Diamonds from the Ural Mountains: their characteristics and the mineralogy and geochemistry of their inclusions

Fernando A. T. P. Laiginhas, B.Sc. (Hons.)

Thesis presented for the degree of Doctor of Philosophy (Ph.D.)

University of Glasgow

Department of Geographical and Earth Sciences

December 2008

Abstract

This thesis has investigated the geological origin of diamonds from the Ural Mountains. A set of inclusion-bearing diamonds from alluvial deposits in the western part of the Urals was characterised on the basis of their morphological features, nitrogen contents and nitrogen aggregation states, carbon and nitrogen stable isotopes, mineral inclusion geochemistry and radiometric isotopic ages of the inclusions.

The vast majority of the studied diamonds are rounded dodecahedra, which indicates that the diamond population has experienced major resorption after crystallisation. The majority of the diamonds are affected by radiation damage and display evidence of transportation. Non-abraded diamonds exhibit similar surface features to those abraded, so they are probably of similar origin. The studied inclusion-bearing set of diamonds shares some characteristics with the overall, mostly inclusion-free, diamond population from the Ural Mountains. This similarity in physical characteristics strongly suggests that the Ural diamonds are all part of a single population.

A Fourier Transform Infra-Red (FTIR) spectroscopy study allowed both the concentration of nitrogen and the aggregation states of this element to be quantified. Diamonds from other known primary deposits in the East European Craton (EEC) have FTIR signatures that do not match that of the studied population. Nitrogen thermometry results suggest that the Ural diamonds probably crystallised under similar pressure-temperature conditions. If a similar overall regime of formation for the Urals alluvial diamonds is considered, then a single primary diamond source or a spatial proximity between primary contributory sources seems likely.

The variations in $\delta^{15}N$ – $\delta^{13}C$ measured in the Ural diamonds of the peridotitic and eclogitic paragenesis suggest derivation from a similar, initially homogenous, mantle carbon source which has been subjected to metasomatic-induced isotopic fractionation. However, for some $\delta^{15}N$-enriched – $\delta^{13}C$-depleted eclogitic diamonds, the possibility of crystallisation from subduction-related metasomatic fluids/melts cannot be excluded.

Based on the chemical composition of syngenetic mineral inclusions recovered from the Ural diamonds, the eclogitic paragenesis (60%) dominates over the peridotitic (26%), with a minor websteritic assemblage also present (2%). The remaining 12% are diamonds with sulphide inclusions of unknown paragenesis. The chemistry of the mineral inclusions almost completely overlaps that of previous electron microprobe studies of inclusions in diamonds from worldwide localities. Geothermobarometric calculations show an overall agreement between the equilibration conditions of the three inclusion parageneses. The Ural diamonds crystallised at temperatures of 1050-1300°C, at minimum depths of about 165 km, within a diamondiferous lithosphere extending to at least 230 km at the time of diamond formation.

The Re-Os isotope genesis age data for syngenetic sulphide inclusions and the $^{40}Ar/^{39}Ar$ laser probe eruption ages of syngenetic clinopyroxene inclusions were determined. Six eclogitic sulphide inclusions, two of which coexist in the same diamond, gave an isochron age of 1280 ± 310 Ma which may be associated with rift-related magmatism that affected the EEC at ca. 1.3 Ga. The determined genesis age is also similar to genesis ages reported for eclogitic diamonds from a number of mines in southern Africa, and this is probably indicative of a global diamond formation event at that time. Five eclogitic clinopyroxenes recovered from four diamonds yielded similar $^{40}Ar/^{39}Ar$ ages averaging 472 ± 28 Ma, which likely approximate the time of source kimberlite/lamproite eruption. This age indicates that the Ural diamonds are not derived either from the diamond-bearing kimberlites of the Siberian craton, nor from presently known Russian and Finnish kimberlite provinces on the EEC.

An integrated model for the genesis, eruption and accumulation of the Ural diamonds in the context of the evolution of the EEC is proposed. The Urals placer deposits are mainly confined to 407-397 Ma sedimentary rocks along the western side of these mountains, with diamond size distribution indicating sediment transportation at that time generally from the north-west. The diamondiferous sedimentary accumulation in the Urals is envisaged as being analogous to that presently found along the Namaqualand / Namibian coastal belt in the western margin of southern Africa. During the construction of the Ural Mountains, the diamondiferous sediments became part of the western accretion zone when the EEC united with the Kazakhstan and Siberia plates during late Devonian through to late Triassic times. The evidence presented in this thesis suggests the existence of an undiscovered kimberlite/lamproite primary source, probably on the Volgo-Uralia crustal segment of the EEC, which gave rise to the Urals diamond deposits.

Table of contents

List of Figures

List of Tables

Acknowledgements

Firstly, my sincerest thanks go my supervisor, Jeff Harris, for being bold enough to offer this project to a young man living out in the sticks of northern Portugal. His interest, assistance and encouragement have never faded over the last three years. Thanks also to my co-supervisor, Tim Dempster, for his advice and guidance, especially during my writing-up.

This project required a collaborative effort of many experts from a number of different institutions, who have allowed me to work in their laboratories. In particular, I owe a great debt to: Gill Parker (formerly of Harry Oppenheimer House, Kimberley) for help with diamond surface features; Gerhard Brey, Heidi Hofer, Timo Luchs, Jan Heliosch and Michael & Sabine Seitz (Institute for Mineralogy, University of Frankfurt) for assistance with EPMA sample preparation and analysis and being the most extraordinary hosts; Pierre Cartigny and Mederic Palot (Institut de Physique du Globe de Paris) for assistance with the FTIR, $\delta^{13}C$ and $\delta^{15}N$ work in the most beautiful city in the world; Graham Pearson, Geoff Nowell, Chris Ottley and Akira Ishikawa (Northern Centre for Isotopic and Elemental Tracing, University of Durham) for introducing me to Re-Os age dating; Ray Burgess (University of Manchester) for showing me the intricacies of the $^{40}Ar/^{39}Ar$ age dating and David Phillips (University of Melbourne) for performing the $^{40}Ar/^{39}Ar$ analyses.

Thomas Stachel is gratefully acknowledged for great discussions and for sharing the worldwide dataset of mineral inclusion chemical analyses. Wolf Skublak (De Beers Group, Russia) provided me with hard to get Russian articles and books, which were translated into English in Glasgow by Mikhail Kabeshov. Mark Newton is thanked for inviting me to present my work at three De Beers Diamond Conferences. The 9th International Kimberlite Conference Committee is also thanked for accepting my paper for an oral presentation and for financial support.

Everybody treated me like a prince during my visit to Lesotho, Namibia and South Africa. I am grateful to Gem Diamonds Ltd. at the Letseng-la-Terae mine in Lesotho, in particular

Keith Whitelock (CEO), Moruti Mphatsoe (General Manager), Debbie Bowen and Ray Ferraris. In Namibia, thanks are due to Bob Burrell and his geology staff of the Mineral Resource Department of Namdeb, Oranjemund, for my two day visit to the diamondiferous alluvial deposits along both the Namibian coast and Orange river. In South Africa, my thanks go to the management of the Finsch diamond mine and in particular their resident geologist Trevor Rowlands for an excellent underground visit. In addition, my visit to Harry Oppenheimer House in Kimberley was most memorable and I thank the management for the opportunity to see their assortment of diamonds.

For keeping me in good spirits, sharing a passion for good food and always giving me excellent advice, I have to say “muchas gracias” to Alberto Perez-Huerta. I am grateful to the staff and technicians at GES for their support. I most sincerely thank Kate Dobson, who brilliantly helped me compile and format the thesis in less than two hours! A special big thank you goes to all postgrads that shared some time of their lives with me in the Gregory Building over the last three years.

Finally, I am grateful to my family for their continued support, despite my long absences from home.

This research was supported by the grant 21-77038-B of the Calouste Gulbenkian Foundation from October to December 2005. From January 2006 to December 2008, the research was supported by the grant SFRH/ BD/ 22174/ 2005 of the Portuguese Foundation for Science and Technology, funded by Measure IV.3 of the POCI 2010 programme. The Calouste Gulbenkian Foundation supported the costs associated with the use of analytical equipment at Durham University. De Beers is greatly acknowledged for providing the diamond samples for this study.

Declaration

Except where specific reference is made to other sources, the work presented in this thesis is the original work of the author, and has not been previously submitted for a degree at this, or any other university or institute of learning.

Fernando Laiginhas

December 2008

1. Introduction

The root word of diamond comes from two Greek words: “diaphanes” and “adamas”. The former means “transparent” and the latter “unconquerable”, two characteristics of diamonds that are evident in their clarity, brightness, and hardness. The ancient Greeks and Romans believed diamonds were tears of the gods and splinters from falling stars. The Hindus believed diamonds were formed by lightning striking rock and attributed them such power they were placed in the eyes of statues (Dickinson, 2001). To the ancients, diamonds were magical, mystical talismans that could bring luck, wealth and success or bestow power, fearlessness and even invincibility. Kings would have large amounts of diamonds set into their breast plates as they marched into battle as protection against arrows and as ornaments. In the Middle Ages, diamonds were used to ward off the effects of poison, illness, and magic spells.

Romance has always been attached to the diamond as the Greeks believed that the dazzle of the diamond reflected the constant dazzling affect of love. However, the diamond engagement ring is a relatively recent tradition started by Austria's Archduke Maximillian, who presented one to his fiancée, Mary of Burgundy, in 1477. He placed the ring on the third finger of her left hand, based on an ancient Egyptian belief that this finger contained a “love vein” running directly to the heart (Hershey, 1940). Ever since, couples around the world have pledged their love and devotion with a diamond.

Diamonds are believed to have been found in alluvial deposits in India between 800 and 600 B.C.. Although diamonds discovered in Borneo around 700 A.D. were an important source for Southeast Asia, for about two thousand years India monopolized world production as it was the only source of diamonds known to Europeans until the 18th century. The diamonds from India travelled two routes, both through the Mediterranean Sea. The southern route was through Egypt, Ethiopia and Aden (present-day Yemen), and the northern route was crossed Turkey, Arabia, Armenia and Persia (Bruton, 1977).

In 1498 the Portuguese navigator Vasco da Gama discovered a direct sea route from Europe to India via the Cape of Good Hope. As a result, a world centre for diamond trade was established in Antwerp because this city's sea port was well situated to receive the vast supplies of rough stones that the Portuguese were sending from Lisbon, as well as the diamond merchants and traders from Venice (Smith, 1912). During the late 17th century, England's interests became stronger towards India and London emerged as a centre for cutting and also became the primary market place of the world for rough diamonds.

In 1725, alluvial diamond discoveries were made in Brazil which turned that country into a major player in the diamond market. At first, exploration was open to anyone who had enough slaves to work a piece of land and paid a tax to the Portuguese crown, which controlled Brazil. In view of the number of diamonds recovered in Brazil, in 1771 the Portuguese crown decided to monopolize both the exploration and exploitation of diamonds by creating a state company, the Diamond Royal Extraction (Hershey, 1940).

Brazil and India remained the two major diamond producing countries until the 1870's, when diamond production of primary deposits using modern techniques started in South Africa after the discovery of the diamond fields in Kimberley (Bruton, 1977). Today, diamonds are found in 26 countries (USGS Minerals Yearbook 2006), including major sources in Canada, Russia, Australia, Botswana, South Africa, Democratic Republic of Congo and Angola. Yet, even with contemporary technology, they remain very difficult to find. Some of the most remote and inhospitable regions on Earth are currently being searched to uncover new diamonds, including the frozen tundra of Siberia and Canada and the arid deserts of Botswana and Australia.

1.1 The Ural Mountains

Extending for nearly 2500 km from the islands of Novaya Zemlya in the north to the Aral Sea in the south, the Uralide orogen of central Russia forms the geographical and geological divide between Europe and Asia (Berzin et al., 1996; Scarrow et al., 2002b; Brown et al., 2006a). For more than a century the Urals have been one of the key areas of geological research in Russia, and have provided much of its mineral and petroleum wealth for the last 50 years (Brown et al., 2002).

In ancient times, the existence of a large mountain range at the eastern fringe of Europe was regarded as being more mythical than real. Not until the 10th century AD does the first mention of the Urals occur, in Arabic sources (Koryakova and Epimakhov, 2007). The

northernmost areas of the Urals were discovered at the end of the 11th century, but the discovery of the entire mountain range only happened in the beginning of the 17th century, when the Russians recognized the economic potential of the minerals that were found in the Urals. The first geographic survey of the chain was made in the early 18th century by the Russian historian and geographer Vasily N. Tatishchev, who undertook the survey for Peter the Great (Yastrebov, 2008).

According to Kukharenko (1955), the first serious scientific study of the Urals was made in 1770–71. Scholars studying the Urals during the 19th century included several Russian scientists and prominent foreign scholars such as the German naturalist Alexander von Humboldt and the English geologist Sir Roderick Murchison, who compiled the first geologic map of the Urals in 1841. A significant amount of work on the geologic structure and associated mineral resources of the Urals was produced during the Soviet period, much of which was not readily available to the global scientific community until the collapse of the Union of Soviet Socialist Republics (USSR).

Both slopes of the Ural Mountains are extremely rich in mineral resources. On the eastern slope, metallic ore deposits, notably magnetite, predominate. Among the non-metallic mineral resources of the eastern slope are asbestos, talc, fireclay, and abrasives. Gems and semiprecious stones have long been known: they include amethyst, topaz, and emerald (Kukharenko, 1955). Among the western deposits there are beds of potassium salts on the upper Kama River and petroleum and natural gas deposits in the Ishimbay and Krasnokamsk areas. There are also large deposits of bauxite, chromite, gold, and platinum. Bituminous coal and lignite are mined on both slopes, the largest deposit being the Pechora bituminous coalfield in the North Urals (Komar and Chikishev, 1968).

Because of its wealth of mineral resources, the leading industries in the Urals are mining, metallurgy, machine building, and chemicals. The metallurgical plants at Magnitogorsk, Chelyabinsk, and Nizhny Tagil; chemical plants at Perm, Ufa, and Orenburg; and large-scale engineering at Yekaterinburg established the Urals as one of the largest industrial regions of Russia (Kukharenko, 1955; Komar and Chikishev, 1968).

1.1.1 *Geological setting and evolution of the Ural Mountains*

From North to South, the Urals are geographically divided into five areas (see Figure 1): Polar (68º N to 65º N), Cis-Polar (65º N to 62º N), Northern (62º N to 60º N), Middle (60º N to 56º N) and Southern Urals (56º N to 48º N) (Puchkov, 1997; Brown et al., 2006a). In

addition, the Urals have traditionally been divided into six longitudinal tectonic zones that extend parallel to the margin of the East European Craton. From west to east, these zones are the Pre-Uralian foredeep, the West Uralian Zone, the Central Uralian Zone, the Magnitogorsk-Tagil Zone, the East Uralian Zone and the Trans-Uralian Zone (Puchkov, 1997; Scarrow et al., 2002a; Brown et al., 2006b).

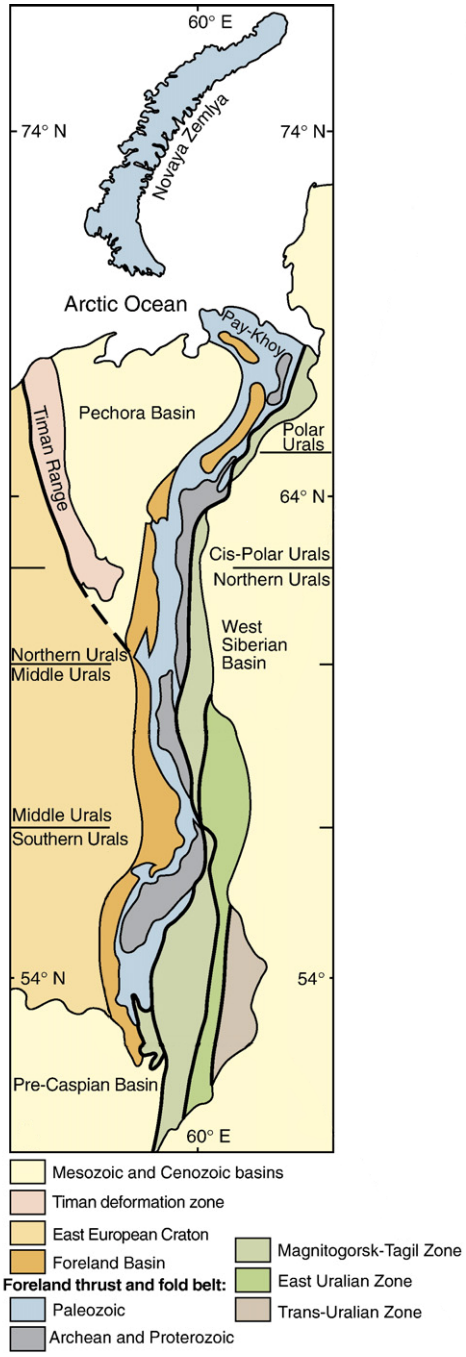

Figure 1 – Sketch map showing the different geographic divisions of the Urals (North to South), and the disposition of the different tectonic zones (West to East). Modified from Brown et al. (2006b).

The Pre-Uralian foredeep is a foreland basin filled with Late Carboniferous to Early Triassic syn-orogenic sedimentary rocks that were derived from the growing Uralide orogen to the east (Scarrow et al., 2002a). The West and Central Uralian zones make up the foreland thrust and fold belt of the orogen and include deformed sedimentary rocks of the foreland basin, Paleozoic platform margin and continental slope rocks, and Archean, Mesoproterozoic and Neoproterozoic rocks of the East European Craton (part of Baltica) (Brown et al., 1997; Brown et al., 2006a). In the Southern Urals, the foreland thrust and fold belt is overlain by an accretionary complex, related to the Middle through Late Devonian collision of the Magnitogorsk island arc with the East European Craton (Brown and Spadea, 1999), while in the Middle Urals the foreland thrust and fold belt is a narrow, N-S trending, west-verging basement thrust stack measuring ~50 to 75 km in width (Brown et al., 2002). The Magnitogorsk-Tagil Zone is composed of Silurian to Devonian intra-oceanic island arc volcanic rocks and overlying volcaniclastic sedimentary rocks of the Tagil and Magnitogorsk island arcs (Herrington et al., 2002).

The Magnitogorsk-Tagil Zone is separated from the first three zones (which belong to the East European Craton) by the Main Uralian fault, the principal suture zone of the Uralide orogen (Berzin et al., 1996). This is a ~10 km wide, east-dipping mélange containing material that was tectonically eroded from the volcanic arc, and, according to seismic data, extends to a depth of ~25 km (Echtler et al., 1996). The East Uralian Zone contains deformed and metamorphosed volcanic island arc fragments and Precambrian and Paleozoic continental-type crust (Puchkov, 1997). This zone was intruded by numerous granitoid batholiths and subordinate diorite and gabbro intrusions during the Carboniferous and the Early Permian, forming the so-called “main granite axis” of the Urals (Bea et al., 2002). The Trans-Uralian Zone only outcrops in the Southern Urals and is not well known due to poor exposure. This easternmost part of the Urals is mainly composed of Devonian and Carboniferous calc-alkaline volcanic and plutonic complexes, with ophiolite material and high pressure rocks also present (Scarrow et al., 2002a). Rocks that unequivocally belong to either the Kazakhstan or Siberia plates do not outcrop in the Uralides (Brown et al., 2006b).

The Uralide orogen developed during the Late Paleozoic as the continental margin of Baltica began to change from a passive setting to an active one (Puchkov, 2002). From the Late Devonian and Early Carboniferous its leading edge was subducted eastward (today’s coordinates) beneath a chain of intra-oceanic island arcs (Magnitogorsk and Tagil) in the palaeo-Uralian ocean (Brown and Spadea, 1999). In the Southern Urals, the collision of Baltica with the Magnitogorsk island arc occurred during the Middle to Late Devonian and

resulted in the development and emplacement of an accretionary complex over the subducting slab (Brown et al., 2006a). By the Early Carboniferous the Magnitogorsk island arc was sutured to the continental margin of Baltica along the Main Uralian fault zone (Brown and Spadea, 1999). In the Late Carboniferous, platform sedimentation along with rift volcanism took place within the accreted Magnitogorsk island arc (Puchkov, 2002). Due to poor exposure, the evolution of the Uralide orogen farther north is less well understood. It is generally accepted, however, that the Tagil volcanic arc collided with the eastward subducting margin of Baltica in the Early Carboniferous.

Meanwhile throughout the orogen, eastward-directed subcontinental subduction of the Uralian oceanic crust was taking place along the margin of the Kazakhstan plate, forming Andean-type continental volcanic arcs. In the latest stages of the Carboniferous the Uralian ocean basin closed and the Kazakhstan plate, followed by the Siberia plate, collided with Baltica (Scarrow et al., 2002a). This continent-continent collision continued until the Early Triassic and was accompanied by westward thrusting of the Precambrian basement and late Paleozoic platform cover of Baltica which resulted in the development of the western foreland thrust and fold belt and foreland basin of the Urals (Puchkov, 1997).

During the late stages of the collision, extensive wrench or transpressive faulting appears to have dominated along the central axis of the Urals orogen, fragmenting the Tagil arc and juxtaposing metamorphic terranes within the East and Trans-Uralian zones (Friberg et al., 2000). This was accompanied by widespread crustal and mantle melt generation and granitoid emplacement took place in the interior part of the Uralides (Bea et al., 2002). Since the Permian-Early Triassic, the Uralide orogen has not been subjected to any major changes. The Middle Urals are the exception, being affected by deformation in the Mesozoic and Tertiary that resulted in folding and thrusting of the Early Triassic deposits in the Tagil zone (Puchkov, 1997). Throughout the Ural Mountains, the East and Trans-Uralian Zones are widely covered by Mesozoic and Cenozoic sediments (Brown et al., 2002).

The Ural Mountains form the only topographic expression currently associated with the Uralide orogen. In the Middle and Southern Urals, the mountains coincide almost exclusively with the foreland thrust and fold belt, except for the Irendik range in the Magnitogorsk arc (Seward et al., 2002). Topographically, the Ural Mountains consist of a series of broad, roughly north-south trending ridges that, in the Middle and especially in the Southern Urals (where the relief is stronger), run parallel to the Uralide geological structures (Borisevich, 1992). In the Southern Urals, these north-south trending ridges and

valleys are crosscut by deeply incised river valleys as the generally north-south flowing rivers turn abruptly west to cut through the mountains (Seward et al., 2002). The timing of river downcutting is not well constrained, but several of the largest rivers have associated raised post-Paleocene river terraces, thus suggesting that surface uplift in the Southern Urals has occurred since the Paleogene period (Borisevich, 1992).

1.2 The alluvial diamond deposits of the Ural Mountains

The alluvial diamond deposits of the Urals have been known since 1829 and were described in detail by Kukharenko (1955). Unfortunately, Kukharenko's excellent book was not readily available to researchers outside Russia and, as a result, most of the scientific community from western countries are not familiar with the key historical facts related to the discovery of diamonds in the Urals. The following is as summary of the principal historical facts mentioned in Kukharenko (1955).

The search for diamonds in Russia started at the beginning of the 18th century. The Russian scientist Mikhail Lomonosov predicted that in the Southern Urals many precious materials, including ores, oil and precious stones would be discovered. The German naturalist and explorer Alexander von Humboldt noticed similarities between alluvial placer sediments in Brazil and in the Urals and predicted that the Urals would be an "Eldorado" for diamonds, gold and all sorts of valuable materials.

Finally, in 1829, Pavel Popov found the first diamond in the Krestovozdvizhenskiy region (also known as Teplaya Gora). At first he thought the stone was a topaz, but after a more careful observation the stone was correctly identified as a diamond. The land where this diamond was found belonged to a wealthy lady named Pole-Butero, who gave the diamond to Alexander von Humboldt, who later offered it to Empress Maria Aleksandrovna.

Shortly after the discovery of the first diamond in the Urals, the Russian government sent Professor M. Engelgardt and a group of scientists and workers to study the placer deposits. In the Krestovozdvizhenskiy region, they found rhombododecahedral diamond crystals and also graphite, iron sulphides, pyrite, anatase, dolomite, talc, amongst other minerals. For roughly a century (1829-1928) the Krestovozdvizhenskiy region was the main diamond producing area in the Urals, with 220 diamonds found. The largest crystal weighed about 3 ct. (590 mg).

Even though the Russian government gave incentives for diamond findings, the majority of findings were accidental during washings of raw materials for gold. In 1888, several French researchers went to the Urals to try to establish a model for the distribution of diamonds in the Krestovozdvizhenskiy region. Despite their continued efforts, no reliable methods for finding and recovering diamonds from the placer sediments could be established. Nevertheless, the drawings and descriptions made at that time by the French researchers confirm that the majority of the Ural diamonds had a typical rounded dodecahedral habit. The area subjected to exploration works gradually increased, and eventually a 87 mg (0.435 ct) stone, similar to the crystals from the Krestovozdvizhenskiy region, was found in the Southern Urals. Together with diamond, an increasing number of other minerals such as pink topaz and chrysoberyl were being found in the Urals, and this abundance of gemstones reinforced the view that the Urals were indeed the "Russian Brazil".

In 1922, the Russian geochemist and mineralogist Alexander Fersman found demantoid garnets in the Nizhne-Tagilsk region, which he believed could be associated with the mother rock of the diamonds. Fersman, who was the first researcher that searched for the primary sources of the Ural diamonds, was of the opinion that dolomite and greenstones could be the possible sources of the diamonds.

In the 1930s the search for primary diamond sources started in the western part of the Urals, but this instead resulted in the discovery of more diamond placers, which were the base for the creation of a powerful diamond industry in Russia. According to Kukharenko (1955), the diamond findings in the 1930s and 1940s in the Urals made Russia the leading country for research in diamond crystallography. In 1955, there were 97 diamond placers known in the Urals, 92 of them in the Middle Urals and of these 73 were on the western slope of the Ural Mountains.

Systematic work began in Middle Urals in 1938 and officially the commercial exploitation started in 1941. All industrial diamond mines were located on the western slope of the Middle and North Urals. Kukharenko (1955) grouped the diamond placers into three sub-meridional fields. The eastern field is the less well known, going from Ilya-Is in the North to Yekaterinburg in the South. Diamonds were found in platinum rich placer sediments around river Tura and Nizhne-Tagilsk. The central field follows roughly the 50ºE meridian, alongside the main Uralian depression, from Kosva in the North to Krestovozdvizhenskiy in the South. The western field goes (north to south) from Kosva to Srebrianka. The western border of this field is not clear. The most important diamond

mines in the Urals were located in the central field, along the rivers Vishera and Chusovaya.

The most important diamond sources of the Urals placers are Devonian rocks of the Takaty (also known as Takata, Takatinian or Takatinskaya) Formation (Bekker et al., 1970). The Takaty Formation is of Emsian age (ca. 407-397 Ma; Gradstein et al., 2004) and is exposed over several hundreds of kilometres along the western slope of the North and Middle Urals (Konstantinovskii and Prokopchuk, 1978). This Formation is composed of quartz sandstones and sands with interlayers of weakly cemented conglomerates and gravelstones in the basal member (Konstantinovskii, 2003). Diamonds are mostly found in the lowermost conglomerate bed which is a lenticular structure composed of alluvial sedimentary rocks subjected to partial rewashing within a coastal-marine zone (Konstantinovskii, 2003). The diamondiferous layers of the Takaty Formation vary in thickness from about 0.1 to 5 metres (Kukharenko, 1955), its thicker sediments being confined to ancient erosional downcuttings or karstic sinkholes in the carbonate bedrock (Konstantinovskii and Prokopchuk, 1978; Konstantinovskii, 2003).

During the Devonian, the diamondiferous sedimentary rocks associated with the Takaty Formation are believed to have accumulated on and along the eastern margin of the EEC under coastal-marine conditions (Stepanov and Sychkin, 1996; Posukhova, 2007). Continuous reworking of the sedimentary rocks of the Takaty Formation liberated and concentrated diamonds in younger Meso-Cenozoic layers (Ishkov, 1966). Thus the Devonian rocks of the Takaty Formation can be seen as secondary diamond collectors that after several cycles of transportation, erosion and re-deposition provided diamonds to tertiary deposits (Konstantinovskii, 2003; Posukhova, 2007). As a result, the diamonds from the Urals have been mined mostly from Quaternary alluvial terrace deposits and from river gravels preserved in Meso-Cenozoic karst depressions (Ishkov, 1966; Konstantinovskii, 2003).

1.3 The quest for a primary source: previous work on the provenance of the Ural diamonds

Despite many decades of exploration and mining activities in the Ural Mountains, no primary diamond sources have yet been found. The problem of the origin of the Urals diamond placer deposits have been addressed by generations of Russian geologists but, to this date, the nature and location of the diamond's native sources remains unknown. The

first explorers, such as Professor M. Engelgardt in the 1830s, thought that the primary sources would be the rocks directly underneath the placer deposits (Kukharenko, 1955). As such rocks were found to be non-diamondiferous, this hypothesis was quickly abandoned.

In the 1920s Alexander Fersman suggested that the Ural diamonds could be related to intrusions of platinum-rich gabbro-peridotites. This hypothesis was favoured by Kukharenko (1955), who said that the sources of the Ural diamonds "will be found very soon". Kukharenko's predictions were not correct, as these rock types did not contain diamonds and mainly occur on the eastern slope of the Ural Mountains and thus were not linked to the economic diamond-bearing placers that are all located on the opposite slope of the Urals (Stepanov, 1971).

In the 1970s, the pioneering study of Sobolev et al. (1971) on garnet and pyroxene inclusions in diamonds from the Urals showed that their chemistry was similar to that of similar minerals from eclogite xenoliths in diamond-bearing kimberlites. This study first substantiated a possible kimberlitic origin for the Ural diamonds. The proximity of the Urals diamondiferous placers to the eastern margin of the East European Craton (EEC), where kimberlite pipes occur, led to the hypothesis that the primary sources of the Ural diamonds were kimberlite pipes in the EEC that have been completely eroded or which are now under a sedimentary cover several kilometres thick (Bekker et al., 1970). This hypothesis has yet to be verified.

A different hypothesis suggests that the primary sources of the Ural diamonds are xenotuffisites (a rock of fluid-magmatic origin with variable content of xenogenic material) of probable ultrabasic or basic composition that have undergone post-magmatic metasomatic changes (Rybal'chenko et al., 1997). Xenotuffisites have been found on the western slope of the Ural Mountains in the form of anostomising, sub-vertical veins and sill-like bodies that have intruded the pre-existing sedimentary layers during the Mesozoic or Cenozoic (Rybal'chenko et al., 1997). Specialists from De Beers (internal report KR97/0515) investigated the areas where diamonds were found in xenotuffisites and observed that in all these areas the xenotuffisites were located near the diamond-bearing sedimentary rocks of the Takaty Formation. They concluded that the diamonds have not derived directly from primary, xenotuffisitic intrusions, but are detrital grains that were mechanically introduced into them from the diamondiferous sedimentary rocks.

Another hypothesis invokes a glacial origin for the origin of the Ural diamond placer deposits (Garanin et al., 2000). According to these authors, the Ural diamonds derived

from kimberlite/lamproite sources located to the northwest of the Urals (e.g. in Finland and the Kola Peninsula) and transported by glaciers over distances of hundreds of kilometres until they were finally concentrated in numerous placers in the Ural Mountains. Garanin et al. (2000) argue that the Finland – Kola Peninsula region would have been the centre (or centres) of a glacier cover situated in Russia during Vendian times, which was later uplifted and then eroded, and hence only a small number of dykes and roots of kimberlite pipes are currently present in that region. This hypothesis assumes that the diamonds from the Urals and those from the kimberlites in Finland and the Kola Peninsula can be linked on the basis of their similar physical characteristics. As diamonds from those two hypothetical primary sources are not readily available for academic studies, the validity of such assumption cannot be verified.

Finally, Anfilogov et al. (2000) proposed that the Ural diamonds have not derived directly from kimberlites, but instead originated from the buried crusts of weathering (crater facies kimberlite) that developed on the top in the kimberlite bodies. It is suggested that diamond-rich clay from the upper part of kimberlites buried under a thick sedimentary cover, migrated to the overlapping rocks by a process of fluid-tectonic mobilization. The upwards migration of the clay was triggered by the movement of a low angle thrust that generates tension cracks in the sediments above the kimberlites (Anfilogov et al., 2000). A major weakness of this very complicated and convoluted theory is that it implies the existence of very proximal primary sources, which is not supported by the presence of surface features in the Ural diamonds which are typical of detrital diamonds that have been subjected to transportation. Instead, Anfilogov et al. (2000) argue that the abrasion features seen in the Ural diamonds were produced when the crystals were transported by the clay solution or suspension.

1.4 Aims of this work

This thesis addresses the fundamental question of the geological origin of diamonds from the Urals. To answer this question, a detailed study of diamonds from the alluvial deposits of the Urals and their mineral inclusions was undertaken. The diamonds used in this study were part of a major purchase by the Diamond Trading Company in London from the then Russian Government, in late 1994. Previously the diamonds had been stored in the Russian Treasury and no details on their geographic and geological origin are known, other that they are from alluvial deposits in the western part of the Ural Mountains. Information on the mining methods used and the representative nature of the purchased parcel relative to

the global Urals production was not given. In 1995, Dr. Jeff Harris was given access to these diamonds and selected a representative set of 217 diamonds containing mineral inclusions. The study of these inclusion-bearing diamonds from the Urals is documented in this thesis.

As such a study is destructive, the work concentrated initially on a thorough characterisation of the diamonds themselves. This aspect evaluated diamond shape, colour, surface features and degree of breakage and/or abrasion. After a full description of the diamonds was completed, all samples were photographed for their surface features and inclusion content (Chapter 2).

Some diamonds were then physically broken to release the inclusions. The diamond fragments were analysed using Fourier Transform Infra-Red Spectroscopy (FTIR) to obtain information about the levels and aggregation states of diamonds' commonest impurity, nitrogen. Such characteristics can be used as a chemical fingerprint to relate the Ural deposits to other diamond populations world-wide and, in so doing, obtain information on their overall regime of formation and mantle residence (Chapter 3). The diamond fragments were further combusted to determine $\delta^{13}C$ and $\delta^{15}N$ signatures as well as the total nitrogen content present. This study of carbon and nitrogen isotopes is useful in defining diamond populations and provides clues to the processes of diamond formation (Chapter 4).

The work then concentrated on mineral inclusions trapped in the diamond during growth. The minerals released from the diamond were subjected to Electron MicroProbe Analysis (EMPA). This analytical procedure provides a very detailed (major and the more common trace elements) and accurate chemistry of the micron-sized minerals, thereby allowing the overall environment in which the diamond grew, to be assessed. Exchange equilibria between co-existing inclusions are used to define the depth and temperature of diamond formation (Chapter 5).

From a set of sulphide inclusions, Negative Thermal Ionization Mass Spectrometry (N-TIMS) isotopic work allowed the determination of femtogramme quantities ($1*10^{-15}$ g) of Re and Os on single sulphide inclusions. This technique was used to determine the genesis age of the diamonds. Additionally, $^{40}Ar/^{39}Ar$ laser probe analysis was carried out on single clinopyroxene inclusions to determine the eruption age of the diamonds (Chapter 6).

The physical characteristics of the diamonds and the mineralogy and geochemistry of their inclusions, combined with the genesis and eruption ages of the diamonds, enable, for the first time, the development of an integrated model for the genesis, eruption and accumulation of the Ural diamonds in the context of the evolution of the East European Craton. The results of this study ultimately lead to an improved model and greater understanding of the diamond-forming regions within the Earth's mantle (Chapter 7).

2. Physical Characteristics

2.1 Introduction

Early studies on diamond characterisation and classification have shown that diamonds from different parts of the world have distinct physical characteristics (Wagner, 1914; Sutton, 1928; Williams, 1932). For example, diamonds from Siberia and Sierra Leone are predominantly sharp-edged octahedra, opaque-coated diamonds are found in various sources in the Democratic Republic of Congo and minor true colours are usually specific to a source (e.g. amber diamonds from Zwartruggens in South Africa and pink diamonds from Argyle mine in Australia) (see Harris, 1992).

In order to fully differentiate diamond sources, two detailed classification schemes, based principally on diamond morphology, have been attempted. The classification scheme of Orlov (1977) was primarily used on Russian diamonds and divided diamond into ten crystal varieties, five for single crystals and five for polycrystalline aggregates. These were further characterised on the basis of colour and surface features. The classification of Orlov (1977) provided much detailed and useful information, but did not take into account such factors as diamond size and locality.

A second classification scheme, which involved a detailed characterization of diamonds from South Africa as a function of size and locality, was proposed by Harris et al. (1975). In this classification, crystal form, crystal angularity and crystal regularity are the main morphological divisions, with further subdivisions being transparency or opacity, colour, the number of inclusions, and surface features. The classification scheme of Harris et al. (1975) established that diamond productions from individual primary sources can be classified on the basis of their physical characteristics, particularly when crystal form and colour are plotted against diamond size.

A wide range of minor surface features are commonly found in diamond and these were first noticed by Sutton (1928) and Williams (1932). A more detailed study was carried out by Orlov (1977), who divided Russian diamonds into six groups according to their surface features. In a subsequent study of diamonds from known kimberlites and alluvial sources in southern Africa, Robinson (1979) indentified and classified 41 pristine surface features recognised on common diamond morphologies into a relative chronological sequence. In alluvial diamonds, pristine surface features are usually still recognisable, and this allows comparisons with diamonds from likely primary sources to be made. For example, from similar surface features observations, Robinson (1979) was able to link the Hlane alluvial diamond field to the Dokolwayo kimberlite in Swaziland.

This chapter presents the results of a study of the physical characteristics of a set of 217 inclusion-bearing diamonds from the alluvial deposits in the western part of the Ural Mountains. The shape, colour, degree of breakage, surface features and transportation features have been determined for all diamonds. As the diamonds were selected solely on the basis of having mineral inclusions suitable for chemical analysis, a bias towards certain shapes, colours, or other physical characteristics may exist.

To describe the physical features of the diamonds such as crystal shape, colour and degree of breakage the classification scheme of Harris et al. (1975) was adopted. With respect to the diamond shapes, diamonds were assigned to the irregular category when they had less than 50% of a specific shape (e.g. octahedra or dodecahedra), adopting the criteria defined by Harris et al. (1975). The classification adopted to describe the surface features of the diamonds is that of Robinson (1979). This classification scheme was preferred relative to others (e.g. Orlov, 1977), because it is widely used by both the industry and the scientific community, and because the author was already familiar with that specific terminology.

2.2 Instrumentation and diamond sizes

A Vickers Instruments binocular microscope at the Department of Geographical and Earth Sciences, University of Glasgow (UK) was used to observe the diamond population. Photographs were taken with a Nikon DN100 Digital Net Camera (1280x960 pixel resolution) attached to a Zeiss Stemi 2000-C microscope. All the photographs were taken in a dark room, and a set of Olympus TYP FLQ 85E fibre optic lights was used to light the specimens.

The sizes of the Ural diamonds were classified according to Diamond Trading Company (DTC) sieve classes, ranging from - 06 + 05 (1.83mm square mesh) to 6 grainers (5.75mm square mesh) sieve sizes (Table 1).

The term "grainer" or "gr" derives from a grain of wheat, of which four would roughly make up a carat. Diamonds are weighed by mass (1 carat equals to 200mg), making it a useful term for the larger stones sieve classes, e.g. 1/4ct = 1grainer, 1ct = 4grainers, 8-10 grainers make up the 2ct range, etc. (Craig Sievewright, DTC pers. comm.).

DTC Sieve Class (circular apertures)	Diameter in mm of aperture (lower screen)	Approximate average weight in carats per stone
6gr	5.75	1.60
4gr	4.95	1.05
3gr	4.35	0.78
-12 +11	3.45	0.37
-11 +09	2.88	0.21
-09 +07	2.46	0.12
-07 +06	2.16	0.09
-07 +05	1.99	0.07
-06 +05	1.83	0.06

Table 1 – The range of sieve classes used for the Ural diamonds and the corresponding diameter of aperture and average weight per diamond.

Figure 2 shows the size distribution of the diamond population from the Urals selected for the present study. The majority of the stones range from approximately 2.5mm to 3.5mm in average diameter (-09 +07 to -12 +11 classes).

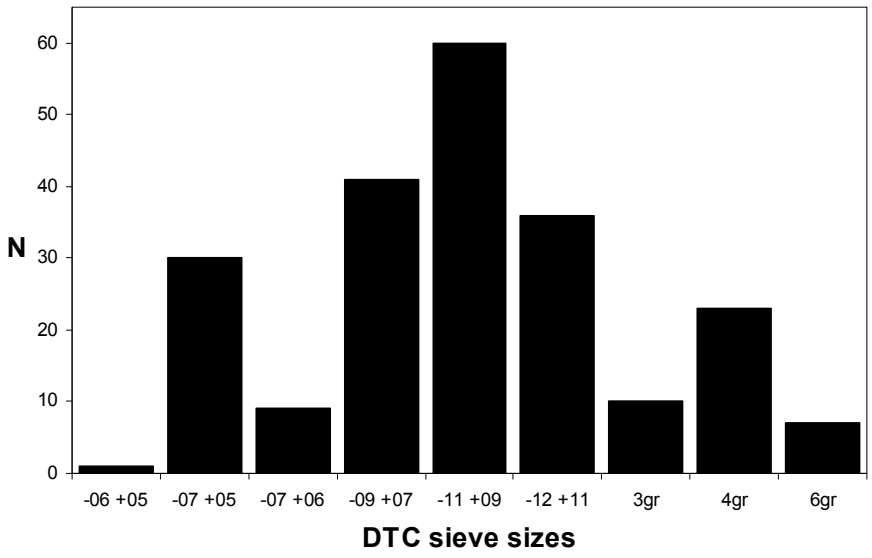

Figure 2 – Size distribution of the 217 inclusion-bearing diamonds from the Urals according to DTC sieve sizes. For corresponding sizes in mm, see Table 1.

2.3 Diamond shape

Diamond crystallizes in the cubic system, occurring in nature as discrete crystals with predominance of the octahedron, cube and rounded dodecahedron forms, and as crypto-crystalline aggregates such as carbonado, ballas, framesite and boart (Robinson, 1978). Cleavage occurs readily parallel to the octahedral faces, giving four directions of possible cleavage. Diamonds commonly have such a brilliant lustre that they lend their name to the term “adamantine”, usually well visible on planar and cleavage surfaces (Bruton, 1977).

Planar surfaces (when present) of diamond crystals almost always belong to octahedral faces. Cubic surfaces may be undulatory and are commonly indented while dodecahedral surfaces are usually curved. The impossibility of describing crystals with curved surfaces using conventional terminology (which assumes crystals to have planar faces) raised a problem when the crystallographic classification of diamond was made. Attempts to partly overcome this problem have resulted in one of the common forms of diamond crystals being referred to as the “rounded dodecahedron” or the “dodecahedroid” (Moore and Lang, 1974).

Diamond crystals frequently exhibit growth twinning. Many twinned crystals are only easily identifiable when the diamond is sawn or polished, but visible manifestations of twinning are commonly encountered in many unpolished crystals (Bruton, 1977). Twinned crystals are of two types: contact twins (also known as macles) and interpenetrant twins, the former being usually more abundant than the latter (Robinson, 1979). A diamond with a contact twin is usually a triangular tabular crystal consisting of two prominent (111) faces divided by a twin plane parallel to these faces, the seam of the twin plane giving a herring-bone pattern to the crystal lattice, the side facets being either proud or re-entrant (Harris et al., 1975). An interpenetrant twin occurs when two crystals appear to have grown within the same space but with different crystal orientations, one appearing to penetrate the other (Bruton, 1977).

As mentioned above, diamond frequently occur as crypto-crystalline aggregates. The small, randomly crystallized, usually yellowish-green or grey to black, masses of diamond, are known as boart (Bruton, 1977). Diamond material known as ballas or shot boart has a spherical form, and ranges in colour from milky white to steely grey, without any crystalline faces or edges and appearing to have no definite lines of cleavage. Both common boart as well as ballas are extremely hard and, when crushed, highly valuable to the abrasive industry.

Carbonado is a black crypto-crystalline variety of diamond, mostly found in Brazil, composed of a mixture of graphite and diamond in compact fine-grained masses. Carbonado nodules are often composed of euhedral grains (up to 200 μm) set in microcrystalline matrix (<0.5 to 20 μm) (Heaney et al., 2005). Framesite is a fine-grained compact form of diamond, commonly found in Southern Africa, which has a bimodal texture similar to carbonado, but with larger (>200 μm) euhedral grains (Bruton, 1977).

Three main crystal shapes have been observed in the Ural diamond single-crystal population: dodecahedra, octahedra and irregular stones (Table 2, Figure 3). Several twinned stones have also been identified with their shape confined to the dodecahedra and irregular crystal forms (Table 2). The diamond crystals were additionally classified as flattened (oblate) or elongate (prolate), according to the particle dimension classification scheme of Zingg (1935). Diamonds of cubic habit and polycrystalline grains are not present in the studied population.

Size (mm)	Single-crystals			Twinned crystals		Totals
	O	D	I	D-m	I-m	
5.75	2	4	0	1	0	7
4.95	2	20	0	1	0	23
4.35	1	7	0	1	1	10
3.45	4	29	0	3	0	36
2.88	3	40	1	13	3	60
2.46	0	33	3	5	0	41
2.16	0	8	0	1	0	9
1.99	0	22	3	4	1	30
1.83	0	1	0	0	0	1
Totals	13	165	7	29	5	217

Table 2 – Morphological classification of the Ural diamonds as a function of size. Diamond size categorised according to largest dimension. O = octahedral, D = dodecahedra, I = irregular shapes, D-m = twinned dodecahedra, I-m = twinned irregulars.

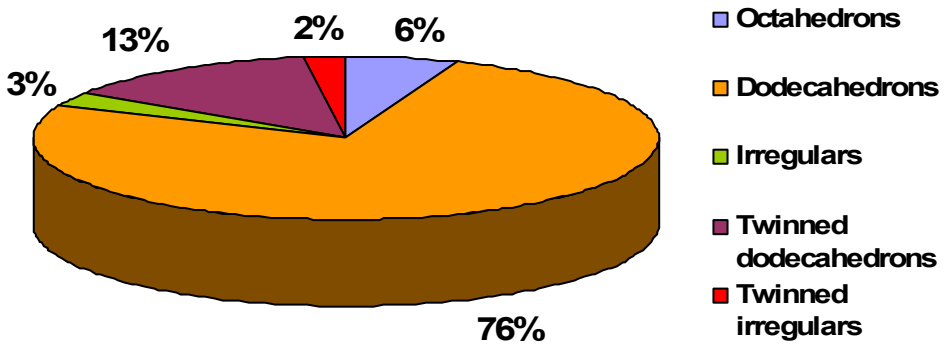

Figure 3 – The relative abundance of the Ural diamonds morphologies.

2.3.1 *Single-crystals*

Single-crystals account for 84% (183 stones) of the population (Table 2). Dodecahedral-shaped diamonds comprising 89% of the single-crystals, octahedra follow with 7% and irregularly shaped diamonds make up the remainder 4%. Dodecahedral-shaped diamond crystals do not represent a primary growth form, but are the result of a resorption or dissolution process operating on octahedra sometime after their formation in the mantle (e.g. Moore and Lang, 1974; Harris, 1987; 1992; Wilks and Wilks, 1994). Resorption processes have, therefore, affected the majority of the studied diamond population.

Figure 4 – Left to right: examples of dodecahedral, octahedral and irregularly-shaped single-crystals from the Ural Mountains, photographed under incident light. Diamond specimens and scale bars are, from left to right: D15A, D4A and D29B; and 250, 500 and 400µm, respectively.

All specimens have been further sub-divided according to their shape (Figure 4). The dodecahedra are dominantly flattened (68%), with equant and elongated crystals comprising, respectively, 18% and 14% of the dodecahedra population. The octahedra were classified as round-edged or flat-faced, with the former being more abundant than the latter (67% and 33%, respectively). All irregular single-crystals are flattened with a remnant shape indicating predominantly towards a dodecahedra form.

2.3.2 *Twinned crystals*

A total of 34 twinned crystals have been characterised in this study (Table 2). This accounts for 16% of the total number of stones. Following the same trend as the single-crystals, the vast majority of the twinned crystals exhibit dodecahedral morphology (85%), the remaining 15% being macle irregulars (Figure 5). Unlike the single-crystals, however,

no octahedral-shaped twinned crystals are present in this population. This absence of octahedral-shaped twins is not surprising, as the resorption processes that affected the original single-crystal octahedra, also most likely affected any original plane-faced twinned octahedra, therefore originating twinned crystals of dodecahedral morphology.

About three-quarters (72%) of the total twinned dodecahedra are flattened, with the remaining 28% of the population being elongate crystals. This contrasts with the twinned irregular crystals population, where all stones are flattened. This dissimilarity may, however, be a statistical artefact, as only 5 irregular twinned crystals were present in the studied population.

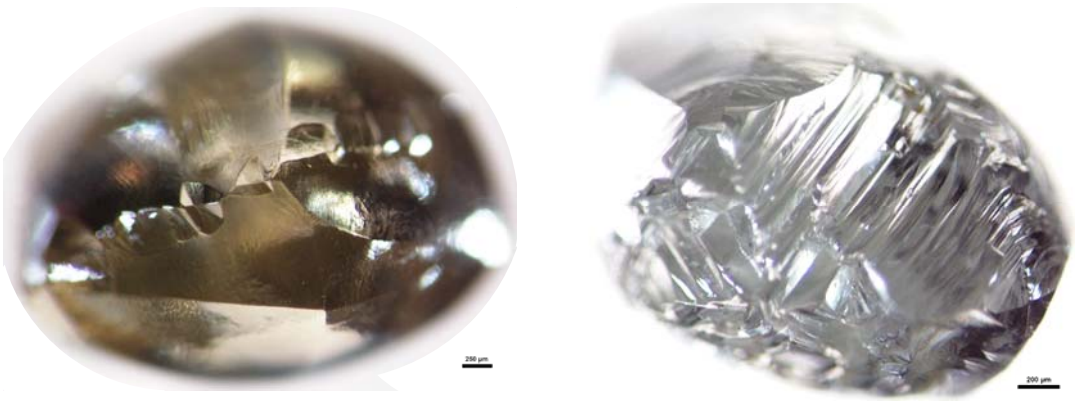

Figure 5 – Examples of a dodecahedral (D23A; left) and an irregularly-shaped twinned crystal (D28; right) from the Ural Mountains. Scale bars are 250µm (left) and 200µm (right).

2.4 Diamond colours

The three body colours which constitute the Ural diamonds population are the same as those which typically dominate the diamond production worldwide: colourless, yellow and brown. In the population studied (Table 3, Figure 6), yellow and colourless are the more common colours, comprising, respectively, 42% and 36% of the total. Taking into consideration that 15% of the stones are brown-coloured, 93% of the Ural diamond population exhibit body colour. The remaining stones (7%) are transparent green-coated diamonds.

Colour	Single-crystals			Twinned crystals		Totals
	O	D	I	D-m	I-m	
Yellow	7	64	5	14	1	91
Colourless	4	64	1	8	1	78
Brown	1	24	1	5	2	33
Tr. green-coat	0	12	0	2	1	15
Totals	13	165	7	29	5	217

Table 3 – Colour as a function of crystal form. Form symbols same as in Table 2.

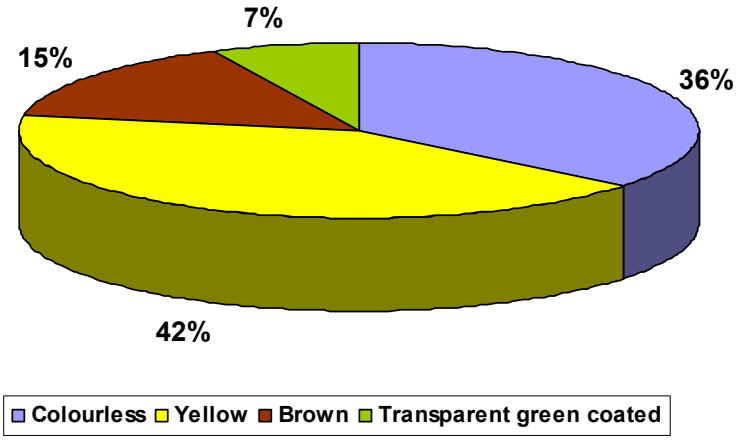

Figure 6 – The distribution of colours in the Ural diamond population.

2.4.1 *Yellow*

Yellow (Figure 7) is the most prominent colour in both single (42%) and twinned crystals (44%). More than half of the octahedra and more than two-thirds of the irregulars are yellow (58% and 71%, respectively). The proportion of yellow single-crystal dodecahedra is smaller (39%).

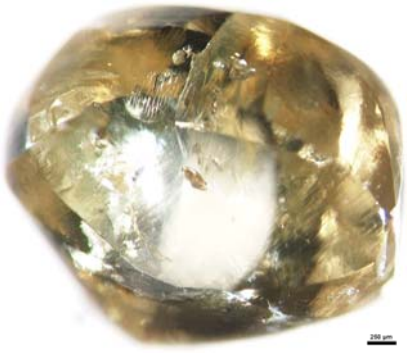

Figure 7 – A yellow diamond (D23A) from the Ural Mountains. Scale bar is 250µm.

The proportions alter in the twinned crystal population, which is composed of 48% of yellow twinned dodecahedra and only 20% of yellow-coloured twinned irregulars.

2.4.2 *Colourless*

Colourless stones (Figure 8) represent 38% of the single-crystals and 27% of the twinned crystals. In the single-crystals, 33% of octahedra and 39% dodecahedra are colourless. By comparison, only a small proportion (14%) of irregularly shaped single-crystals is colourless.

Figure 8 – A colourless diamond (D61C) from the Ural Mountains. Scale bar is 250µm.

The same trend can be seen in the twinned crystal population, where 28% of the dodecahedra *versus* 20% of the irregulars are colourless. The small number of irregular colourless stones may be a characteristic of the Urals diamond population, or, more likely, a statistical artefact due to the comparative small number of irregular crystals that were present in the studied population.

2.4.3 *Brown*

Brown (Figure 9) is the least common body colour observed. Brown is slightly more common in the twinned crystals (21%) relative to the single-crystals (14%). Brown dodecahedral and irregularly shaped single-crystals are present in similar proportions (15% and 14%, respectively). Only 8% of the octahedra are brown, which is a much lower proportion than that observed for the other body colours of the Ural specimens.

In the twinned crystal population, the proportion of irregularly shaped brown stones is more than double than that of the dodecahedra (40% and 17%, respectively). Brown colour is known to be correlated to plastic deformation in diamond (Harris, 1992) and all but one of the Urals brown diamonds exhibit up to three sets of lamination lines (see 2.6.3.4). This trend is very similar to what has been observed for some diamond mines worldwide (e.g. Finsch and Argyle, see Harris (1992)) and suggests that the Urals brown stones (and especially the twinned irregulars) have experienced high levels of plastic deformation.

Figure 9 – A brown diamond (D25) from the Ural Mountains. Scale bar is 400µm.

2.4.4 *Transparent green-coated*

Transparent green-coated diamonds (Figure 10) constitute about 7% of the single-crystals and 9% of the twinned stones from the Urals population. Transparent green-coated irregulars and octahedral single-crystals are absent from the specimens observed in this study. Single-crystal and twinned crystal dodecahedra show identical proportion (7%) of transparent green-coated specimens. Twinned irregulars possessing a transparent green coat are more frequent, 20% of the stones exhibiting this colour. This is likely to be a statistical artefact given the small number of twinned irregular diamonds studied (see Table 2).

Green colour in diamond is not a true body colour, but a ca. 20 µm transparent coat which results from radiation damage to the diamond surface by alpha-particles generated by the decay of uranium or thorium atoms in the kimberlite, the damage occurring after the rock had solidified (Vance et al., 1973). Diamonds with complete green coats are commonly

found in the upper oxidized zones of kimberlites/lamproites (see Vance et al., 1973), where radioactive materials are dissolved in the groundwater. Transparent green-coated diamonds are also very common in alluvial deposits, due to the presence of radioactive material in the sedimentary environment (Harris, 1992), but more commonly a localised damage in the form of spots or small clusters is recognised due to the particulate nature of the radioactive species (see section 2.7.1). Experiments by Vance et al. (1973) have shown that natural transparent green-coated diamonds appear to have received an alpha-dose of $5x10^{13}$ to $1x10^{14}$ $\alpha.cm^{-2}$, which would require ~10 Ma to produce an homogenous green coat on an otherwise colourless diamond.

Figure 10 – A transparent green-coated diamond (D18F) from the Ural Mountains. Scale bar is 400µm.

2.5 Degree of breakage

Forty-nine diamonds (23% of the total population) show some degree of breakage. Breakage affected a higher proportion of the single-crystals (24%) relative to those that are twinned (15%).

Breakage surfaces have been divided into two types: old and fresh break (Figure 11). Old breakage refers to the natural breakage that occurred prior to and during kimberlite emplacement, i.e. breakage that existed before the diamond was liberated from the kimberlite. The surfaces of these broken diamonds would then have been subjected to slight resorption from the molten kimberlite which might etch or mark the broken surfaces (Robinson, 1979).

Figure 11 – Left stone (D52A): old breakage surface with signs of etching; Right stone (D55F): fresh, sub-conchoidal breakage surface. Scale bars are 400µm (left) and 250µm (right).

When pressure, force or stress is applied to the diamond, the resultant fracture or break will be characterised by a series of sub-conchoidal steps. This fresh, unetched breakage will usually run across the grain until a weakness in the stone forces it to split on a natural cleavage plane. In the broken diamonds examined, the majority (61%) of the breakage surfaces are fresh, sub-conchoidal fracture surfaces. Fresh breakage may be originated by natural processes such as during subsequent alluvial transportation, but may also occur during diamond recovery. When green surface spotting is present in fresh broken surfaces, the breakage can be inferred to be of a natural origin.

	Old breakage	Fresh breakage
75 - 95% (slightly broken)	4	12
50 - 75% (broken)	6	6
25 - 50% (mostly broken)	7	9
<25% (extremely broken)	2	3
Totals	**19**	**30**

Table 4 – Number of broken diamonds, divided by type of breakage.

The extent to which a diamond has been broken has also been assessed in this study. Four divisions have been established to classify the degree of breakage according to the percentage of the whole stone that has not been broken. Thus, 95% stands for a stone exhibiting breakage surfaces on up to 5% of its whole surface area; a 75% crystal will have breakage surfaces from 5% to 25% of its entire surface area; from 25% to up to half of the stone will be broken on a 50% diamond; from 50% to 75% of the original crystal has been lost on a 25% stone (see Table 4).

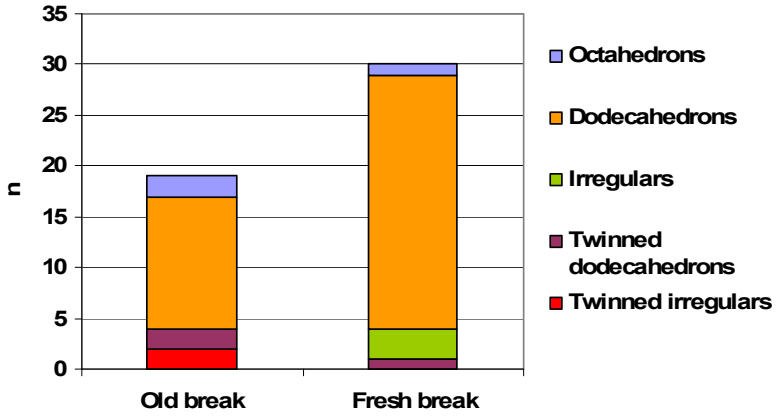

Figure 12 – The distribution of diamonds affected by breakage.

Figure 12 shows the prevalence of old and fresh breakage for each of the diamond shapes. The prevalence of the slightly broken category in diamonds with fresh breakage surfaces is a characteristic of placer deposits worldwide because cracked diamonds tend to disintegrate into small fragments during transportation, and thus only the high-quality, less broken stones are likely to be recovered (Orlov, 1977; Robinson, 1979).

2.6 Surface features

A total of 17 surface features have been recognized, using a conventional binocular microscope, in the Ural diamond population. The surface features were listed according to the specific diamond shapes on which they occur. The nomenclature utilised follows the classification scheme of Robinson (1979), which also describes the formation process of all surface features in detail (see 2.1).

2.6.1 *Octahedral surface features*

2.6.1.1 Incomplete octahedral growth

This feature is present on five diamonds. It resembles positive trigons (see 2.6.1.3), but are much larger (up to 500μm) and usually results from preferential nucleation on octahedral faces creating upraised trigonal structures (Figure 13). Sometimes a false negative trigon type hollow is found between these structures.

Figure 13 – Incomplete octahedral growth. Note the false negative trigon type hollows in between the upraised trigonal structures. Sample D123.

2.6.1.2 Shield-shaped laminae

Shield-shaped laminae consist of superimposed laminae of progressively diminishing areal extent (Figure 14). Near the edges of octahedral crystal faces, the laminae normally form terrace-like structures, the size of the steps being about 10 to 50 µm. This structure has been observed on 21 diamonds. Shield-shaped laminae are thought to be associated with resorption (Robinson, 1979), where the outermost laminae are exposed soonest and therefore recede furthest, particularly from octahedral corners which are susceptible to resorption. As shield-shaped laminae develops throughout the diamond surface, this eventually leads to octahedral crystal edges being replaced by more curved dodecahedral surfaces.

Figure 14 – Shield-shaped laminae on an octahedral crystal face. Also note the presence of a green spot on the diamond surface (see 2.7.1). Scale bar is 100µm. Sample D36C.

2.6.1.3 Negatively-oriented trigonal etch pits (trigons)

Trigonal shaped etch pits with edges aligned parallel to the diamond cleavage directions are good examples of etch features that are typically present in octahedral-shaped diamonds (Wilks and Wilks, 1994). These etch pits develop where growth or strain dislocations, which indicate defects or weakness points of a crystal, tangentially intersect the crystal face (Lang, 1964). The pits initiate as small pyramidal forms and continued resorption increases their width and flattens their bases. Large concentrations of small shallow trigonal etch pits may be derived from etching of near-surface micro-defects such as shallow dislocations or platelets (Sunagawa, 1984; Mendelssohn and Milledge, 1995a). Trigonal etch pits can also be found concentrated along weaknesses such as lamination lines (Jeff Harris, pers. comm.).

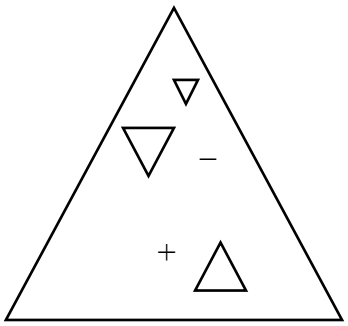

Figure 15 – Schematic representation of the "positive" (+) and "negative" (-) orientations of surface features on octahedral diamond faces. Modified from Robinson (1979).

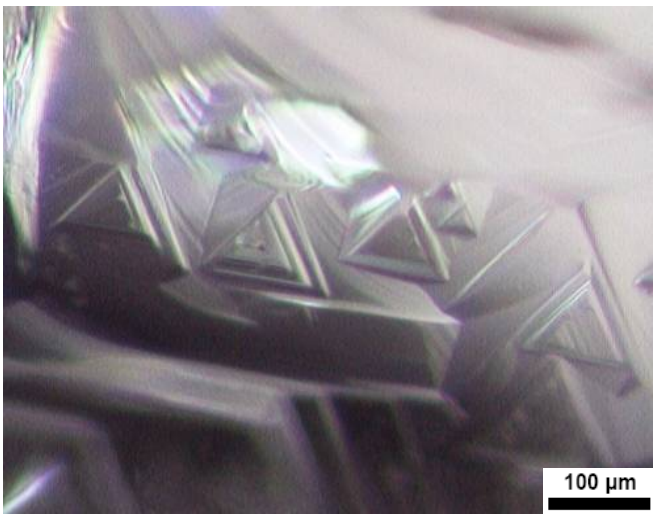

Figure 16 – Terraced, flat-bottomed negatively-oriented trigonal etch pits (trigons). Sample D14C.

Trigonal etch pits are referred to as being positive if they are aligned in the same orientation as the octahedral diamond edges and negative if the orientation of the apices of the etch pits and the octahedron faces differ by 180° (Figure 15). Experiments by Yamaoka et al. (1980) showed that the orientation of trigons varies as a function of the partial pressure of oxygen and temperature (800°C to 1400°C). At an oxygen partial pressure of 0.21 atm and a total pressure of 15 kbar, positive etch pits change into negative orientation for temperatures above 1130°C (Yamaoka et al., 1980). Thus for the geological temperatures and oxygen partial pressures expected in kimberlite/lamproite, this experimental result is consistent with the observation that positive trigonal etch pits are rarer than their negative counterpart in natural diamond (Harris, 1992). Positively-oriented trigonal etch pits were not found in the studied population.

Commonly referred to as trigons (Frank et al., 1958; Lang, 1964), negatively-oriented trigonal pits of edge lengths between 50 – 200 μm are very common octahedral surface features, present on 51 stones of the Urals population (Figure 16). In the present study, trigons occur as point-bottomed, flat-bottomed or terraced structures of 10 – 40 μm in depth, the first two varieties being predominant in the Urals population.

2.6.1.4 Hexagonal etch pits

Hexagonal etch pits of edge lengths between 50 – 300 μm were recognised on 28 diamonds (Figure 17). Likely formed at the transitional temperature of positively- to negatively-oriented trigonal pits, hexagonal pits are flat-bottomed structures which are relatively larger than trigons and may indicate etching in relatively oxidising environments which are required to enable the formation of the positively-oriented component of the pits (Yamaoka et al., 1980).

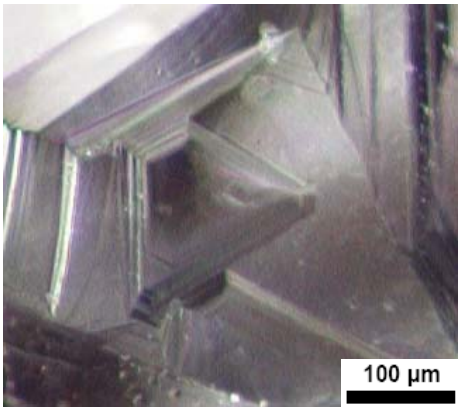

Figure 17 – Example of a hexagonal etch pit on an octahedral crystal face. Sample D12C.

2.6.1.5 Hexagonal etch pits containing trigonal etch pits

A total of seventeen diamonds exhibit large, flat-bottomed, hexagonal etch pits (edge lengths usually larger than 150 μm), containing flat-bottomed trigonal etch pits with edge lengths between 50 – 100 μm (Figure 18). It is likely that the trigonal pits formed separately, and subsequently, to the etching event that produced the hexagonal pits (Robinson, 1979). In the Ural diamond population, the trigonal pits found inside the hexagonal pits were always of the negatively-oriented type.

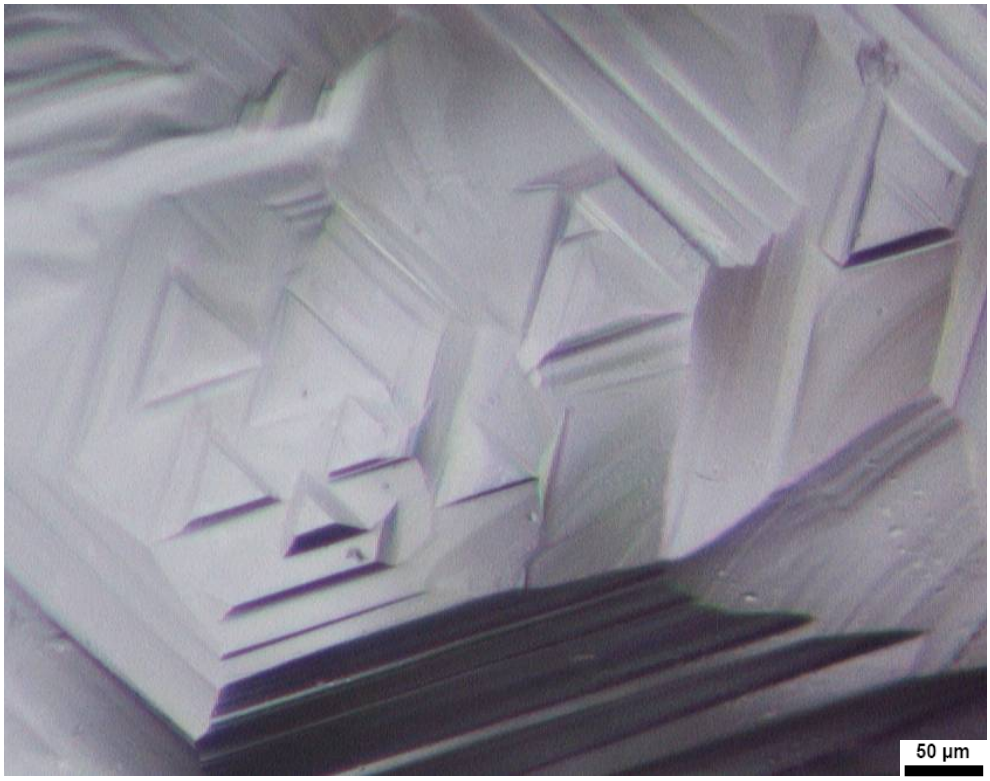

Figure 18– Hexagonal etch pits containing flat-bottomed trigonal etch pits. Sample D52A.

2.6.1.6 Serrate laminae

Truncated superimposed laminae of progressively diminishing areal extent with a step size of about 10 – 50 μm occur on 13 stones (Figure 19). These structures are designated serrate laminae and they are distinct from shield-shaped laminae because they do not normally form terrace-like structures (see section 2.6.1.2). According to Robinson (1979), serrate laminae are likened to a coalescence of laterally-expanding, flat-bottomed trigons, mostly initiated at the edges of successively exposed, octahedral growth layers.

Figure 19 – Serrate laminae on an octahedral crystal face. Note the irregular edges of each superimposed laminae. Sample D3B.

2.6.2 *Cubic surface features*

2.6.2.1 Negatively-oriented tetragonal etch pits (tetragons)

Eleven Ural diamonds contain negatively-oriented tetragonal pits of edge lengths between 50 – 200 µm, which are usually deeper (>100 µm in depth) than trigons and of pyramidal shape (Figure 21). Tetragonal etch pits are etch features which form in the same way as trigons (see 2.6.1.3), but have a tetragonal shape because they occur on cubic faces. Also, similarly to trigonal etch pits, tetragonal etch pits can exhibit positive or negative (also called tetragons) orientations (Figure 20). Compared with trigons, tetragons tend to form deeper pits because the (100) surface of diamond is softer than the (111) surface (Phaal, 1965).

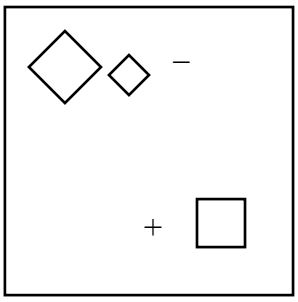

Figure 20 – Schematic representation of the "positive" (+) and "negative" (-) orientations of surface features on cubic diamond faces. Modified from Robinson (1979).

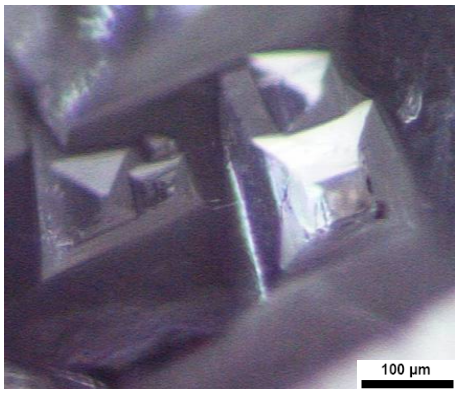

Figure 21– Point-bottomed, negatively-oriented tetragonal etch pits (tetragons) on a cubic crystal face. Sample D38.

2.6.3 *Dodecahedral surface features*

2.6.3.1 Terraces

Terraces are concentric surface features, normally developed about the points where the three-fold octahedral axes emerge (Figure 22). Because of the high proportion of dodecahedral diamonds in the studied population, terracing is extremely common, being observed on 179 stones. The size of each of the steps usually varies between 20 to 50 µm. The presence of terracing is the result of the resorption process which changes octahedra to dodecahedra. The terraces represent the now exposed original octahedral growth planes in the diamond.

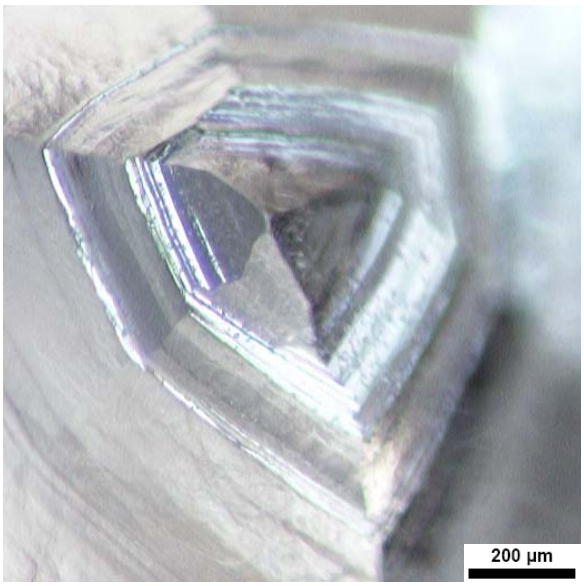

Figure 22– Prominent terraces on a dodecahedral crystal face. Sample D2.

A dodecahedron displaying prominent terraces is likely to have been less resorbed than one displaying insignificant, or no, terraces (Robinson, 1979). Terracing is very faint in 24 of the diamonds examined, and so those dodecahedra are likely to have been resorbed to a very high degree.

2.6.3.2 Elongate hillocks

Occurring on 161 stones, hillocks which are elongated in the direction of the major rhombic axes are very common features of dodecahedral crystal surfaces. In the current study, the shape of individual hillocks varies from semi-cylindrical to semi-ellipsoidal (Figure 24), the latter also referred to as "boat-shaped" (Gill Parker, pers. comm.). The length of the hillocks is variable, long hillocks (>150μm) are present on 46 diamonds.

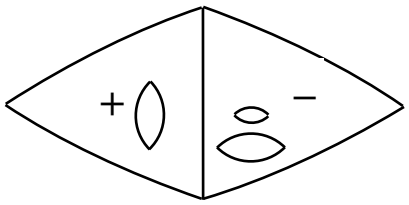

Figure 23 – Schematic representation of the "positive" (+) and "negative" (-) orientations of surface features on dodecahedral diamond faces. Modified from Robinson (1979).

The two fold symmetry of hillocks relates to the dodecahedral face on which they occur, with hillocks being referred to as positive or negative according to their orientation on the diamond crystal surface (see Figure 23). Hillocks develop initially as pyramidal shapes that can be subsequently affected by resorption, which rounds hillocks to elongate- and drop-shaped forms (Orlov, 1977).

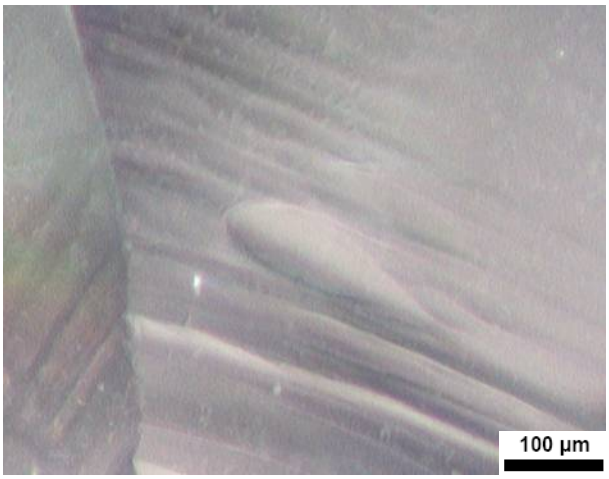

Figure 24 – A prominent elongate hillock of semi-ellipsoidal shape. Sample D12C.

2.6.3.3 Pyramidal hillocks

Pyramidal hillocks were observed on 85 diamonds. The hillocks have triangular-pyramidal form and their edges are conspicuously rounded (Figure 25). They are usually between 50 to 200 µm in length and occur isolated or scattered on one or more dodecahedral surfaces of the diamonds. The processes that lead to the formation of pyramidal hillocks are not fully understood, with Urusovskaya and Orlov (1964) and Robinson (1979) suggesting a possible formation at the intersections between three lamination lines which would offer a relative resistance to resorption. In the present study, lamination lines were observed on 63 of the 85 diamonds that contained pyramidal hillocks and thus an association between these two surface features cannot be fully confirmed or dismissed.

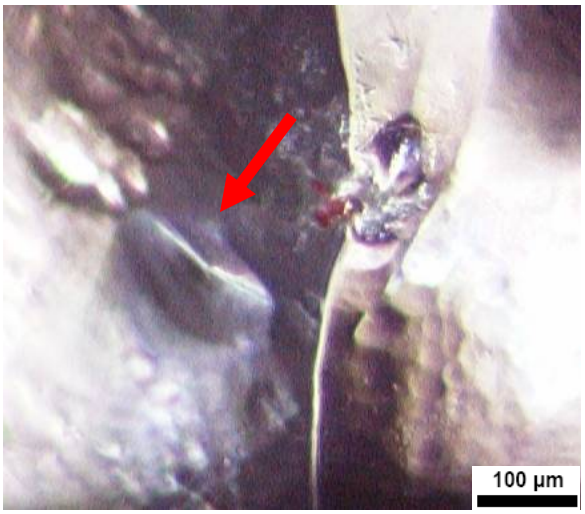

Figure 25– A pyramidal hillock (indicated by the arrow) on a dodecahedral crystal face. Sample D14A.

2.6.3.4 Lamination lines

Lamination lines are series of closely spaced lineations, which run partially or wholly across a diamond surface, parallel to cleavage planes (Figure 26). Frequently, lamination lines extend across the ridges between adjacent dodecahedral surfaces. This very common feature is present on 155 diamonds, including 32 of the 33 brown stones. In the present study, a maximum of three transecting sets of lamination lines have been identified. Lamination lines most commonly occur as 2 sets (n=88) or 1 set (n=63), 3 sets of lines were observed only on four stones. Lamination lines are also more commonly observed on twinned crystals (about 79%) than on the single-crystal population (about 67%).

A strong indication that a diamond has been plastically deformed, up to four transecting sets of lamination lines are possible to occur on diamond (Harris, 1992). For unresorbed diamonds, lines of trigons running across octahedral faces are also indicative of plastic deformation (see 2.6.1.3). Plastic deformation occurs while the diamonds are resident in the mantle and may result from stresses associated with the development of kimberlite/lamproite pipes (Robinson et al., 1989; Harris, 1992).

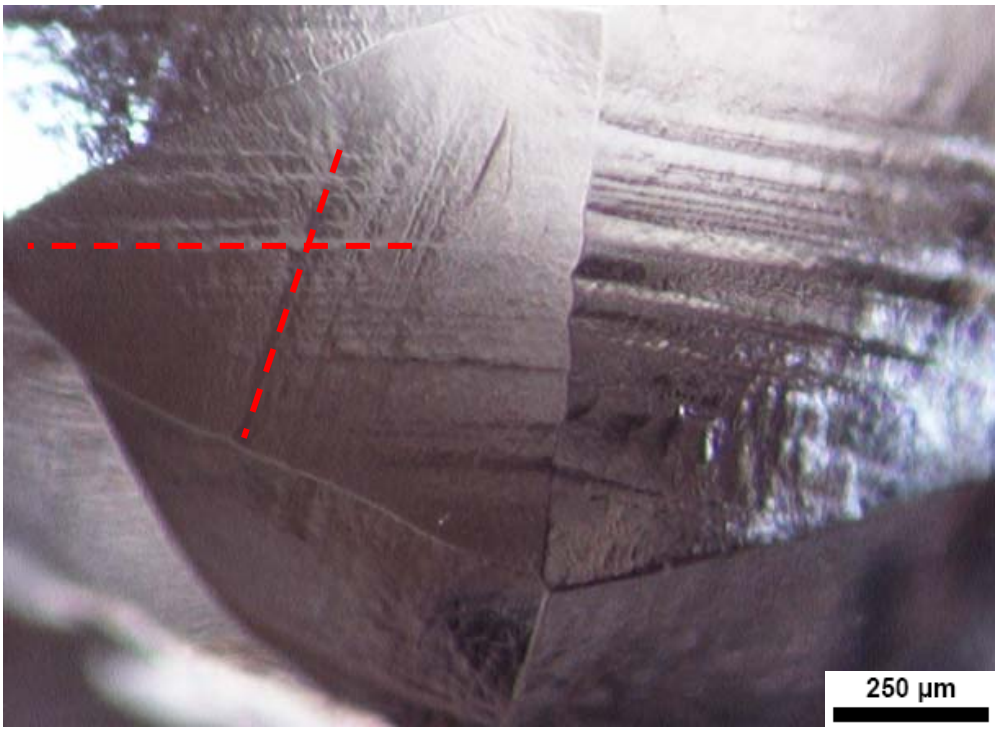

Figure 26 – Diamond with 2 sets of lamination lines (illustrated in red). Sample D55.

Plastic deformation is correlated with brown colour in diamond (see 2.4.3), this colour being originally attributed to incipient graphitization on dislocation planes in response to the deformation (Urusovskaya and Orlov, 1964). If graphitization is indeed present in brown diamonds, then the plastic deformation process is likely to have occurred when mantle *PT* conditions approached those of the diamond-graphite equilibration curve (see Kennedy and Kennedy, 1976). Experimental results by DeVries (1975) showed that for the pressures relevant to the diamond stability curve (>40 kbar), the existence of visible slip planes or deformation lamellae is mostly controlled by temperature, with deformation taking place as low as 900°C (at 60 kbar), even though resistance to plastic flow increases dramatically below about 1200°C.

More recently, the origin of the brown colouration of diamond has moved again into the focus of research after it was shown that high pressure high temperature treatment (HPHT)

treatment of diamond can lead to a removal of the brown colour and hence generate colourless, more valuable gems. During HPHT treatment of brown diamond, positron annihilation measurements indicate that vacancy clusters (several tens of atoms missing) in the crystal lattice gradually disappear in conjugation with the loss of colouration (Maki et al., 2007). Although still under discussion, these experiments indicate that the brown colour is likely to be caused by vacancy-type extended defects in the diamond lattice (David Fisher, pers. comm.).

2.6.3.5 Zigzag texture

Zigzag texture has been observed on seventeen stones. The zigzag pattern normally consists of a series of 5 to 10 closely spaced (about 20 μm in between) lines, restricted to small areas of the diamond surface (Figure 27). Through resorption, the zigzag pattern traces the intersections between two sets of the octahedral layers not generally expressed on dodecahedral surfaces (Robinson, 1979).

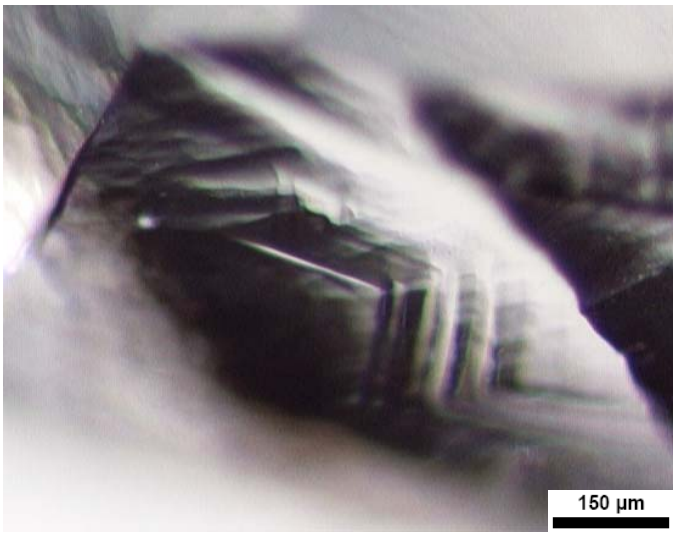

Figure 27 – Zigzag texture on a dodecahedral crystal face. Sample D9.

2.6.3.6 Enhanced crystal edges

Two diamonds exhibit ridge-like dodecahedral crystal edges. This feature is present in both "A" and "C" edges (see Figure 28), which stand at a higher elevation (about 100 to 300 μm) than the crystal faces (Figure 29). In the two diamonds that have enhanced crystal edges, this surface feature affects the entire diamond surface. Enhanced crystal edges may be the result of short periods of etching (Robinson, 1979). Nevertheless, it is not understood why the crystal edges are less etched than the dodecahedral surfaces.

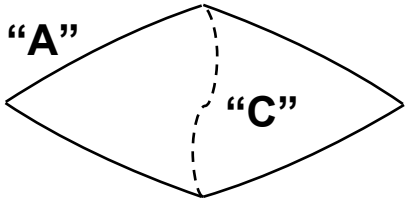

Figure 28 – The location of “A” and “C” crystal edges on a rounded dodecahedron according to the terminology of Dana (1958). The figure shows a pair of dodecahedral surfaces joined at a “C” edge.

Figure 29 – A dodecahedral-shaped diamond with enhanced “A” and “C” crystal edges. Sample D102.

2.6.3.7 Corrosion sculpture

Corrosion sculptures are depressions of irregular outline, usually containing striated bottoms (Figure 30). Found on 12 Urals stones, the depressions are generally between 50 µm and 150 µm in depth and 50 µm and 400 µm in maximum diameter. Coalescence of the depressions may occur on the diamonds when corrosion sculpture is a common surface feature. Corrosion sculpture is probably produced by rapid, brief, etching of diamond (Orlov, 1977). Corrosion sculptures that extend over dodecahedral edges are indicative of etching that post-dates the resorption of the diamond.

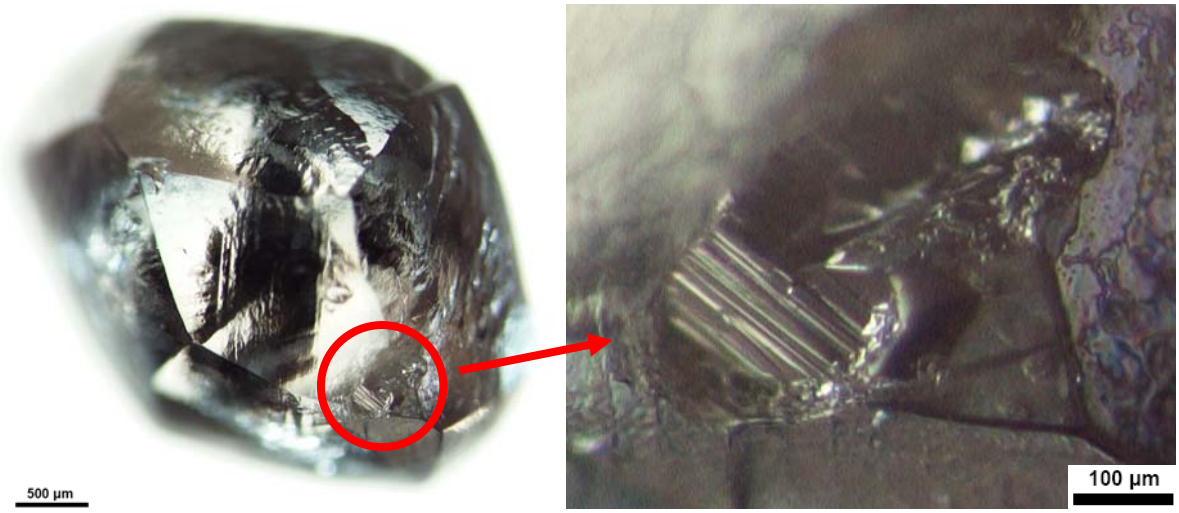

Figure 30 – Corrosion sculpture on a dodecahedral diamond. Note the striated bottom and irregular outline of the depression (right picture). Sample D46.

2.6.3.8 Enhanced lustre

Fifty-six crystals of the Ural diamond population exhibit a nearly perfect adamantine lustre, with a typical "melted" surface when observed under the binocular microscope (Figure 31). When present, enhanced lustre always occurs throughout the entire diamond surface. This surface feature post-dates crystal resorption and pre-dates all abrasion features and thus is likely the result of a chemical polishing process (Orlov, 1977). A possible etching agent capable of chemically polishing the surface of diamond could be CO_2 gas flowing through kimberlite/lamproite at temperatures above 950°C (Robinson, 1981).

Figure 31 – Diamond with enhanced lustre. Note the smoothly-polished surfaces of the dodecahedral faces and edges. Sample D18.

2.6.4 *Unrestricted surface features*

Two distinct surface features that are not restricted to any particular crystal surface of diamond have been identified in the Ural diamond population.

2.6.4.1 Ruts

Ruts have been identified on 42 diamonds. Typically only one rut, up to 1 mm in length and 600 μm in width, is present per diamond, but occasionally two or more can occur on the same stone. The "walls" of the ruts are generally ragged, extending to a depth of about 200 – 600 μm, while the edges are usually rounded (Figure 32). Some ruts develop from inclusion cavities, others from crystal fractures, and others appear not to be associated with any other surface feature. Ruts can be straight or sinuous and represent either planar zones of weakness or fractures widened by resorption or etching.

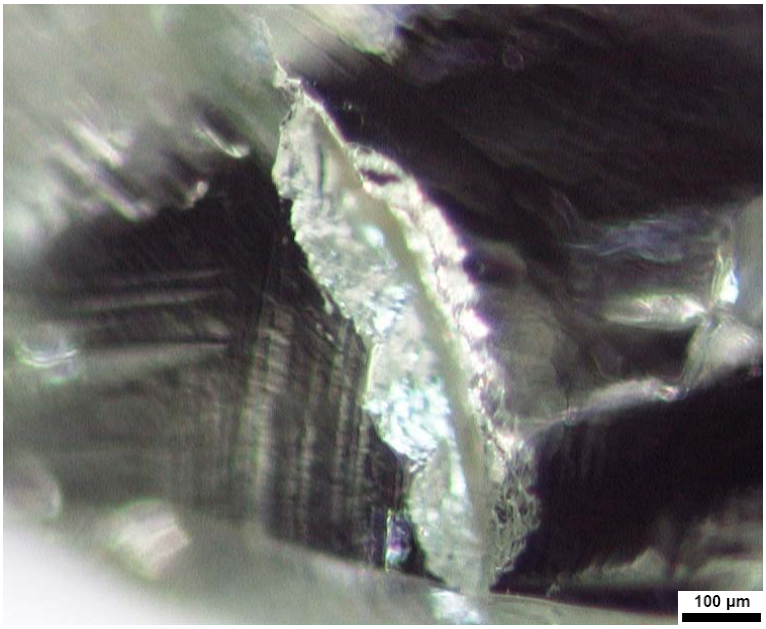

Figure 32 – Rut with irregular, ragged "walls", which has developed on a dodecahedral crystal face. Sample D18.

2.6.4.2 Inclusion cavities

Isolated depressions with octahedral sides are present on 95 diamonds (Figure 33). Such depressions can be up to 500 μm in length and 300 μm in width, and represent hollows vacated by syngenetic mineral inclusions, which typically have a cubo-octahedral external shape (see 2.9). The cavities (that may reach a depth of up to 200 μm), are thus sites of pre-

existing mineral inclusions which were plucked from, or dissolved out of (during the diamond acidizing process), their hosts. In the current study, inclusion cavities are common in broken diamonds, where they are present on 51% of the stones. Inclusion cavities on rounded dodecahedral crystals commonly have sharp edges, indicating that the mineral inclusions must have departed after crystal resorption.

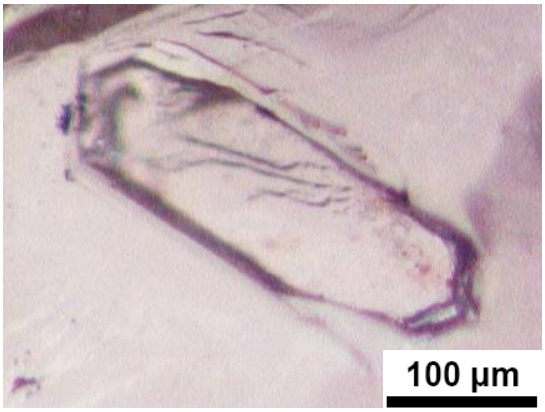

Figure 33 – Sharp-edged inclusion cavity with a cubo-octahedral external shape, on a dodecahedral diamond crystal. Sample D57B.

2.7 Radiation damage

2.7.1 *Green spots*

Green surface spotting is a common feature throughout the Ural diamond population, affecting more than half of the stones. Green spotting usually occurs as single, isolated, rounded spots of about 50 µm to 20 µm in diameter (Figure 34), though loose clusters of several green spots are not uncommon. In some specimens, green spots or localised areas of green colour may also occur within fractures in the stone. The intensity of the colour in the spots can vary considerably on the same and between different specimens from faint to intense, but in the majority of the cases faint green spots are predominant.

Green spotting is generated by alpha-particle irradiation of the diamond surface when a radioactive mineral lies adjacent to it (Vance et al., 1973). The intensity of green is directly proportional to the level of alpha-particle attack, with dark green spots taking about 10 Ma to appear (Vance and Milledge, 1972). Both single-crystals and twinned stones are affected by alpha-particle radiation damage in similar proportions (56%). Nevertheless it should be noted that green spotting affects about 83% of the octahedra, which represents a higher incidence than in the other single and twinned crystal forms (between 54% and 60%).

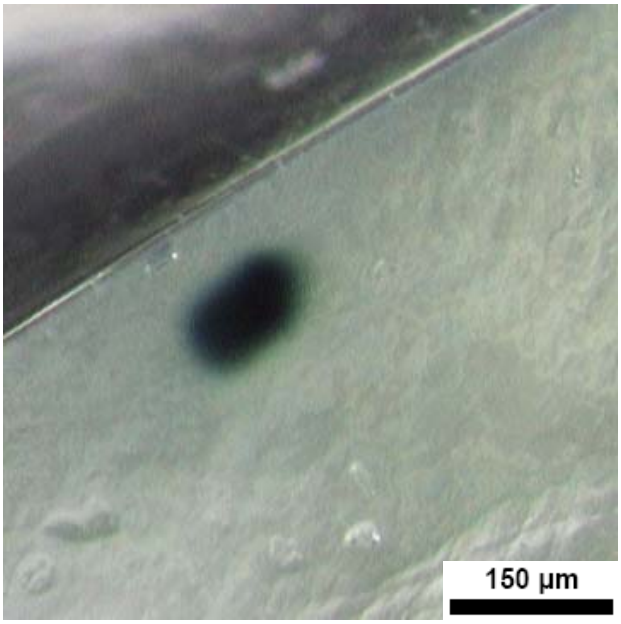

Figure 34 – Intense green spot near the "A" edge on a dodecahedral crystal face. Sample D18.

2.7.2 *Brown spots*

Brown surface spotting is rare in the Ural diamonds, occurring in only 4% of the total population. The intensity of colour in the brown spots varies from faint to intense, but with a slight predominance to faint spots. Brown surface spotting occurs in both single-crystals and twinned stones, but only in the specimens exhibiting well-defined crystal morphology (i.e. octahedra and dodecahedra), being absent from irregularly shaped stones. It should be noted that the octahedra show a higher incidence (8%) of brown surface spots than the other crystal forms, and the single-crystal dodecahedra are less affected by brown spots than their twinned counterparts (3% and 7%, respectively).

Vance et al. (1973) observed that the green spots converts readily to brown if heated to temperatures of about 600ºC. Based on this observation, brown surface spotting reflects the heating of pre-existing green spots during a deep seated metamorphic event. However, more recent evidence (Harris, 1992) suggests that the green to brown change is more likely to be a kinetic reaction, i.e. one that considers temperature and time and not just temperature as thought before. Assuming that the green to brown transition is a kinetically controlled process that takes place over a reasonable geological timescale (~50 to ~150 Ma), then the conversion temperature is not likely to exceed 300ºC (Jeff Harris, pers. comm.).

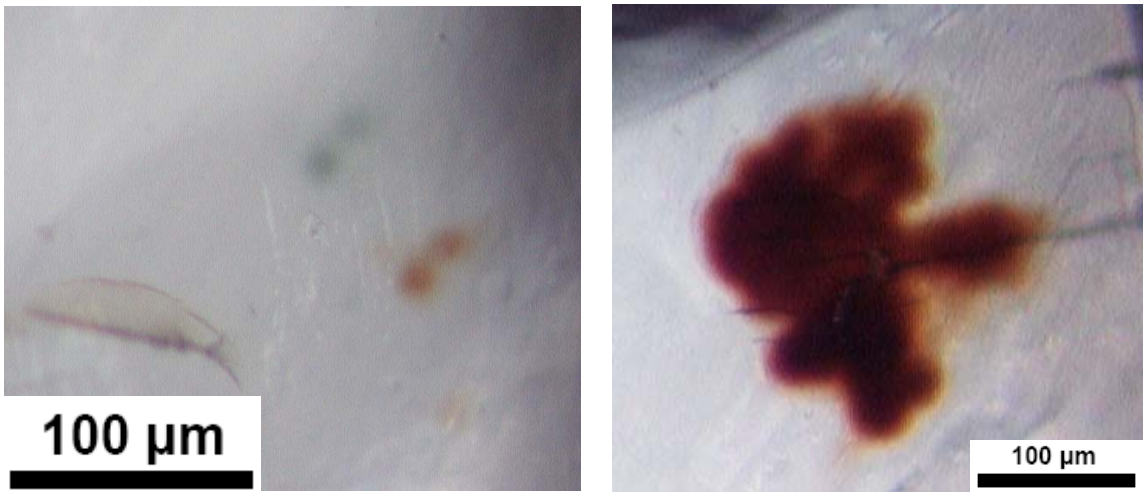

Figure 35– Paired green and brown spots (left) and an irregularly-shaped, intense brown spot (right). Samples D93A (left) and D37 (right).

Except in one dodecahedral single-crystal (Figure 35), the brown spots encountered are unaccompanied by superimposed or matching green spots, The occurrence of this matched pair may be explained by alpha-particle radiation hitting the diamond surface at one spot (generating a couple of green spots which have, with time, changed to brown) and then the diamond moving slightly, inflecting radiation damage on a new adjacent area of the diamond surface (forming the couple of "younger" green spots that are visible in Figure 35).

2.8 Transportation features

Evidence of diamond transportation is present on 56% of the total population. Once diamonds enter an alluvial environment, abrasion and impact during transportation create an additional suite of surface textures. In the Ural diamond population, three different types of surface textures relating to transportation have been observed.

2.8.1 *Point and edge abrasion*

Edge abrasion is manifested in the grinding of crystal points and, eventually, all crystal edges of the diamond (Figure 36). Seven crystals are ground at the points of emergence of three-fold axes; 16 crystals are ground along crystal edges; 15 stones are ground at all "A" dodecahedral edges; and 16 diamonds are ground at all "A" and "C" dodecahedral edges (see Figure 28).

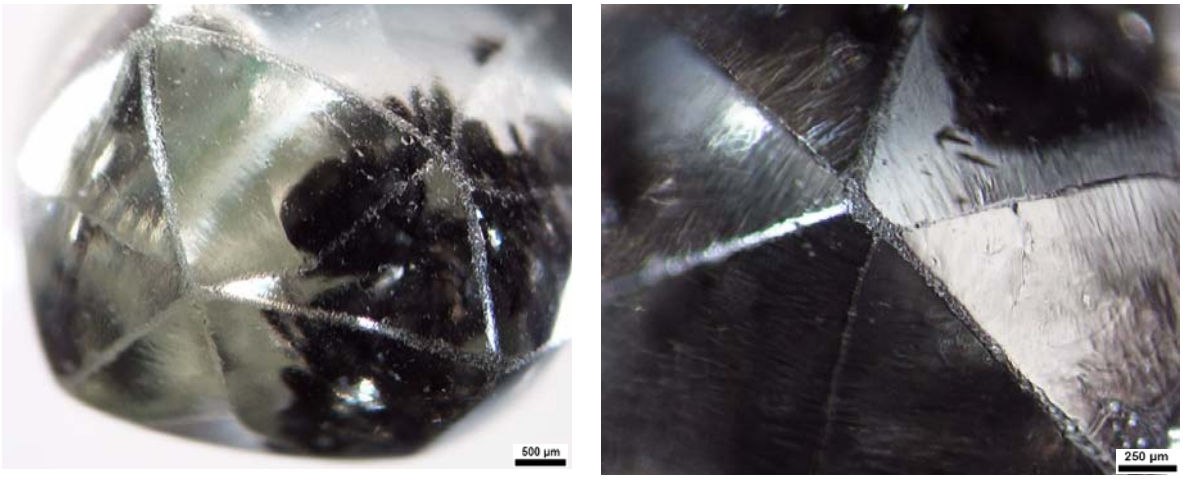

Figure 36 – Two examples of point and edge abrasion. Samples D3A (left) and D4B (right).

2.8.2 *Network pattern*

Rhombic network patterns consist of a crosswork of highly curved, shallow ruts. In all cases the network patterns define the intersecting traces of octahedral planes. Network patterns have been found on the dodecahedral surfaces of 25 Ural diamonds. The grooves tend to be narrow and shallow (<10 µm in width), and their depth tends to be uniform on any dodecahedral surface (Figure 37).

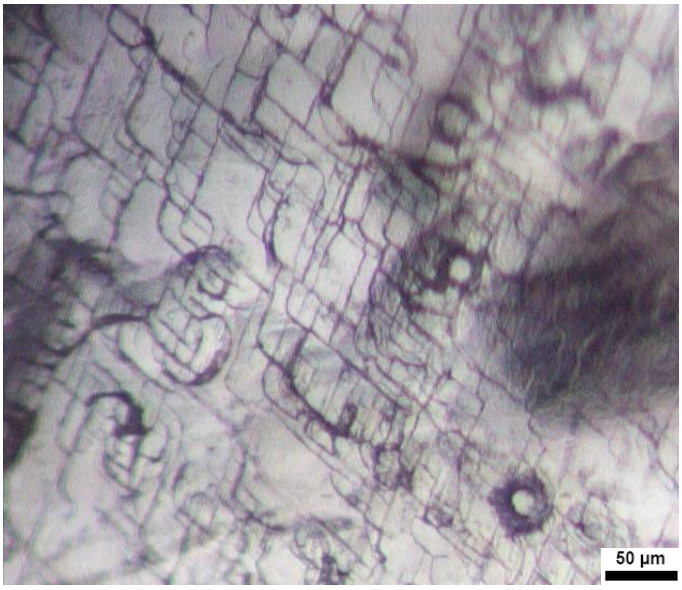

Figure 37 – Example of a network pattern. Note the strong curvature developed at groove intersections. Sample D29A.

Network patterns are typically observed in alluvial diamonds and are very rare or absent in diamonds collected directly from kimberlite/lamproite rocks (Orlov, 1977; Robinson,

1981). In the Ural samples, network patterns post-date diamond resorption and etching and occur together with the other abrasion features. Thus they are most likely the result of mechanical abrasion operating during diamond transportation.

2.8.3 *Percussion marks*

Percussion marks are shallow, surface cracks of characteristic crescentic outline (Figure 38). At dodecahedral crystal edges, percussion cracks are represented mainly by straight lines crossing the edges at an angle of 90º. Often percussion marks are associated with small (ca. 10 μm), rough-bottomed, trigonal etch pits. These irregularly shaped pits resemble very small trigons and are also know as spall scars (Robinson, 1979). Diamond is the hardest mineral known and therefore is extremely resistant to scratching. However, diamond is also brittle and its easy cleavage along octahedral planes makes it vulnerable to breakage from falls or impacts. Experimental data shows that percussion marks in diamond do not require impact with other diamonds to be formed, as surface cracks are produced by transfer of kinetic energy when softer materials impact against the diamond surface (see Wilks and Wilks, 1994). In geological terms, this means that percussion marks are likely to result from impact with rock pebbles or boulders when diamond is transported in an alluvial environment.

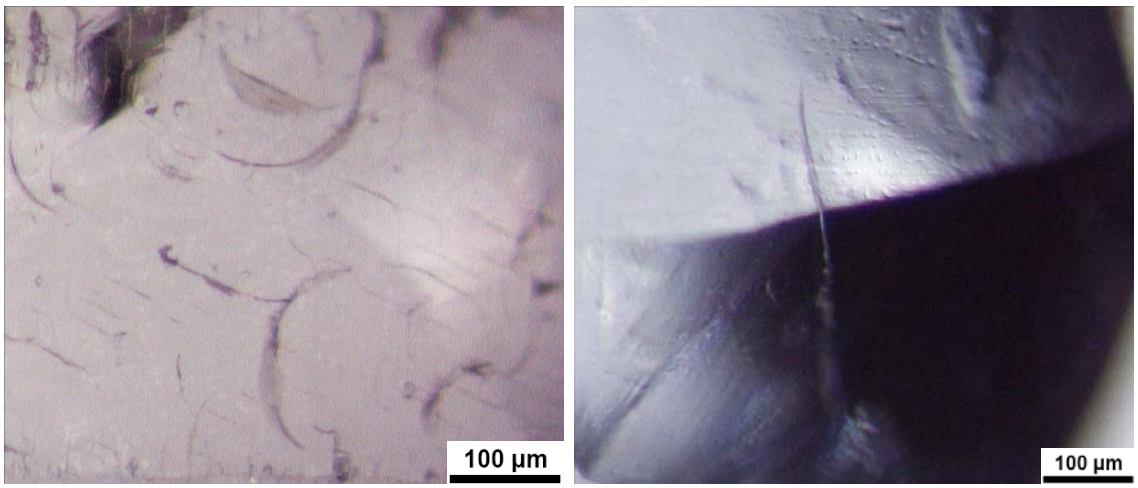

Figure 38 – Left: crescentic percussion marks. Right: straight percussion mark crossing a dodecahedral edge. Samples D62A (left) and D45B (right).

In this study, small percussion marks (about 10 to 50 μm) are more abundant than large (over 100 μm) ones, occurring in 83 and 31 diamonds, respectively. Straight small surface cracks which traverse unabraded dodecahedral edges are not uncommon, occurring on 36 stones.

2.9 Inclusion abundance and parageneses

An important aspect revealed by geochemical studies of typical mineral assemblages inside single diamonds, was the recognition of three main inclusion suites: 1) a peridotitic (also called ultramafic) suite, commonly subdivided into harzburgitic, lherzolitic and wherlitic parageneses, 2) an eclogitic suite, and, 3) a websteritic suite (e.g. Meyer and Svisero, 1975; Robinson, 1978; Harte et al., 1980; Meyer, 1987; Harris, 1992). The names attributed to the first two inclusion suites were chosen because they show a mineralogical similarity with the two most important xenolith types found in kimberlites and lamproites. The websteritic suite is not as common as the others and the term "websteritic" is normally used to describe inclusions which are chemically transitional between the eclogitic and peridotitic suites.

Generally, the members of these suites are mutually exclusive, i.e. minerals of one suite do not coexist in the same diamond with minerals of other suite. Nevertheless, some studies (e.g. Prinz et al., 1975; Hall and Smith, 1985; Griffin et al., 1988; Moore and Gurney, 1989) have found diamonds containing mixed paragenesis inclusions. Diamonds with peridotitic suite mineral inclusions may coexist, in the same kimberlite, with diamonds containing mineral inclusions belonging to the eclogitic suite. This discovery (Meyer and Boyd, 1972) was the first evidence that diamonds could originate in more than one geochemical environment. Sulphides are the most common mineral inclusions in diamonds, with Ni-rich and Ni-poor sulphide inclusions being commonly assigned to the peridotitic or eclogitic paragenesis, respectively, when coexisting silicate or oxide inclusions of known paragenesis are absent (Bulanova et al., 1996).

With regard to eclogitic suite inclusions, the typical minerals comprise orange pyrope-almandine garnet, omphacitic clinopyroxene, kyanite, rutile, coesite and sulphides. Peridotitic suite diamond mineral inclusions mainly consist of olivine, enstatite, purple chrome-pyrope garnet, chrome-diopside, chromite and sulphides. Websteritic suite mineral inclusions are indentified by their "unusual" chemical composition, and may include "peridotitic" inclusions with very low Mg# (Gurney et al., 1984), as well as "eclogitic" inclusions with very high Mg# and Cr# (see Grutter et al., 2004). In this thesis, diamonds containing inclusions of these parageneses are designated as "E"-, "P"- and "W"-types.

Visual observation of all 217 inclusion-bearing diamonds (Table 5) and subsequent chemical analysis of 93 stones indicates that 62% are eclogitic, with inclusions of orange

garnet, pale-green clinopyroxene, colourless coesite, blue kyanite, light brown rutile and sulphide.

Diamond parageneses	n	%
E-type	134	62
P-type	34	15
W-type	2	1
Others	47	22
Totals	217	100

Table 5 – Paragenetic classification of the Urals inclusion-bearing diamonds.

Fifteen percent of the diamonds belong to the peridotitic growth environment, containing inclusions of purple garnet, dark cherry-red chromite and colourless olivine (Table 5). A small number of diamonds (1% of the total) enclose inclusions which were assigned to the websteritic paragenesis after chemical analysis. The inclusions are colourless enstatite, colourless olivine and pale-green clinopyroxene.

Twenty-two percent of the diamonds contain sulphide, graphite and colourless inclusions which in the absence of coexisting minerals of known paragenesis cannot be assigned to a specific growth environment. These minerals are categorised as unknown paragenesis.

Irrespective of their paragenesis, the mineral inclusions analysed in this study were unrelated to cracks in diamond and have cubo-octahedral shapes. Elongate or flattened shapes, orientated parallel to the octahedral plane of the diamond, also occur. The enclosed minerals display cubo-octahedral shapes because diamond has a greater form energy relative to other minerals so it imposes its morphology on the inclusions that are entrapped during simultaneous growth (Harris, 1992). All inclusions analysed in this study are regarded as being syngenetic with diamond and thus their composition can be used to characterize the sources of the Ural diamonds in the Earth's mantle (see Chapter 5).

Mineral inclusion sizes vary from 50 to 580 μm in largest dimension, normally occurring as only one inclusion per diamond, although clusters of inclusions of one or several distinct minerals also occur (see below). The location of the inclusions in the diamond was very variable, and although most were positioned in central zones, the presence of inclusions at intermediate or near-surface zones was also common.

2.9.1 *Eclogitic inclusions*

A total of 134 diamonds containing minerals of the eclogitic paragenesis have been identified (Table 6). The diamonds contain either inclusions of only one mineral, or enclose an assemblage of several distinct but separate minerals.

E-type inclusions	Single-crystals			Twinned crystals		Totals
	O	D	I	D-m	I-m	
Gt	6	52	4	15	4	81
Cpx	2	8	0	4	0	14
Ky	0	2	0	0	0	2
Coe	0	1	0	1	0	2
Cpx + Sul	0	1	0	0	0	1
Gt + Cpx	0	3	0	0	0	3
Gt + Col	1	0	0	0	0	1
Gt + Sul	1	21	1	1	0	24
Gt + Coe + Sul	0	2	0	0	0	2
Gt + Ru + Sul	0	1	0	0	0	1
Gt + Cpx + Sul	0	1	0	1	0	2
Gt + Cpx + Coe + Sul	0	0	0	1	0	1
Totals	11	92	5	23	3	134

Table 6 – Variation in abundance of E-type inclusions as a function of crystal form. Gt = garnet, Cpx = clinopyroxene, Ky = kyanite, Coe = coesite, Col = colourless, Ru = rutile, Sul = sulphide. Key to form symbols: O = octahedral, D = dodecahedra, I = irregular shapes, D-m = twinned dodecahedra, I-m = twinned irregulars.

Of the latter, eight distinct mineral assemblages have been observed: clinopyroxene + sulphide; garnet + clinopyroxene; garnet + colourless; garnet + sulphide; garnet + coesite + sulphide; garnet + clinopyroxene + sulphide; garnet + rutile + sulphide; garnet + clinopyroxene + coesite + sulphide (see Table 6).

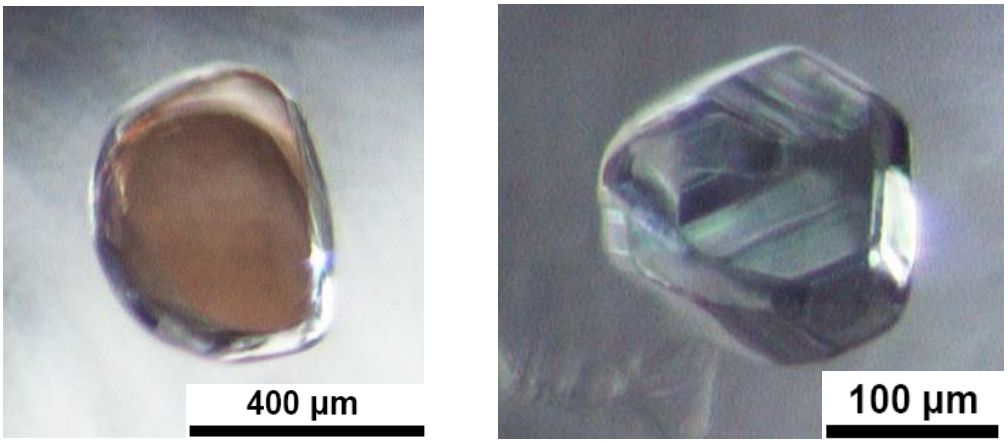

Figure 39 – Left: orange garnet. Right: pale-green clinopyroxene. Samples D122A (left) and D132 (right).

The garnet + sulphide assemblage is the most common, occurring in 24 stones (see Table 6). This is not a surprise, since garnet is the most abundant silicate inclusion in eclogitic diamonds (see Stachel and Harris, 2008) and sulphides are the most common mineral inclusions in diamonds overall (Harris and Gurney, 1979).

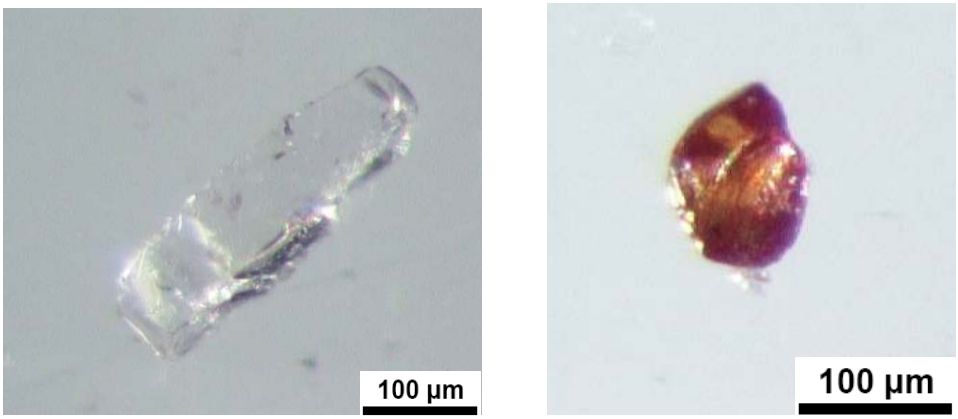

Figure 40 – Left: colourless coesite. Right: light brown rutile. Samples D39 (left) and D47A (right).

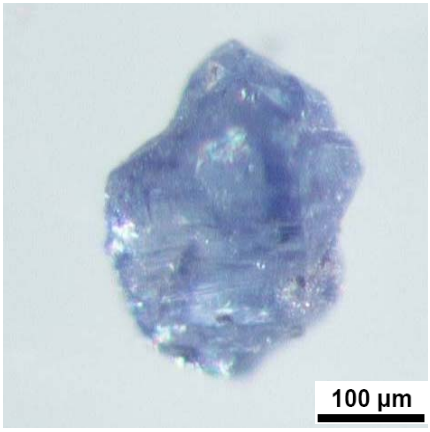

Figure 41 – A blue kyanite inclusion. Sample D128.

Garnet, clinopyroxene (Figure 39), coesite (Figure 40) and kyanite (Figure 41) are also present as single mineral phases within a diamond. Kyanite is rare and only two stones contain it as a single mineral. Another two diamonds contain coesite inclusions. Clinopyroxene is more common and can be found as a single inclusion in 14 diamonds. Nonetheless, by far the most abundant single mineral inclusion is garnet, occurring in 81 of the 134 eclogitic diamonds (Table 6).

The relative abundance of these minerals in the Ural diamonds is in good agreement with the worldwide database, where eclogitic rutile, kyanite and coesite are much less common than clinopyroxene and garnet inclusions. The proportion of clinopyroxene inclusions relative to garnet is low when compared to the worldwide database of (56% garnet, 39% clinopyroxene; Stachel and Harris (2008)), and this may be due to the inclusion's natural abundance, sampling bias, or both.

2.9.2 *Peridotitic inclusions*

A total of 34 diamonds enclosing minerals of the peridotitic paragenesis have been identified (Table 7). Two distinct mineral assemblages have been observed in the diamonds that contain inclusions of this paragenesis: garnet + olivine and garnet + chromite. However, coexisting peridotitic inclusions were only found in five diamonds (Table 7).

P-type inclusions	Single-crystals			Twinned crystals		Totals
	O	D	I	D-m	I-m	
Ol	0	9	0	2	0	11
Gt	0	2	0	0	0	2
Chr	1	12	1	1	1	16
Gt + Ol	1	3	0	0	0	4
Gt + Chr	0	1	0	0	0	1
Totals	2	28	1	3	1	34

Table 7 – Variation in abundance of P-type inclusions as a function of crystal form. Ol = olivine, Gt = garnet, Chr = chromite. Key to form symbols: O = octahedral, D = dodecahedra, I = irregular shapes, D-m = twinned dodecahedra, I-m = twinned irregulars.

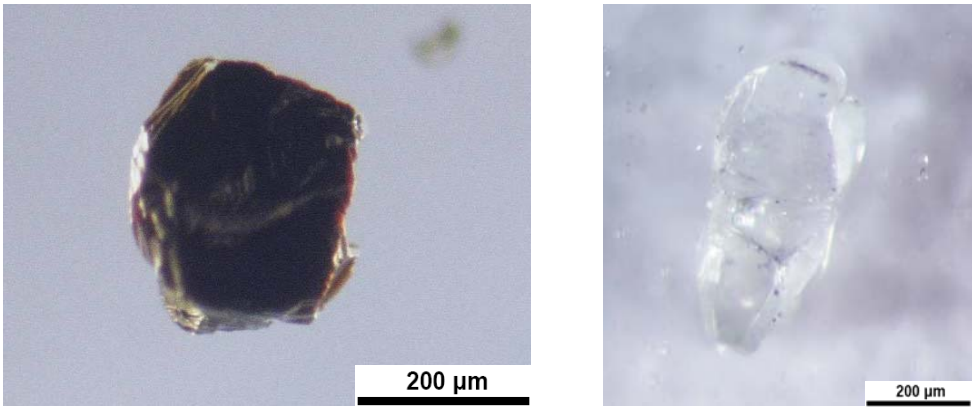

Figure 42 – Left: dark cherry-red chromite. Right: colourless olivine. Samples D124 (left) and D94 (right).

Peridotitic diamonds with single-inclusions are much more abundant than crystals enclosing several minerals. Three minerals of the peridotitic paragenesis (olivine, garnet and chromite) are also present as single-inclusions within the diamond (Table 7). Olivine and chromite (Figure 42) are the most common inclusions, found in 11 and 16 stones, respectively. Peridotitic garnet (Figure 43) is less abundant, being present in only two stones.

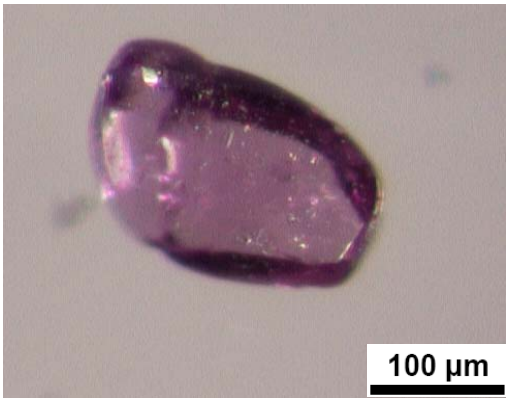

Figure 43 – A purple garnet inclusion. Sample D67.

Relative to the worldwide distribution of inclusions in diamonds, the distinctive feature of the Ural diamonds is their low contents of peridotitic garnet. This is probably due to garnet-bearing diamonds from other localities worldwide being often preferentially picked for geothermobarometric studies (Stachel and Harris, 2008). As this was also the case with the diamonds selected in the present study (see 1.4), it may be reasonable to assume that garnet inclusions are naturally less abundant than olivine and chromite in the Urals alluvial diamonds.

2.9.3 *Websteritic inclusions*

After chemical analysis of their inclusions (see Chapter 5), two diamonds have mineral inclusions which are chemically transitional between the eclogitic and peridotitic parageneses and therefore they have been assigned to the websteritic paragenesis (Table 8). One stone contains the mineral association colourless olivine + pale-green clinopyroxene, and six colourless enstatite grains (Figure 44) are present in one diamond specimen.

All websteritic inclusions displayed typical cubo-octahedral shapes which were undistinguishable form their eclogitic and peridotitic counterparts. The low number of inclusions does not allow any meaningful comparison with the worldwide database of

Stachel and Harris (2008) to be established, and the olivine inclusion analysed in this study is only the third such olivine ever to be reported.

W-type inclusions	Single-crystals			Twinned crystals		Totals
	O	D	I	D-m	I-m	
Enst	0	1	0	0	0	1
Ol + Cpx	0	1	0	0	0	1
Totals	0	2	0	0	1	2

Table 8 – Variation in abundance of W-type inclusions as a function of crystal form. Gt = garnet, Enst = enstatite, Ol = olivine, Cpx = clinopyroxene. Key to form symbols: O = octahedral, D = dodecahedra, I = irregular shapes, D-m = twinned dodecahedra, I-m = twinned irregulars.

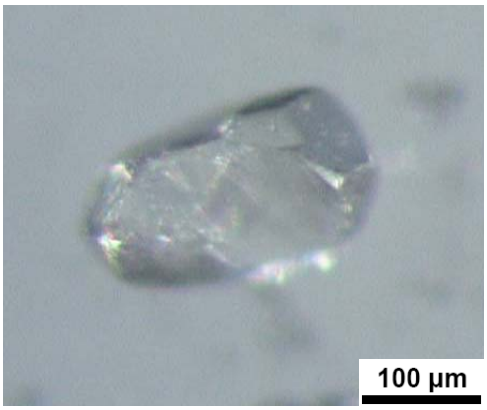

Figure 44 – A colourless websteritic enstatite inclusion. Sample D16A.

2.9.4 *Inclusions of unknown paragenesis*

A total of 47 diamonds enclosing minerals of unknown paragenesis were found (Table 9). Five stones contain solely black graphite inclusions which are unsuitable for electron microprobe analysis. Graphite occurs as clusters of flake-like inclusions (four diamonds), and as a monocrystalline crystal (one stone, see Figure 45). Graphite inclusions of the first type are the product of internal graphitisation after diamond growth, which takes place in lattice defects in all four (111) cleavage directions, when diamond experiences lower temperature conditions (Harris, 1972). Graphite inclusions of the latter type have been interpreted as primary phases that could have acted as nucleation points and/or catalysts for the process of diamond nucleation and growth (Bulanova, 1995). Six diamonds with colourless inclusions were not crushed for analysis and therefore their growth environment remains unknown.

Unknown paragenesis	Single-crystals			Twinned crystals		Totals
	O	D	I	D-m	I-m	
Sulphide	1	34	0	1	0	36
Colourless	0	4	1	1	0	6
Graphite	0	4	0	1	0	5
Totals	1	42	1	3	0	47

Table 9 – Variation in abundance of inclusions of unknown paragenesis as a function of crystal form. Key to form symbols: O = octahedral, D = dodecahedra, I = irregular shapes, D-m = twinned dodecahedra, I-m = twinned irregulars.

The bulk of the "unknown paragenesis" group is formed by sulphides (36 diamonds), typically surrounded by metallic black, rosette-, or disc-shaped fracture systems which, nevertheless, do not reach the surface of the diamond host (see Figure 45). The high number of sulphide inclusions in this "unknown paragenesis" group reflects their status as the most abundant mineral inclusion in diamond (Harris and Gurney, 1979).

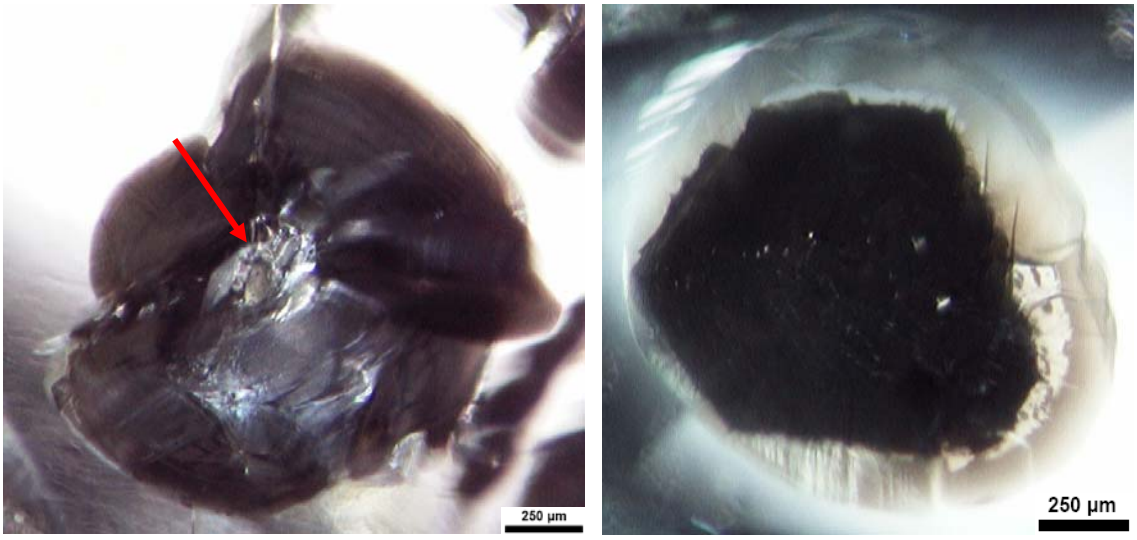

Figure 45 – Left: sulphide (indicated by red arrow) in the centre of a typical black, rosette-shaped fracture system. Right: black graphite. Samples D5B (left) and D40A (right).

2.10 Comparison with the work of Kukharenko (1955)

As mentioned in Chapter 1, the Russian academic A. A. Kukharenko carried out a pioneering study of the physical properties of the Ural diamonds and summarized his findings in the book "Diamonds from the Urals" (1955). Kukharenko's work was published during the secretive Soviet Period and the exact number of diamonds analysed is not mentioned. Nevertheless, Kukharenko points out that 95% of "several thousands" of diamonds studied from the Urals were inclusion-free, this high number of samples studied being most likely representative of the global Urals production at that time.

Diamond characteristics	Kukharenko (1955)	This work
Mean size	0.32 carats	0.21 carats
Shape	82% Dodecahedra 15% Octahedra 2% Irregulars 1% Cubes Twinned crystals comprise ~5% of total stones	89% Dodecahedra 6% Octahedra 5% Irregulars Twinned crystals comprise ~16% of total stones
Colour	70% Colourless 23% Yellow 5% Transparent green-coat 1% Brown 0.8% Pink 0.2% Blue	36% Colourless 42% Yellow 7% Transparent green-coat 15% Brown
Breakage	27% of total stones	23% of total stones
Surface textures	Shield-shaped laminae Trigons Hexagonal etch pits Terraces Hillocks Corrosion sculpture Enhanced lustre Ruts	A total of 17 surface features were recognized (see 2.6), including all the textures identified by Kukharenko (1955)
Radiation damage	Green spots – 33% of total stones Brown spots not very common	Green spots – 56% of total stones Brown spots – 4% of total stones
Abrasion	59% of total stones Percussion marks are the most common feature	56% of total stones Percussion marks are the most common feature
Mineral inclusions	Garnet Chromite Ilmenite Coesite Sulphides Graphite ~95% of diamonds are inclusion-free	Garnet Clinopyroxene Orthopyroxene Olivine Chromite Coesite Kyanite Rutile Sulphides Graphite

Table 10 – Characteristics of the overall Ural diamond population described in Kukharenko (1955) and of the inclusion-bearing Ural diamonds analysed in the present study.

Information on diamond size, shape, colour, breakage, surface textures, radiation damage, abrasion and mineral inclusions in Ural diamonds, presented in Kukharenko (1955) and in the present study, is listed in Table 10. This allows a comparison of the studied inclusion-bearing set of diamonds with the overall, mostly inclusion-free, diamond population from the Ural Mountains described in Kukharenko (1955).

Overall, the studied sub-set of diamonds appears very similar to the diamonds studied by Kukharenko (Table 10). On both studies, resorption is common, dodecahedral-shaped crystals being clearly predominant over the other crystal shapes. A higher percentage of octahedra and the occurrence of cube-shaped crystals is presented in the 1955 study, while twinned crystals are about three times more abundant in the inclusion-bearing sub-set.

In terms of colour, the inclusion-bearing diamonds have about half of the proportion of colourless stones and twice the percentage of yellow stones relative to Kukharenko (1955). Brown coloured crystals are much more common in the present study (15% versus 1%; see Table 10), while pink and blues diamonds were only identified in Kukharenko's study. Both studies present similar results with respect to the percentage of broken and abraded stones, and similar types of surface features were identified (Table 10).

In Kukharenko's work, green spots were identified on a third of the diamonds. Radiation damage is more common in inclusion-bearing diamonds, green spots being present in more than half of the studied population (Table 10). Only limited information is presented in Kukharenko (1955) on the different minerals found inside diamond. Although the relative abundances of mineral inclusions were not recorded by Kukharenko, the minerals described (with the exception of ilmenite) were all recognised in the present study.

2.11 Summary

In terms of their physical characteristics, the vast majority of the studied Ural diamonds are rounded dodecahedra, which indicates that this diamond population have experienced major resorption after crystallisation. Both single- and twinned-crystals were affected by similar resorption processes. Yellow, colourless and brown are the diamond body colours which constitute the studied population. These three body colours are the same as those which typically dominate the diamond production worldwide.

A total of 17 similar and common surface features have been recognized throughout the diamond population. The majority of the diamonds display evidence of transportation, mostly in the form of percussion marks. Non-abraded diamonds exhibit similar surface features to those abraded, so they are probably of similar origin. More than half of the stones are affected by radiation damage, illustrated by the presence of green spots or coats on the surface of the diamonds. Diamonds with such complete green coats are also commonly found in alluvial deposits from other localities worldwide, due to the presence of radioactive material in the sedimentary environment.

The studied inclusion-bearing set of diamonds shares some characteristics with the overall, mostly inclusion-free, diamond population from the Ural Mountains described in Kukharenko (1955). This similarity in physical characteristics strongly suggests that the Ural diamonds are all part of a single population.

3. Nitrogen contents and aggregation states

3.1 Introduction

The presence or the absence of nitrogen in diamond, and its mode of occurrence (known as aggregation state or speciation) is an important way to classify this mineral (Robertson et al., 1934) (see 3.2). The study of the physical and chemical properties of nitrogen occurring in natural diamond also provides information that enables a better understanding of the conditions of diamond formation (see 3.3.2.1).

This chapter presents the results of an infrared spectroscopy study that quantifies the concentration of nitrogen and identifies the aggregation states of this element in the Ural diamonds. The kinetics of nitrogen aggregation in diamond is considered as they provide an insight into the thermal conditions during diamond residence in the mantle (e.g. Taylor et al., 1990; Navon, 1999). Finally, the results of a paleothermometry study of the Ural diamonds are discussed.

3.2 Infrared classification of diamond

Nitrogen is similar in ionic radius and charge to carbon and, therefore, may substitute in the diamond lattice, with concentrations that usually range from less than 20 ppm to more than 2500 ppm (Robinson, 1978). Optical absorption measurements show that nitrogen is present in almost all natural diamonds and occurs in several different aggregation states. This evidence led to the creation of a specific classification based on the nitrogen content and aggregation states of diamond crystals (Robertson et al., 1934). This classification scheme is non-destructive and makes it possible to classify diamonds according to the principal features of their infrared spectra. The widely used infrared classification scheme of diamond divides diamond into two main Types, which are then subdivided, as follows:

Type I: Diamonds with detectable nitrogen content; subdivided into:

Type Ia: Diamonds that contain aggregated nitrogen (A-, B-, N3-centres, platelets; see definition below and in section 3.3.2.1); subdivided into:

Type IaA: Diamonds with nitrogen mainly (≥ 90%) in A-centres.

Type IaB: Diamonds with nitrogen mainly (≥ 90%) in B-centres.

Type IaAB: Diamonds with nitrogen in A- and B- centres.

Type Ib: Diamonds with single substitutional nitrogen.

Type II: Diamonds with very low or non-detectable nitrogen.

Type IIa: Nitrogen free diamonds.

Type IIb: Diamonds with boron as main impurity.

The nitrogen atoms are substitutionally trapped in the diamond lattice at high pressures and temperatures during diamond growth, gradually migrating along the crystalline lattice, towards other nitrogen atoms hereby forming aggregates (see Figure 46). Such atomic migration can only occur whilst diamond is in the Earth's mantle, a situation confirmed by high pressure-temperature experiments that induced nitrogen migration in synthetic diamonds (Evans and Harris, 1989).

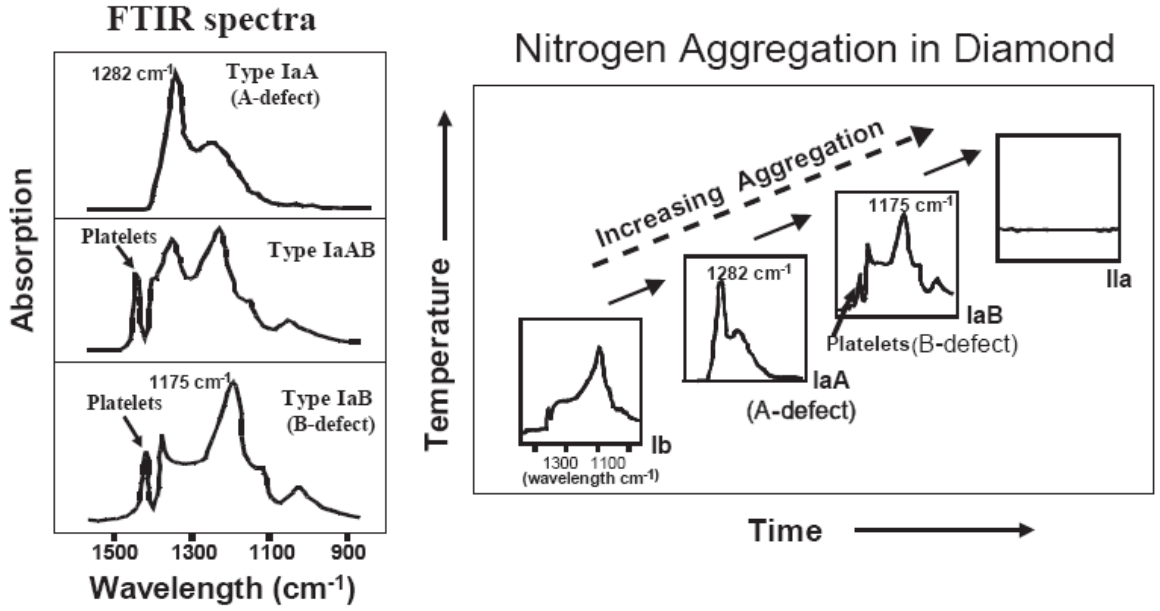

Figure 46 – Fourier-Transform Infrared Spectroscopy (FTIR) spectra of diamond illustrating the different types of nitrogen substitution for carbon in the diamond structure. The development of the type and degree of nitrogen aggregation as a function of time and temperature is illustrated on the right. From Taylor and Anand (2004).

Further aggregation states of nitrogen which are recognised in natural Type Ia diamonds, but which were not quantitatively determined for this study, include N3-centres and platelets. N3-centres consist of three nitrogen atoms and one vacancy and they cause a yellow colouration to diamonds in the visible region at 24,000 cm^{-1} (Evans and Harris, 1989; Evans, 1992). Platelets are planar defects, which range in size from ~10 nm to a few micrometres and form on cubic (001) planes (Evans et al., 1981). Platelets can be observed both by X-ray diffraction and electron microscopy techniques (Woods, 1976; Allen and Evans, 1981). They are also detected by infrared spectroscopy through a pronounced absorption peak at ~1370 cm^{-1} (Allen and Evans, 1981).

Type II diamonds can be subdivided on the basis of their electrical conductivity, Type IIa being non-conducting and Type IIb having semiconducting properties due to presence of substitutional boron as the major impurity (Chrenko, 1973). The amount of boron present in Type IIb diamonds is between 0.02 and 0.26 ppm (Bibby, 1982).

3.3 Fourier-Transform Infrared Spectroscopy

Fourier-Transform infrared spectroscopy (FTIR) is an analytical technique that allows the identification of the molecular species in a sample (qualitative information) and their concentration (quantitative information). It is a fast and non destructive method that can be used to determine both the concentration and aggregation states of nitrogen in diamond.

The use of an infrared microscope enables the attainment of spectra from sub-millimetre areas of individual diamonds, thus providing a means of identifying the presence of nitrogen A and B centres and platelets. In addition, the spectra also provides information on any hydrogen impurity (3107 cm^{-1} peak in the diamond infrared spectra) (Woods and Collins, 1983). It is also a method that can be used for the determination of mantle temperature conditions when diamond crystallised (Evans and Qi, 1982; Evans and Harris, 1989; Mendelssohn and Milledge, 1995b). Thus, infrared studies of diamond may aid in a) paleotectonic reconstructions (the platelet degradation state is sensitive to thermomechanical events in the lithosphere and may be indicative of continental rifting or migration) (Taylor et al., 1990); b) deducing the thermal evolution of continental lithosphere (by combining nitrogen paleothermometry calculations with additional geothermometric and geochronological data) (Stachel and Harris, 2008); and c) determining the provenance of detrital diamonds (by comparing their FTIR signatures with that of diamonds from known primary occurrences) (Kaminsky and Khachatryan, 2001).

3.3.1 *Sample preparation and analytical techniques*

Fragments from the 93 Ural diamonds that were crushed to release their mineral inclusions were used to determine nitrogen contents and aggregation states. Since the infrared microscope measures transmitted light, as far as possible the fragments chosen were suitably flat pieces with parallel faces and sufficient clarity and surface quality in order to minimise diffraction. In the case of diamond, this is particularly important because of its high refractive index (2.417).

Sample thickness is also important and needs to be taken into account during sample selection. Too thin a fragment (<100 μm) does not absorb enough of the infrared beam and normally produces a noisy signal, characterised by the presence of fringes in the 1600 – 900 cm^{-1} spectral range. Thick samples (>2 mm) absorb too much of the primary beam causing the intensity of the transmitted signal to be lower than the equipment's detection limit. It was found that diamond fragments of thickness between 100 μm – 1 mm were most suitable, and these were oriented normal to the infrared beam. This approach reduced the effects of beam scattering, which also causes low transmission values and spectral fringing.

3.3.1.1 Fourier-Transform Infrared Spectroscopy (FTIR)

Infrared absorbance spectra of the diamond samples were recorded by a Nicolet Magna-IR 550 optic bench. It was equipped with an Ever-Glo™ infrared source and a KBr beam-splitter which covers a spectral range of 74000-350 cm^{-1} with a resolution of up to 0.125 cm^{-1}.

The optic bench was linked to a Spectra Tech IR-Plan infrared microscope and the infrared signals were recorded with a liquid nitrogen cooled MCT-A detector that covers a frequency interval of 11700-600 cm^{-1}. The spectra were acquired in transmission mode from 300 scans over a spectral range from 4000 – 650 cm^{-1}. A fixed aperture of 100 μm at a spectral resolution of 4 cm^{-1} was used for all measurements. The instrument was purged with CO_2 free air and was operated under controlled humidity conditions. Background spectra were recorded after every five analyses for later subtraction from the diamond spectra to correct for non-sample contributions.

The optic bench was controlled using the Nicollete OMNIC™ 3.1a software, which also automatically deconvoluted the signals into infrared absorption spectra by performing a mathematical Fourier transform on them.

3.3.1.2 Calculation of nitrogen contents and aggregation states

In order to determine the nitrogen contents and the extent of nitrogen aggregation in the Ural diamonds, the software programme went through a number of procedures. Firstly, the spectra were baselined by simply taking a straight line between about 4000 and 650 cm^{-1}. For the noisier spectra, generated when optimum diamond fragments were not available, the baseline was applied intuitively "by eye". Subsequent to this step, all spectra were converted to absorption coefficients by normalising to a 1 cm thick diamond standard, which has an absorption coefficient of 11.64 cm^{-1} at the 1995 cm^{-1} wavenumber (Pierre Cartigny, pers. comm.).

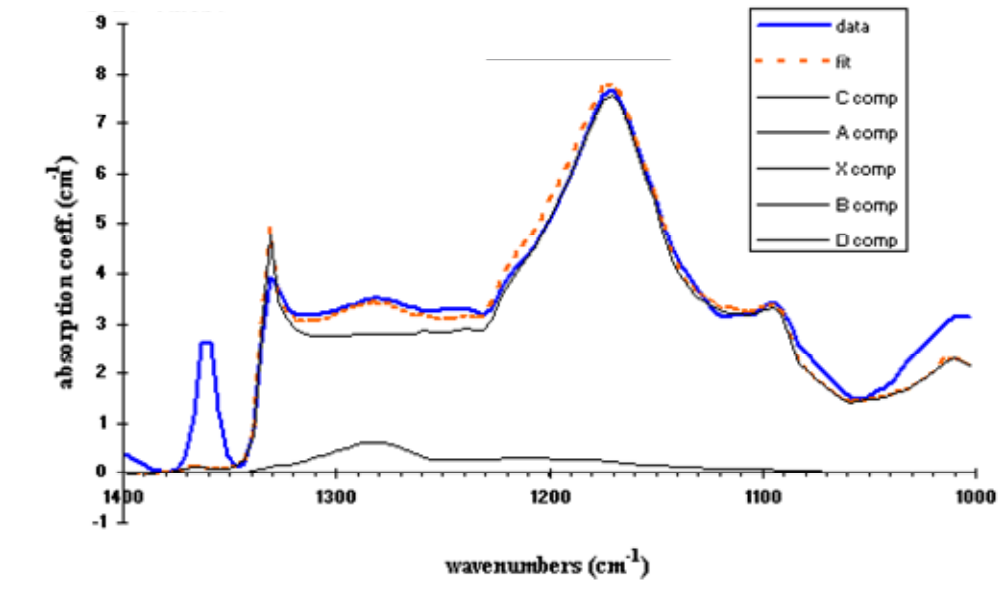

type Ib	μ(1130cm^{-1})	0,00 cm^{-1}	[N_C]	0,0 ppm	**95,6 %**
type IaA	μ(1282cm^{-1})	0,63 cm^{-1}	[N_A]	10,3 ppm	
N^+	μ(1332cm^{-1})	0,00 cm^{-1}	[N^+]	0,0 ppm	**271,5 ppm**
type IaB	μ(1282cm^{-1})	2,80 cm^{-1}	[N_B]	222,4 ppm	*fit range*
D	μ(1282cm^{-1})	0,00 cm^{-1}	[N_T]	232,7 at.ppm	*1100 to 1399*

Figure 47 – Example of a deconvolution of an infrared spectrum (sample U3). The program determines the proportion of type IaA and IaB diamond that fits best the measured spectrum (in blue), as well as the nitrogen concentration in the sample [N_T].

The quantification of the nitrogen contents and aggregation states was determined by deconvolution of the normalised infrared spectral envelope in the 1400 – 1000 cm^{-1} region (see Figure 47) using software written by Pierre Cartigny (see Cartigny, 1997). The software deconvolutes the spectra into components generated by the different centres, using a least-squares regression approach. As illustrated in Figure 47, the software varies the proportions of Type IaA and Type IaB diamond until a best fit to the measured spectrum is achieved. The concentrations of nitrogen, in atomic ppm, are calculated from absorption coefficient values of 16.5 at.ppm cm^{-1} and 79.4 at.ppm cm^{-1} for the A-centre B-centres, respectively (Boyd et al., 1994a; 1995a).

The detection limits for the infrared data were largely dependant on spectral quality, with typical values on the order of 10-30 ppm. The analytical precision is deconvolution-dependant and was ±20% for nitrogen content and ±5% on aggregation state (total errors).

3.3.2 *Results and discussion*

The nitrogen contents and aggregation states for the 93 Ural diamonds are presented in Table A.1. The samples show a large range in nitrogen contents, from 46 to 1528 atomic ppm. Nitrogen aggregation states cover a wide range, from pure Type IaA diamond to pure Type IaB diamond. Type IaAB diamonds (between 10 and 90% of nitrogen in the fully aggregated B-centre) comprise 90% of the population (84 stones). Five stones are Type IaA diamonds (>90% of nitrogen in the poorly aggregated A-centre), with nitrogen contents of about 520-692 atomic ppm. Three stones have >90% of nitrogen in the fully aggregated B-centre (Type IaB), their nitrogen contents varying between 211-393 atomic ppm. Only one nitrogen-free diamond (Type II) was present in the studied population.

On a worldwide basis, nitrogen contents tend to be higher in diamonds with eclogitic inclusions (mean value of 378 atomic ppm) compared to peridotitic samples (mean of 72 atomic ppm) (Stachel et al., *submitted*). In the Urals samples there is a correlation between nitrogen contents and mineral inclusion paragenesis (Figure 48), the average of all nitrogen content data acquired on the eclogitic diamonds being somewhat higher (655 atomic ppm) than the average nitrogen content of the peridotitic and the websteritic diamonds (320 and 311 atomic ppm, respectively). Therefore, although the Ural diamonds are nitrogen-rich relative to the worldwide average, the higher nitrogen contents in eclogitic diamonds relative to the peridotitic ones is in keeping with a similar trend worldwide (Stachel et al., *submitted*). The diamonds with sulphide inclusions of unknown paragenesis have nitrogen contents similar to those belonging to the eclogitic growth environment (average of 630

atomic ppm). Nitrogen aggregation states and mineral inclusion paragenesis do not appear to be correlated (Figure 48).

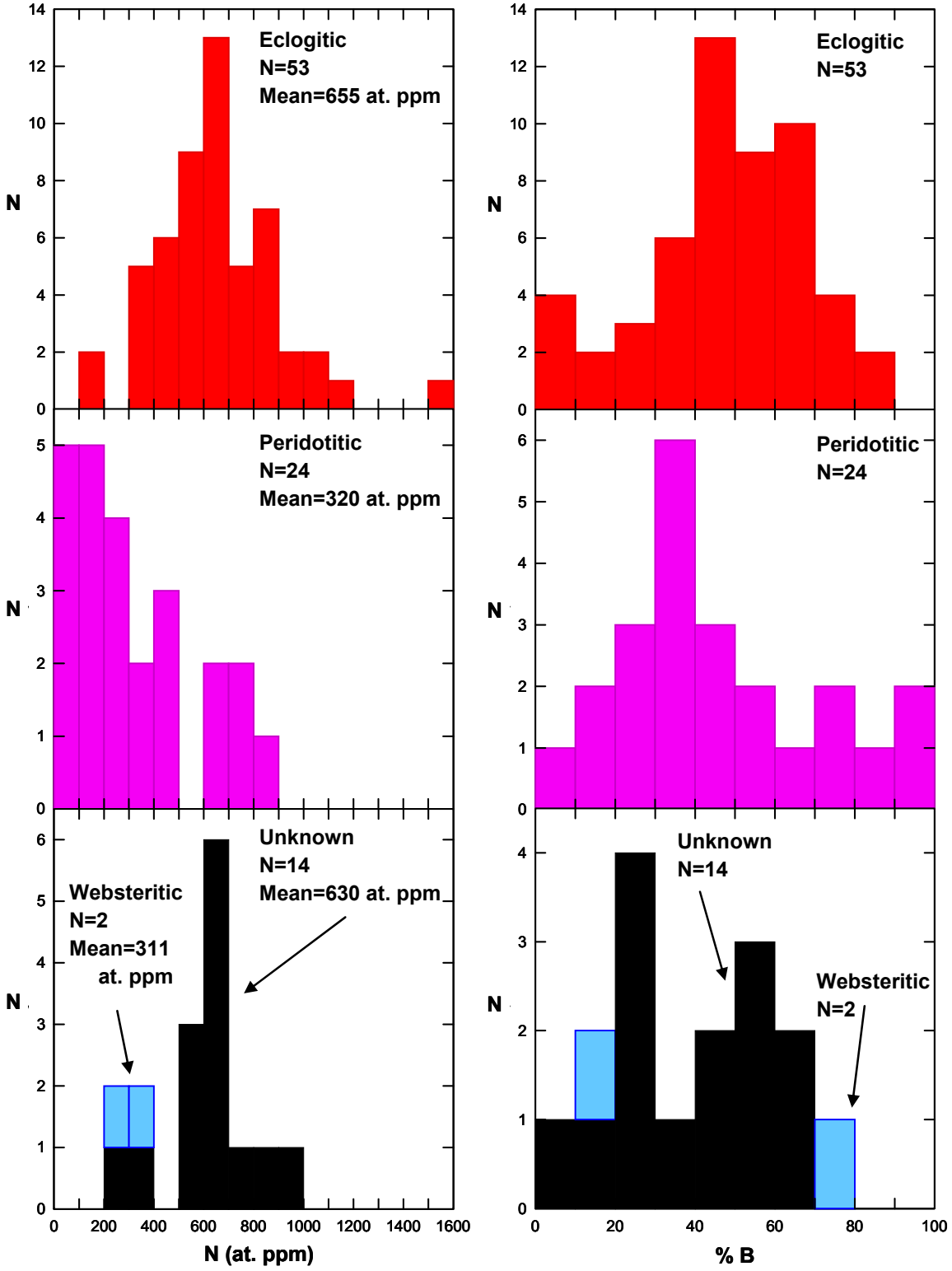

Figure 48 – Histograms of the nitrogen content (atomic ppm) and nitrogen aggregation state (the percentage of nitrogen in the B-centre) for 93 diamonds of the eclogitic, peridotitic, websteritic and unknown parageneses from the Ural Mountains.

Structurally bonded hydrogen, as evidenced by a sharp peak at 3107 cm^{-1} in the infrared spectra (Woods and Collins, 1983), is present in 72% of the diamonds. In this study, the 3107 cm^{-1} hydrogen peak shows no obvious relationship to nitrogen content or mineral inclusion paragenesis (see Table A.1). Even though the concentration of hydrogen was not determined, all diamonds with more than 80% of nitrogen in the highly aggregated B-centre contain infrared-active hydrogen. Therefore there is a tendency for structurally bonded hydrogen to be present in the diamonds with an advanced nitrogen aggregation state.

3.3.2.1 Nitrogen paleothermometry

The aggregation of nitrogen defects in diamond is a kinetic phenomenon in which the degree of aggregation depends on the mantle residence temperature, diamond nitrogen content and the mantle residence time of the specimen (Evans and Qi, 1982; Evans and Harris, 1989; Evans, 1992; Taylor et al., 1996). Experimental studies (see review by Evans, 1992) have shown that upon heating, the single nitrogen atoms (C-centres) that replace single carbon atoms in the diamond lattice, aggregate first to pairs of nitrogen atoms (A-centres) and then to larger, B-type aggregates (four nitrogen atoms and one vacancy). The kinetics of the conversion from C- to A-centres suggest it is relatively fast (in the order of millions of years) and in consequence only a small number of natural diamonds (Type Ib) still retain their C-centres. The kinetics associated with A- to B-centre conversion is much slower (in the order of billions of years), and most nitrogen-bearing natural diamonds fall into this category (Taylor et al., 1996). In theory, therefore, the kinetic equation (see below) can constrain either the mantle residence time or the residence temperature of a diamond from the concentration and aggregation of nitrogen impurities (Navon, 1999). In practice, however, the reaction has a very high sensitivity to temperature and an equally weak dependence on mantle residence time. This situation makes nitrogen aggregation a useful geothermometer but a very poor geochronometer (Cartigny et al., 2004; Stachel and Harris, 2008).

Figure 49 shows diamond mantle residence temperatures as a function of mantle residence time, calculated for the Ural diamonds. An assumption is made that the aggregation of A defects to form B defects is a second order kinetic process (i.e. the rate-determining step involves the combination of two A-centres) and could be fitted into the rate equation given below (Evans and Qi, 1982; Evans and Harris, 1989).

$1/[IaA] - 1/[N] = (A.Exp^{-Ea/RT}).t$

where: T = Time-averaged mantle residence temperature in Kelvin; R = Ideal gas constant; N = Total nitrogen concentration of the diamond ([N] = [IaA] + [IaB]); Ea = Activation energy in eV; A = Arrhenius constant, proportional to the frequency at which two A-centres encounter each other during random diffusion through the diamond structure; t = assumed diamond mantle residence time in seconds from crystallisation to kimberlite eruption.

Isotherms and mantle residence temperatures were calculated using Ea=7.0 eV, R=8.314 $J.mol^{-1}.K^{-1}$ and A=674.8 $kJ.mol^{-1}$ (Cooper et al., 1989; Taylor et al., 1990). A mantle residence time of 1.0 Ga was assumed, but even if a longer residence time was considered, for example 2 Ga, the calculated isotherms are still robust because they would only change by about 35°C (see Evans and Harris, 1989).

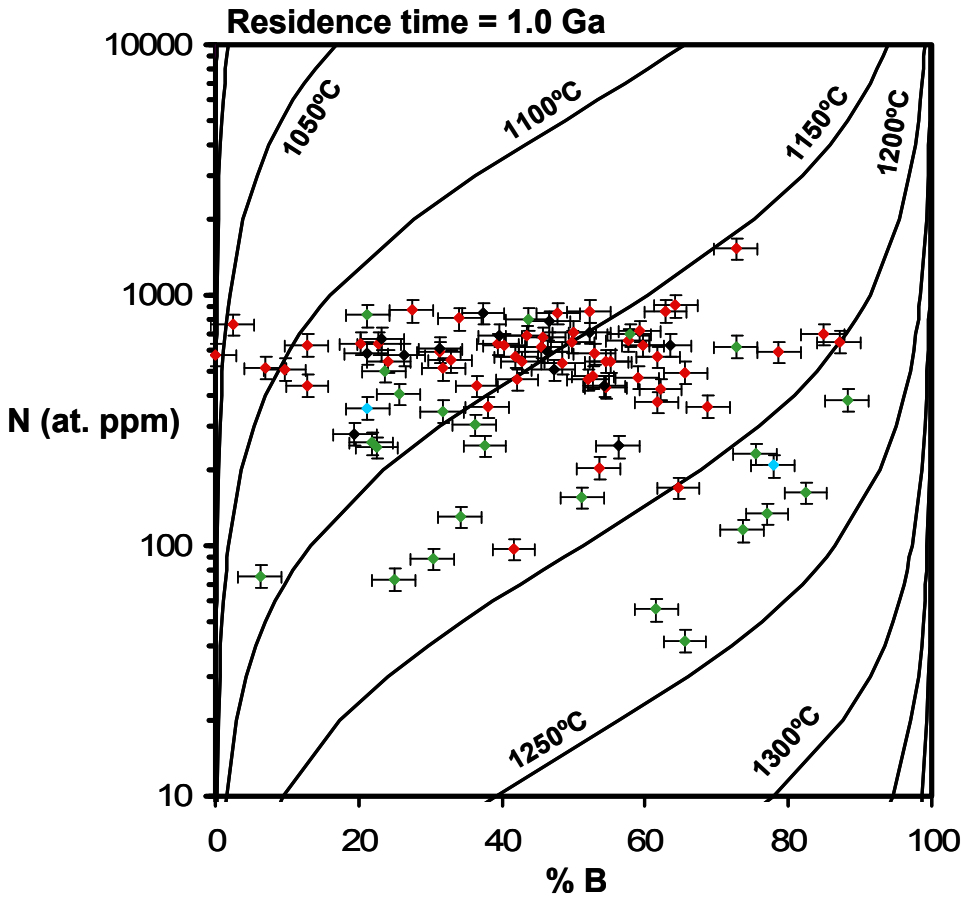

Figure 49 – Total nitrogen concentration (atomic ppm) versus nitrogen aggregation state (expressed as relative percentage of the fully aggregated nitrogen B-centre) for the Ural diamonds. Colours represent mineral inclusion paragenesis: eclogitic in red, peridotitic in green, websteritic in blue and unknown in black. Error bars are ±20% for nitrogen content and ±5% for nitrogen aggregation state. Isotherms are calculated for a mantle residence time of 1.0 Ga using constants from Taylor et al. (1990). Note that although the results exhibit a wide spread, the actual temperature range is not too wide: 1150 ± 100ºC.

The calculated mantle residence temperatures represent an unweighted average for the whole time of residence, with, for example, a diamond residing for 10 Ma at 1250°C and then stored at 1100°C for 2 Ga, receiving heavier weight in the average that a sample that experienced constant mantle temperatures of 1130°C for the same time period (Taylor et al., 1990; Stachel and Harris, 2008). Under the above-mentioned conditions, the Urals data plots between the 1050ºC and the 1250ºC isotherms (Figure 49), which is in good agreement with the temperatures derived from the mineral inclusions that were analysed in this study (see Chapter 5).

Stachel and Harris (2008) argued that an agreement between nitrogen thermometry and inclusion-based geothermometry cannot be taken as evidence against diamond formation during brief heating events followed by diamond storage at cooler temperatures. The same authors pointed out, however, that there seems to be an overall agreement between calculated time-averaged residence temperatures for diamonds from different parageneses and localities worldwide, which implies that the majority of diamonds formed within a narrow depth interval in the Earth's mantle.

The present FTIR results can be compared against the FTIR database of almost 600 diamond crystals from different deposits in the East European Craton, compiled by Khachatryan and Kaminsky (2003) (Figure 50). These authors determined an average nitrogen concentration and aggregation state for diamonds from the Arkhangelsk region kimberlites (Arkhangelskaya, Karpinsky-1, Pomorskaya and Lomonosov); the Kola Peninsula Yermakovskaya-7 pipe; the Middle and Northern Timan alluvials; and the Middle and Northern Ural alluvials. Although the ranges of nitrogen contents and aggregation states in diamonds from these East European Craton localities do overlap, Khachatryan and Kaminsky (2003) showed that their respective means are generally different and can be used for "fingerprinting" of diamonds from distinct sources. To establish a comparison, the average nitrogen concentration and aggregation states for the diamonds analysed in the present study have been determined and these values (505 atomic ppm; %B= 46) are plotted on Figure 50.

Khachatryan and Kaminsky (2003) noted that the diamonds in placers along the western slope of the Middle (Koivo-Vizhai area) and Northern (Vishera area) of the Ural mountains do not show the same FTIR systematics. In particular, among the Middle Urals suite, the authors were able to distinguish two different populations: one consisting of low-nitrogen, highly aggregated diamonds (termed Middle Urals I), the other being a high-

nitrogen, poorly aggregated set (termed Middle Urals II). The Northern Urals suite has similar FTIR characteristics to the Middle Urals II population (see Figure 50).

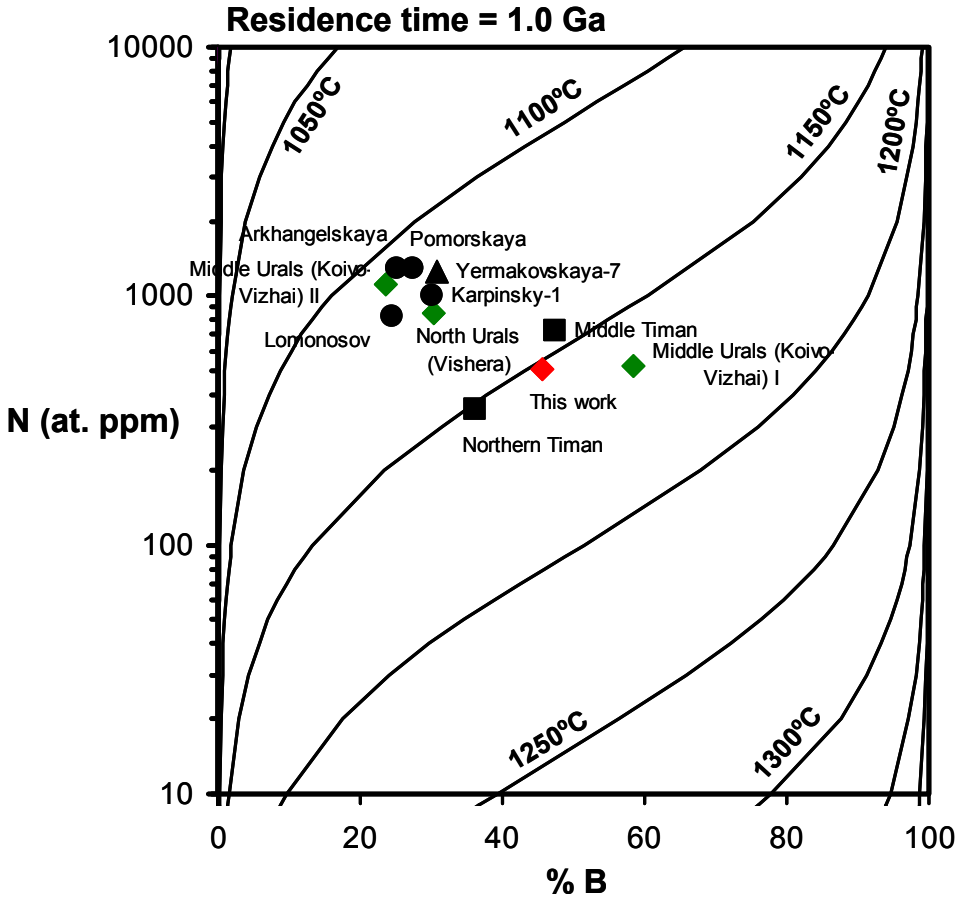

Figure 50 – Total nitrogen concentration (atomic ppm) versus nitrogen aggregation state (expressed as relative percentage of the fully aggregated nitrogen B-centre) for diamonds from different locations within the East European Craton. The symbols represent average values obtained by Khachatryan and Kaminsky (2003) for diamonds from the following deposits: Arkhangelsk region (black circles); Kola Peninsula (black triangle); Timan (black squares); Urals (green diamonds). The average results from the present study are illustrated by the red diamond. Isotherms are calculated for a mantle residence time of 1.0 Ga using constants from Taylor et al. (1990).

The average nitrogen concentration of the present analysed diamond population is closest to the Middle Urals I suite, but the percentage of B-centre nitrogen is about 10% less. Data for the Middle Ural II and Northern Urals (Figure 50) have slightly elevated nitrogen concentration and even less B-centre aggregation. This supports the view that the studied diamond population is a "blend" from several Urals placers, with perhaps a slight predominance of crystals similar to the Middle Urals I population.

By comparison with the studied Ural samples, the diamonds from the other, mostly non-alluvial diamond deposits in the East European Craton have distinct FTIR signatures (see Figure 50). The primary deposits of the Kola Peninsula and the Arkhangelsk region are

relatively high-nitrogen, poorly aggregated suites which appear to have experienced a lower mantle residence temperature. The diamonds from the alluvial deposits of the Timan region plot alongside the same 1150ºC isotherm which is typical of the studied Ural diamonds, but they have different nitrogen concentration and aggregation states characteristics (Figure 50). Nevertheless, this could be an indication that the Timan diamonds and those from the Urals analysed in the present work have evolved under similar mantle conditions.

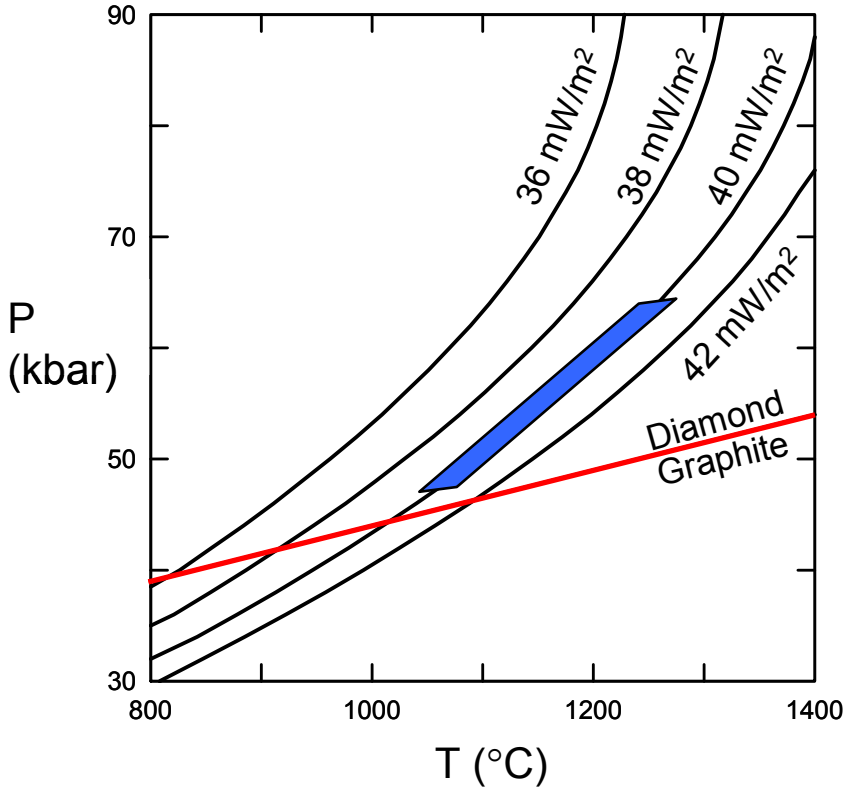

Figure 51 – Pressure-temperature diagram showing the range of temperatures (in blue) obtained by nitrogen-based thermometry for the Ural diamonds, plotted along a conductive continental geotherm based on a surface heat flow of 40 mW/m^2. The associated pressure range (from about 45 to 65 kbar) corresponds to a depth range of about 148 to 215 km (assuming a pressure gradient of 3.3 km/ kbar). Curves for 36, 38, 40 and 42 mW/m^2 conductive continental geotherms calculated according to Pollack and Chapman (1977). Diamond-graphite univariant reaction curve from Kennedy and Kennedy (1976).

Figure 51 shows the range of nitrogen thermometry results for the Ural diamonds plotted along a typical (surface heat flow of 40 mW/m^2) conductive cratonic geotherm. The inferred pressures correspond to a depth range of about 148-215 km (~45 to ~65 kbar), which is also in good agreement with the mineral inclusion geobarometry results (see Chapter 5).

Even if one considers that the scattered nature of the nitrogen thermometry results may not be consistent with the formation of all Ural diamonds during a single growth event (i.e. the nitrogen concentration and aggregation states of the full set of samples are not well correlated along any specific isotherm in Figure 49), it should be noted that any supposedly distinct generations of diamonds from the Urals have most likely crystallised under similar pressure-temperature conditions. This may be indicative of a single primary diamond source or of a spatial proximity between primary contributory sources of the Urals alluvial deposits.

4. Carbon and nitrogen isotopes

4.1 Introduction

Fragments from the Ural diamonds that were crushed to release their mineral inclusions were used to determine their $\delta^{13}C$ and $\delta^{15}N$ isotopic compositions by dual-inlet and static gas source mass spectrometry, respectively. The $\delta^{13}C$ isotopic compositions were determined using the 93 fragments previously selected for nitrogen FTIR analysis (see Chapter 3). Subsequent to the $\delta^{13}C$ work, fragments from 16 diamonds were chosen for $\delta^{15}N$ determination. These diamonds covered the full range of the $\delta^{13}C$ values determined for the initial set of 93 fragments. The $\delta^{15}N$ analytical procedure also allowed the $\delta^{13}C$ and nitrogen content to be determined by bulk combustion, as a second analysis. The results of these stable isotope studies are presented and discussed in this chapter.

4.2 Carbon isotopes in diamond

Carbon has two stable isotopes, ^{12}C and ^{13}C, that occur in nature with abundances of 98.8% and 1.11%, respectively. The carbon isotopic composition is given in "delta" notation ($\delta^{13}C$) and corresponds to the difference in the $^{13}C/^{12}C$ ratio between the sample and a standard of known composition, expressed as: $\delta^{13}C= [(^{13}C/^{12}C)_{sample}/(^{13}C/^{12}C)_{standard}-1]\times1000$. The internationally accepted standard for carbon is the Pee Dee Belemnite (PDB) and thus the carbon isotopic compositions are expressed in terms of how they deviate, in parts per thousand or per mil (‰), relative to the PDB (Hoefs, 2004).

The carbon isotopic composition of a diamond was first measured by Nier and Gulbrasen (1939). Subsequent early studies (mostly focusing on Russian diamonds) have unsuccessfully attempted to correlate diamond properties such as morphology and colour with the carbon isotopic composition of diamonds in some form of classification scheme (e.g. Vinogradov et al., 1966; Koval'skiy and Cherskiy, 1972; Koval'skiy et al., 1973; Galimov et al., 1978; Galimov, 1985). More recently, carbon isotopes are used to

understand the formation of diamond and especially to examine the geochemical cycle of carbon in the mantle focusing on the relative roles of primordial carbon versus recycled crustal carbon (e.g. Deines, 1980; Galimov, 1991; Kirkley et al., 1991; Harris, 1992; Van Heerden et al., 1995; Cartigny et al., 1998a; Haggerty, 1999; Navon, 1999; Cartigny, 2005).

The carbon isotopic composition of diamonds worldwide varies over a wide range, from -38.5 to +5.0‰, with about 72% of the $\delta^{13}C$ values between -8 and -2‰, which is within the range of $\delta^{13}C$ mantle values (Cartigny, 2005). Different diamond localities have distinct carbon isotopic distributions, but if all localities are considered, the worldwide $\delta^{13}C$ distribution has a characteristic peak at about -5‰ (Galimov, 1991; Navon, 1999; Cartigny, 2005).

There is a general relationship between $\delta^{13}C$ values and the two principal diamond parageneses (Sobolev et al., 1979). The carbon isotope compositions of peridotitic diamonds record a narrower range ($\delta^{13}C$ from -26.4 to +0.2‰) than those of the eclogitic growth environment ($\delta^{13}C$ from -38.5 to +2.7‰) (e.g. Deines, 1980; Deines et al., 1984; 1989; Otter and Gurney, 1989; Galimov, 1991; Kirkley et al., 1991; Cartigny, 1997; Cartigny et al., 1998a; 1998b; Deines et al., 2001). In addition, only 2% of the worldwide peridotitic diamonds have $\delta^{13}C$ values lower than -10‰, which is in sharp contrast with the much higher proportion (34%) of eclogitic diamonds (Cartigny, 2005).

While most diamonds sampled by kimberlites and related rocks originate at the base of the cratonic lithosphere (~100–250 km depth), they can also form at much greater depths including the Earth's lower mantle (≥660 km depth) (see Stachel et al., 2005). These lower-mantle diamonds show a narrow range of $\delta^{13}C$ values, from -8.5 to -0.5‰ (Cartigny, 2005).

The carbon isotope compositions of fibrous/coated diamonds range from -8.1 to -4.9‰, while impact-related and metamorphic diamonds (microdiamonds formed in subducted metamorphic rocks) vary in $\delta^{13}C$ from -22 to -8‰ and -30 to -3‰, respectively (Cartigny, 2005). Carbonados have a light carbon isotopic signature, with $\delta^{13}C$ varying from -30 to -23‰, excluding two known outliers at -6 and -8‰ (see Kamioka et al., 1996; Shelkov et al., 1997; Heaney et al., 2005).

4.2.1 *Origin of $\delta^{13}C$ variability in diamond: existing models*

The carbon isotopic compositions of diamond have implications for the understanding of both the source of carbon and the processes of diamond formation. Three main models have been proposed in an attempt to explain the observed variability of carbon isotopic values in natural diamonds. A description of each of these models is presented below.

4.2.1.1 Introduction of heterogeneous subducted carbon

The $\delta^{13}C$ values in mantle-derived materials such as mid-ocean ridge basalts, ocean island basalts, carbonatites and kimberlitic carbonate cover a relatively narrow range, from about -10 to 0‰ (see Deines and Gold, 1973; Exley et al., 1986; Deines, 1989; Kirkley et al., 1989; Javoy and Pineau, 1991). By contrast, sedimentary carbon shows a range in $\delta^{13}C$ values from an average of about -25‰ in organic matter (Strauss, 1986) and about 0‰ in marine carbonates (Veizer and Hoefs, 1976).

The range of the carbon isotopic compositions of sediments is similar to that of eclogitic diamond ($\delta^{13}C$ from -38.5 to +2.7‰) and led to the suggestion that eclogitic diamond formed from crustally-derived carbon recycled into the mantle by subduction, whereas peridotitic diamond, with a narrower $\delta^{13}C$ distribution (-26.4 to +0.2‰) would have formed from mantle-derived carbon (e.g. Kesson and Ringwood, 1989; Kirkley and Gurney, 1989; Kirkley et al., 1991; Jacob et al., 1994; Nisbet et al., 1994; Navon, 1999).

This hypothesis has, however, some weaknesses. To account for eclogitic diamonds with an average $\delta^{13}C$ values of -5‰, mass-balance considerations indicate the need to recycle one part of organic matter (average $\delta^{13}C$ of -25‰) and four parts of carbonates (average $\delta^{13}C$ of 0‰), in order to confirm that these diamonds are indeed the product of recycled carbon (Cartigny et al., 1998b). However, as most eclogitic diamonds have $\delta^{13}C$ values between -25 and -5‰, this is in disagreement with the $\delta^{13}C$ distribution around -5 to 0‰ that would be expected if carbonates were to make up 80% of the carbon in eclogitic diamond (Cartigny, 2005). In fact, diamonds from upper-mantle sources with high $\delta^{13}C$ values (from -1 to +3‰) are only common in the alluvial deposits of New South Wales, Australia (see Sobolev, 1984; Davies et al., 1999) and are very rare in other mines worldwide. This discrepancy between the expected $\delta^{13}C$ distribution produced by mixing organic matter and carbonates and the observed $\delta^{13}C$ values in eclogitic diamond is a strong argument against the formation of diamond from subducted carbon.

Another argument against a recycled origin is that, during subduction, the carbon isotopic compositions of carbonates and organic matter tend to homogenise when temperatures reach in excess of 700ºC (Satish-Kumar et al., 2002). Based on this evidence, Cartigny (2005) argues that the re-equilibration of the two sedimentary carbon components in the mantle would result in eclogitic diamonds having very similar carbon isotopic compositions and not to an extreme $\delta^{13}C$ variability, as is commonly observed. The scarcity of $\delta^{13}C$ values around -5‰ for crustal-derived metamorphic diamonds contrasts with the $\delta^{13}C$ distribution for eclogitic diamonds and also suggests that the latter are not subduction-related (Cartigny et al., 2001a).

4.2.1.2 Primordial isotopic variability

A comprehensive study of the physical characteristics, mineral inclusion chemistry, carbon isotopes and nitrogen contents and aggregation states of diamonds from several mines of the Kaapvaal craton, enabled Deines et al. (1984; 1987; 1989; 1991a; 1991b; 1993; 1997) to establish that several diamond subpopulations can be sampled by a single kimberlite pipe. These authors found that the diamond subpopulations were dissimilar in terms of all of the above criteria and therefore suggested that the observed range of carbon isotopic values was inherited from a heterogeneous primordial carbon source that had existed since the accretion of the Earth and was not homogenised by mantle convection.

This model supports the observations of Deines and Wickman (1975), who noted a close resemblance between the carbon isotopic composition of enstatite chondrites (which are considered to represent a significant part of the Earth's mantle) and that of diamond. This similarity in $\delta^{13}C$ values of diamonds and meteorites led to the suggestion that the diamonds have sampled primordial mantle heterogeneities that would have been preserved since the Earth's accretion (Deines, 1980).

There are, however, some inconsistencies in this model. The existence of isolated primordial reservoirs with distinct carbon isotopic compositions cannot be evoked as the sole reason for the observed isotopic variations in diamonds since it would require that distinct lithospheric mineralogies (e.g. peridotite versus eclogite) consistently tap distinct primordial reservoirs (Stachel et al., *submitted*).

Also, as pointed out by Cartigny (2005), the preservation of primordial $\delta^{13}C$ variability in the Earth's mantle is not supported by data from other fields of mantle isotope geochemistry, which show almost no evidence for preservation of primitive mantle

compositions, since the effects of melting or convection processes would tend to homogenise any initial $\delta^{13}C$ heterogeneity.

4.2.1.3 Fractionation of stable isotopes at mantle temperature

Stable isotopes are unique in that coexisting chemical compounds in equilibrium will display different stable isotope compositions (Cartigny, 2005). This fractionation process is controlled mainly by temperature (it becomes less important as temperature increases) and the species involved (e.g. CO_2, CH_4) (Bottinga, 1969). In order to explain the full range of $\delta^{13}C$ values in diamond, the fractionation model proposes that diamond crystallisation occurs from a single homogeneous fluid in an open system, where minute amounts of diamond form under isotopic equilibrium and remain isolated from their growth medium (e.g. Javoy et al., 1986; Galimov, 1991; Cartigny et al., 1998a; 1998b; 2001b). This open system fractionation process, where material is removed continuously under conditions of a constant fractionation factor, is termed Rayleigh distillation and can create a very large range in carbon isotopic compositions, in some cases in excess of 40‰ (Cartigny, 2005).

Of the different carbon-bearing phases in the mantle (e.g. carbonate, carbide, methane, carbon dioxide), CH_4 and CO_2 were considered by Deines (1980) to be the ones from which diamond would more likely precipitate. Fractionally precipitating diamond from CH_4 and CO_2 with an initial $\delta^{13}C$ value of -5‰ (representative of the worldwide diamond $\delta^{13}C$ mode) produces model $\delta^{13}C$ distributions with distinct modes and shapes, but which could actually account for the pronounced overlap of both peridotitic and eclogitic diamonds in the $\delta^{13}C$ range of -8 to -2‰ (Deines, 1980). This is in agreement with the suggestion that the diamonds from the two principal parageneses may have crystallised from high-temperature fractionation of mantle-derived carbon with an initial carbon isotopic composition of about -5‰ (Javoy et al., 1986; Galimov, 1991).

Cartigny et al. (1998a; 1998b) suggested that high-temperature fractionation of mantle fluids might account for the complete $\delta^{13}C$ range for diamonds, given that these fluids evolved separately in peridotitic and eclogitic environments. The loss of CO_2 from eclogitic sources is thought to leave a $\delta^{13}C$ -depleted residue that may crystallize diamonds with a broad $\delta^{13}C$ range.

Nevertheless, the fractionation hypothesis also has some weaknesses, the most significant being the difficulty in explaining the distinct carbon isotopic composition distributions of peridotitic and eclogitic diamonds solely on the basis of a stable isotope fractionation

mechanism. In addition, if a unique carbon source with an initial $\delta^{13}C$ value of about -5‰ truly reflects the mantle conditions worldwide, then the $\delta^{13}C$ distributions diamonds from Argyle and Guaniamo (centered around -11 and -15‰, respectively) cannot be readily explained (Van Heerden et al., 1995; Kaminsky et al., 2000). Furthermore, a simple Rayleigh distillation model is incapable of explaining the bimodal $\delta^{13}C$ distribution of diamonds from the Jagersfontein and Orapa kimberlites (Deines et al., 1991a; 1993).

4.2.2 *Sample preparation and analytical techniques*

The 93 diamond fragments selected for $\delta^{13}C$ analysis were weighed on a CAHN C-31 microbalance with a precision of 0.5×10^{-5} mg. Diamond chips between 1 and 1.5 mg were specifically selected, as this is the optimum weight for diamond combustion (Pierre Cartigny, pers. comm.). The fragments were placed inside quartz glass tubes and left for at least 30 minutes inside an oven at 600ºC to eliminate any organic carbon contamination. The samples were then introduced into the CO_2 extraction line and left overnight under vacuum (10^{-6} torr) conditions.

4.2.2.1 CO_2 extraction line

The CO_2 was extracted by combusting the diamond inside a furnace in a pure oxygen atmosphere (5.0 purity = 99.995% O_2) at a temperature of 1100ºC. Depending on the mass of the fragment, total combustion of the diamond typically occurred after 15 to 30 minutes. The CO_2 produced was then separated cryogenically from other gases using a liquid N_2 trap and collected in a gas sample tube for mass spectrometry analysis.

4.2.2.2 Dual-inlet gas source mass spectrometry

The $\delta^{13}C$ isotopic compositions were obtained from the analysis of the CO_2 molecule (intensity of the masses 44, 45 and 46) on a Finnigan Delta plus XP dual-inlet gas source mass spectrometer. The correction of Craig (1957) was applied to the 45/44 and 46/44 mass ratios. The instrumental precision and accuracy of the $\delta^{13}C$ isotopic compositions, as established on the basis of standard analyses, was better than 0.05‰ (2σ).

4.2.3 *Results*

Table A.2.1 reports the weight (mg), $\delta^{13}C$ and nitrogen content (from FTIR analysis, see Chapter 3) determined on 93 diamonds of the eclogitic, peridotitic, websteritic and

unknown parageneses from the Urals placer deposits. As illustrated in Figure 52, the studied diamonds range in $\delta^{13}C$ values from -18.9‰ to +2.3‰, with a mean of -5.6‰ and a mode in class -6 to -5‰. This $\delta^{13}C$ distribution is in agreement with previous carbon isotope studies of diamonds from the Urals (Galimov, 1985; Galimov et al., 1978; 1990), which also show a mode in the -6 to -5‰ class, although the mean of previous studies is slightly shifted towards lighter carbon isotopic compositions ($\delta^{13}C$= -6.9‰; see Figure 52).

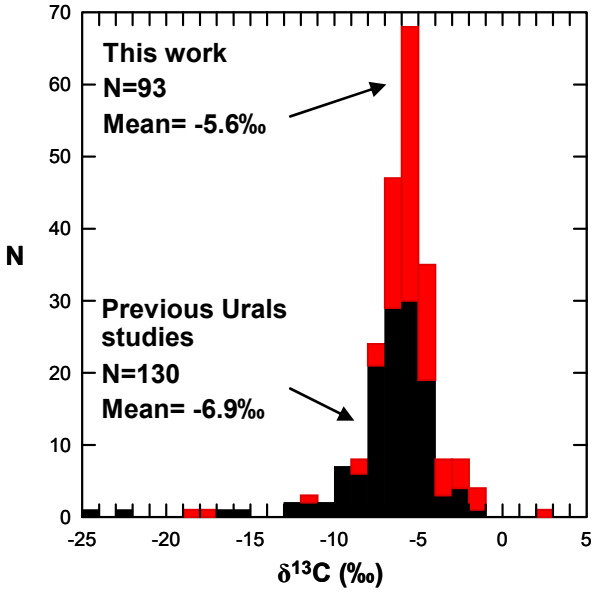

Figure 52 – The $\delta^{13}C$ isotopic composition of diamonds from the Ural Mountains. The data from previous studies is from Galimov (1985) and Galimov et al. (1978; 1990).

A more detailed assessment of the $\delta^{13}C$ distribution of the studied diamond population can be made by grouping the diamonds in terms of their mineral inclusion paragenesis (Figure 53). The fifty-three eclogitic diamonds vary in $\delta^{13}C$ from -18.9‰ to -4.9‰, 94% of them being between -8.3‰ and -4.9‰, which is typical of diamonds of this paragenesis from worldwide sources and within the range of $\delta^{13}C$ mantle values (Cartigny, 2005). The $\delta^{13}C$ mean for eclogitic diamonds is -6.9‰, and their distribution peaks in the -6 to -5‰ class (Figure 53).

The twenty-four peridotitic diamonds range in $\delta^{13}C$ values from -8.9‰ to +2.3‰, the positive value reflecting the very heavy carbon isotopic composition of one sample (U5; see Table A.2.1). The peridotitic diamonds show a tendency to be isotopically heavier (average $\delta^{13}C$= -3.9‰) than the eclogitic ones, with a mode in the -5 to -4‰ class (Figure 53). With the exception of sample U5, the Urals peridotitic diamonds have carbon isotopic compositions within the mantle range, and their $\delta^{13}C$ distribution is in good agreement with the worldwide database of Cartigny (2005).

Only two websteritic diamonds, U23 and U45, have been analysed for carbon isotopic compositions, their $\delta^{13}C$ values (-3.7‰ and -5.8‰, respectively; Figure 53) being again within the mantle range. The fourteen diamonds of unknown paragenesis are restricted to a narrow range in $\delta^{13}C$, from -6.1‰ to -3.9‰ (Table A.2.1). Their $\delta^{13}C$ mean is -5.5‰, with a mantle-like mode again in the -6 to -5‰ class (Figure 53).

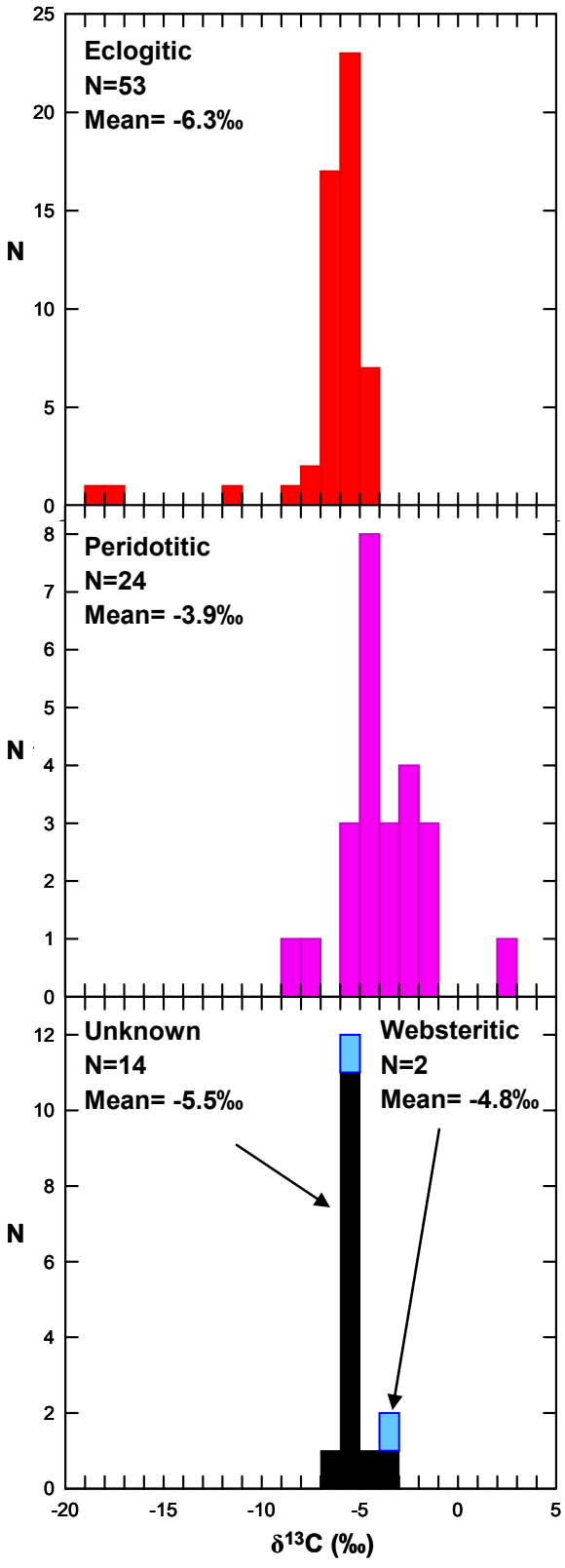

Figure 53 – Histograms of $\delta^{13}C$ values for 93 diamonds of the eclogitic, peridotitic, websteritic and unknown parageneses from the Ural Mountains.

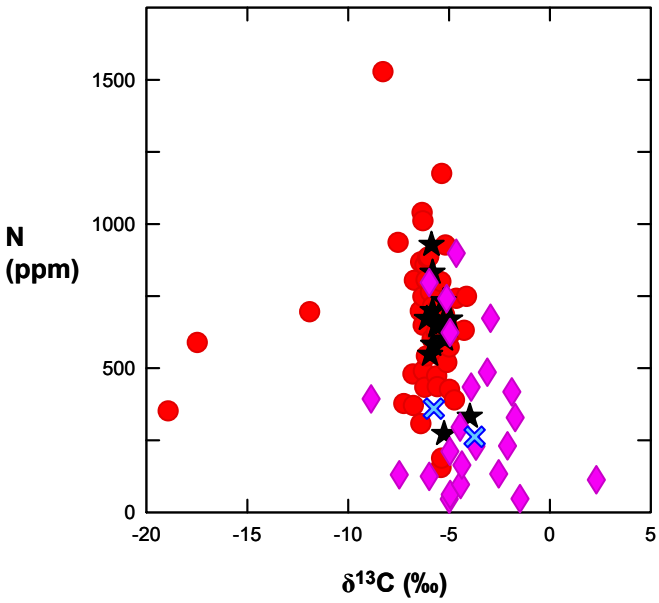

Figure 54 – $\delta^{13}C$ versus nitrogen content (determined by FTIR) for diamonds from the Urals. Colours represent mineral inclusion paragenesis: eclogitic in red, peridotitic in pink, websteritic in blue and unknown in black.

On a worldwide basis, a relationship of decreasing $\delta^{13}C$ with decreasing nitrogen content has been identified (e.g. Stachel and Harris, 1997; Cartigny et al., 2001a; 2001b), but with exceptions such as the diamonds from the Namibian placers (Cartigny et al., 2004). Figure 54 compares the nitrogen contents of the studied diamonds as determined by FTIR, with their $\delta^{13}C$ isotopic composition. Almost all diamonds plot within a $\delta^{13}C$ range that is too narrow (~ -8‰ to ~ -1‰) to establish any meaningful correlation with the large range in nitrogen contents (0 to 1528 ppm) that has been observed. Thus and irrespective of their paragenesis, no correlation appears to exist between $\delta^{13}C$ and nitrogen content of the Ural diamonds. The $\delta^{13}C$ values are also not correlated to any of the physical characteristics of the Ural diamonds.

4.3 Nitrogen isotopes in diamond

Nitrogen has two stable isotopes, ^{14}N and ^{15}N, that occur in nature with abundances of 99.64% and 0.36%, respectively. The nitrogen isotopic composition is given in "delta" units ($\delta^{15}N$) and corresponds to the difference in the $^{15}N/^{14}N$ ratio between the sample and molecular nitrogen in the atmosphere, expressed as: $\delta^{15}N = [(^{15}N/^{14}N)_{sample}/(^{15}N/^{14}N)_{atm}-1]\times1000$. The nitrogen isotopic compositions are expressed in terms of how they deviate, in parts per thousand or per mil (‰), relative to atmospheric nitrogen (Hoefs, 2004).

The application of nitrogen isotopic analyses to diamonds is now well established by the work of Javoy and co-workers (e.g. Javoy et al., 1984; 1986), Boyd and co-workers (e.g. Boyd et al., 1987; 1992; Boyd and Pillinger, 1994) and Cartigny and co-workers (e.g. Cartigny et al., 1997; 1998a; 1998b; 2001a; 2003; 2004). The data set for $\delta^{15}N$ is less extensive than that for $\delta^{13}C$, primarily because nitrogen concentrations in diamond are much lower (average of ~300 ppm, Deines et al. (1993)) and the extraction techniques are more complicated. Particularly, it is very difficult to check the completeness of the N_2 extraction and there are interference problems with much more abundant species (isobaric CO, CH_4 and H_2 giving rise to C_2H_5 and N_2H^+, respectively) (see Javoy et al., 1986).

In general terms, the $\delta^{15}N$ isotopic composition of diamonds is spread over a larger range and does not display a clear paragenetic distinction such as that seen for $\delta^{13}C$. For example, with the exception of the unusually large $\delta^{15}N$ range seen in P-type diamonds from Pipe 50, China (Cartigny et al., 1997), the majority of P-type and E-type diamonds from worldwide localities have overlapping $\delta^{15}N$ values ranging from -12 to +4‰ (Cartigny et al., 1998b). Close examination of the worldwide nitrogen isotope data shows that peridotitic diamonds vary over a range from -25 to +15‰, with about 65% of the $\delta^{15}N$ values between -8 and -2‰, whereas eclogitic diamonds worldwide have a $\delta^{15}N$ range between -12 and + 18‰, with most values (~70%) being negative (Cartigny, 2005). Fibrous and metamorphic diamonds display relatively more homogeneous $\delta^{15}N$ ranges, of -9 to -2‰ and -2 to +12‰, respectively (Javoy et al., 1984; Boyd et al., 1987; 1992; Cartigny et al., 2001a).

4.3.1 *$\delta^{15}N$-based models for diamond forming processes*

Relative to atmospheric nitrogen ($\delta^{15}N$= 0), the Earth's surface is ^{15}N-enriched ($\delta^{15}N\approx$ +2‰; Marty and Humbert (1997)). Nitrogen in sedimentary rocks occurs typically as ammonium ions (Honma and Itihara, 1981) and is characterised by positive $\delta^{15}N$ values, with an average of about +6‰ (Peters et al., 1978; Fogel and Cifuentes, 1993). Due to similarities in charge and ionic radius, nitrogen substitutes for potassium in such sedimentary K-bearing minerals as mica and clays (Honma and Itihara, 1981). With increasing metamorphism, the nitrogen content in rocks composed of these minerals decreases because of devolatilization of NH_4^+ to N_2, and the $\delta^{15}N$ signatures shift towards more ^{15}N-enriched values (Haendel et al., 1986). Thus the $\delta^{15}N$ isotopic composition of ammoniacal nitrogen in metasediments ranges from +2 to +15‰ relative to air (Bebout and Fogel, 1992). The $\delta^{15}N$ isotopic composition of metasediments have remained relatively constant, from the Archean to recent geological periods (Peters et al., 1978).

Studies of nitrogen isotopes in mid-ocean ridge basalts (Javoy and Pineau, 1991; Marty and Humbert, 1997), fibrous/coated diamonds (Javoy et al., 1984; Boyd et al., 1987; 1992) and peridotitic diamonds (Cartigny, 1997) have been used to estimate the $\delta^{15}N$ isotopic composition of the Earth's upper mantle. These studies have shown that about 65% of the $\delta^{15}N$ values for these mantle samples are negative and centred around -5 ±3‰ (Cartigny, 2005). Thus there is an isotopic imbalance between the external (^{15}N-enriched sediment, metasediment and crust), and the deep (^{15}N-impoverished upper mantle) reservoirs of the Earth. This means that $\delta^{15}N$ data can be used as a tool to constrain models of diamond forming processes and trace the origin of nitrogen in the mantle.

The three proposed hypotheses for the origin of diamonds from their $\delta^{13}C$ characteristics (see 4.2.1) are further constrained by $\delta^{15}N$ data. If eclogitic diamonds formed from crustally-derived carbon recycled into the mantle by subduction (see 4.2.1.1), then they should contain positive to highly positive $\delta^{15}N$ values, particularly when displaying low $\delta^{13}C$ values, matching those of the original organic matter. However, a large majority (~70%) of eclogitic diamonds worldwide have negative $\delta^{15}N$ values, and about half of the eclogitic diamonds with negative $\delta^{13}C$ values also display low $\delta^{15}N$ values (Cartigny, 2005). This observation led Cartigny et al. (1998a; 1998b) to suggest that eclogitic diamonds are unlikely to crystallise from recycled carbon and most probably have a mantle origin.

A variation to the recycled carbon model has been proposed by Navon (1999), whereby the carbon and nitrogen systematics of eclogitic diamond would be best explained as a mixture of mantle and subducted components. This model requires mantle and sedimentary mixing end-members that have variable compositions, possible nitrogen isotopic fractionations during diamond growth and a variable carbon/nitrogen ratio of the diamond-forming fluid (Navon, 1999). However, the model cannot explain the fact that both peridotitic and eclogitic diamonds show a positive correlation between nitrogen content and $\delta^{13}C$, when a drop in nitrogen content (which decreases with metamorphism, see above) with increasing $\delta^{13}C$ values would be expected (Cartigny et al., 2004). Also, taking the high $\delta^{15}N$ (-2 to +12‰) metamorphic diamonds as an example of crustal-derived diamonds, the model of Navon (1999) would predict an overlap between the $\delta^{13}C$ values of metamorphic and eclogitic diamonds, and thus does not account for metamorphic diamonds being less depleted in $\delta^{13}C$ than some eclogitic diamonds (Cartigny, 2005).

If eclogitic diamonds originated from several distinct locations of a primordial isotopically heterogeneous mantle (see 4.2.1.2), then several distinct $\delta^{15}N$ isotopic signatures would be

expected. Also, because nitrogen is less abundant than carbon, nitrogen isotopes should be more sensitive to a primordial mantle heterogeneity than carbon isotopes (Cartigny et al., 1998a). On a stable isotope study of diamonds from the Jwaneng mine, Botswana, Cartigny et al. (1998a) noted that eclogitic diamonds showed relatively little variability in $\delta^{15}N$ (-10 to -1‰) compared with their $\delta^{13}C$ range (-21 to -5‰) and concluded that this was incompatible with diamond formation in several distinct mantle environments, as had been previously suggested by Deines et al. (1997).

To explain the eclogitic diamonds with anomalously low $\delta^{13}C$ and high $\delta^{15}N$ isotopic signatures that fall outside the normal mantle range, Cartigny et al. (1998a; 1998b; 2001b) argued for a stable-isotope fractionation process in the diamond forming fluid prior to diamond growth (see 4.2.1.3). The model has since been refined to consider the presence of a metasomatic agent in diamond formation (Cartigny et al., 2004; Cartigny, 2005), which would allow minute amounts of diamond to form under isotopic equilibrium whilst remaining isolated from their peridotitic/eclogitic growth medium (Thomassot et al., 2007). This isotope fractionation model is supported by a number of studies that suggest a direct link between diamond formation and mantle metasomatism, such as: 3D X-ray tomography of eclogite xenoliths (Schulze et al., 1996; Taylor and Anand, 2004); work on fibrous (Navon et al., 1988; Schrauder and Navon, 1993; Klein-BenDavid et al., 2004) or gem diamonds (Taylor et al., 1998; Cartigny et al., 2001b; 2004; Cartigny, 2005); and the trace element chemistry of mineral inclusions in diamonds (Stachel et al., 2004). The oxidized (i.e. CO_2/carbonate-rich) or reduced (i.e. methane-rich) nature of the metasomatic agent remains debatable, with the model of Thomassot et al. (2007) providing evidence in favour of diamond crystallization via a Rayleigh distillation from a methane-bearing fluid.

4.3.2 *Sample preparation and analytical techniques*

For $\delta^{15}N$ analysis, 16 inclusion free diamond fragments were specifically selected after the initial $\delta^{13}C$ and FTIR measurements. Nitrogen rich representative samples of each of the inclusion parageneses, covering the entire observed range of $\delta^{13}C$ values, were selected and analysed for $\delta^{15}N$, total nitrogen content (N Comb.) and $\delta^{13}C$ (as a second analysis) by bulk combustion (see Table A.2.2).

The diamond fragments, between 0.5 and 2.2 mg in weight, were subjected to the same analytical procedures described in section 4.2.2. The CO_2 produced during the combustion was collected and analysed for $\delta^{13}C$ following the procedure described earlier (see sections 4.2.2.1 and 4.2.2.2). Nitrogen was separated from CO_2 and any nitrogen oxides were

reduced to N_2 using a CaO/Cu mixture, as described in Boyd et al. (1994b). Nitrogen concentrations were measured with a Baratron^{TM} capacitance manometer with a precision better than 5% (2σ) (see Boyd et al., 1993; 1995b).

4.3.2.1 Static gas source mass spectrometry

After quantification, N_2 was directly introduced and isotopically analysed in a specially constructed VG-type static mass spectrometer. The mass spectrometer includes a Nier-type ion source, a flight tube of 8 cm radius across a Hall probe-stabilized magnetic field and three single Faraday cup collectors. The $\delta^{15}N$ isotopic compositions were obtained from the analysis of the N_2 molecule at masses 28, 29 and 30.

In addition to blank determinations, ^{40}Ar was also monitored in the mass spectrometer as an indicator of potential atmospheric contamination for both sample and blank. The blank contribution was below 9 ng of nitrogen with $\delta^{15}N$ of -9 ± 3‰. No correction was applied to the nitrogen isotopic measurements. The precision on the $\delta^{15}N$ measurements was better than 0.5‰ (standard error of the mean based on 2σ), estimated from the reproducibility of international standards (IAEA-N1 and IAEA-N2; Boyd et al. (1995b)) that were run during the period of analysis.

4.3.3 *Results*

Table A.2.2 reports the weight (mg), $\delta^{15}N$, $\delta^{13}C$ and nitrogen content determined by bulk combustion on 16 Ural diamonds of the peridotitic, eclogitic, websteritic and unknown parageneses, selected from the initial set of 93 stones (see 4.2.2).

As shown in Figure 55, the six peridotitic diamonds show a large spread in $\delta^{15}N$, from -24.1‰ to +8.3‰, the lower value reflecting the very light nitrogen isotopic composition of sample U5 (Table A.2.2). Apart from this sample, the other diamonds of the peridotitic paragenesis have $\delta^{15}N$ values ranging from -9.4‰ to +8.3‰. The eight eclogitic diamonds cover a comparatively narrower $\delta^{15}N$ range, between -6.9‰ and +4.4‰ (Figure 55). The nitrogen isotopic composition of one websteritic diamond and one diamond of unknown paragenesis (which contained a sulphide inclusion) has also been determined, their $\delta^{15}N$ values being -4.7‰ and -4.4‰, respectively (Table A.2.2; Figure 55).

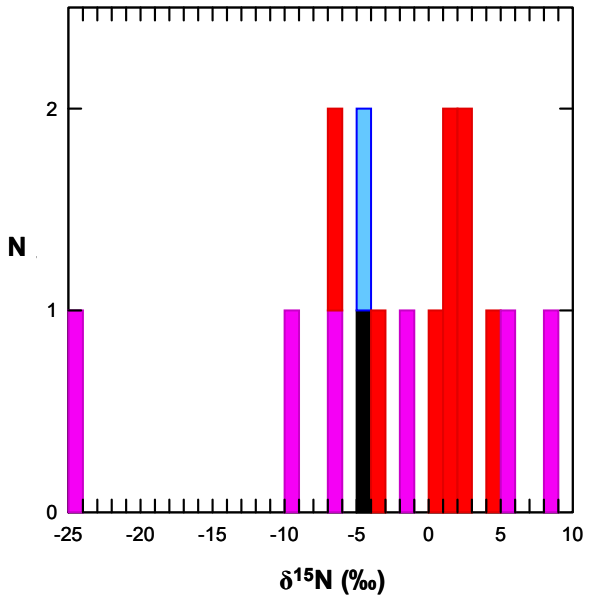

Figure 55 – The $\delta^{15}N$ isotopic composition of diamonds from the Ural Mountains. Colours represent mineral inclusion paragenesis: eclogitic in red, peridotitic in pink, websteritic in blue and unknown in black.

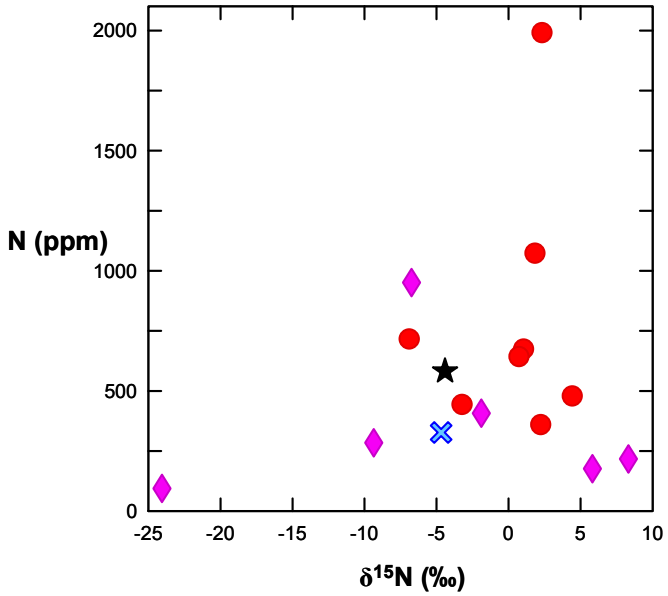

Figure 56 – $\delta^{15}N$ versus nitrogen content (determined by bulk combustion) for diamonds from the Urals. Colours represent mineral inclusion paragenesis: eclogitic in red, peridotitic in pink, websteritic in blue and unknown in black.

Worldwide data indicate a general tendency for an positive increase in $\delta^{15}N$ with decreasing nitrogen content (Cartigny et al., 2001b). In the case of the studied diamonds, no clear correlation between $\delta^{15}N$ and nitrogen content was observed (Figure 56). This absence of co-variation of $\delta^{13}C$ (see 4.2.3) or $\delta^{15}N$ values with nitrogen contents appears to be similar to that observed in diamonds from Namibia, where several samples were too nitrogen-rich for their high $\delta^{15}N$ signatures (see Cartigny et al., 2004). There is no correlation between $\delta^{15}N$ values and the physical characteristics of the Ural diamonds.

4.4 The variation of $\delta^{13}C$ and $\delta^{15}N$ in the Ural diamonds

For the 16 Ural diamonds analysed for $\delta^{15}N$, an assessment of the relationship between their nitrogen and carbon isotopic compositions was made. For the six diamonds from the peridotitic paragenesis, there is a correlation (r^2= 0.90) with an increase in $\delta^{15}N$ while decreasing $\delta^{13}C$ (Figure 57). Five of the eight diamonds of the eclogitic paragenesis follow a trend in $\delta^{15}N$ – $\delta^{13}C$ space that is similar to the one defined by the peridotitic diamonds (Figure 57). The other three eclogitic diamonds show an even more marked increase (r^2= 0.94) in $\delta^{15}N$ with decreasing $\delta^{13}C$.

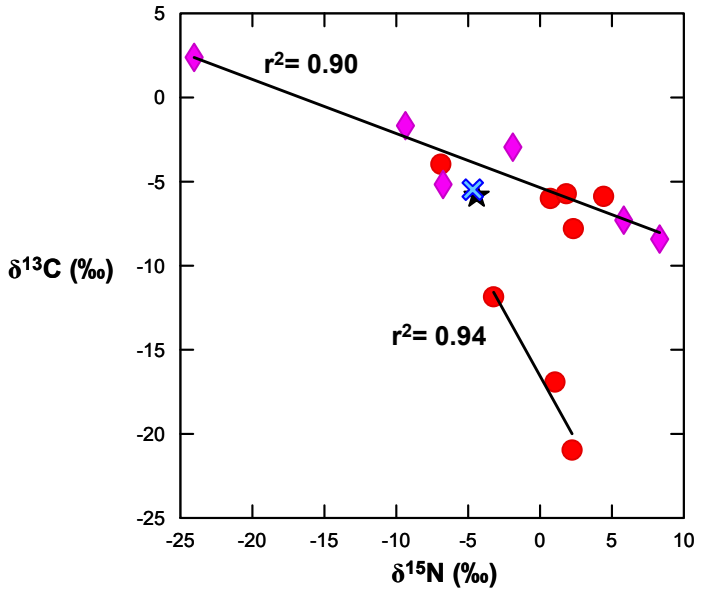

Figure 57 – $\delta^{15}N$ versus $\delta^{13}C$ for diamonds from the Urals. Colours represent mineral inclusion paragenesis: eclogitic in red, peridotitic in pink, websteritic in blue and unknown in black. Correlation coefficients (given as r^2) and their respective regression lines for the peridotitic and three of the eclogitic diamonds, are also shown.

The relatively narrow $\delta^{13}C$ distribution of the peridotitic diamonds, excluding a sample with positive $\delta^{13}C$, is in reasonable agreement with the model that these diamonds have formed from mantle carbon. However, the peridotitic diamond with a positive $\delta^{13}C$ value (Figure 57) is not likely to have derived directly from mantle carbon, which has an average $\delta^{13}C$ of -5‰. Also, the positive $\delta^{15}N$ signature observed for two other peridotitic diamonds is not compatible with direct crystallisation from mantle-derived fluids. The total $\delta^{15}N$ – $\delta^{13}C$ variation recorded by the peridotitic diamonds most likely reflects the existence of isotopic fractionation of mantle fluids/melts introduced into peridotites through metasomatic processes (Cartigny et al., 1999; 2004).

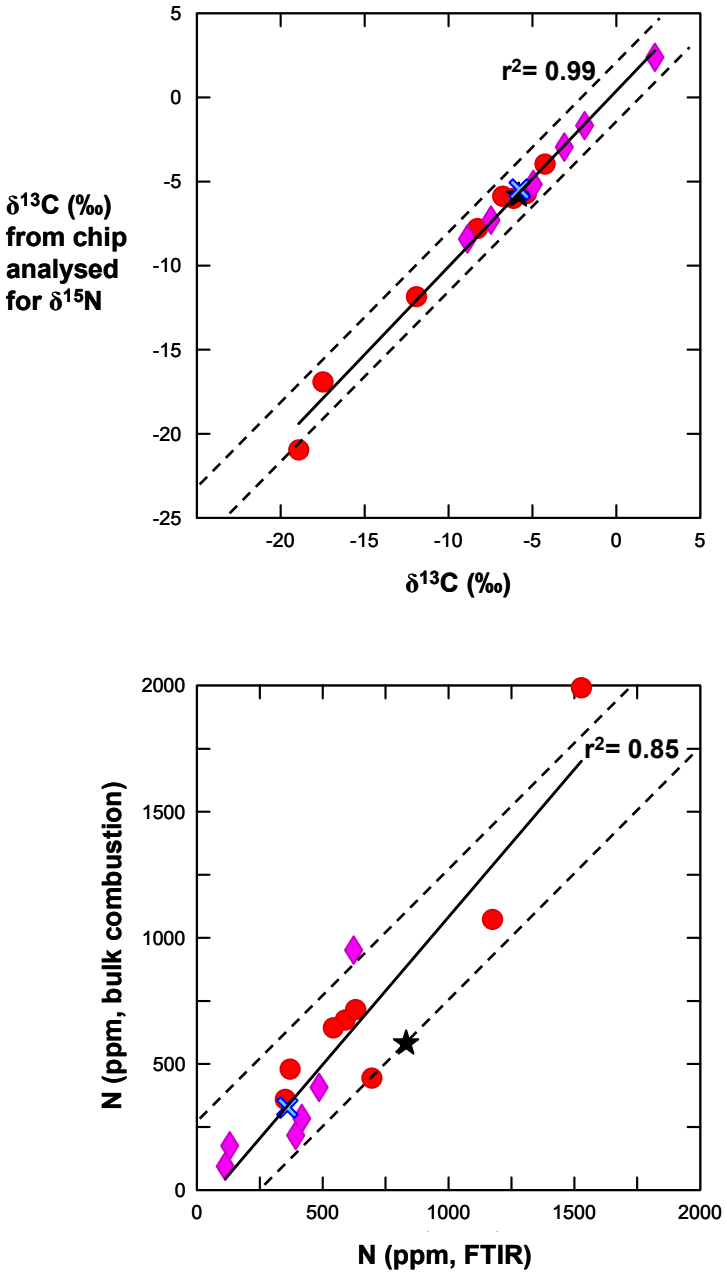

Figure 58 – Top: comparison of $\delta^{13}C$-values measured on two fragments from the same diamond. Dashed lines indicate variations of 2‰. Bottom: nitrogen contents as determined by FTIR and by bulk combustion using the same diamond fragment. Dashed lines indicate a difference of 250 ppm. Colours represent mineral inclusion paragenesis: eclogitic in red, peridotitic in pink, websteritic in blue and unknown in black. Dashed lines variation from Cartigny et al. (2004). Correlation coefficients (given as r^2) and their respective regression lines were calculated for all diamonds.

In light of the $\delta^{15}N$ – $\delta^{13}C$ data, the similarity between the peridotitic and five eclogitic diamonds suggests derivation from a similar isotopic source (Cartigny et al., 1998b). Thus both eclogitic and peridotitic diamonds are believed to have derived from a common, initially homogenous, mantle carbon source, which has been subjected to metasomatic-induced isotopic fractionation. For the three eclogitic diamonds with a lighter carbon isotopic signature, their evolution towards positive $\delta^{15}N$ values may indicate formation

from subduction-related metasomatic fluids/melts (Cartigny et al., 2004). A continuum of values from high $\delta^{13}C$ – negative $\delta^{15}N$ towards low $\delta^{13}C$ and positive $\delta^{15}N$ has also been noted in eclogitic samples from the Orapa mine, Botswana (Cartigny et al., 1999). According to these authors, this $\delta^{13}C$ – $\delta^{15}N$ trend suggests that both kinetic fractionation of nitrogen isotopes during diamond growth (see Boyd and Pillinger, 1994) and preferential diffusion of carbon relative to nitrogen (or vice-versa) within the diamond lattice after crystallisation (see Hauri et al., 1998), are small or negligible relative to the isotopic variations recorded by the diamonds.

The two $\delta^{15}N$ stable isotope analyses carried out on diamonds of websteritic and unknown paragenesis do not allow their precise origin to be addressed. Nevertheless, both diamonds have a well defined mantle signature, with $\delta^{13}C$ and $\delta^{15}N$ values of about -5‰ (Figure 57). Although it would be tempting to suggest crystallisation from a pure mantle origin, it seems more likely that these diamonds have been affected by the same isotopic fractionation processes proposed above for the peridotitic and eclogitic diamonds.

A comparison of the $\delta^{13}C$ isotopic compositions measured on two different fragments of the same diamonds reveals isotopic homogeneity better than 2‰ for all samples (Figure 58). Nitrogen contents measured on the same diamond fragment by combustion and by FTIR compare well (r^2= 0.85), heterogeneity being usually smaller than 250 ppm, with only samples U30 and U53 being relatively more variable (difference of ~300 and ~500 ppm, respectively) (see Figure 58). The Urals results compare well with studies of other localities worldwide using similar analytical techniques (e.g. Cartigny et al., 2004), which shown that the heterogeneity of diamonds is usually restricted to a few per mil in $\delta^{13}C$ isotopic composition, and less than 200 ppm in nitrogen contents.

5. Inclusion geochemistry

This chapter presents the results of electron microprobe quantitative chemical analysis carried out on silicates, oxides and sulphide mineral inclusions released from diamonds recovered in the alluvial deposits of the Ural Mountains.

The aim of this study was to determine which minerals occur as inclusions in diamonds from the Ural Mountains, and to find the range in chemical composition for individual mineral species. The Urals mineral inclusion chemistry results were then integrated and compared with a pre-existing data set from other localities worldwide (Stachel and Harris, 2008). It was also intended to investigate the conditions under which these minerals would have crystallised and hence to gain an insight into the processes of diamond formation in the Urals.

5.1 The study of the minerals included in diamond

The importance of the study of mineral inclusions in diamond with regard to mantle characterization and the genesis of diamond was appreciated early (by the end of the 19th century). However, apart from some studies using optical and X-ray diffraction procedures, little work was done until the second half of the 20th century, when electron microprobe techniques finally allowed to routinely carry out chemical analyses on micron-sized minerals (Meyer, 1968; Meyer and Boyd, 1969; Meyer and Boyd, 1972). Since then many others have contributed significantly to the study of the minerals enclosed in diamond (e.g. Gurney and Switzer, 1973; Meyer and Svisero, 1975; Harte et al., 1980; Svisero, 1981; Svisero, 1983; Deines et al., 1984; Gurney et al., 1985; Moore and Gurney, 1985; Canil and Wei, 1992; Griffin et al., 1992; Eldridge et al., 1995; Griffin and Ryan, 1995; Bulanova et al., 1996; Griffin et al., 1999a; 1999b; Pearson and Shirey, 1999; Stachel et al., 2000a; 2000b; Barron, 2003; Shirey et al., 2003; Taylor et al., 2003; Stachel et al., 2004; Stachel and Harris, 2008).

The mineral inclusions in diamonds are commonly characterised according to their generic relationship to the host (Harris, 1992). Epigenetic inclusions usually occur in surface fractures and, in most cases, are minerals which are either not stable in the diamond stability field (e.g. calcite) or alteration products of pre-existing inclusions (e.g. serpentine). Syngenetic inclusions are those which formed synchronously with the diamond host. Some of these inclusions exhibit specific orientations with respect to their diamond host. Others have principle surfaces closely related to those of diamond so that cubo-octahedral morphology is exhibited, even by inclusions of minerals such as olivine which has a non-cubic crystalline structure (Robinson, 1978). Such epitaxially related inclusions and inclusions where the diamond host imposes its morphology on the enclosed mineral, must have nucleated on growing diamond surfaces and are believed to represent pristine and chemically unaltered samples of the mantle (Meyer, 1987).

Criteria for the identification of syngenetic inclusions have been outlined by several authors who carried out work on the relationship between diamond and its inclusions (Harris, 1968b; Harris, 1968a; Orlov, 1977; Sobolev, 1977; Meyer, 1987). In general, syngenetic mineral inclusions are shown to 1) have an imposed cubo-octahedral morphology such that the inclusion is a negative crystal of the host; 2) be epitaxially and topotaxially intergrown with diamond; and 3) have specific elongations and bifurcations following the crystallographic directions of their host, frequently varying in thickness along their length.

Meyer (1987) suggested the existence of a third, protogenetic, group of inclusions with irregular morphologies, or morphologies consistent with the inclusions's crystal structure. Both epigenetic and protogenetic inclusions do not permit to estimate the formation conditions of natural diamonds as they post- or pre-date their diamond hosts, respectively.

All of the mineral inclusions analysed in this study were unrelated to cracks in diamond and exhibited imposed morphology. The results of this study will be discussed on the premise that all the inclusions recovered are syngenetic and hence the data obtained can be used to estimate the formation conditions of the Ural diamonds.

5.2 Inclusion selection

From an initial population of 217 inclusion-bearing diamonds, a total of 93 stones were crushed to release the mineral inclusions. Two diamonds had inclusions (a chromite and an eclogitic garnet, respectively) which were lost during polishing. Another four stones had

large sulphides that were reserved for Re-Os isotopic analysis. The inclusion contents for the remaining 87 diamonds are listed in Table 11.

Many stones contained more than one inclusion, normally of the same mineral, but occasionally of two or even three different minerals, thus allowing P-T estimates to be made (on the assumption of different phases being in equilibrium) and providing more detailed information on mineral parageneses. In total, 181 mineral inclusions were recovered and analysed on the electron microprobe (Table 12).

Mono-mineralic assemblages	*n*	Bi-mineralic assemblages	*n*	Tri-mineralic assemblages	*n*	Poli-mineralic assemblages	*n*
Olivine (ol)	11	ol, p-gt	4	e-gt, rutile, sul	1	e-gt, e-cpx, coe, sul	1
Cr-bearing pyrope (p-gt)	1	p-gt, chr	1	e-gt, coe, sul	1		
Eclogitic pyrope-almandine (e-gt)	23	w-ol, w-cpx	1				
Websteritic Enstatite (w-opx)	1	e-gt, e-cpx	4				
Eclogitic omphacitic cpx (e-cpx)	7	e-gt, sul	9				
Chromite (chr)	6	e-cpx, sul	1				
Coesite (coe)	2	coe, sul	1				
Kyanite (ky)	2						
Sulphide (sul)	10						
Total diamonds	63		21		2		1

Table 11 – Inclusion abundance for the 87 Ural diamonds analysed.

Paragenesis	Inclusion mineral	*n*
Peridotitic	ol	18
	gt	8
	chr	12
Eclogitic	gt	69
	cpx	16
	ky	2
	rut	1
	coe	6
	sul	26
Websteritic	cpx	1
	opx	6
	ol	1
Unknown	sul	15
Total inclusions		181

Table 12 – Number of inclusions analysed on the electron microprobe. gt: garnet; ol: olivine; chr: chromite; cpx: clinopyroxene; opx: orthopyroxene; ky: kyanite; coe: coesite; rut: rutile; sul: sulphide.

Based on the composition of the inclusions ~26% of the analysed diamonds from the Urals belong to the peridotitic suite, ~60% are eclogitic and ~2% are websteritic (see Table 13). The remainder ~12% are all diamonds with sulphides of unknown paragenesis.

Paragenesis	Inclusion assemblage	*n*
Peridotitic	ol	11
	gt	1
	chr	6
	ol, gt	4
	gt, chr	1
Eclogitic	gt	23
	cpx	7
	coe	2
	ky	2
	gt, cpx	4
	gt, sul	9
	gt, rut, sul	1
	gt, coe, sul	1
	cpx, sul	1
	coe, sul	1
	gt, cpx, coe, sul	1
Websteritic	opx	1
	ol, cpx	1
Unknown	sul	10
Total diamonds		87

Table 13 – The paragenesis of the Ural diamonds analysed on the electron microprobe. gt: garnet; ol: olivine; chr: chromite; cpx: clinopyroxene; opx: orthopyroxene; ky: kyanite; coe: coesite; rut: rutile; sul: sulphide.

With the exception of one eclogitic clinopyroxene (U13A), compositional variations within individual silicate and oxide inclusions were minor and within the error of microprobe analysis. The grains therefore may be regarded as homogeneous. This was not the case with the majority of the sulphide inclusions, were exsolution patterns were often present.

Electron microprobe data of mineral inclusions in diamond from occurrences worldwide has been compiled by Stachel & Harris (2008). In the present study, these data are referred to as the worldwide data and used as a basis for comparison with the Ural diamond inclusions.

5.3 Sample preparation and analytical techniques

The mineral inclusions, ranging from 50-580 μm in largest dimension, were released from their host diamonds using a stainless steel crusher equipped with a glass window to observe the process under a binocular microscope. The inclusion grains were then placed on top of glass slides covered with a thin layer of release agent, and separately mounted in 6 mm brass rings using Araldite epoxy (using a 9:1 resin-hardener mix ratio). Mechanical polishing of the inclusions was made on a 90% Pb - 10% Sb plate using diamond abrasives to attain a 0.25 μm finish. All samples were coated with carbon. Additionally, a thin line of Silverdag^{TM} was applied from the mineral to the sample holder on all the brass rings containing sulphide inclusions to increase sample conductivity. Electron backscattered imaging was carried out for all samples.

Major and minor elements were determined by wavelength-dispersive spectrometry (WDS) using a JEOL JXA-8900 RL electron microprobe equipped with five spectrometers at the Institute for Mineralogy, University of Frankfurt. A minimum of three analyses per inclusion were completed. All measurements were carried out with spot beam, using an accelerating voltage of 20 kV and a beam current of 20 nA.

For silicate and oxide minerals, peak count times were 60 seconds for Si, Ca, Ni, Mg, Cr, P, Al and Ti, and 30 seconds for K, Ca, Zn, Mn and Fe. Background times were half the peak times, except for Si, Na, Mg, Al and Mn, where background times were the same as peak times. The crystal spectrometers used were TAP (for Si, Na, Mg and Al), PET (for K, Ca, Cr, P and Ti) and LIF (for Ni, Zn, Mn and Fe). The standards were the following: $CaSiO_3$ for Si and CaO; $KTiOPO_4$ for K and P; $NaAlSiO_3$ for Na; NiO for Ni; Mg_2SiO_4 for Mg; Cr_2O_3 for Cr; ZnO for Zn; Al_2O_3 for Al; $MnTiO_3$ for Ti; MnO for Mn; Fe_2SiO_4 for Fe. Typical detection limits are of about 100 ppm. Accuracy and precision were checked against secondary standards and are better than 1% relative for major element analysis.

For sulphide minerals, peak count times were 200 seconds for S, Cr and Se, and 40 seconds for Fe, Ni, Co, Cu and Zn. Background times were half the peak times, except for Co, where background time was the same as peak time. TAP (for Se), PET (for S and Cr) and LIF (for Fe, Ni, Co, Cu and Zn) crystal spectrometers were used. The standards were FeS_2 for S and Fe and pure metals for all remaining elements. Typical detection limits are of about 100 ppm.

5.4 Inclusion compositions

5.4.1 *Garnet*

Garnet (77 inclusions released from 45 diamonds) is the most common inclusion in the Ural diamond population. The mineral occurs either as a single inclusion or together with other mineral phases (see Table 11). The eclogitic suite predominates over the peridotitic, 69 grains being orange pyrope-almandines and 8 grains purple Cr-pyropes. The chemical composition of garnet inclusions is presented in Tables A.3.1 and A.3.2. A refinement of the more usual value of Mg# [100Mg/(Mg+Fe^{2+})], $Mg\#_{Ca\text{-}corr}$ ($Mg\#_{Ca\text{-}corr}$ = Mg# + 2Ca, Ca as cations calculated on a basis of 24 oxygens) is given for garnet inclusions to account for the effect of CaO on Mg/Fe partitioning between garnet and Mg-Fe silicates (O'Neill and Wood, 1979).

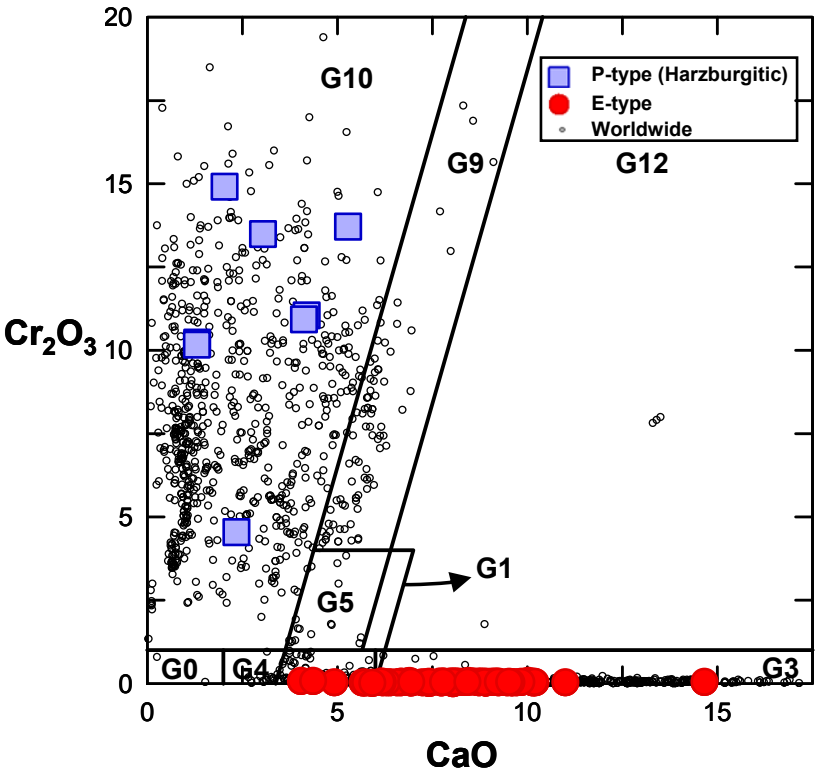

Figure 59 – Plot of CaO versus Cr_2O_3 (wt%) for garnets recovered from the Ural diamonds. The compositional fields are those of Grutter et al. (2004). Worldwide data from Stachel and Harris (2008).

According to the classification scheme of Grutter et al. (2004), all the peridotitic Cr-pyropes belong to the harzburgitic paragenesis (Figure 59). The values for $Mg\#_{Ca\text{-}corr}$ range from 87 to 92 (Figure 60) and are consistent with the average $Mg\#_{Ca\text{-}corr}$ of 88 for "normal"

harzburgitic garnet inclusions worldwide. Two grains (U5A and U5B) coexisting with olivine in the same diamond are highly depleted low-Ca garnets (<1.8 wt% CaO, see Grutter et al. (1999)) with $Mg\#_{Ca\text{-}corr}$ of 92.

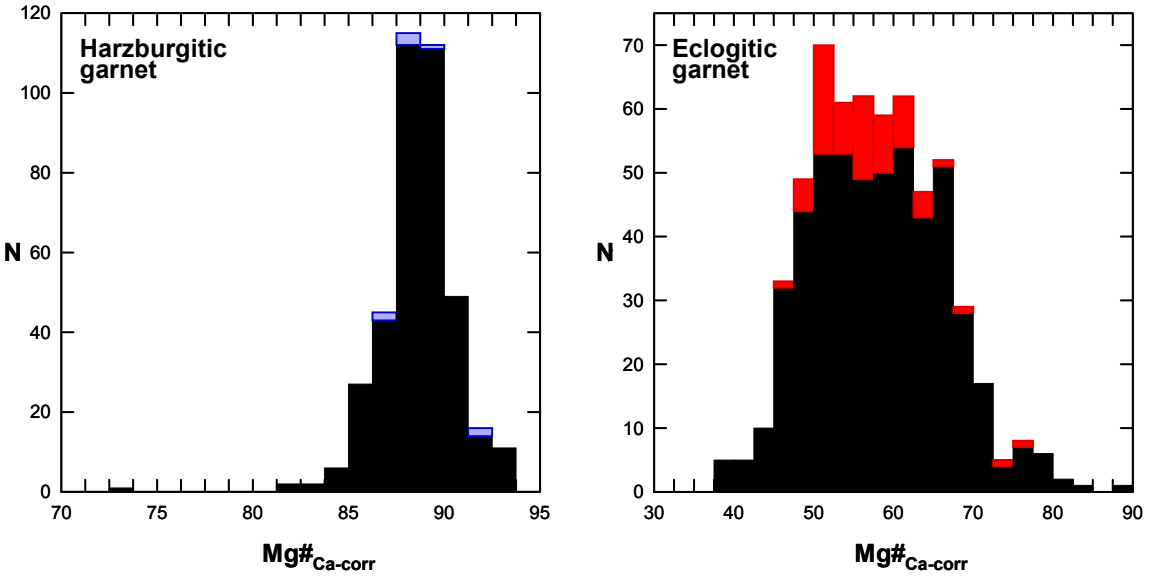

Figure 60 – Histograms showing the $Mg\#_{Ca\text{-}corr}$ (see text for definition) of garnet inclusions in diamonds of the harzburgitic and eclogitic parageneses. The worldwide database of Stachel and Harris (2008) is represented in black and the Ural garnets belonging to each suite are plotted in colour.

Stachel and Harris (2008) suggested that high TiO_2 contents (>0.04 wt%) in garnet may be indicative of metasomatic re-enrichment, as Ti is removed from garnet during melt depletion of cratonic peridotites. Accordingly, the Urals peridotitic garnets were divided into low- (≤0.04 wt% TiO_2) and high-Ti (>0.04 wt% TiO_2) groups. Four garnets (U1A, U3A, U4A and U29A) fall into the low-Ti group, although one of them (U1A) only by a small margin. The other four garnets belong to the high-Ti group, with Ti contents reaching as high as 1.0 wt% TiO_2 in sample U3A.

The high-Ti garnets also have the highest chromium content of the studied set, ranging from 11.05 to 14.91 wt% Cr_2O_3 (Figure 61). With respect to the Ural diamond source, these high-Cr, high-Ti harzburgitic garnets are likely to have formed under higher pressure conditions based on the Cr in garnet geobarometer of Grutter et al. (2006), and hence may indicate increasing metasomatism towards the base of the lithosphere (Stachel and Harris, 2008).

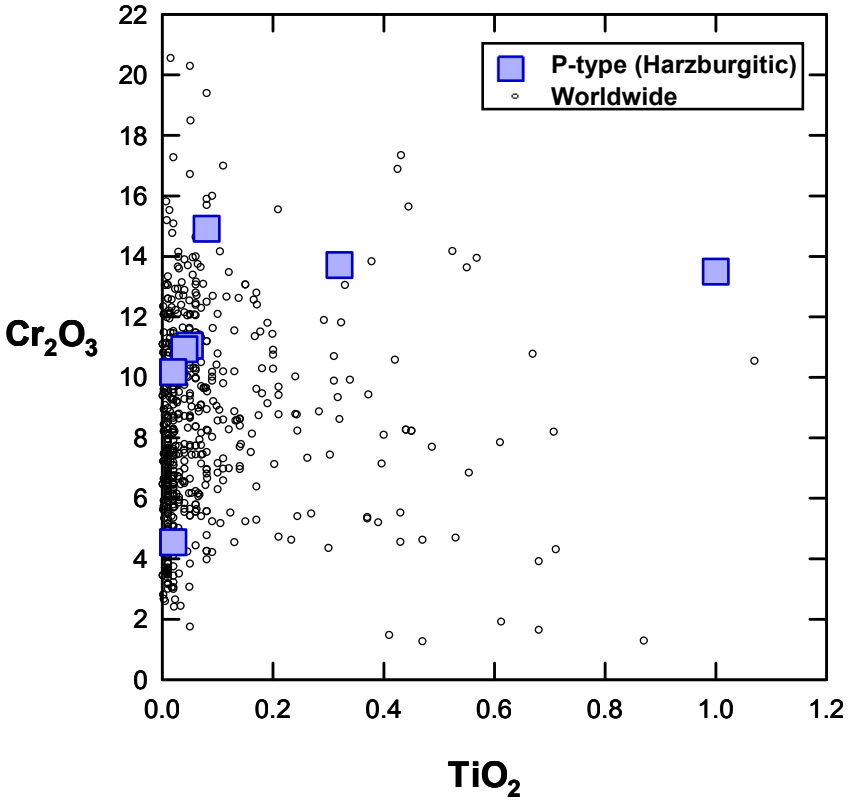

Figure 61 – Plot of TiO_2 versus Cr_2O_3 (wt%) for peridotitic garnet inclusions in diamonds. Worldwide data from Stachel and Harris (2008).

Taking the Al/Cr ratio in peridotitic garnets (Table A.3.1) as a measure of the fertility of the diamond source (Stachel and Harris, 1997), all peridotitic garnets, with the exception of grain U6A, are from highly depleted sources. The high (6.7) Al/Cr ratio of garnet U6A also reflects a low knorringite content [100 Cr/(Cr+Al) = 13 mol%], characteristic of more fertile origin.

The atomic proportions of Si (calculated on a basis of 24 oxygens per formula unit) lie close to the ideal value of 6, and a majorite component (> 6.12 cations Si per formula unit based on 24 oxygens; see Irifune (1987)) is not considered to be present in the Ural garnets. However, one inclusion (U1B) has a value of 6.119 Si cations per 24 oxygens, which is very close to the "normal" garnet / majorite garnet boundary referred above. Applying the criteria of Irifune (1987), a pressure of up to about 70 kbar could be suggested for this garnet. Knorringite solubility in garnet is a function of bulk composition and is favoured mainly by pressure, thus being a good indicator for minimum crystallisation pressures (Brey et al., 1991). The low knorringite content [calculated as 100 Cr/(Cr+Al)] of 33.4 mol% in grain U1B does not suggest unusually high (>70 kbar) crystallisation pressures for this garnet.

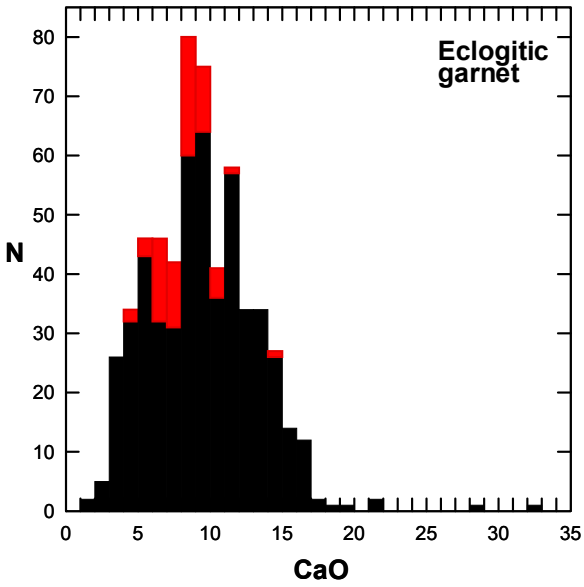

Figure 62 – Histogram showing the CaO content (wt%) of eclogitic garnet inclusions in diamonds. Urals inclusions shown in red and worldwide data (Stachel and Harris, 2008) in black.

All eclogitic pyrope-almandines have extremely low Cr_2O_3 contents (maximum Cr_2O_3 = 0.08 wt%) and therefore plot well below the 1% cut-off between eclogitic and peridotitic garnets of Grutter et al. (2004) in Figure 59. With the exception of six garnets with CaO < 6 wt% which plot in the low-Ca (G4) field of the classification scheme of Grutter et al. (2004), all grains are high Ca (G3) eclogitic garnets. A histogram of the CaO content of eclogitic garnets (Figure 62), shows a predominance of values around 7-9 wt% CaO, with only one grain (U49A) having very high CaO contents (14.66 wt%).

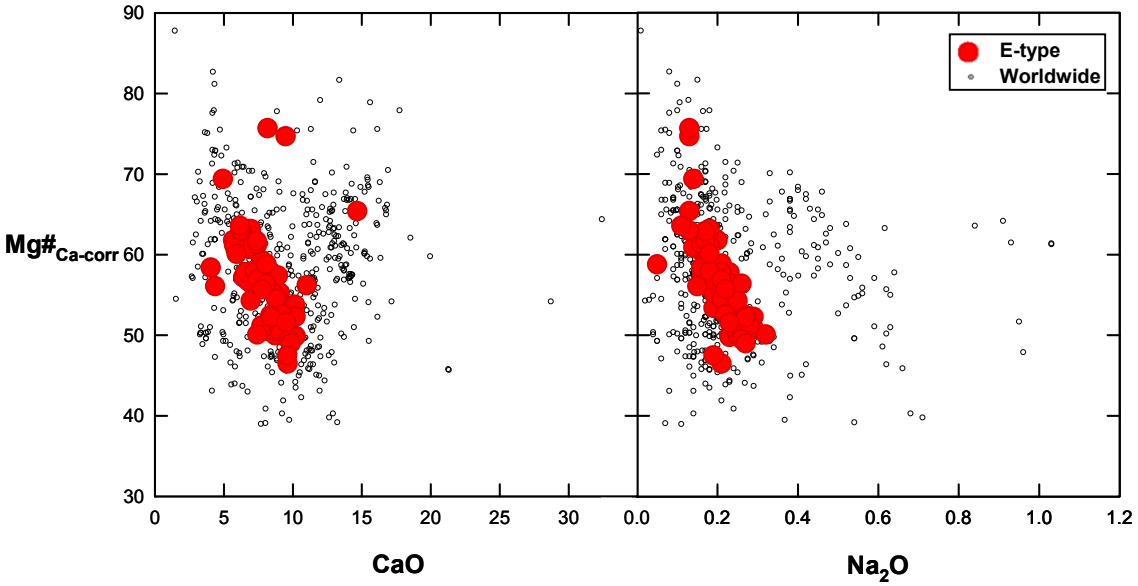

Figure 63 – CaO and Na_2O content (wt%) versus $Mg\#_{Ca\text{-}corr}$ (see text for definition) for eclogitic garnet inclusions in diamonds. Worldwide data from Stachel and Harris (2008).

The eclogitic garnets have $Mg\#_{Ca\text{-}corr}$ ranging from 46 to 76 (see Figure 60), which is reflected in pyrope contents from 32-59 mol%. Figure 63 shows that for values of $Mg\#_{Ca\text{-}corr} < 65$ a negative correlation exists between CaO contents and $Mg\#_{Ca\text{-}corr}$. A strong negative correlation between $Mg\#_{Ca\text{-}corr}$ and Na_2O is also evident from Figure 63. A similar correlation (though at lower Na_2O contents) was observed for Argyle eclogitic garnets by Jaques et al. (1989) who interpreted it as indicating the presence of recycled crustal materials. On a cation basis, Na is positively correlated with P and Ti, a slight excess of Na over Ti being present, as was also noticed by Stachel and Harris (2008) for several diamond mines worldwide.

5.4.2 *Clinopyroxene*

Clinopyroxene (17 inclusions recovered from 14 diamonds) occurs in the Ural diamonds samples either as a single inclusion or together with other mineral phases, namely olivine or eclogitic garnet (see Table 11). Similarly to the garnet inclusion population, the eclogitic suite predominates, 16 grains being pale green omphacites and one grain a colourless websteritic clinopyroxene. The chemical composition of clinopyroxene inclusions is presented in Table A.3.3.

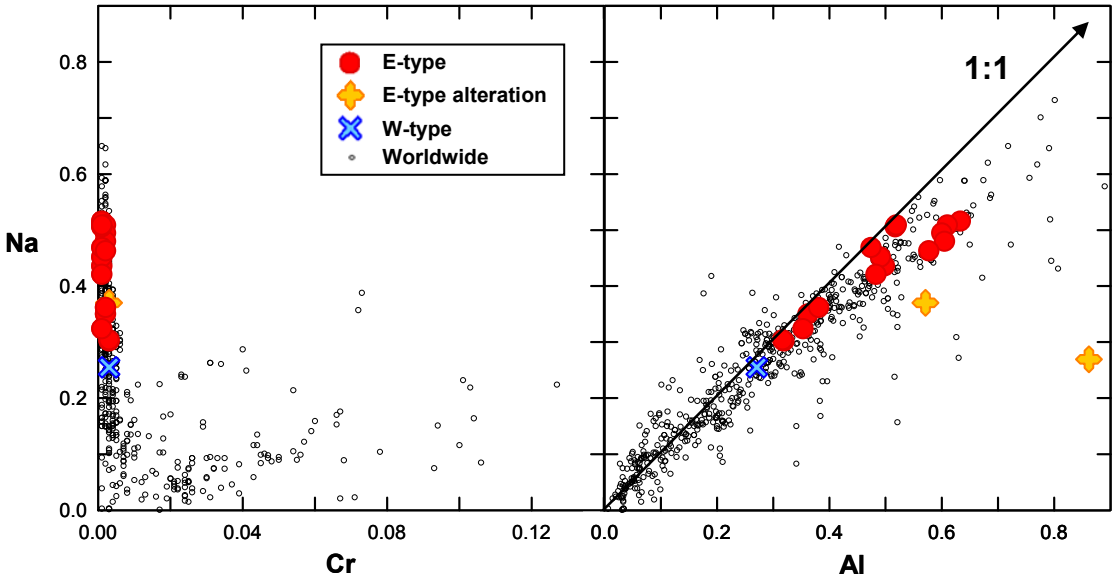

Figure 64 – Cr and Al versus Na (cations, calculated for 6 oxygens per formula unit) for clinopyroxene inclusions in diamonds. The Urals websteritic clinopyroxene shows a near 1:1 correlation between Al and Na, which indicates Na accommodation as a jadeite component. For eclogitic clinopyroxenes, excess of Al over Na indicate the presence of an additional Tschermaks component. Worldwide data from Stachel and Harris (2008).

The clinopyroxene U23A coexists with olivine in the same diamond. As it is compositionally distinct from the typical peridotitic clinopyroxene inclusions in diamond (see Stachel and Harris, 2008), a websteritic parageneses has been suggested for this grain. This inclusion has a Mg# of 76 and a Ca# of 49 mol% (Table A.3.3). It is poor in chromium (Cr_2O_3 = 0.12 wt%) and potassium (K_2O = 0.07 wt%), and the Cr# value of 1 is more typical of eclogitic clinopyroxenes. Sodium is intermediate between the peridotitic and eclogitic suites (Na_2O = 3.59 wt%). Although slightly Al-rich, a correlation of almost 1:1 exists between Na and Al, indicating that Na is accommodated as a Jadeite ($NaAlSi_2O_6$) component (Figure 64).

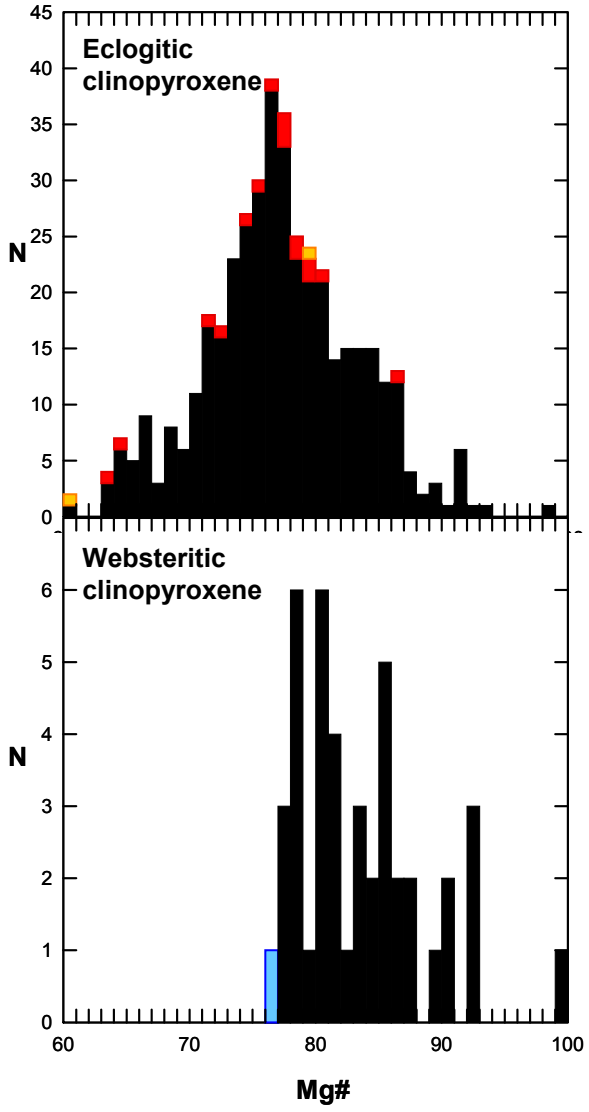

Figure 65 – Histograms showing the Mg# of clinopyroxene inclusions in diamonds of the eclogitic and websteritic parageneses. The Urals clinopyroxenes belonging to each suite are represented in colour and worldwide data in black (worldwide database of Stachel and Harris (2008)). Note the Mg# values of the two exsolved phases from an eclogitic zoned clinopyroxene shown in yellow.

The eclogitic omphacites recovered from the Ural diamonds have Mg# between 74-86, with the exception of grains U37A and U37B (coexisting in the same diamond) which have a lower Mg# of 64 (see Figure 65). The Ca ratio ranges from 27.2 to 46.7 mol% and Cr_2O_3 contents are very low (0.03-0.12 wt%), resulting in low Cr# values of 0.2 to 1.0. The omphacites are rich in Al (7.50-15.34 wt% Al_2O_3), which is in excess over Na (Figure 64) indicating the presence of a Tschermaks ($(Fe,Mg)^{vi}Si^{iv} \leftrightarrow Al^{vi}Al^{iv}$) component. Potassium contents are low, ranging from 0.09-0.45 wt% K_2O (Figure 66). These values may be indicative of a low pressure of crystallisation in a relatively K-poor environment (Harlow and Davies, 2004).

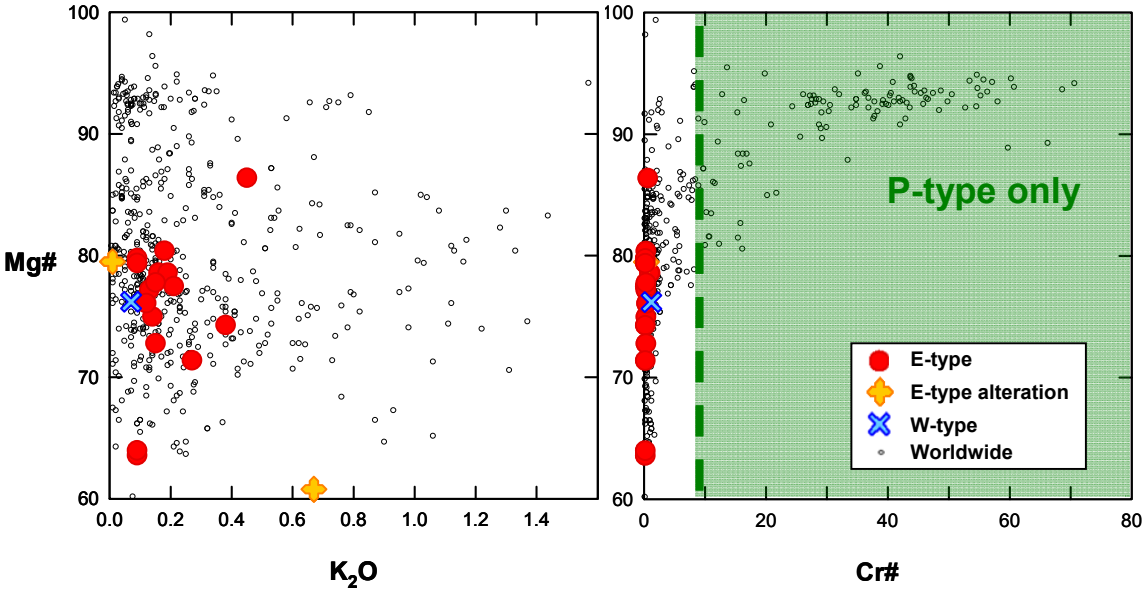

Figure 66 – The K_2O content (wt%) and Cr# versus Mg# for clinopyroxene inclusions in diamonds. Note that peridotitic clinopyroxenes would only occur at Cr# higher than 7 (green field). Worldwide data from Stachel and Harris (2008).

The variations in the major components of coexisting eclogitic clinopyroxene and garnet inclusions are represented in Figure 67. The Ca-Mg-Fe compositions of the Urals garnet-clinopyroxene pairs are within the range of diamond inclusions worldwide (Stachel and Harris, 2008). The inclusions are likely to have coexisted in equilibrium conditions, as there is no overlap or cross cutting between any of the tie lines connecting the inclusion pairs (Rickard et al., 1989).

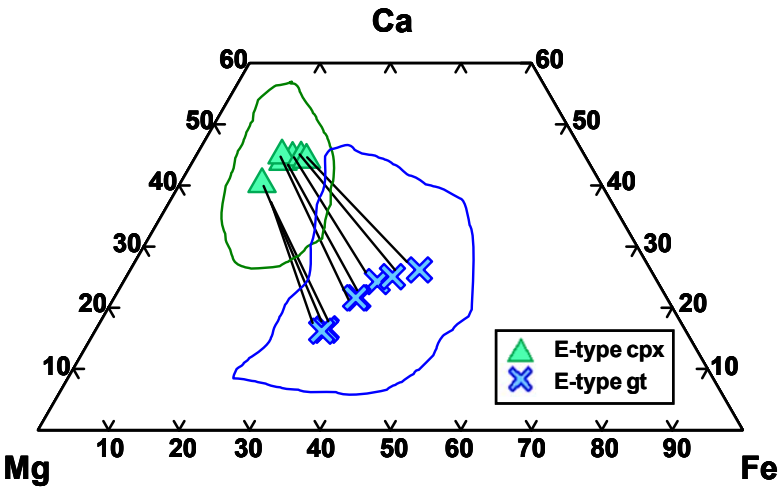

Figure 67 – Ca-Mg-Fe (atomic proportions) ternary diagram showing Urals eclogitic garnet-clinopyroxene inclusion pairs relative to their worldwide compositional fields (green and blue lines for clinopyroxene and garnet, respectively). The tie lines connect the Urals inclusions coexisting in single diamonds. Worldwide data used to plot the compositional fields is from Stachel and Harris (2008).

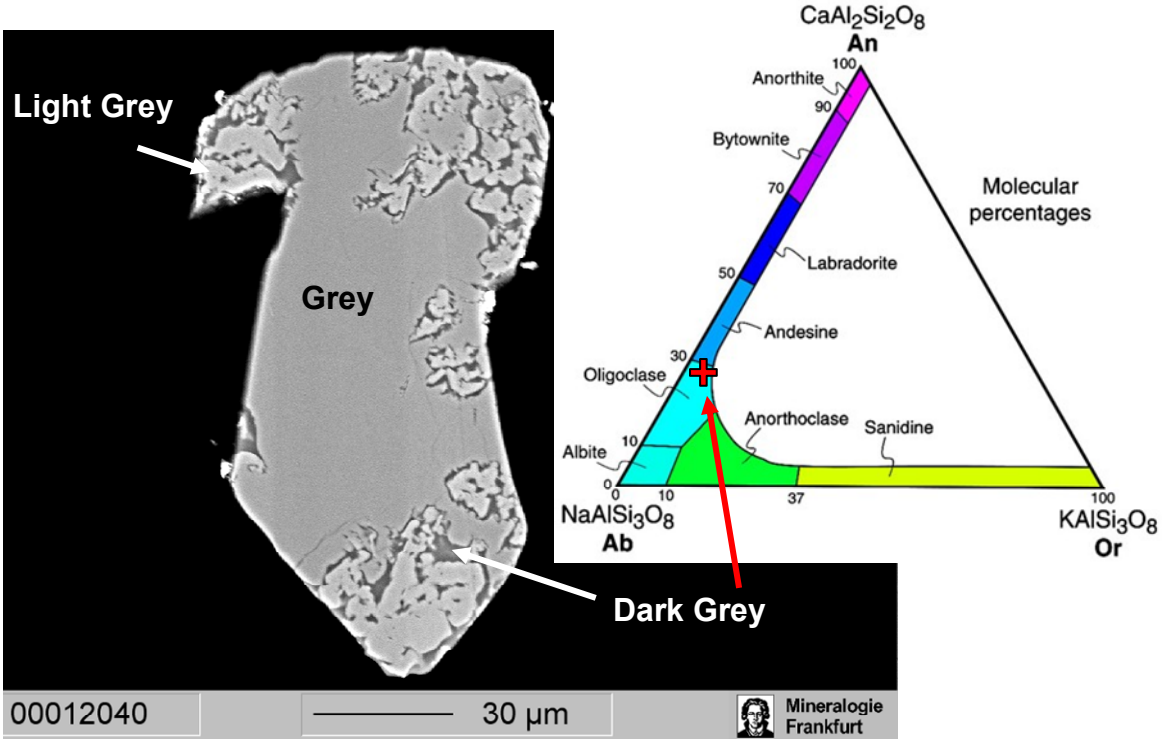

Figure 68 – Electron backscattered image of the clinopyroxene U13A. Note the three different phases (grey, light grey and dark grey) present. The composition of the dark grey phase in terms of its Ab-An-Or components is represented in the feldspar ternary by a red cross.

Sample U13A was the only silicate inclusion that showed a compositional variation. As shown by the electron backscattered image (Figure 68), three different phases (grey, light

grey and dark grey in order of abundance) are present in this mineral. As shown in Table A.3.3, the compositions for the two main phases could be determined accurately. Measurements of the dark grey phase closed at a total of 97.73 wt% and therefore the values obtained may not be representative of a true composition. The main grey phase is a typical eclogitic clinopyroxene. The chemistry of the minor dark grey phase fits that of a sodic plagioclase approximating to oligoclase (see Figure 68), but the phase has abnormally high Mg and Fe contents. These latter elements were probably "picked up" from the surrounding phases during analysis because of the beam size resolution. The light grey phase approximates to a clinopyroxene but is depleted principally in SiO_2, is K-free and is very enriched in Ca (Table A.3.3). The chemical analyses of the two minor peripheral phases in clinopyroxene U13A are best explained by partial alteration of the main inclusion probably by introduction of a Si-enriched fluid through a crack.

5.4.3 *Orthopyroxene*

The 6 colourless enstatite inclusions analysed in this study were all recovered from the same diamond. Their chemical compositions are very similar with a Mg# of 90 (Table A.3.4). The high calcium contents (0.59-0.63 wt% CaO) indicate that these enstatites could have crystallised in equilibrium with clinopyroxene and therefore a lherzolitic origin would be possible (Stachel et al., 1998) (Figure 69).

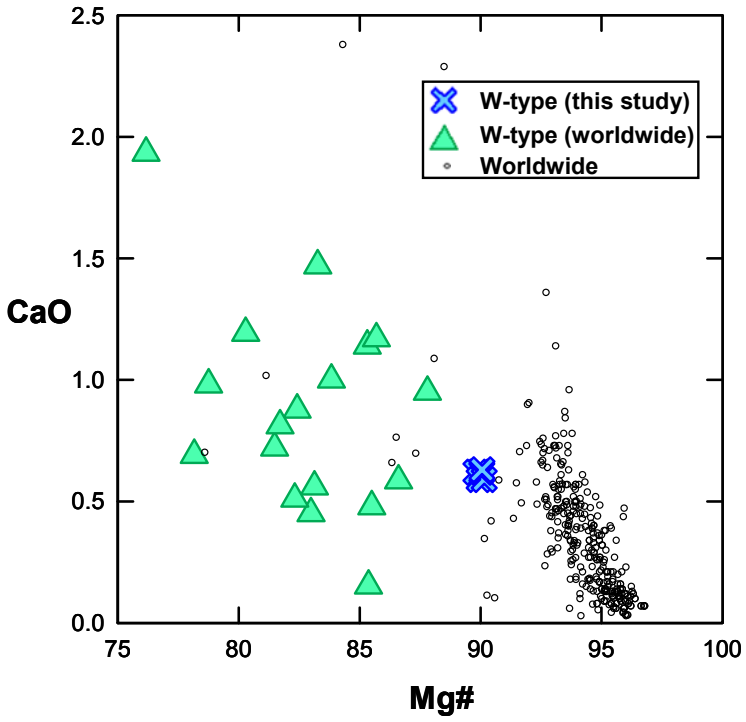

Figure 69 – CaO (wt%) versus Mg# for orthopyroxene inclusions in diamonds. Worldwide data from Stachel and Harris (2008).

However, adopting the classification scheme suggested by Stachel and Harris (2008), which allocates orthopyroxenes to the websteritic suite if the Mg# is <86, or Na_2O >0.25 wt%, or TiO_2 >0.12 wt%, such an origin for the studied orthopyroxenes seems likely. Although both Mg# and TiO_2 contents (0.08-0.09 wt% TiO_2) do not meet the condition referred above, the very high Na contents measured (0.35-0.39 wt% Na_2O) (Figure 70) are typical of the websteritic clinopyroxene inclusions that have been analysed worldwide (Stachel and Harris, 2008).

The enstatite inclusions are very poor in Cr (0.09-0.10 wt% Cr_2O_3) and rich in Al (1.17-1.20 wt% Al_2O_3). Similarly low Cr contents were reported by Tappert et al. (2005) for a websteritic orthopyroxene from Jagersfontein (South Africa) thus further supporting a websteritic origin for the orthopyroxenes analysed in the present study.

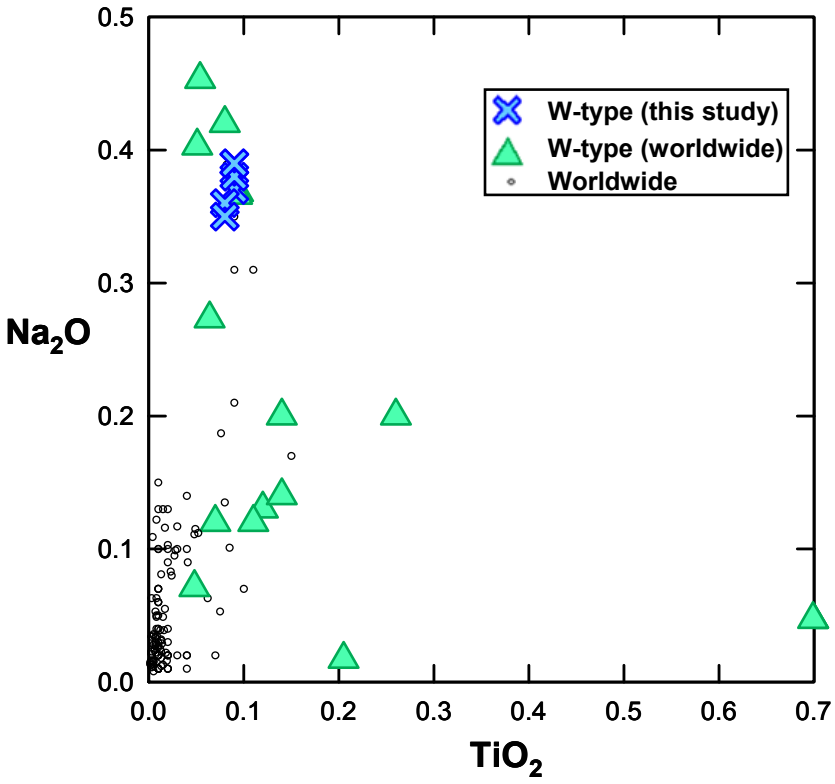

Figure 70 – Na_2O versus TiO_2 (wt%) for orthopyroxene inclusions in diamonds. The Urals orthopyroxenes have Na_2O >0.25 wt% and hence were allocated to the websteritic paragenesis, following the suggestion of Stachel and Harris (2008). Worldwide data from Stachel and Harris (2008).

5.4.4 *Olivine*

The 19 colourless olivine inclusions (released from 16 diamonds) were found mostly as single grains but occasionally with other mineral phases, mostly garnet (see Table 11).

Chemical compositions are presented in Table A.3.5. The forsterite content ranges from 91.1 to 95.6 mol%, excluding one grain (U23B) with 83.2 mol% which will be treated separately (see below). The 5 olivines coexisting with harzburgitic garnet have a range of Mg# between 92.2 and 95.6. The two grains (U1C and U1D) with the lower Mg# coexist with two harzburgitic garnets which also have low Mg#, therefore representing a slightly less depleted diamond source. The Mg# in the remaining harzburgitic olivines is consistent with the worldwide average of 93.2 (Stachel and Harris, 2008). Grain U5C, with the highest Mg# (95.6), coexists with two garnets showing the highest $Mg\#_{Ca\text{-}corr}$ of the studied set, therefore suggesting diamond formation in an extremely depleted source.

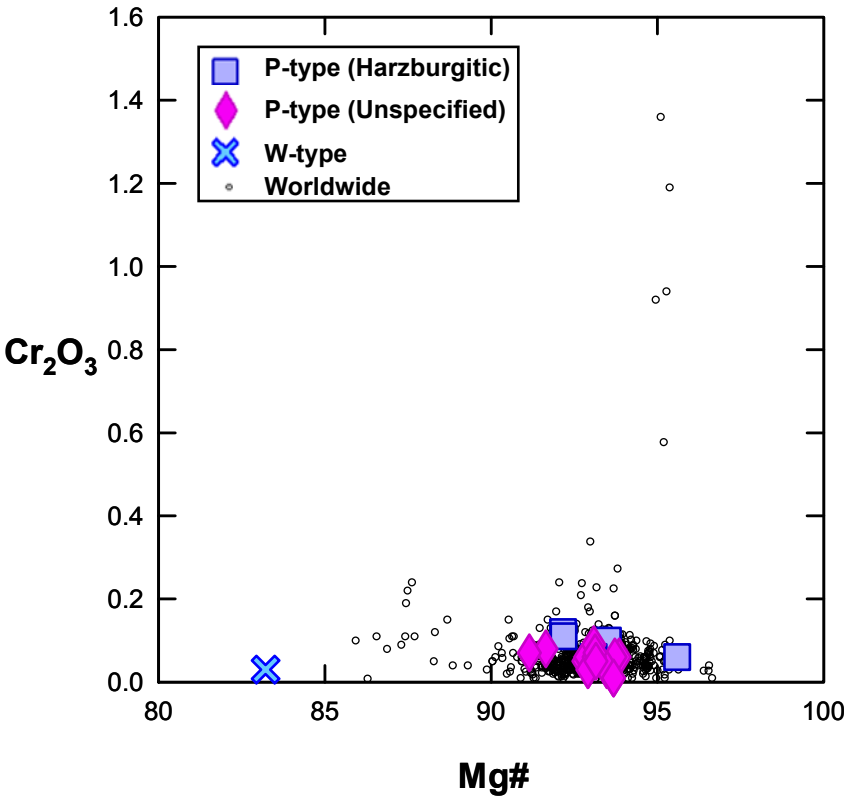

Figure 71 – Cr_2O_3 (wt%) versus Mg# for olivine inclusions in diamonds. Worldwide data from Stachel and Harris (2008).

Nickel contents range from 0.34 to 0.39 wt% NiO and are in agreement with the worldwide average of 0.36 wt% (Stachel and Harris, 2008). For chromium (0.01-0.12 wt% Cr_2O_3), harzburgite inclusions have the higher content of the set analysed (0.06-0.12 wt% Cr_2O_3), all values falling within the compositional range defined by the worldwide database (Figure 71). Calcium contents are variable (0.01-0.07 wt% CaO) but low, reflecting the Ca-depletion of the source region (Figure 72). Sodium contents are too low (0.00-0.03 wt% Na_2O) to allow accurate correlations with other elements to be made.

Nevertheless, this is a common feature of olivines of the harzburgitic paragenesis, as reported by Stachel and Harris (2008).

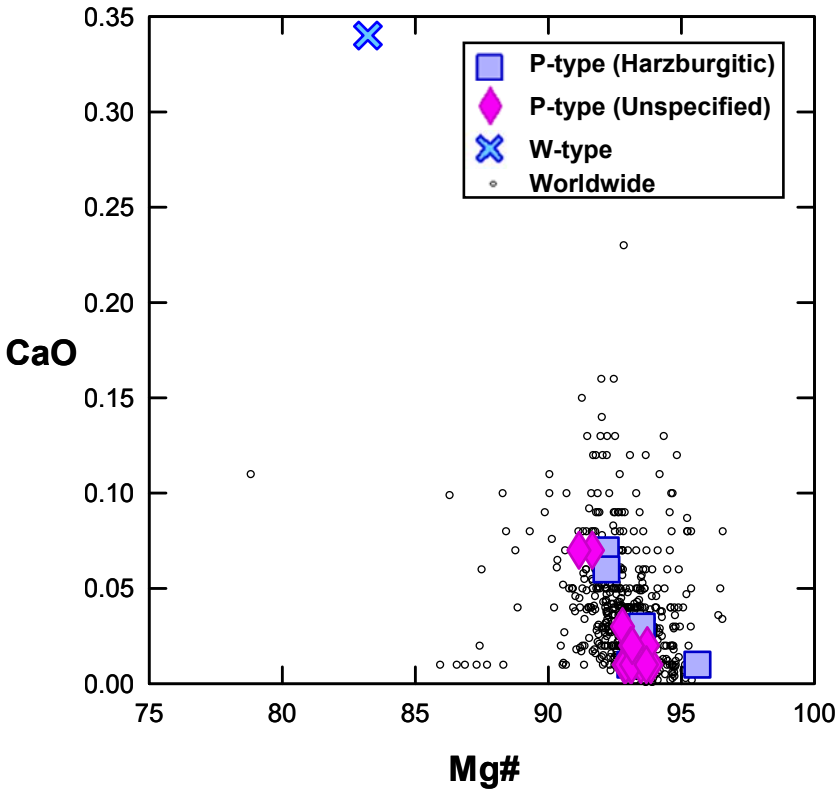

Figure 72 – CaO (wt%) versus Mg# for olivine inclusions in diamonds. Worldwide data from Stachel and Harris (2008).

As mentioned above, one olivine (U23B) is chemically distinct from the rest of the set. It coexists with clinopyroxene U23A in diamond D84 (see 5.4.2). The Mg# is very low (83.3), see Figure 71, as well as the nickel contents (0.19 wt% NiO). Manganese and total iron contents are extremely high (0.23 wt% MnO; 15.75 wt% FeO) by comparison with the worldwide average of 0.10 wt% and 6.97 wt%, respectively. Calcium contents are much higher (0.34 wt% CaO) than the highest value reported for a peridotitic olivine inclusion (0.23 wt% CaO) and imply diamond formation in a much more fertile source than the one that originated the other olivine-bearing diamonds. Thus, and in agreement with the analysis of the associated clinopyroxene, a websteritic, rather than peridotitic, origin seems likely for this olivine grain.

5.4.5 *Chromite*

With the exception of one grain where it coexists with garnet, dark cherry-red chromites (12 inclusions released from 7 diamonds) occur as separate grains within the diamond host.

One chromite inclusion was lost during the polishing process. Another grain (U8A) had a "rotten" appearance and, even though it was re-polished and re-analysed several times, its highly irregular surface did not permit an accurate chemical composition to be obtained. The chemical compositions of the remaining chromites are listed in Table A.3.6. Ferric iron (Fe^{3+}) contents have been calculated from stoichiometry using the method proposed by Droop (1987).

The Mg# values range between 63-71 and Cr# from 80-89 (Figure 73). All grains derived from "normal" peridotitic sources, as experimental data (e.g. Doroshev et al., 1997) shows that only chromites with Cr# of at least about 80 are stable in cratonic lherzolites and harzburgites within the diamond stability field. The lack of associations of chromite with other minerals does not allow the exact paragenesis to be known, except for sample U29B, which coexists with a harzburgitic garnet and has Mg# and Cr# of 67 and 88, respectively.

The chromites have FFM ratios [FFM ratio = $100Fe^{2+}/(Fe^{2+}+Mg)$] between 29.3-37.0 mol% (Figure 74) and the recalculated ferric iron ratio [$100Fe^{3+}/(Fe^{3+}+Fe^{2+})$] ranges from 2.9 to 22.70 mol%. Two chromites coexisting in the same diamond (U12a and U12B) have the lowest ferric iron ratio of the analysed set (2.9 and 10.8 mol%, respectively) and this may indicate a growth environment that is more reduced than usual (Figure 73).

Zinc contents (see Figure 73) range between 0.03-0.10 wt% ZnO and are consistent with the worldwide database. Silica contents (0.14-0.25 wt% SiO_2) are "normal" to slightly Si-rich when compared with the worldwide database (Figure 74). Manganese is also very constant, with MnO ranging from 0.25 to 0.29 wt%. The harzburgitic chromite has the same unusual enrichment in Ti (0.66 wt% TiO_2) as the garnet which coexists with it. This suggests an unusually Ti rich environment during diamond formation. All other chromites have variable Ti contents, ranging from 0.03-0.40 wt% TiO_2.

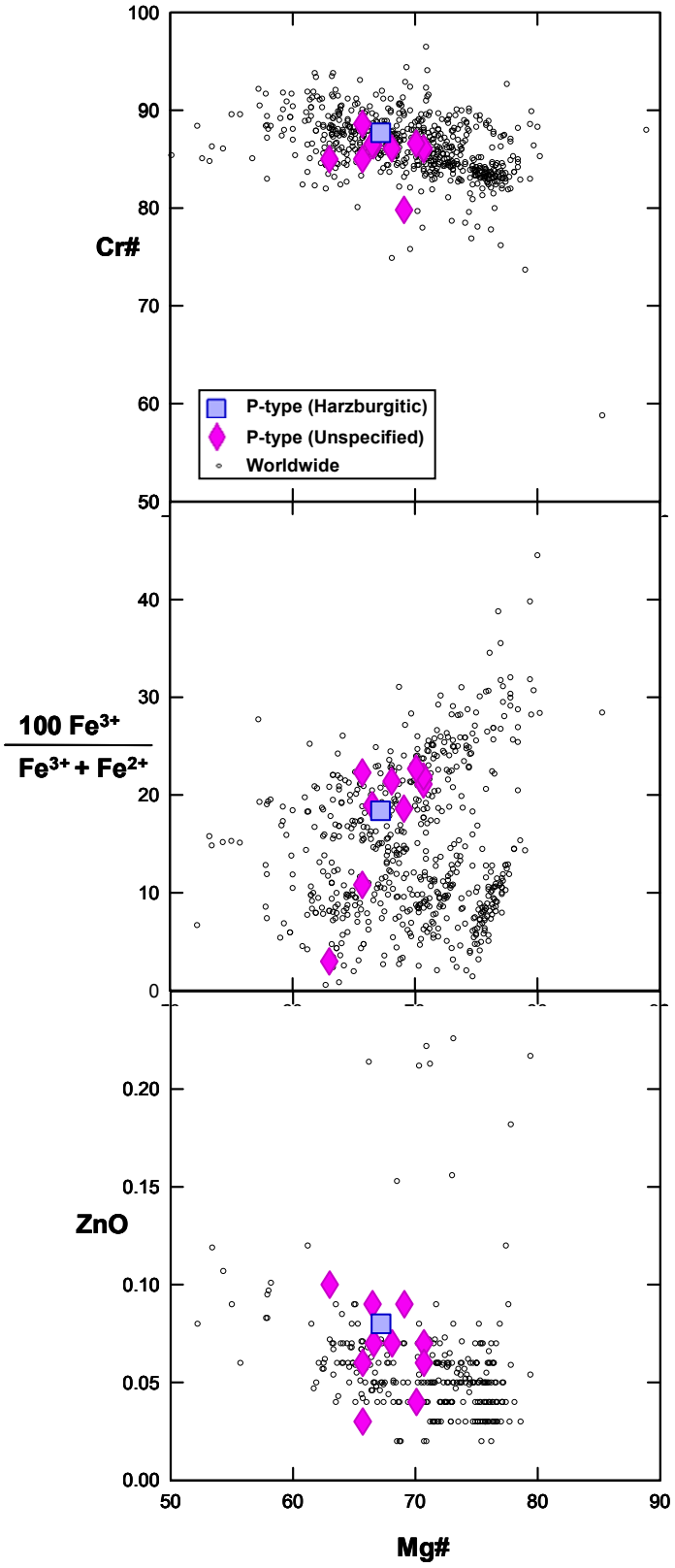

Figure 73 – ZnO content (wt%), molar ferric iron and Cr# versus Mg# for chromite inclusions in diamonds. Ferric iron (Fe^{3+}) contents calculated from stoichiometry after Droop (1987). Worldwide data from Stachel and Harris (2008).

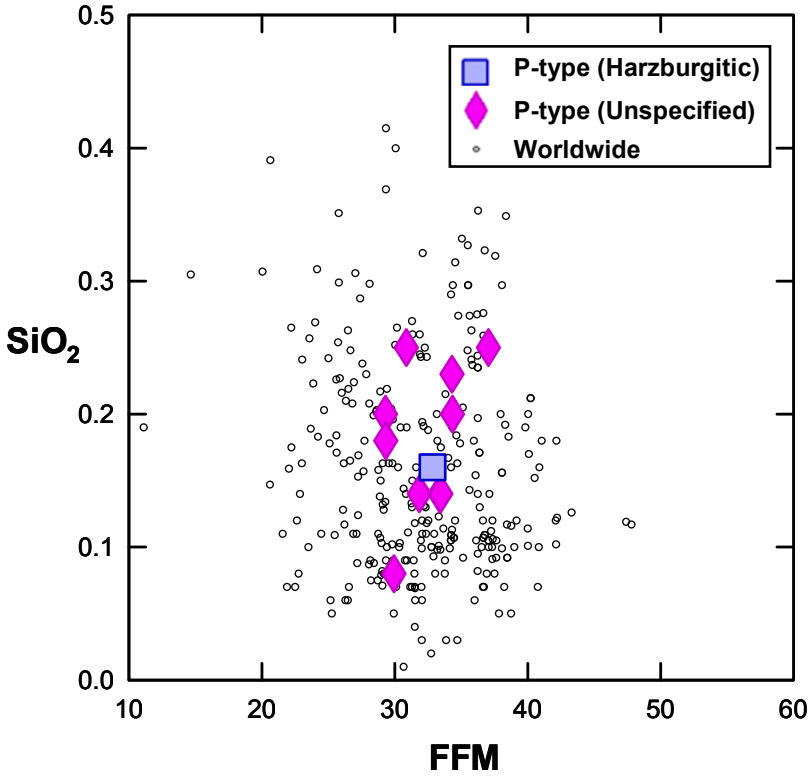

Figure 74 – SiO_2 (wt%) versus FFM (see text for definition) for chromite inclusions in diamonds. Worldwide data from Stachel and Harris (2008).

5.4.6 *Rutile*

One brown rutile inclusion was recovered from a diamond which also contained two pyrope-almandine garnets and 2 sulphides, showing that the rutile belongs to the eclogitic paragenesis. Elemental abundances for the rutile inclusion are listed in Table A.3.7 and fall within the ranges of the worldwide database.

5.4.7 *Kyanite*

Two light blue kyanite inclusions, occurring as isolated crystals, were released from 2 diamonds. Their chemical composition is given in Table A.3.8. Both inclusions have the same silica content (36.90 wt% SiO_2), with aluminium ranging from 61.64 to 62.05 wt% Al_2O_3. Total iron varies from 0.24-0.39 wt% FeO, titanium between 0.14-0.30 wt% TiO_2 and magnesium from 0.10-0.18 wt% MgO.

5.4.8 *Coesite*

Six colourless coesite inclusions (released from 5 diamonds) were found as isolated grains or associated with other mineral phases. Chemical compositions are presented in Table A.3.9. Coesite is assigned to the eclogitic paragenesis, as grains U42E and U85C coexist with E-type garnet and an E-type garnet + clinopyroxene assemblage, respectively.

5.4.9 *Sulphide*

A total of 41 sulphide inclusions (released from 24 diamonds) were analysed. All inclusions were surrounded by metallic black, rosette-, or disc-shaped fracture systems which did not reach the surface of the diamond host. Within the diamond, the typical chalcopyrite yellow colour of the sulphide at the centre of the rosette fractures was invariably masked due to total reflection, and a colourless or white appearance was commonly observed. The sulphides occur as separate single grains (15 inclusions) or in association with silicate minerals of the eclogitic paragenesis (26 inclusions).

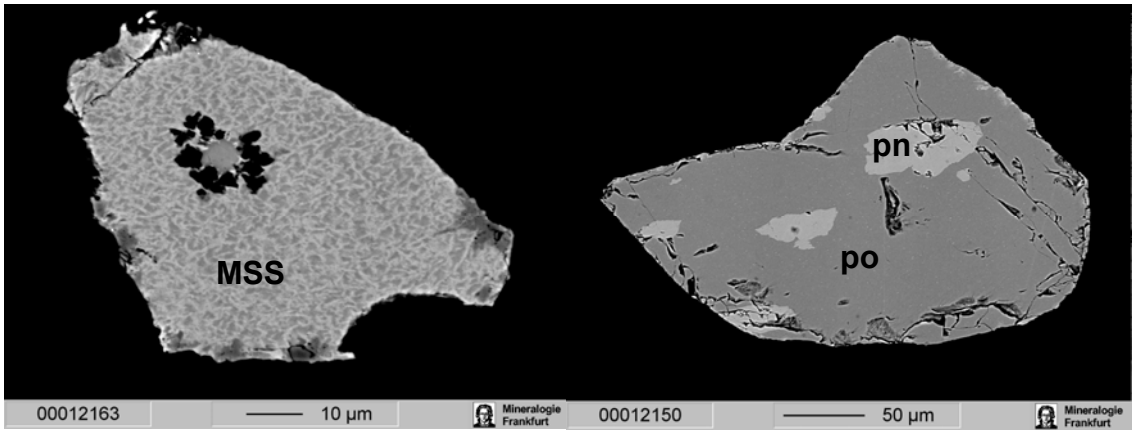

Figure 75 – Backscattered electron images of a monosulphide solid solution (MSS) grain (sample U65A, left) and a pyrrhotite (po) grain with pentlandite (pn) exsolutions (Sample U54A, right).

The majority of the sulphide inclusions analysed are polyphase grains showing intense sub-solidus re-equilibrations into several low-temperature phases. Careful backscattered electron (BSE) imaging and multiple analyses were made on each inclusion to accurately define the composition of each phase. By observation of the BSE images (see Figure 75), it was commonly found that a mostly grey inclusion contained light grey (Ni-rich) and sometimes dark grey (Ni-poor) domains. Wherever possible, several spot measurements

were made on these individual exsolution phases to determine their chemistry. The chemical composition of the sulphide inclusions is presented in Table A.3.10.

According to the well-known phase relations of the Fe-Ni-S system (Craig and Kullerud, 1969), at 1 atm monosulphide FeS appears on the liquidus at about 1200 ºC and with decreasing temperature increasingly Ni-rich monosulphide solid solution (MSS) is precipitated from the sulphide melt. Subsequent sub-solidus exsolutions lead to a mineral sequence pyrite (py), pyrrhotite (po), pentlandite (pn), chalcopyrite (cp), cubanite (cu), and heazlewoodite (hz), as temperature decreases (Craig and Kullerud, 1969).

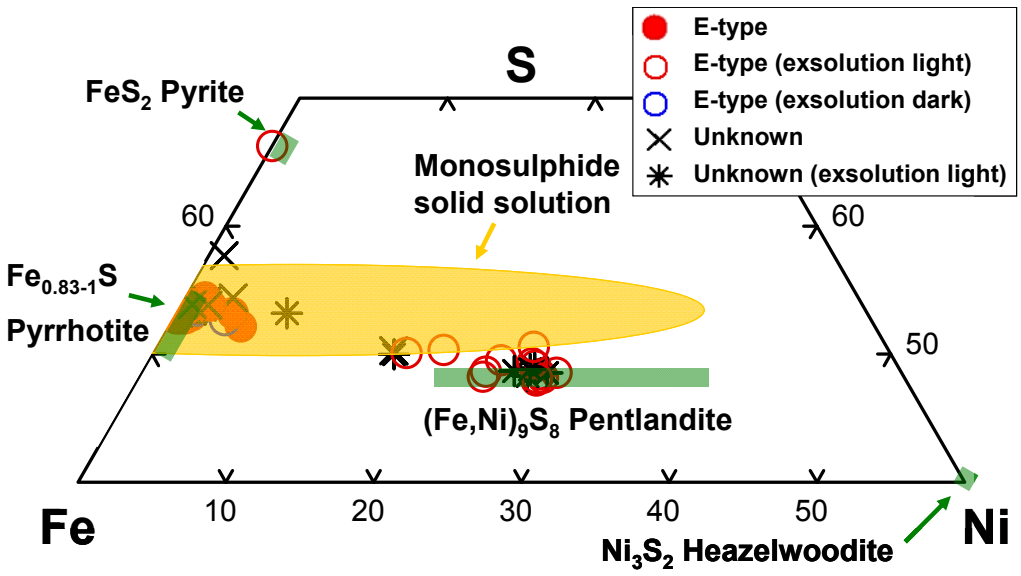

Figure 76 – The composition of the sulphide inclusions from the Ural diamonds in the Fe-Ni-S quadrilateral (based on atomic proportions).

Figure 76 shows sulphide composition in terms of the ternary components Fe-Ni-S, together with the approximate extent of homogeneous MSS at 1 atm and 1000ºC. Eclogitic sulphides consist of a) MSS with Ni-richer and Ni-poorer domains (grain U2A has a small blocky pentlandite exsolution); b) pyrrhotite with or without small blocks or lamellae of pentlandite; and c) pyrrhotite with small exsolution blocks of chalcopyrite (grain U85D). Sulphide inclusions of unknown paragenesis consist of a) MSS with or without Ni-richer and Ni-poorer domains (grain U70A has small blocky pentlandite exsolutions); b) pyrrhotite with or without small blocks or lamellae of pentlandite; and c) Cu-rich MSS with Cu-poor MSS lamellae (inclusion U69A).

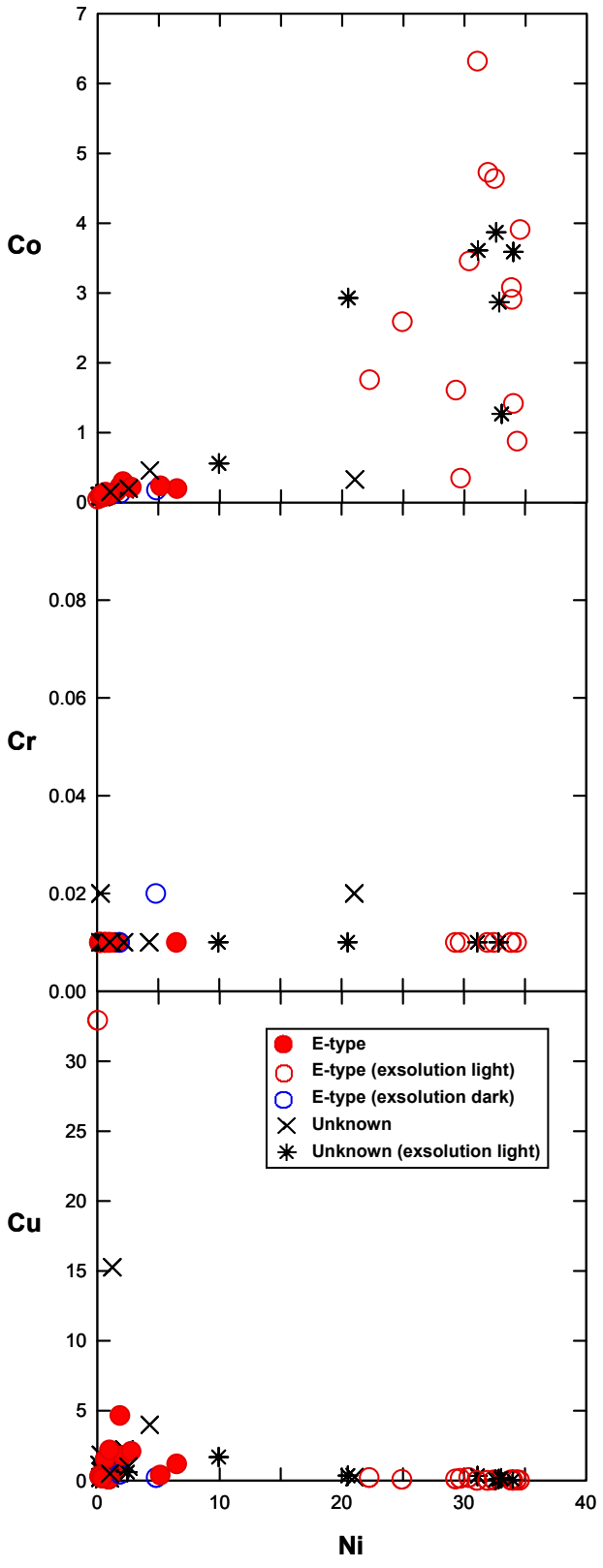

Figure 77 – Co, Cr and Cu versus Ni (wt%) for sulphide inclusions from the Ural diamonds. Note that only the exsolved phases have Ni contents >22 wt% and Co contents >1 wt%. Cr contents are low in all sulphide phases.

In the common case that coexisting silicate or oxide inclusions are absent, Bulanova et al. (1996) assigned Ni-rich (22-36 wt% Ni) sulphide inclusions to the peridotitic paragenesis

and Ni-poor (0-12 wt% Ni) ones to the eclogitic paragenesis. The present study shows that this assumption is ambiguous for compositions determined by electron microprobe analysis, as a spot analysis carried on an exsolved phase of an eclogitic sulphide may give high Ni contents (>22 wt% Ni) which are "typical" of peridotitic sulphides (see Figure 77).

Figure 77 shows that Cr contents are low (<0.02 wt%) in both eclogitic and unknown sulphides, which according to Stachel and Harris (2008) may indicate a common eclogitic origin for all samples analysed. In the present study, however, no sulphide inclusions were associated with silicate minerals of the peridotitic paragenesis, and thus it was not possible to use the sulphide's Cr contents to discriminate between parageneses. Cobalt is also present in all inclusions analysed, but high (>2 wt% Co) concentrations are restricted to the Ni-rich exsolved phases (Figure 77). For eclogitic sulphides, Cu contents range from 0.01 to 4.66 wt% Cu, with the exception of the chalcopyrite exsolution in grain U85D, which has 32.94 wt% Cu.

Sulphides of unknown paragenesis have Cu contents ranging between 0.04-15.26 wt% Cu, the highest value measured on the main phase of a MSS inclusion (U69A). Excluding this grain, Cu contents are similar to the ones measured for the bulk of the eclogitic sulphides and range from 0.04-3.99 wt% Cu (Figure 77). In all sulphide inclusions, Se contents are at or below the detection level and Zn contents are very low (0-0.05 wt% Zn).

5.5 Geothermobarometry

Estimates of equilibration conditions for diamond formation are based on chemical analysis of the syngenetic inclusions, utilizing the various geothermometers and geobarometers that are also used in determining pressure and temperature regimes in which peridotite and eclogite xenoliths have crystallized (e.g. Boyd, 1973; MacGregor, 1974; Wood, 1974; Lindsley and Dixon, 1976; Mitchell, 1977; Wells, 1977; Ellis and Green, 1979; O'Neill and Wood, 1979; Irifune et al., 1982; Irifune and Hariya, 1983; Finnerty and Boyd, 1984; Nickel and Green, 1985; Powell, 1985; Krogh, 1988; Brey and Kohler, 1990; Brey et al., 1990; Griffin and Ryan, 1995; Canil, 1996; Ryan et al., 1996; Nimis and Taylor, 2000; Grutter et al., 2006).

There is no basic thermodynamic distinction between a geothermometer and a geobarometer, either may be considered as an exchange reaction that may be represented in *P-T* space by isopleths or isopartition curves (Finnerty and Boyd, 1984). Compositional analyses for the components involved in a particular exchange reaction define a curve in *P-*

T space. The intersection of two such curves defines a *P-T* point that, ideally, represents the conditions under which the mineral or rock was last equilibrated. Due to propagation of analytical errors, each one of the curves should be thought of as a band (Figure 78).

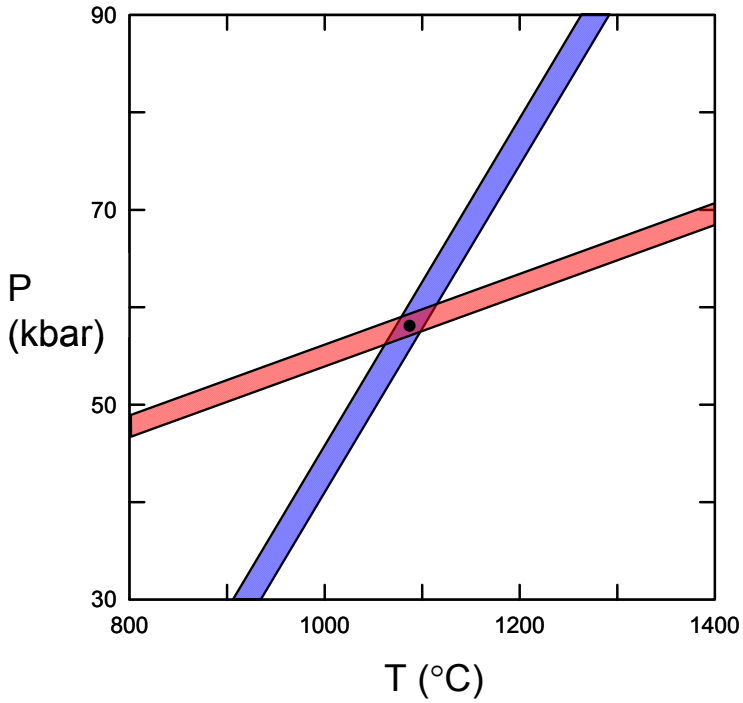

Figure 78 – Schematic illustration of the error bands produced by a geothermometer (in blue) and a geobarometer (in red). A P-T estimate is given by the central point (black dot) defined by the intersection of the two bands.

The precision of a *P-T* estimate is related to the area of the quadrilateral formed by the interaction of two such bands, whereas the accuracy is related to the localization of the central point defined by them (see Figure 78). The precision is maximized for bands that intersect at direct angles, and the width of the bands is minimized for reactions strongly affected by pressure or temperature (or both), using elements that can be analyzed precisely (Finnerty and Boyd, 1984).

When methods that incorporate analyses of many elements are used, or when the uncertainty in one determined element (e.g. Fe^{2+}/Fe^{3+}) is high, the propagation of analytical errors increases considerably, leading to the attainment of less precise values.

Despite the probability of error occurrence that the use of geothermometers and geobarometers always involves, the equilibration pressures and temperatures obtained for diamonds are, in most cases, within the same range (900 to 1300 ºC; 45 to 65 kbar) and are

similar to those obtained for most peridotite and eclogite xenoliths, including those which contain diamond (Meyer, 1985).

5.5.1 *Limitations and applicability*

Syngenetic mineral inclusions in diamond offer the opportunity to calculate the pressures and temperatures under which the diamonds originated. However, there are some problems related to the interpretation of such P-T estimates.

Single-mineral geothermobarometry (e.g. Nimis and Taylor (2000) for clinopyroxene) may result in the attainment of meaningful values for specific stages of diamond growth, especially when the inclusions are studied in situ, as shown by Bulanova (1995). However, the composition of single inclusions should not be used alone to estimate the P-T conditions of diamond crystallisation, as these conditions can only be uniquely constrained if all minerals of a given paragenesis coexist, in equilibrium, in the same diamond. Unfortunately, the occurrence of a full mineral assemblage in a single diamond is extremely rare, so it is common that pressure and temperature assumptions have to be made when making geothermobarometric calculations (e.g. Stachel et al. (1998) assume a pressure of 50 kbar to estimate temperatures and a temperature of 1150ºC to estimate pressures).

Another difficulty related to the geothermobarometric study of mineral inclusions is that they can occur as discrete crystals or as touching minerals in the diamond host. According to Sobolev et al. (1997), when two or more mineral phases are intergrown as a single inclusion, the estimation of pressure and temperature may reflect ambient conditions at the time the diamond was entrained in the kimberlite (and quenched by eruption), or may reflect heating events that would have occurred before or during kimberlite eruption. It is conceivable that touching crystals of such small dimension (~100 μm) will be able to re-equilibrate very quickly when subject to heating. Griffin et al. (1992; 1993) and Bulanova (1995), among others, have demonstrated that a set of minerals imprisoned in single diamonds may yield a wide range of temperatures, suggesting that at least some diamonds grew during heating or cooling events over significant temperature ranges.

If a diamond crystallises over a wide range of temperatures, the minerals trapped at different growth stages will not be in equilibrium with one another, even though each may have been in equilibrium with its immediate environment when it was captured. Stachel and Harris (1997) noticed, when studying non-touching inclusions in diamonds from the

Birim field, Ghana, that these produced highly inconsistent results (calculation of very low or negative pressures), suggesting that the inclusions have not grown simultaneously but were incorporated during successive stages of diamond growth. In these conditions, any estimate of pressure or temperature obtained by the combination of such minerals will not correspond to the real conditions of the diamond growth environment.

A comprehensive study of non-touching and touching inclusion pairs by Phillips et al. (2004b) strongly suggested that the non-touching inclusions record the conditions at the time of diamond crystallisation, whereas the touching inclusions reflect subsequent re-equilibration in a cooling (decrease in ambient temperature of about 150ºC) mantle until the time of kimberlite eruption. According to Stachel and Harris (2008), the majority of the inclusions (touching and non-touching) analysed worldwide reflect equilibration temperatures along conductive geothermal gradients equivalent to 36 to 42 mW/m^2 surface heat flow (calculated according to Pollack and Chapman (1977)) at pressures below 65 kbar. As a decrease in mantle ambient temperature of about 150ºC implies a decrease of about 2 to 3 mW/m^2 in the geothermal gradient, it can be reasonably assumed that conductive geotherms calculated for a surface heat flow between 36 and 38 mW/m^2 are more likely to represent conditions of mantle storage, rather than diamond formation. Based on this assumption, a conductive continental geotherm calculated for a 38 mW/m^2 surface heat flow will intercept the diamond-graphite univariant reaction curve of Kennedy and Kennedy (1976) at about 900ºC. This value is important when interpreting the results of geothermometric calculations, as it can be used as the lower cut-off for diamond formation temperatures.

Assuming an upper limit of 250 km for the subcratonic lithosphere (about 75 kbar, pressure gradient of 3.3 km/ kbar), an upper cut-off for diamond formation can be placed at 1400°C (Stachel and Harris, 2008) since higher temperatures exceed the intersection of a conductive geothermal gradient calculated for a 42 mW/m^2 surface heat flow with the mantle adiabat.

Touching inclusion pairs were not found in the diamonds analysed. It is assumed that the diamond hosts have not reacted with the enclosed minerals and have prevented the inclusions from reacting with each other, for that the chemical compositions of the inclusions can be considered representative of diamond formation. Therefore, pressure and temperature calculations based on the chemistry of the inclusions are interpreted as indicative of the P-T conditions of diamond formation and not of any later P-T event.

5.5.2 *Estimated P-T equilibration conditions for the Ural diamonds*

Equilibration pressures and temperatures for the Ural diamonds were estimated from the chemical composition of mineral inclusions pairs and single inclusions. Several geothermometers and geobarometers available for mantle silicate and oxide assemblages were applied and results are summarised in Table 14. To differentiate between diamonds and their inclusions (which are numbered separately), the suffix "D" was applied to the former, while the latter are designated in the text by the suffix "U". All geothermobarometric calculations were made using the *PT*-Excel software, developed by Dr. Thomas Kohler.

In agreement with previous geothermobarometric studies of mineral inclusions in diamonds from diverse worldwide sources (e.g. Stachel and Harris, 1997; Stachel et al., 1998; Phillips et al., 2004b) geothermometers were applied for an assumed pressure of 50 kbar and pressure was calculated using a temperature of 1150°C. All uncertainties are given as one standard deviation.

Diamond D84 contained a websteritic olivine (U23B) and clinopyroxene (U23A) inclusion pair that produced inconsistent results with independent geothermometers and geobarometers. For this diamond, the Ca content in olivine coexisting with clinopyroxene calibrated as a geothermometer (T_{KB}) of Kohler and Brey (1990) and the enstatite content in clinopyroxene geothermometer (T_{NT}) of Nimis and Taylor (2000), produce temperatures of 1625°C and 1011°C, respectively. Pressures of -15.9 and 27.1 kbar were obtained using the Ca content in olivine coexisting with clinopyroxene geobarometer (P_{KB}) of Kohler and Brey (1990) and the Cr-in-clinopyroxene geobarometer (P_{NT}) of Nimis and Taylor (2000), respectively. These results reflect disequilibrium between the inclusion phases probably due to incorporation of the two inclusions at different stages of diamond growth and thus will not be considered further.

For eclogitic garnet-clinopyroxene pairs, the Fe^{2+}/Mg exchange geothermometer of Krogh (1988) was used. The same exchange reaction was also used to estimate temperatures of harzburgitic olivine-garnet pairs, according to the calibration of O'Neill and Wood (1979), with corrections by O'Neill (1980). Considering the small number of samples analysed, both thermometers reflect similar thermal conditions (modes in class 1100 to 1150°C, mean of 1190±52°C for T_{Krogh} and 1200±114°C for $T_{O'Neill}$) for the two inclusion parageneses (see Figure 79).

Diamond	Inclusion	Paragenesis	Mineral	T_{KB}	T_{Krogh}	$T_{O'Neill}$	T_{BK}	T_{NT}	T_{Ryan}	P_{BKN}	P_{KB}	P_{NT}	P_{38}
D67	U1a, U1c	p(H)	gt, ol			1318							49.8
	U1b, U1d	p(H)	gt, ol			1339							49.6
D87	U3a, U3b	p(H)	gt, ol			1218							68.8
D148	U4a, U4b	p(H)	gt, ol			1067							61.1
D94	U5a, U5c	p(H)	gt, ol			1107							55.9
	U5b, U5c	p(H)	gt, ol			1130							55.7
D112	U29a, U29b	p(H)	gt, chr						972				55.0
D37	U6a	p(H)	gt										*[32.8]*
D99-C	U34a, U34b	e	gt, cpx		1250								
D99-E	U35a, U35c	e	gt, cpx		1216								
	U35b, U35d	e	gt, cpx		1204								
D16-B	U74b, U74d	e	gt, cpx		1261								
D122-B	U59a, U59b	e	gt, cpx		1131								
	U59a, U59c	e	gt, cpx		1130								
	U59a, U59d	e	gt, cpx		1142								
D132	U85a, U85b	e	gt, cpx		1193								
D84	U23a, U23b	w	ol, cpx	*[1625]*				*[1011]*			*[-15.9]*	*[27.1]*	
D16-A	U45a	w	opx				1105			52.2			
	U45b	w	opx				1107			52.4			
	U45c	w	opx				1093			53.2			
	U45d	w	opx				1092			52.2			
	U45e	w	opx				1102			53.4			
	U45f	w	opx				1111			53			
D115-B	U30a	p	chr						1079				
D60-C	U8a	p	chr						*[655]*				
	U8b	p	chr						1030				
	U8c	p	chr						1103				
D123	U31a	p	chr						1277				
D57-B	U12a	p	chr						*[880]*				
	U12b	p	chr						*[1509]*				
D38	U27a	p	chr						918				
D149	U28a	p	chr						1011				
	U28b	p	chr						1005				
	U28c	p	chr						948				

Table 14 – Geothermobarometry of mineral inclusions from the Ural diamonds. Temperature is given in ºC, pressure in kbar. Geothermometers were applied assuming a fixed pressure of 50 kbar and pressure was calculated assuming a temperature of 1150°C. T_{Ryan} is assumed to be independent of pressure. Values in square brackets indicate disequilibrium conditions and were not considered. *p*: peridotitic; *p(H)*: harzburgitic; *w*: websteritic; *e*: eclogitic; gt: garnet; ol: olivine; chr: chromite; cpx: clinopyroxene; opx: orthopyroxene.

T_{KB} (Kohler and Brey, 1990); T_{Krogh} (Krogh, 1988); $T_{O'Neill}$ (O'Neill and Wood, 1979; O'Neill, 1980); T_{BK} (Brey and Kohler, 1990); T_{NT} (Nimis and Taylor, 2000); T_{Ryan} (Ryan et al., 1996); P_{BKN} (Brey and Kohler, 1990); P_{KB} (Kohler and Brey, 1990); P_{NT} (Nimis and Taylor, 2000); P_{38} (Grutter et al., 2006).

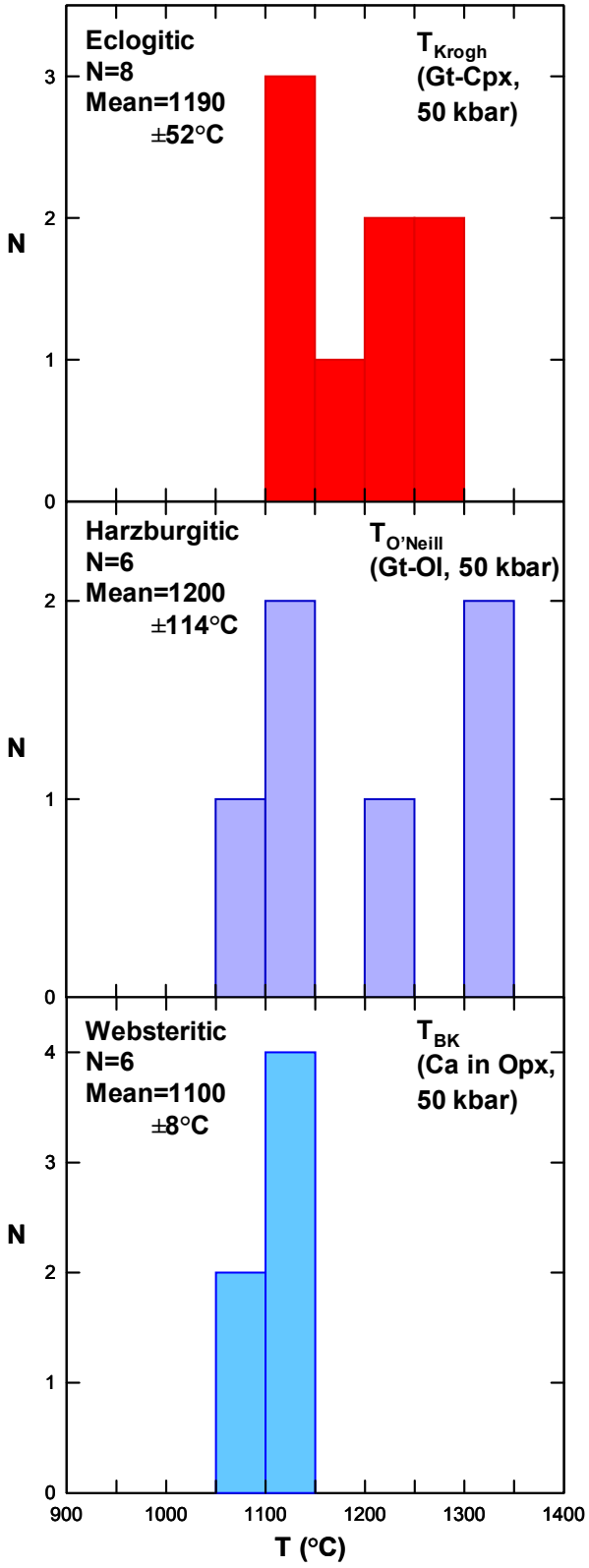

Figure 79 – Temperature estimates using (top to bottom) the Fe^{2+}/Mg exchange between garnet and clinopyroxene (Krogh, 1988), between garnet and olivine (O'Neill and Wood, 1979), and the Ca content in orthopyroxene assuming coexistence with clinopyroxene (Brey and Kohler, 1990). All geothermometers were calculated for an assumed pressure of 50 kbar. Notwithstanding the use of different geothermometers, the histograms show an overall agreement between the three inclusion parageneses.

Assuming crystallisation in equilibrium with clinopyroxene, the Ca content of orthopyroxene may be used to calculate temperatures (Brey and Kohler, 1990). The T_{BK} geothermometer was applied to the six websteritic orthopyroxenes recovered from diamond D16-A, producing a narrow temperature distribution with a mean of 1100±8°C and a mode in class 1100 to 1150°C (Figure 79). This range of estimated equilibration temperatures is in good agreement with those calculated for the eclogitic (T_{Krogh}) and harzburgitic ($T_{O'Neill}$) inclusion assemblages.

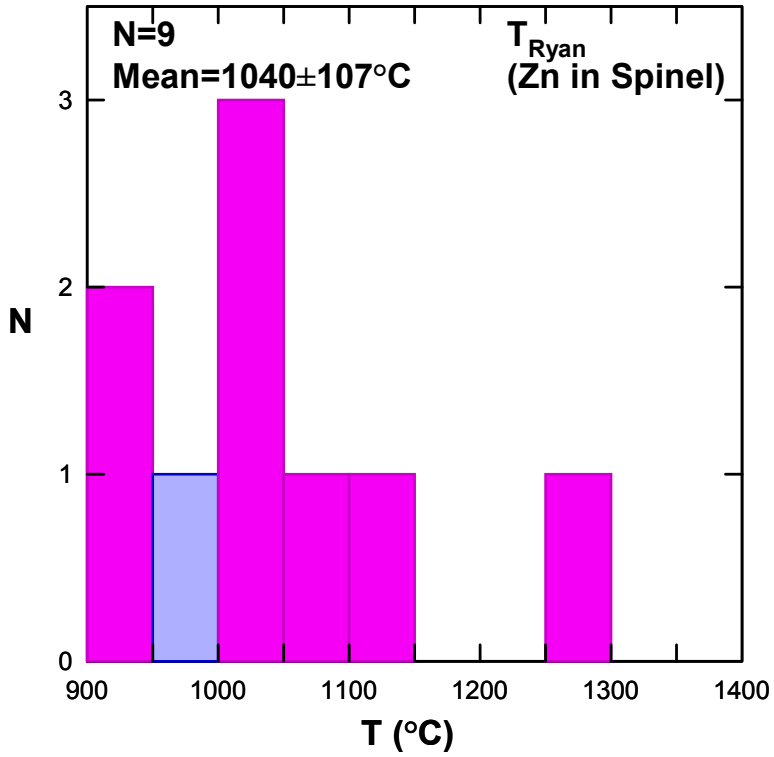

Figure 80 – Temperature estimates based on the Zn content in spinel geothermometer of Ryan et al. (1996). One chromite grain that gave a temperature higher than 1400°C and two others that yielded temperatures below 900°C were assumed to reflect disequilibrium (crystallisation outside the lithospheric diamond window, see 5.5.1) and were excluded. One chromite coexists with a harzburgitic garnet (in blue); all others do not coexist with other minerals and therefore can only be assigned to an "unknown" peridotitic paragenesis (in pink). T_{Ryan} is assumed to be independent of pressure.

For 12 chromite inclusions the Zn content in spinel geothermometer of Ryan et al. (1996) was used. Temperature cut-offs at <900°C and >1400°C were applied and three grains were excluded from the calculations as results outside this range are likely to represent disequilibrium (see 5.5.1). The remaining 9 chromite grains yielded T_{Ryan} temperatures between 918 and 1277°C, with a mean of 1040±107°C and a mode in class 1000 to 1050°C (Figure 80). One chromite could be assigned to the harzburgitic paragenesis as it coexists with a harzburgitic garnet in the same diamond (D112). The estimated temperature for this grain (T_{Ryan}= 972°C) is much lower than the $T_{O'Neill}$ mean of 1200±114°C for harzburgitic

garnet-olivine pairs and may reflect disequilibrium between the chromite and garnet included in diamond D112. All other chromites do not coexist with other minerals and therefore equilibrium cannot be tested.

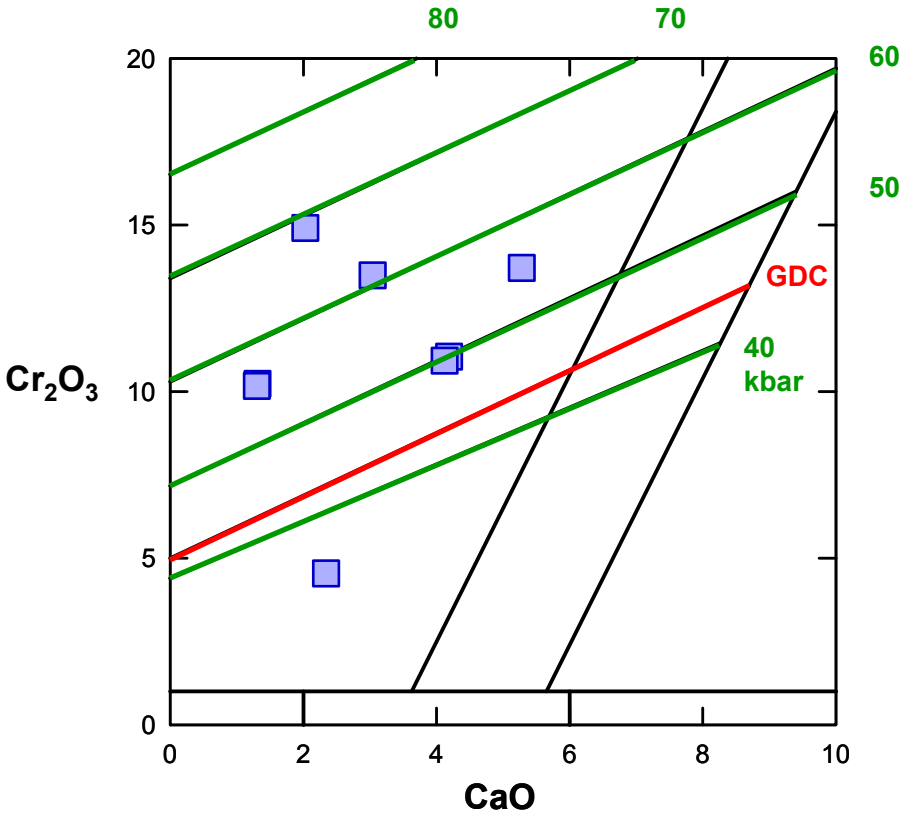

Figure 81 – Cr_2O_3 versus CaO (wt%) plot of peridotitic garnets with Cr-in-garnet isobars (green lines, pressure in kbar) calculated for a conductive continental geotherm with a 38 mW/m^2 surface heat flow. GDC: graphite–diamond constraint of Grutter et al. (2006).

For individual peridotitic (harzburgitic) garnet inclusions, pressures were estimated using the single phase Cr-in-garnet geobarometer (P_{38}) of Grutter et al. (2006). The results are shown in Figure 81. It is worth noting that this geobarometer assumes equilibration of garnet with chromite and therefore the calculated values will be minimum estimates of the real pressure at which the garnets were trapped if chromite is not present in the diamond. Grutter et al. (2006) found that the garnet compositions define a unique chromite-saturated trend that transects the harzburgite compositional field in Cr_2O_3 – CaO space, and named this relationship as the graphite–diamond constraint (GDC). Garnets plotting below the GDC line (in red) are not in equilibrium with chromite. In Figure 81, the green isobars were calculated for a conductive continental geothermal gradient of 38 mW/m^2, which the GDC intercepts at a pressure of about 43 kbar.

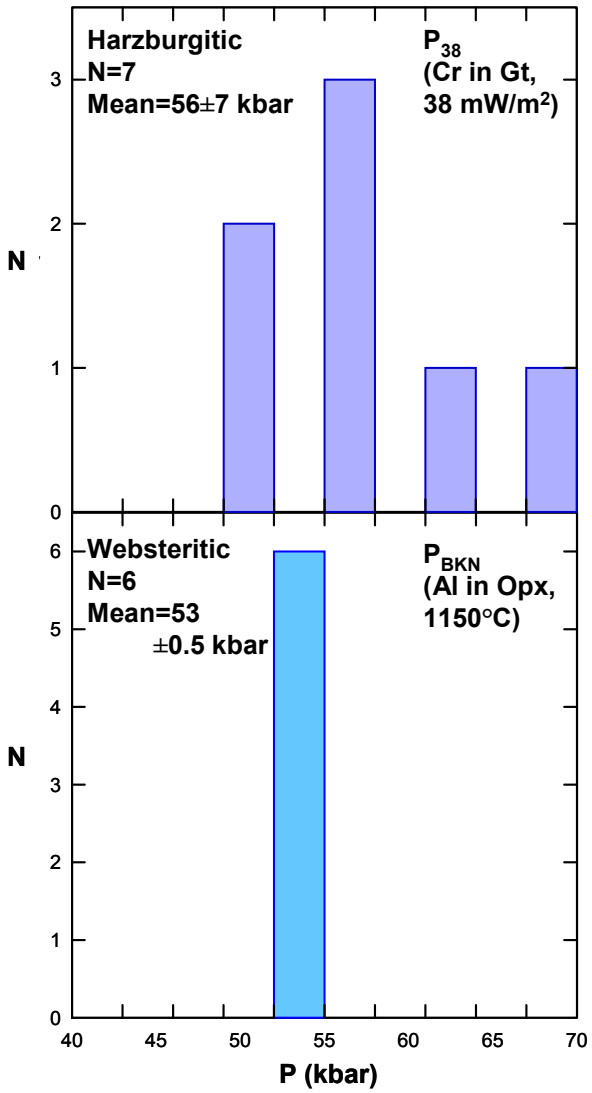

Figure 82 – Equilibration pressures calculated for garnet and orthopyroxene inclusions in the Ural diamonds. For garnets (top), pressures were estimated using the single phase Cr-in-garnet geobarometer (P_{38}) of Grutter et al. (2006), calculated for a conductive continental geotherm with a 38 mW/m^2 surface heat flow. One garnet (U6A) with P_{38}= 33 kbar falls outside the range of the histogram. For orthopyroxenes (bottom), the Al content in orthopyroxene assuming coexistence with garnet geobarometer (P_{BKN}) of Brey and Kohler (1990), was used. P_{BKN} was calculated for a temperature of 1150 °C and equilibration with garnet of an estimated chemical composition (the median of websteritic garnet inclusions worldwide, from Stachel and Harris (2008)) was assumed.

With the exception of one Cr-poor grain (U6A; 4.54 wt% Cr_2O_3) that is likely to represent a chromite-free environment, all Ural garnet inclusions plot above the GDC. Sample U29A coexists with chromite in the same diamond (D112) and thus the calculated equilibration pressure of 55 kbar can be interpreted as indicative of the true crystallisation pressure of diamond. For all other garnets plotting above the GDC, the absence of chromite in the same diamond means that the calculated values represent only minimum pressures. The range in pressures (50 to 69 kbar) obtained for the Ural peridotitic garnet inclusions is consistent with the worldwide data (see Stachel and Harris, 2008) and suggest that the

peridotitic Ural diamonds formed at minimum depths of about 165 km, within a diamondiferous lithosphere extending to at least 230 km at the time of diamond formation.

Orthopyroxene inclusions in equilibrium with garnet enable the application of the Al-in-orthopyroxene geobarometer (P_{BKN}) of Brey and Kohler (1990). The six enstatite inclusions recovered from one diamond analysed with this study have chemical compositions which fall within the 1 sigma range of the websteritic enstatites analysed worldwide (see Stachel and Harris, 2008). Based on this evidence, the Urals orthopyroxenes were assumed to be in equilibrium with websteritic garnet and an estimated chemical composition (the median of websteritic garnet inclusions worldwide, from Stachel and Harris (2008)) was used. The P_{BKN} geobarometer, calculated for an assumed temperature of 1150°C, yielded similar pressures for all inclusions of about 53 kbar (Figure 82). These pressures are in reasonable agreement with the 56 ± 7 kbar average estimated for the Urals harzburgitic garnets using the single phase Cr-in-garnet geobarometer (P_{38}) of Grutter et al. (2006) and suggest similar crystallisation conditions for the websteritic and harzburgitic inclusion parageneses.

5.6 Summary

The chemistry of syngenetic mineral inclusions in the Ural diamonds indicates an almost complete overlap with previous electron microprobe studies of mineral inclusions in diamonds from other localities worldwide. Pressure and temperature calculations of inclusion equilibration conditions show an overall agreement between the eclogitic, peridotitic and websteritic inclusion parageneses. The inclusion geothermometry results suggest that the Ural diamonds crystallised at temperatures of 1050-1300°C, which is in good agreement with the 1050-1250°C temperature range given by nitrogen thermometry (see Chapter 3). Inclusion geobarometry calculations indicate diamond crystallisation at pressures of 50 to 69 kbar, which corresponds to a depth range of about 165 km to 230 km within a diamondiferous lithosphere.

6. Radiometric dating of inclusions in diamond

6.1 Diamond age determinations

Diamonds are probably the most unreactive of all minerals at the Earth's surface (Meyer, 1987); the carbon in natural terrestrial diamond has no long lived radioactive decay scheme that can be used as a geochronometer, and the diamond lattice contains no other useful radioisotope in significant quantities (Richardson et al., 1984; Pearson and Shirey, 1999). Consequently, direct age determinations cannot be obtained from diamond itself.

To surpass this obstacle, the research on the age of diamond has focused on the analysis of the mineral inclusions that are present in some of the diamonds (Harris, 1992). Assuming that the integrity of the diamond host is maintained and the inclusion is protected from subsequent reaction, then its primary chemical signature is preserved and the isotopic composition of the inclusion can be used as an indication of the age of the diamond host.

All of the mineral inclusions selected for radiometric age determinations were unrelated to cracks in diamond and exhibited imposed morphology. The results of this study will be discussed on the premise that all the inclusions recovered are syngenetic and hence the isotopic data obtained can be directly related to diamond crystallization and eruption events.

6.1.1 *Isochron age versus model age*

Diamond ages are always reported as isochron ages or model ages. This terminology refers to the two different methods that are used to determine the age of diamond from the various radiogenic isotope systems currently available for their mineral inclusions.

An isochron is the straight line defined by plotting the isotope ratios for a cogenetic sample suite (e.g. $^{187}Os/^{188}Os$) against the parent/daughter ratio in those samples (e.g. $^{187}Re/^{188}Os$).

The slope of the isochron line is proportional to the age of the system. However, since both quantities involved are measured experimentally, errors are inevitable and must be considered when fitting a straight line to an array of points (Dickin, 1995). The traditional approach to isochron age calculation (Pearson and Shirey, 1999) is based on a multisample least-squares linear regression of samples that are assumed to have been in isotopic equilibrium at the time of formation.

In the present study, all isochron ages were generated by the program Isoplot/Ex 3 (Ludwig, 2003). Isoplot uses 3 distinct regression models for the manipulation and plotting of the radiogenic-isotope data. The calculation method for each regression model is briefly presented below.

The Model 1 fit assumes that the assigned errors are the only reason the data-points scatter from a straight line. The points are therefore weighted proportional to the inverse square of these errors (taking into account the error correlations). Isoplot always attempts a Model 1 fit first.

The Model 2 fit (not valid for classical isochrones such as Re-Os, Ar-Ar or Sm-Nd) assigns equal weights and zero error-correlations to each point. This is seldom justified, but at least avoids weighting the points according only to analytical errors (the Model 1 approach) when some other cause of scatter is involved.

The Model 3 fit (for classical isochrones such as Re-Os, Ar-Ar or Sm-Nd) assumes that the scatter is due to a combination of the assigned errors plus an unknown but normally distributed variation in the Y-values. This model may be the most realistic if the isochron data show variable initial ratios. For this model, the program will solve for the unknown Y-variation (= initial ratio variation) as well as for the best-fit line, allowing to judge whether or not the solution is realistic.

In addition to an indication of the regression model used, two other important parameters, the Probability of Fit and MSWD, are calculated by Isoplot and presented for every isochron age calculated in this study.

The Probability of Fit is the probability that, if the only reason for scatter from a straight line is the analytical errors assigned to the data points, the scatter of the data points will exceed the amount observed for the data.

The Mean Square of Weighted Deviates (MSWD) is a measure of the ratio of the observed scatter of the points (from the best-fit line) to the expected scatter (from the assigned errors and error correlations). If the assigned errors are the only cause of scatter, the MSWD will tend to be near unity. MSWD values much greater than unity generally indicate either underestimated analytical errors, or the presence of non-analytical scatter. MSWD values much less than unity generally indicate either overestimated analytical errors or unrecognized error-correlations. An isochron age with small age uncertainty, high Probability of Fit and MSWD close to unity is statistically sound, and the reason why the isochron methodology is commonly considered a very robust and reliable process for determining the age of diamond.

A model age is based on the intersection of a radioisotope growth curve of a single sample with a geochemical reservoir of interest (Pearson and Shirey, 1999). Since the initial isotopic ratio of the sample is predicted by a model rather than measured directly, model ages are less reliable than isochron ages as it is not possible to check statistically the validity of the age uncertainty or if the system has evolved according to a different model than the one predicted. Despite these disadvantages, the model age approach is the best option available when several hundreds of inclusions need to be combined for analysis (a typical procedure for several isotopic systems). When multigrain composites of potentially related inclusions are used, the resulting "age" implied by the model can be interpreted as an average of that inclusion population and therefore may have a geologic significance (Pearson and Shirey, 1999). However, the isochron approach is, in many cases, both statistically and geologically valid and therefore should be preferred over the model age method.

6.2 Isotope systems

Several radiogenic isotope systems have been used to date the minerals included in diamond. The established methods are Sm-Nd in garnets and clinopyroxenes, Ar-Ar in clinopyroxenes, U-Pb in zircon, and Pb-Pb and Re-Os in sulphides (Harris, 1992; Pearson and Shirey, 1999). Additional age constraints can be obtained from the Rb-Sr system for garnets and clinopyroxenes and from the kinetics of the nitrogen aggregation within the diamond hosts. Table A.4.1 presents a compilation of published diamond dating studies.

The radiometric approaches are quite distinct but they all require the following assumptions to be made in order to obtain meaningful isochron or model ages that represent the formation of the diamonds (Navon, 1999): 1) there was a discrete event of

diamond formation (common to all analysed diamonds when multigrain composites are used); 2) this event reset the isotopic systems in the inclusions; and 3) the inclusions remained a closed system since diamond formation.

Data published during the last decades from many diamond mines within the Kalahari craton, allowed Shirey et al. (2004b) to establish a correlation between all the radiometric ages of mineral inclusions in diamond and major thermal/tectonic events affecting the lithospheric mantle below southern Africa. These results provide strong evidence in favour of episodic rather than continuous diamond formation. It seems therefore that diamonds are formed in discrete events and the results obtained from the analysis of both single inclusions and composite samples can be used to generate isochron or model ages of their diamond hosts.

To understand the resetting of the inclusion's isotopic systems, it is useful to remember that the typical blocking temperatures for most isotopic systems are well below (up to several hundred degrees lower) the ca. 900ºC – 1400ºC "diamond window" that constrains the growth temperature of the majority of mantle derived diamonds (Pearson and Shirey, 1999). For example, while in an eclogite, garnets, clinopyroxenes and sulphides maintain isotopic equilibrium, but once completely enclosed by diamond, each inclusion isotopic system is isolated and the evolution of the Sm/Nd ratio (for garnet and clinopyroxenes), $^{40}Ar/^{39}Ar$ ratio (for clinopyroxenes) and Re/Os ratio (for sulphides) can be dated.

The third requirement is the easiest to check. When a diamond encapsulates a mineral, the inclusion is completely isolated and cannot interact with any other mineral or fluid. The system should remain perfectly closed until a geologist breaks the diamond to recover and analyse the inclusion.

6.2.1 *Historical review of diamond age determinations*

6.2.1.1 Uranium-Lead (U-Pb) ages of zircon

The occurrence of syngenetic inclusions of zircon in diamonds is particularly rare (Meyer, 1987). Meyer and Svisero (1975) first reported the presence of zircon in a study of Brazilian diamonds but it was not until two decades later that the first (and so far the only) zircon inclusion was dated. In a systematic study of 200 diamonds from Mbuji-Mayi, Democratic Republic of Congo, Kinny and Meyer (1994) found a 140 μm by 100 μm

zircon inclusion and analysed it in an instrument known as SHRIMP or "sensitive high-resolution ion microprobe".

The absence of any coexisting silicate mineral inclusions of known paragenesis in the diamond containing the zircon studied by Kinny and Meyer (1994) meant that the results could not be linked to a specific paragenetic association. Nevertheless, the determined U-Pb age of 628 ± 12 Ma (see Table A.4.1) had a small uncertainty and was older than the kimberlite pipe eruption age of 73.1 ± 1.1 Ma. (Scharer et al., 1997). Kinny and Meyer (1994) were surprised by this results and proposed that the diamond and its inclusion could have been somehow transported at this time from deeper levels in the mantle and lodged at a depth where ambient conditions were cool enough to allow Pb to accumulate. At mantle temperatures, continuous diffusion of radiogenic Pb from zircon to the diamond-inclusion interface could occur, in a similar way to the diffusion of Ar in clinopyroxene inclusions (Burgess et al., 1992). This hypothesis is supported by experimentally-derived Pb diffusion parameters which indicate that, for temperatures in excess of 1000°C, Pb diffusion in zircon occurs for some hundreds of microns up to one millimetre in crystal length (see Cherniak and Watson, 2003).

Despite the limitations regarding the interpretation of the age given by the model, the work of Kinny and Meyer (1994) showed that the U-Pb system can be applied to constrain the age of diamonds with syngenetic zircon inclusions. The rarity of the zircon inclusions, however, is the major drawback of the method.

6.2.1.2 Samarium-Neodymium (Sm-Nd) ages of garnet and clinopyroxene

Among the common silicate inclusions in diamonds, garnets and clinopyroxenes were found to contain enough Sr and Nd to be analysed accurately using the Rb-Sr and Sm-Nd isotope systems (Richardson et al., 1984; Richardson, 1986).

However, as most garnet and clinopyroxene inclusions carry almost no Rb (Navon, 1999), these silicates have very low $^{87}Rb/^{86}Sr$ ratios. Despite this, $^{87}Sr/^{86}Sr$ ratios are relatively high and this signature is commonly referred to as "unsupported radiogenic Sr" (Dickin, 1995), meaning that the high $^{87}Sr/^{86}Sr$ ratio cannot be explained by a close system radioactive decay of ^{87}Rb in the inclusions. Richardson et al. (1984) suggested that the decoupling of the Rb-Sr isotope system could be due to growth of the diamond and inclusions in contact with an "asthenosphere-derived, alkali, LREE and CO_2 enriched interstitial melt", which would have contained almost no Rb. After entrapment in the

diamond, the inclusion would have preserved the original radiogenic Sr whilst maintaining the very low levels of Rb. The complexity of the Rb-Sr data meant that precise diamond formation ages could not be obtained by using this isotope system. Nonetheless, the Rb-Sr information can be used to constrain a possible common origin between different inclusion populations (Pearson and Shirey, 1999).

By comparison with the Rb-Sr isotope system, the Sm-Nd system is less problematic to apply to garnet and clinopyroxene inclusions in diamonds. A main reason for this is that Sm is more abundant than Rb in both silicates (Navon, 1999). Garnet incorporates Sm in preference to Nd and thus allows a high $^{143}Nd/^{144}Nd$ to develop through time, in contrast with clinopyroxene which has a low Sm/Nd ratio and consequently a low $^{143}Nd/^{144}Nd$. The other reason pointed out by Richardson et al. (1984), is the lack of diffusion of Sm and Nd to the diamond-inclusion interface, meaning that the results from the Sm-Nd system effectively date the last time $^{143}Nd/^{144}Nd$ equilibrated.

However, some problems still exist related with the interpretation of Sm-Nd data. Apart from one study (Smith et al., 1991) which used very large single inclusions, the low Nd concentrations in the majority of the inclusions mean that up to several hundred grains had to be combined for analysis (e.g. Richardson et al., 1984). Even considering diamonds that were all recovered from the same mine, it is very difficult to prove consanguinity of these many different grains, as the kimberlite may have sampled diamonds that have formed during distinct events. This problem was partly addressed by carefully grouping the inclusion minerals on the basis of their colour and chemical composition. Garnet inclusion grains were analysed by EPMA and grouped according to colour and their position in the CaO versus Cr_2O_3 wt.% plot (Gurney and Switzer, 1973), while clinopyroxenes were grouped mostly by colour (e.g. Richardson et al., 1984; Richardson, 1986; Richardson et al., 1990).

For P-type garnet composites showing a limited range in $^{147}Sm/^{144}Nd$ values, the age of the diamonds was inferred from a model age approach (e.g. Richardson et al., 1984), with all the inherent uncertainties regarding the choice of the reference reservoir and the divergence of the Nd isotope growth curve from that reservoir (Pearson and Shirey, 1999). When the P-type garnet composites showed enough spread in the $^{147}Sm/^{144}Nd$ ratio, the age was obtained by the more robust isochron methodology (e.g. Richardson and Harris, 1997).

For P- and E-type inclusions where a set of garnet inclusion composites and at least one clinopyroxene composite were analysed, the Sm-Nd age was obtained by isochron

regression (e.g. Richardson, 1986). The wide range of $^{147}Sm/^{144}Nd$ values between the two E-type composites produces a more precise isochron age than the P-type composites, the largest uncertainty being the possibility of grouping potentially unrelated grains.

In a study of P-type harzburgitic garnets included in diamonds from the Finsch and Kimberley Pool mines in South Africa, Richardson et al. (1984) were the first to determine diamond genesis ages by using the Sm-Nd isotope system (see Table A.4.1). The inclusion composites for both mines gave model genesis ages of 3200 ± 100 Ma. A subsequent study of inclusion composites of E-type clinopyroxene and garnet gave Sm-Nd isochron ages of 1580 ± 60 Ma for Argyle (Australia) and 1150 ± 60 Ma for Premier (South Africa) (Richardson, 1986).

Inclusion composites of E-type garnets and clinopyroxenes also provided isochron ages of 990 ± 50 for Orapa (Botswana) and 1580 ± 50 Ma for Finsch (Richardson et al., 1990). For Finsch, comparable Sm-Nd model ages of 1443 ± 166 Ma and 1657 ± 77 Ma (Smith et al., 1991) were obtained from large E-type single garnet inclusions. Smith et al (1991) also analysed a large clinopyroxene recovered from a diamond with a websteritic inclusion assemblage (clinopyroxene, orthopyroxene, garnet) from the Kimberley Pool. The clinopyroxene yielded a Sm-Nd model age of 2111 ± 120 Ma and is the only age of a websteritic diamond reported so far (Table A.4.1).

A further study (Richardson et al., 1993) involved composites of P-type lherzolitic garnets and clinopyroxenes from the Premier mine giving an isochron age of 1930 ± 60 Ma, which is significantly older that the previously determined isochron age of 1150 ± 60 Ma from E-type garnets and clinopyroxenes from the same mine (Richardson, 1986). Another old isochron age, 2010 ± 60 Ma, was obtained by Richardson and Harris (1997) for P-type harzburgitic garnet composites from the Udachnaya mine in Siberia. For the Jwaneng mine in Botswana, Richardson et al. (1999) reported an isochron age of 1540 ± 20 Ma from composites of E-type clinopyroxenes and garnets. The most recent study using the Sm-Nd isotopic system focused on the analysis of P-type harzburgitic garnet inclusion composites from the Venetia mine (South Africa), which gave an isochron genesis age of 2300 ± 40 Ma (Richardson et al., 2006).

A quarter of a century of systematic work using the Sm-Nd isotopic system in silicate inclusions in diamonds has resulted in major advances for diamond research. One important breakthrough was the determination of the genesis age of diamonds from eight mines (Kimberley, Finsch, Premier, Venetia, Orapa, Jwaneng, Argyle and Udachnaya, see

Table A.4.1) in three different continents (Africa, Asia and Australia). The validity of the ages obtained is supported by the coherence in the Sm-Nd isotopic composition of the inclusions compared with the very scattered correlations found on Sm-Nd isochron diagrams of garnet megacrysts from each individual mine (Richardson et al., 1984). Richardson and co-workers have attributed this difference to the closed system behaviour of the inclusions versus the open system behaviour of the kimberlite megacrysts. The other important conclusion that became evident from the Sm-Nd isotopic studies was the difference in ages between P- and E-type silicate inclusion composites: for this system, P-type inclusions give older ages than E-type inclusions. And finally, for Southern Africa, the Sm-Nd ages appear to be correlated with major depletion events with high degrees of melting affecting the lithospheric mantle (see Shirey et al., 2004a), providing strong evidence in favour of episodic rather than continuous diamond formation in the Earth's mantle.

6.2.1.3 Argon-Argon (Ar-Ar) ages of clinopyroxene

By comparison with the other common mineral inclusions in diamond, clinopyroxenes contain elevated levels of potassium and hence can potentially be dated by the $^{40}Ar/^{39}Ar$ system (Phillips et al., 2004a). In order to convert ^{39}K to ^{39}Ar, the clinopyroxene inclusions need to be placed in a nuclear reactor, where they are irradiated with fast neutrons. This causes an n,p (neutron capture, proton emission) reaction that permits the potassium determination for a K-Ar age to be made as part of the argon isotope analysis (Dickin, 1995).

The $^{40}Ar/^{39}Ar$ technique that has been applied to date single clinopyroxene inclusions in diamond makes use of a laser probe system attached to a gas mass spectrometer and was first used by Burgess et al. (1989) and Phillips et al. (1989). The advantage of the laser probe technique is that it can precisely measure the very small amounts of radiogenic Ar released in several laser outgassing steps by the individual clinopyroxene inclusions.

In this procedure, known as $^{40}Ar/^{39}Ar$ laser step-heating analysis, laser shots are repeatedly fired into an inclusion to produce a large pit of between 40 and 100 μm diameter. The gas liberated from each of the shots is measured and the analysis of an inclusion is completed when all the argon is released (Burgess et al., 1989). The argon released in each step is measured by a mass spectrometer and "step ages" with an associated analytical error are calculated. At the end of the series of experiments, the step ages are plotted against the cumulative amount of ^{39}Ar released and the resulting figure is called an age spectrum

(Dickin, 1995). When a reasonable number of consecutive steps, carrying a substantial amount of the total argon released, give the same age, the resulting average value carries geological significance.

The laser probe $^{40}Ar/^{39}Ar$ technique also allows the calculation of Ca/K ratios from the measured $^{39}Ar/^{37}Ar$ ratios. As noted by Phillips et al. (2004a), across step-heating increments the Ca/K ratios are normally uniform within individual clinopyroxene inclusions from the same diamond. This uniformity attests the mineralogical and compositional purity of the clinopyroxene inclusions (Pearson and Shirey, 1999).

Initial attempts to date diamond formation events using the $^{40}Ar/^{39}Ar$ isotopic system focused on E-type clinopyroxene inclusions in diamonds from the Premier mine, South Africa, which yielded apparent ages of 1185 ± 94 Ma (Burgess et al., 1989) and 1198 ± 28 Ma (Phillips et al., 1989). The results were within error of the time of kimberlite emplacement (1180 ± 30 Ma; (Allsopp et al., 1989)) and were consistent with the 1150 ± 60 Ma isochron genesis ages obtained for E-type inclusions using the Sm-Nd isotope system (Richardson, 1986). This consistency led Burgess et al. (1989) and Phillips et al. (1989) to initially interpret the $^{40}Ar/^{39}Ar$ results as reflecting the diamond genesis age.

A subsequent study by Burgess et al. (1992) on E-type clinopyroxene inclusions from the Argyle (Australia), Udachnaya (Siberia), Orapa and Jwaneng (both in Botswana) mines showed that the $^{40}Ar/^{39}Ar$ technique was more complex than previously assumed. Rather than cracking the diamonds to release the inclusions, the authors opted to cleave them in order to expose the inclusions at the diamond surface. Surprisingly, the calculated apparent ages were intermediate between the times of kimberlite eruption and the diamond formation ages that have been determined by other dating methods. Burgess et al. (1992) suggested that this was due to the diffusion at mantle temperatures (>1000ºC) of radiogenic ^{40}Ar to the interface between the inclusion and diamond. After kimberlite eruption and cooling below the closure temperature for argon diffusion, radiogenic argon is retained by the clinopyroxene inclusions. Burgess et al. (1992) argued that the Ar trapped in the diamond/inclusion interface region was partially lost when the diamond was cleaved. As a result, in addition to the Ar contained in the inclusion, the laser heating technique also released any remaining argon still trapped at the diamond/inclusion interface region, resulting in $^{40}Ar/^{39}Ar$ apparent ages intermediate between the age of diamond crystallisation and the age of kimberlite emplacement.

To overcome this problem, Burgess et al. (1992) analysed the Ar content of a clinopyroxene inclusion from Udachnaya without cleaving the diamond host. This was achieved by laser drilling the diamond until the inclusion has been reached (to recover the Ar trapped at the diamond/inclusion interface), and then laser melt the inclusion (to release the Ar generated since eruption of the kimberlite). Once this two-stage analysis was complete, the results were combined and an age calculated from the total $^{40}Ar/^{39}Ar$ ratio, give the time at which the inclusion was trapped in the diamond. The results were inconclusive, as the calculated apparent age of 1149 ± 37 Ma was indeed considerably older than the eruption age of the Udachnaya kimberlite (361 ± 6 Ma; (Kinny et al., 1997)) but still much younger than the youngest Sm-Nd isochron genesis age of 2010 ± 60 Ma (Richardson and Harris, 1997) that has been determined for diamonds from the same mine (see Table A.4.1).

Further studies by Phillips et al. (1998) and Phillips et al. (2004a) focused on E- and P-type clinopyroxene inclusions from Orapa, Jwaneng (both in Botswana) and E-type clinopyroxene inclusions from Mbuji Mayi (Democratic Republic of Congo). These studies assumed that total extraction of the clinopyroxene inclusions from their host diamonds should induce loss of all argon trapped at the diamond/inclusion interface region, and therefore provide ages in close agreement with the kimberlite eruption age. Although these studies showed that the $^{40}Ar/^{39}Ar$ method could be applied to clinopyroxene inclusions of both paragenesis, the results from all locations gave apparent $^{40}Ar/^{39}Ar$ ages that were intermediate between kimberlite eruption and the diamond genesis ages constrained by Re–Os or Sm–Nd dating. Phillips et al. (2004a) discussed possible explanations for the intermediate apparent ages and favoured an explanation involving the release, during the step-heating analysis, of radiogenic ^{40}Ar produced during mantle residence and trapped in fluid inclusions or defects within the clinopyroxene. If this hypothesis is correct, then the model of total diffusion of pre-eruption Ar to the diamond/inclusion interface is not simple and the results must be interpreted as maximum estimates for kimberlite emplacement ages.

The refinement of the $^{40}Ar/^{39}Ar$ technique allowed Burgess et al. (2004) to analyse E-type clinopyroxene and garnet inclusions in diamonds from Orapa (Botswana), and E-type clinopyroxene inclusions from Venetia (South Africa). The Venetia diamonds were drilled down into the clinopyroxene inclusions using an ultraviolet laser and then step-heated using a Ta-resistance furnace. Furnace stepped heating of the diamond to extract Ar was used in preference to laser heating because the former has the potential to discriminate between Ar released from the clinopyroxene (at temperatures below 1800 ºC) and the host

diamond (released during graphitisation at >2000 ºC). The Orapa diamonds were not drilled and Ar was extracted, during furnace stepped heating, by mechanical rupture of the diamonds induced by melting of the silicate inclusions.

None of the Venetia diamonds that were probed with the laser released significant amounts of ^{40}Ar from the diamond–inclusion interface, and the majority of apparent ages were in close agreement with the host kimberlite age of 519 Ma (Phillips et al., 1999). On the other hand, stepped heating ages obtained from most clinopyroxene inclusions from Orapa were in the range 906–1032 Ma, similar to the Sm–Nd isochron genesis age of 990 ± 50 Ma (Richardson et al., 1990) but much older than the kimberlite age of 93 Ma (Allsopp et al., 1989). Orapa garnets were also shown to contain measurable K contents, and recorded a range of ages between 1000 and 2500 Ma (Burgess et al., 2004). A few of the Orapa and one Venetia inclusions gave apparent ages older than 2500 Ma, supporting the suggestion that pre-eruption radiogenic ^{40}Ar and mantle-derived ^{40}Ar components are trapped in defects and microinclusions within the clinopyroxene and garnet inclusions (Phillips et al., 2004a).

An important application of the $^{40}Ar/^{39}Ar$ technique is that it offers the possibility to constrain the ages of alluvial diamond deposits, thus enabling their source kimberlite/lamproite intrusions to be traced. Burgess et al. (1998) extracted four E-type clinopyroxene inclusions from diamonds recovered in the Copeton alluvial field in New South Wales (Australia) and analysed them using the laser probe step-heating technique. The inclusions gave an average apparent age of 325 ± 25 Ma, which was interpreted as the eruption age of the diamond source. Given that no kimberlites/lamproites of that age exist in south-east Australia, and that at 325 Ma ago, Australia was attached to Antarctica, the alluvial diamonds may have been derived from that continent and subsequently transported by glaciers (Burgess et al., 1998).

Burgess et al. (1998) showed that step-heating $^{40}Ar/^{39}Ar$ ages obtained from several inclusions from alluvial diamond deposits can be linked to known kimberlite/lamproite eruption ages in potential source regions. This information is especially valuable for diamond mining companies, as it has important implications for diamond exploration in focussing exploration targets with respect to primary kimberlites/lamproites as well as the discovery of intermediate alluvial deposits from the study of the paleo-river systems.

To test the applicability of the $^{40}Ar/^{39}Ar$ method to diamond provenance studies, Phillips and Harris (2008) analysed 50 eclogitic clinopyroxene inclusions from the ~93 Ma (Davis,

1977) Orapa kimberlite in Botswana. These authors found that 35% of fusion ages were within error of the time of Orapa kimberlite eruption (~93 Ma; Davis, 1977), with 77% of results within +50 Ma, and 92% within +100 Ma of this time. Thus individual $^{40}Ar/^{39}Ar$ fusion ages should be regarded as maximum estimates of source kimberlite/lamproite eruption; however, the youngest ages from an inclusion population should approximate the time of kimberlite eruption. Subject to these limitations, Phillips and Harris (2008) concluded that the $^{40}Ar/^{39}Ar$ inclusion dating method can provide unique information on diamond provenance and palaeo-landscape evolution.

6.2.1.4 Lead-Lead (Pb-Pb) ages of sulphide

Sulphides are the most common mineral inclusions in diamonds (Meyer, 1987). Not surprisingly, the first attempt to provide information on the genesis age of diamond (Welke et al., 1974) focused on the analysis of sulphide inclusions. The most common sulphides have sufficiently low U and Th concentrations (<50 ppb) that these elements cannot be measured precisely on the very small inclusions in diamonds (Pearson and Shirey, 1999). This is not a disadvantage, as the resulting low U/Pb and Th/Pb values mean that corrections for in situ decay are negligible (Eldridge et al., 1991) and thus the measured Pb isotope ratios can be used to estimate the age of the sulphide inclusions.

The evolution of the Pb isotopes in the terrestrial mantle has been theoretically modelled as growth curves that describe a single-stage variation in the $^{207}Pb/^{206}Pb$ versus $^{208}Pb/^{206}Pb$ ratios with time (Cumming and Richards, 1975). Although the terrestrial Pb evolution can also be approximated by a two-stage model (Stacey and Kramers, 1975), the single-stage model has been favoured for Pb-Pb dating of sulphide inclusions in diamonds as it is less complex and easier to interpret.

A simple, single-stage Pb isotope evolution diagram commonly contains a curved and a straight line (see Figure 83). The curved line is the assumed Pb growth curve. The straight line, known as geochron, connects present-day average mantle Pb to the initial Pb isotopic composition at the formation of the Earth (Pearson and Shirey, 1999). Data plotting on the growth curve can be used to calculate Pb-Pb model ages. Data plotting between the growth curve and the geochron cannot be used to calculate Pb-Pb model ages directly but will still permit some general age inferences to be made. Data plotting elsewhere in the diagram will produce unrealistically young or old ages and should not be used.

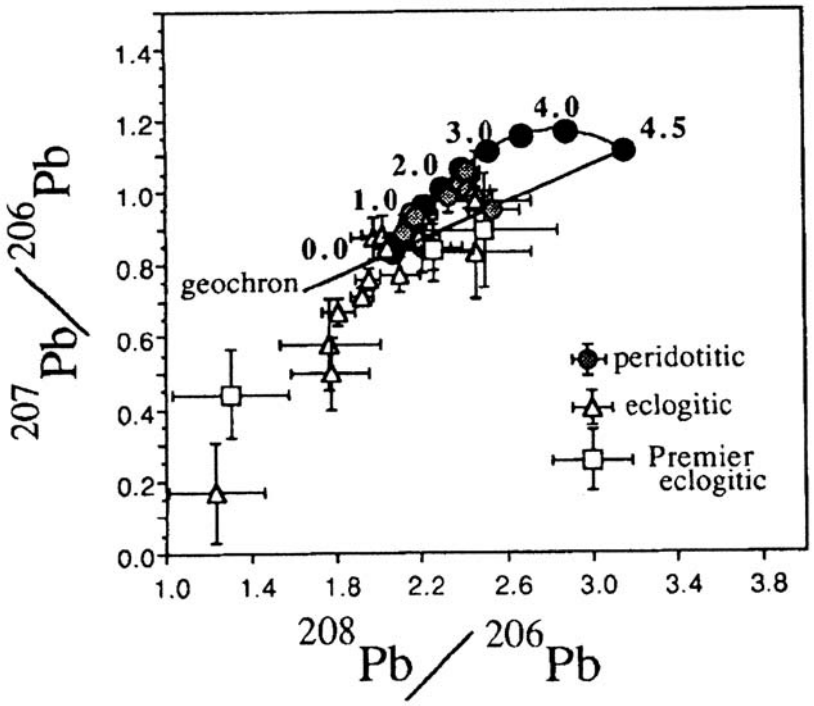

Figure 83 – Example of a single-stage Pb isotope evolution diagram, showing the assumed Pb growth curve (curved line) and the geochron (straight line). Diagram from Eldridge et al. (1991).

Pb-Pb sulphide ages are determined using the model age methodology and, as such, are subject to the assumptions and the uncertainty in the evolution of mantle Pb used for the model. The complexity of Pb isotopes in sulphide inclusions in diamonds means that Pb-Pb model ages are not easy to interpret and should only be taken as a broad indication of the age of the diamond host (Pearson and Shirey, 1999).

In their pioneering thermal ionization mass spectrometry (TIMS) study, Welke et al. (1974) determined the U and Pb contents and the Pb isotopic ratios of composites of sulphide inclusions of unknown paragenesis from selected diamonds from the Premier mine, South Africa. The large blank corrections led to imprecise Pb isotope measurements that suggested a diamond genesis age of about 1500 Ma (see Table A.4.1). A subsequent TIMS study of sulphide inclusion composites of unknown paragenesis from the Premier, Kimberley Pool and Finsch mines in South Africa, gave more precise Pb isotope results (Kramers, 1979). The Pb-Pb model age of ca. 1200 Ma for the Premier diamonds was in reasonable agreement with the results of Welke et al. (1974) and close to the 1180 ± 30 Ma pipe emplacement age (Allsopp et al., 1989). The Kimberley Pool and Finsch results were an important development for diamond geology, as they gave Pb-Pb model ages in excess of 2000 Ma, which were significantly older than the 118 ± 3 Ma (Finsch) and 95 Ma (Kimberley Pool) kimberlite eruption ages (Allsopp et al., 1989). This age discrepancy was

the first evidence that diamonds were much older than the kimberlite intrusions and therefore should be considered as xenocrysts in the host kimberlite.

It was only after the introduction of the SHRIMP instrument that the analysis of single sulphide inclusions with high precision became possible. This in-situ technique was first used by Eldridge et al. (1991) to date sulphide inclusions in diamonds from Southern (Premier, Roberts Victor, Koffiefontein, Jagersfontein, Finsch and Orapa) and Western (Sierra Leone) Africa mines. Sulphides with high levels of Ni and Pb were assigned to the peridotitic paragenesis and the remainder to the eclogitic paragenesis. The ages of the diamonds from each mine were not presented, but the results showed that most P-type sulphides plotted between the Pb isotope growth curve and the geochron whereas most E-type sulphides plotted below the geochron line. Eldridge et al. (1991) suggested a genesis age of ca. 2000 to 2500 Ma for the P-type sulphides and a younger, undeterminable age for the E-type sulphides.

Using a similar approach, Rudnick et al. (1993) analysed sulphide inclusions in diamonds from Siberia. A total of thirty three sulphides from the Mir, Udachnaya and 23rd Party Congress mines were extracted from their host diamonds and analysed by SHRIMP. An additional diamond from Udachnaya was mechanically polished until the sulphide inclusions were exposed on the surface. All sulphides were classified as E-type or P-type on the basis of their Ni content. The results of this study were somewhat similar to those of Eldridge et al. (1991) for the African mines, with the sulphides giving the P-type Siberian diamonds a genesis model age of about 2000 Ma. For E-type sulphides, the $^{207}Pb/^{206}Pb$ and $^{208}Pb/^{206}Pb$ ratios plotted outside of the area delimited by the Pb growth curve and the geochron, suggesting unrealistic genesis ages. The only individual source specified in the study of Rudnick et al. (1993) was the Udachnaya mine, where the polished diamond with P-type sulphide inclusions gave a Pb-Pb model age of ca. 2000 Ma (see Table A.4.1).

The Rudnick et al. (1993) study was the last work to have used the Pb-Pb system, as it became clear that the imprecise knowledge of the Pb isotopic evolution of the Earth's mantle meant that the diamond ages could not be safely assigned on the basis of the Pb isotopic composition of single sulphide inclusions. The Pb-Pb system has since been replaced by the more precise Re-Os system developed for single sulphide inclusions in diamonds.

6.2.1.5 Rhenium-Osmium (Re-Os) ages of sulphide

Sulphides included in diamonds are known to have high platinum group elements (Ru, Rh, Pd, Os, Ir and Pt) contents (Bulanova et al., 1996). Of the six platinum group elements, Os can be used to date geological processes as part of Re-Os decay system and therefore is uniquely useful for the analysis of sulphide inclusions in diamond (Richardson et al., 2001). Relative to the other isotopic systems, the Re-Os system has some differences, the most evident being the siderophile/chalcophile nature of these elements, making this a useful system to address questions about core/mantle evolution (Dickin, 1995). In addition, whereas all the other isotopic systems make use of incompatible elements which are enriched in the melt, Os is a highly compatible element which is strongly retained in mantle minerals. As Re is a moderately incompatible element, there is good potential for strong fractionation of Re from Os during melt generation. This potential for Re-Os fractionation means that there is enough spread in the Re/Os ratios of sulphide inclusions in diamond to allow the use of the Re-Os system to date these minerals (Pearson et al., 1998b).

A further advantage of the Re-Os isotopic system is that it offers the possibility to date single sulphide inclusions. The results of some early studies (Pearson et al., 1998b; Pearson et al., 1999) showed insufficient spread in the Re/Os ratios to accurately define isochrones and the less reliable model age approach had to be used. The Re-Os model age method applied to sulphide inclusions in diamonds assumes single-stage, closed-system evolution (Pearson et al., 1999). In simple terms, the sulphides are assumed to have experienced a single-stage evolutionary history in which the sulphide Os was extracted from a chondritic reservoir, followed by entrapment in the diamond in a perfectly closed system. As with all models, there are some limitations that must be taken into account when one tries to determine an age. For the Re-Os system, the main source of uncertainty, which greatly affects the precision of the model age obtained, is that the Os isotope evolution in the mantle is not fully understood. Depending on which particular Os evolution model is chosen, the model ages can differ by at least ±300 Ma (Pearson and Shirey, 1999). Fortunately, the majority of sulphide inclusions in diamond that have been studied show enough spread in Re/Os ratios and have been dated using the isochron approach.

The only method currently capable of analysing femtogramme (10^{-15} g) levels of Re and Os within sulphide inclusions in diamonds is negative thermal ionization mass spectrometry (N-TIMS). In order to extract the pure separates of Re and Os required by this type of analysis, two dissolution techniques can be employed: 1) direct micro-

distillation of Os from the sulphide inclusions in sealed Teflon beakers (e.g. Pearson et al., 1998b), or, 2) digestion of sulphides in micro-Carius tubes and subsequent distillation (e.g. Pearson et al., 1999). The first method is more advantageous, as it produces lower analytical Re and Os blanks and sample loss is minimised (Pearson et al., 1998b). After Os distillation, Re is separated by micro-column anion-exchange chemistry and analysed by ICP-MS. The Fe, Ni and Cu contents of the sulphide inclusions can be obtained from the solutions washed off the anion columns prior to Re elution (e.g. Richardson et al., 2001) and analysed by ICP-MS. If a mixed platinum group element (PGE) spike is added to the sample before distillation (e.g. Pearson et al., 1998b), other PGE can also be eluted and analysed by ICP-MS.

Sulphide-bearing diamonds frequently do not contain any coexisting silicate or oxide inclusions. This peculiarity complicates the classification of the sulphides into the paragenetic suites that have been defined for the silicate inclusions. Bulanova et al. (1996), using evidence from Siberian diamonds (Yefimova et al., 1983), assigned Ni-rich (22-36 wt% Ni) sulphide inclusions to the peridotitic paragenesis and Ni-poor (0-12 wt% Ni) inclusions to the eclogitic paragenesis. Work on African diamonds by Deines and Harris (1995) showed that a paragenetic distinction of sulphides based on their Ni content alone was ambiguous, as a continuum from Ni-poor to Ni-rich compositions, regardless of the sulphide paragenesis, was observed. Further studies on African and Siberian diamonds analysed both Ni and Os contents of sulphide inclusions and showed that low Ni eclogitic sulphides are lower in Os (Os <700 ppb) than high Ni peridotitic sulphides (Os from 2000 to 20000 ppb) (Pearson et al., 1998b; Pearson et al., 1999). In addition, these authors also noted that the Re/Os ratios in eclogitic and peridotitic sulphide inclusions are similar to those observed in the respective mantle xenoliths. The combined use of Ni and Re/Os systematics in sulphide inclusions appears to provide helpful information with regard to possible paragenetic associations.

The Re-Os isotopic system was first applied to single sulphide inclusions, in a study of diamonds from Koffiefontein (South Africa) (Pearson et al., 1998b). Two P-type sulphide inclusions provided an isochron genesis age of 69 ± 30 Ma, within error of the kimberlite eruption age of 90 Ma (Allsopp et al., 1989). This young age was supported by Pb-Pb systematics and the kinetics of nitrogen aggregation in diamond, which defined a mantle residence time of ca. 10 Ma at 1100ºC before kimberlite emplacement. Five E-type sulphide inclusions gave an isochron age of 1048 ± 120 Ma (see Table A.4.1) which was interpreted as a single period of diamond growth (Pearson et al., 1998b).

In a subsequent study, Pearson et al. (1999) re-examined a polished diamond from Udachnaya (Siberia) containing P-type sulphide inclusions that had previously given a Pb-Pb model age of ca. 2000 Ma (Rudnick et al., 1993). Although no isochron could be defined, the sulphides yielded Re-Os model ages varying from 3100 ± 300 to 3500 ± 300 Ma, indicating that the crystallisation of different zones of diamond growth was not separated by substantial time intervals. In an attempt to obtain information on the origin of diamonds from the alluvial deposits of Wellington (Australia), two sulphide inclusions from two diamonds belonging to the peridotitic paragenesis were analysed (Pearson et al., 1998a). The sulphides gave Re-Os model ages of 2374 ± 300 Ma and 3609 ± Ma, much older than the eruption age calculated for diamonds from the same alluvial deposits (Burgess et al., 1998) and supporting the derivation of the diamonds from a distal cratonic source (Pearson et al., 1998a).

A further study using the Re-Os system (Richardson et al., 2001) was carried out on E-type sulphide inclusions from the De Beers Pool kimberlites, Kimberley, South Africa. Grouping 4 of the 18 sulphides analysed, Richardson et al. (2001) were able to define a Re-Os isochron genesis age of 2890 ± 60 Ma (see Table A.4.1) and suggested that if E-type diamonds were formed by oceanic crustal recycling, then a subduction-related process may have had occurred as early as the middle Archean in the Kaapvaal craton. In a study of diamond-bearing kimberlites in the Kaapvaal-Zimbabwe cratons, Shirey et al. (2001) presented Re-Os isotope data for E-type sulphide inclusions from the Orapa mine in Botswana. The results, plotted against reference isochrones, suggest diamond formation at two distinct events, the first at ca. 2500 – 3000 Ma, and the second at a later stage (ca. 1000 Ma), in good agreement with the Sm-Nd isochron age of 990 ± 50 Ma previously reported (Richardson et al., 1990). A study of E-type sulphide inclusions from Jwaneng also revealed the presence of two diamond generations (Richardson et al., 2004). The genesis ages obtained approximate reference Re-Os isochrones of 2900 Ma (similar to the Re-Os isochron age obtained for E-type Kimberley sulphide inclusions (Richardson et al., 2001)) and 1500 Ma (in agreement with the Sm-Nd isochron age of 1540 ± 20 Ma from Jwaneng silicate inclusions (Richardson et al., 1999)).

A refinement of the Re-Os technique allowed Pearson and Harris (2004) to present new data on E-type sulphide inclusions from Koffiefontein (South Africa). A single diamond containing four separate sulphide inclusions defined a Re-Os isochron age of 2600 ± 300 Ma, while five other sulphides from different diamonds gave a Re-Os isochron age of 1000 ± 40 Ma. These results confirmed the occurrence of episodic diamond growth in the mantle beneath the cratons of southern Africa.

A recent Re-Os study of sulphide inclusions in diamonds was carried out on samples from the Panda kimberlite in north-west Canada. Westerlund et al. (2006) obtained a Re-Os isochron age of 3520 ± 170 Ma from 11 P-type sulphides recovered from 5 diamonds. This very old genesis age obtained for northern American diamonds is in agreement with the oldest ages obtained for diamonds from Siberia (3100 to 3500 ± 300 Ma; (Pearson et al., 1999)) and southern Africa (3200 ± 100 Ma; (Richardson et al., 1984)), suggesting that diamond formed relatively early in the Earth's history.

6.3 Re-Os isotope study of sulphide inclusions in the Ural diamonds

6.3.1 *Sample preparation and classification*

A total of 15 diamonds containing syngenetic sulphide inclusions were selected for Re-Os analysis. One diamond contained two sulphides and two diamonds enclosed three sulphides, which resulted in a total of 20 sulphides being recovered for this study.

The inclusions were manually extracted from the diamonds by cracking. Inclusion sizes ranged from 50 μm to 330 μm in longest dimension (Table A.4.2). The sulphides exhibited a typical cubo-octahedral morphology, with facets mirroring the diamond symmetry. The majority of the sulphides crystals, however, were broken during extraction, which resulted in two or more (up to twenty) thin, irregular sulphide fragments. Each of the pieces was carefully examined under a binocular microscope to avoid misclassifying any metal fragment from the crusher as a sulphide fragment.

Some diamonds also contained silicate inclusions and, where possible, these were assigned to a specific paragenesis. Of the 15 diamonds, 8 belong to the eclogitic paragenesis, the remainder are of unknown paragenesis. No silicate inclusions of the peridotitic paragenesis coexist with the set of sulphides selected for Re-Os analysis.

In addition to the 20 sulphides, 5 total procedure blanks (labelled Blk_1 to Blk_5) were prepared by the same procedure but with sample material omitted. For an unknown reason, the total procedure blank Blk_2 did not run successfully in both Os and Re analyses and was not included in the results of this study.

6.3.2 *Chemistry*

6.3.2.1 Sample and spike weights

All chemical procedures and instrumental analyses were carried out at the Northern Centre for Isotopic and Elemental Tracing, based in the University of Durham.

Sulphide inclusion weights ranged from 1.9 μg to 80.3 μg and were determined using a Mettler UMT-2 ultra-micro-balance with a sensitivity of 0.1 μg (see Table A.4.3) The precision of the balance was assessed by weighing a mass of ca. 5 μg in several runs of 10 measurements each, giving a reproducibility better than 0.2 μg.

Samples were placed in "weighing boats" made of aluminium foil and weighed three times each. Mass reproducibility was better than 0.3 μg. Weight determinations were carried out mostly overnight during an 18 hour non-stop period, in a room under controlled temperature and air flow conditions. Subsequently, a "Department of Terrestrial Magnetism mixed sulphide" spike solution was weighed onto a cone-shaped hole drilled on the centre of the inverted cap of a conical 7 ml screw-top Teflon (PFA) vial (Savillex). The spike solution was dried down on a hotplate at 80 ºC under flowing air, ensuring that the spike drop remained in the central area of the vial.

The small size of the sulphide inclusions makes them very susceptible to static electricity. The vials utilised in this study are made of Teflon, which is a good electrical insulator. This also means that Teflon is good at both generating, and holding, a surface charge and therefore tends to build up static electricity easily. When placed inside the Teflon vials, the sulphide inclusions tend to "jump" from one spot to another and even to the outside of the vial. To avoid this, a small drop of double distilled, deionised water with a measured resistance of >18.2 MΩ (Milli-Q water) was added to the cap of the vial exactly on the spot where the spike had been previously dried down and the sulphide inclusions placed directly on top of the Milli-Q water drop.

Even after taking all these precautionary measures, several fragments of sample U67a "jumped" to the outside of the vial and were lost. To prevent the loss of more samples, all other sulphide fragments and blanks were manipulated without the use of gloves and lab coats. No other sulphide fragments were lost and the results from the total procedure blanks show that the samples were not subjected to any additional contamination.

6.3.2.2 Direct micro-distillation of Os

20 µl of a 0.05 g/g CrO_3 solution in 6 *N* H_2SO_4 was placed on the top of the sulphide inclusions. The threads of the vial base were wrapped with Parafilm PTFE tape and 20 µl of 9 *N* HBr added to its apex. The vial base was then carefully inverted assuring the HBr drop stayed in place. The vial was sealed, wrapped in Al-foil and placed on a heating block at 80 ºC for 3 hours. During the heating process, the Re fraction stays in the CrO_3 solution while the Os fraction oxidises (OsO_4) and is distilled into the HBr "trap".

Each vial was removed from the heating block, the Al-foil was taken out and the cap gently unscrewed and inspected with a binocular microscope for undigested samples. All sulphide inclusions were fully digested. To collect any Os that may be present near the HBr drop on the vial base, about 10 µl HBr was placed at the tip of a pipette and dragged along the area in the vicinity of the apex of the vial and then released onto the HBr drop. The vial base was then placed on a hotplate at 90 ºC until only a very small volume of the initial HBr drop containing the Os fraction remains, ready to be loaded for mass spectrometry.

6.3.2.3 Micro-column anion-exchange separation of Re

The drop of CrO_3 solution containing the Re fraction was transferred to a clean, flat-bottomed, 7 ml Teflon (PFA) vial. The reduction of Cr^{6+} to Cr^{3+} was achieved by adding 60 µl of Milli-Q water and 20 µl of H_2O_2 to the drop of CrO_3 solution. The effectiveness of the chemical reaction can be easily monitored, as the drop of CrO_3 solution changes in colour, from deep orange to a characteristic Prussian blue. The vial was then closed and placed on a hotplate at 90 ºC for 30 minutes to allow fully homogenisation of the solution.

The Re fraction was separated on micro-anion columns using 100 µl of resin. To minimise sample contamination, the resin was cleaned with 400 µl 8 *N* HNO_3, 600 µl Milli-Q water and 400 µl 4 *N* H_2SO_4. The sample was added to the column and the Cu, Fe and Ni fractions eluted with 1200 µl Milli-Q water and 400 µl 0.8 *N* HNO_3, and recovered in micro-centrifuge tubes.

The flat-bottomed, 7 ml Teflon (PFA) vial that contained the sample was further cleaned with several drops of 0.8 *N* HNO_3 and placed on a hotplate at 90 ºC while the Cr, Fe and Ni fractions were being collected. This procedure allowed the re-use of the Teflon vials to collect the Re fraction by elution with 800 µl 4 *N* HNO_3 and also minimized sample

contamination by reducing the use of Teflon vials. The Re fractions were dried down overnight on a hotplate at 90 ºC and diluted with 250 µl of a 0.8 *N* HNO_3 + 50 ppb Ir solution, ready to be analysed by Inductively Coupled Plasma Mass Spectrometry (ICP-MS).

6.3.3 *Experimental procedures*

6.3.3.1 Negative thermal ionization mass spectrometry (N-TIMS)

The Os fractions were loaded onto Pt filaments from the dried HBr trapping solution and dried under a 150 W lamp. Once the Os fraction dried out, 0.7 µl of $Ba(OH)_2$ (the activator solution utilised to improve sample ionisation) was added to the filament making sure that it covered all the sample.

The samples were analysed by negative thermal ionization mass spectrometry (N-TIMS) on a Thermo Finnigan Triton mass spectrometer operating in ion-counting mode. The total Os blank (including mass spectrometer Pt filament blank) from four blank determinations was 7.7 ± 1 fg. The $^{187}Os/^{188}Os$ blank isotopic composition was 0.2162 ± 0.0065 (see Table A.4.3).

6.3.3.2 High resolution magnetic sector field inductively coupled plasma mass spectrometry (HR-ICP-MS)

The spiked Re fractions were analysed by ICP-MS on a Thermo Finnigan Element2 high resolution magnetic sector field mass spectrometer. The 50 ppb Ir present in the 0.8 *N* HNO_3 solution containing the Re fraction monitored and confirmed that there were no changes in the instrument's stability and sensitivity throughout the run (see results in Table A.4.3).

A 1 ppb Re standard solution was analysed after every five analyses and at the beginning and the end of the run to monitor drift in mass fractionation. Also, five column blanks (prepared using all the reagents utilised for micro-column anion-exchange separation of Re, but with no sample added) were analysed at the beginning of the run. A 0.8 *N* HNO_3 wash solution was used for a minimum of 2 minutes after each analysis. The Re levels measured in the column blanks were similar to the washing solution, indicating very high purity of all the chemical reagents used. The total procedural Re blank from four blank determinations was 35.3 ± 5 fg.

6.3.3.3 Collision/reaction cell inductively coupled plasma mass spectrometry (CCT-ICP-MS)

The bulk major element (Fe, Ni, Cu) and trace element (Co) compositions of the sulphide inclusions were determined from the column washes of the micro-distillation residue. These solutions were analysed by ICP-MS (Thermo Scientific Xseries2) using a collision cell fed with a mixed H/He gas source to reduce Ar-based interferences. Calibration was via a range of mixed synthetic Fe-Ni-Cu-Co solutions. A 500 ppb Fe+Ni+Cu+Co standard solution was analysed after every five analyses and at the beginning and the end of the run to monitor drift. A 0.8 N HNO_3 wash solution was also used for a minimum of 2 minutes after each analysis. Assuming all cations in the sulphide consist of Fe, Ni, Cu and Co, element concentrations for the first three were normalised to a total of 100 atom %, with the latter reported in ppm. The results are shown in Table A.4.3.

6.3.4 *Results*

Backscattered electron imaging and multiple chemical analyses made on a separate set of sulphide inclusions from the Urals (see Chapter 5) showed that almost all sulphides were polyphase grains (mostly pyrrhotite with exsolved small blocks or lamellae of pentlandite and with rare chalcopyrite), meaning that careful recovery of all broken fragments was necessary to obtain accurate results.

Eclogitic sulphide inclusions from South Africa (Richardson et al., 2001) range in Fe contents from 74.3-91.5 at.%. The Urals inclusions have predominantly higher Fe contents (84.4-98.1 at.%), with 17 of the 20 samples having Fe >91.3 at.%. Ni (1.2-12.8 at.%) and Cu (1.2-3.6 at.%) contents are lower than those reported by Richardson et al. (2001), at 7.0-20.9 and 1.5-7.2 at.% for Ni and Cu, respectively (see Table A.4.3). Co is present in variable amounts (711-4165 ppm) and is positively correlated with Ni. The (Ni+Co)/Fe and Cu/(Fe+Ni+Cu+Co) ratios are between 0.01-0.11 and 0.01-0.04, respectively. As shown by Deines and Harris (1995), both ratios are too low to be in equilibrium with mantle olivine and these values further indicate that all sulphide inclusions analysed in this study belong to the eclogitic paragenesis.

Additional evidence for this conclusion comes from Figure 84, which shows a comparison of the Re and Os contents of the Urals sulphides with those from eclogitic diamonds from Siberia and Southern Africa. The range in Os and Re concentrations of the Ural sulphides is typical of eclogitic sulphide inclusions (e.g. Pearson et al., 1998b; Richardson et al.,

2001). The Os and Re concentrations of the Ural sulphides are positively correlated (see Table A.4.3) and vary from 87 – 967 ppb for Re, and from 3 – 775 ppb for Os.

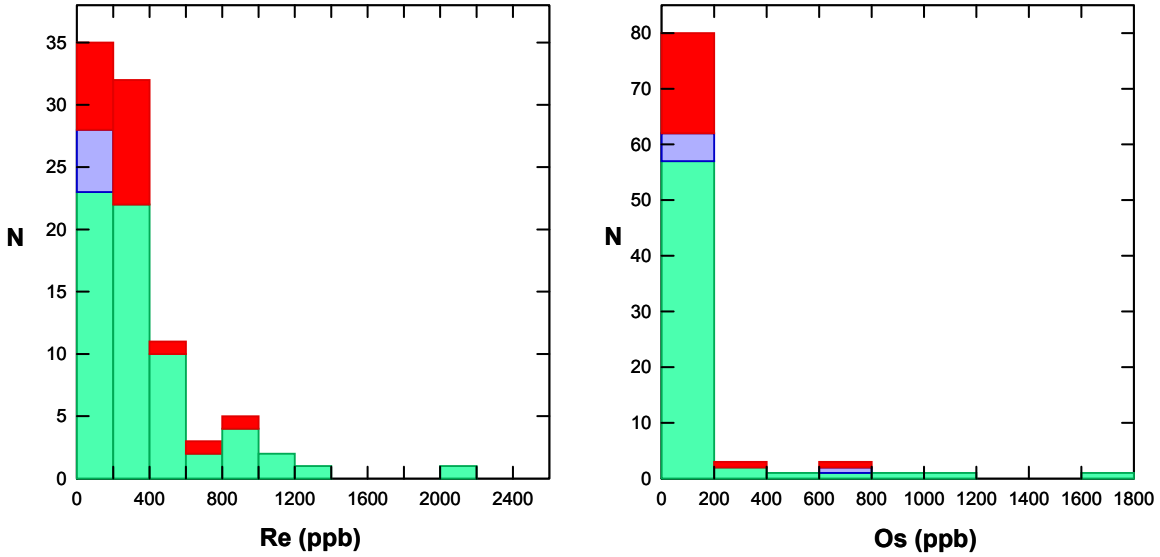

Figure 84 – Comparison of the Re and Os contents (in ppb) of sulphide inclusions in eclogitic diamonds from the Urals (blue), Siberia (red) and Southern Africa (green). The Siberia and Southern Africa inclusion data is from Pearson et al. (1998b; 1999), Richardson et al. (2001) and Aulbach et al. (in press).

The results of the Re-Os isotopic analysis are presented in Table A.4.3. The absolute 2σ errors reported in Table A.4.3 are the sum of all sources of error. Errors in $^{187}Os/^{188}Os$ are the sum of Os run precision (2σ), weighing errors and uncertainty in Os blank correction (variation in blank abundance, blank isotopic composition and spike calibration). Errors in $^{187}Re/^{188}Os$ are the sum of $^{187}Re/^{185}Re$ and $^{190}Os/^{188}Os$ run precision (2σ), weighing errors, Re and Os spike calibration and uncertainty in Re and Os blank correction.

All sulphides successfully ran in the N-TIMS instrument, but the Os levels obtained from some of the smaller sulphide samples were only approximately 10 times higher than the blank levels. Consequently, some loss of in-run precision was inevitable with uncertainties being compounded further by the magnitude of the blank correction. In addition, these minute low Os-bearing sulphides produced larger uncertainties in both $^{187}Os/^{188}Os$ and $^{187}Re/^{188}Os$ ratios due to larger weighing errors and larger blank corrections.

Globally, the Ural sulphides display a large range in the $^{187}Re/^{188}Os$ ratios (2.3 to 804) which appears to be controlled largely by the variation in Os abundance, rather than by the Re contents of the sulphides. In terms of Os isotope compositions, all samples are very radiogenic, with $^{187}Os/^{188}Os$ ratios between 1.28 and 24.3.

6.3.5 *Re-Os isochron systematics and the genesis age of the Ural diamonds*

The large spread in $^{187}Re/^{188}Os$ and $^{187}Os/^{188}Os$ ratios of the Urals sulphide inclusions (see Table A.4.3) would normally make them particularly amenable to dating using the isochron approach. However, a single, well-correlated linear array was not obtained when all samples were considered (Figure 85). This might be expected for an alluvial deposit, the wide scatter indicating that the Urals alluvial deposits contain more than one population of diamonds, with different formation ages and distinct $^{187}Os/^{188}Os$ initial ratios.

Accordingly, in order to better constrain these data, the sulphide-bearing diamonds were examined for characteristics which would indicate a shared temperature-time history. Diamond morphology and surface features are not helpful in this regard, as all are similar (see Chapter 2). It was considered that nitrogen aggregation systematics was the best means of identifying such diamonds because this process is sensitive to both temperature and time.

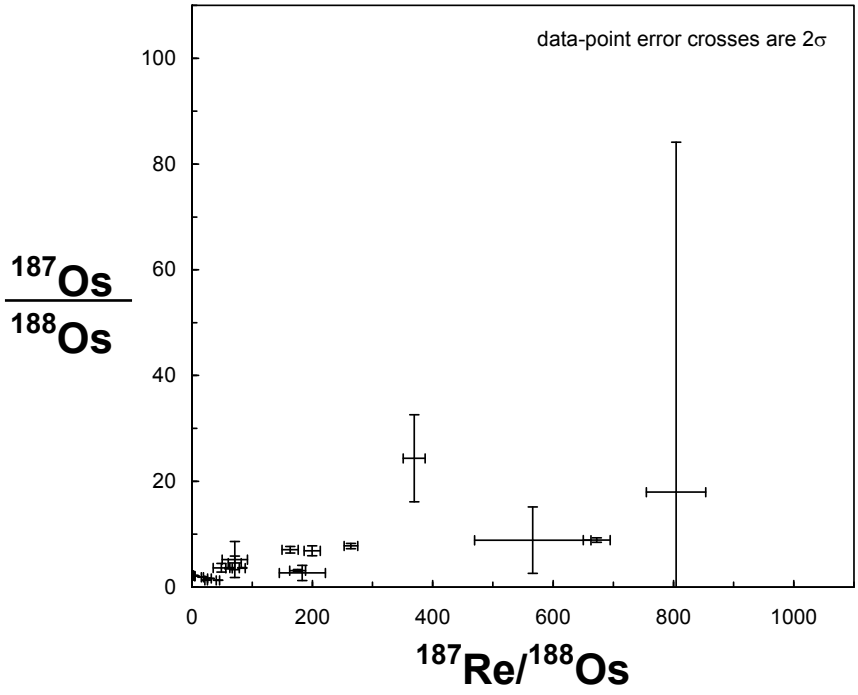

Figure 85 – Re-Os isochron diagram showing the 20 Urals sulphide inclusions analysed.

FTIR analysis identified a sub-set of 8 diamonds defining a slightly elongate trend with similar nitrogen contents and nitrogen aggregation (% B) adhering closely to the 1150°C isotherm for a residence time of 1 Ga (Figure 4). On the basis of nitrogen aggregation

kinetics, this suite of samples has experienced the same temperature-time history and hence is possibly derived from the same "population" of diamonds. The 1150ºC residence temperature also agrees with geothermometry data obtained for the principal eclogitic silicate inclusions from the Urals (see Chapter 5). From the present data, no other combination of nitrogen characteristics versus mantle residence temperature for this diamond suite provided a credible isochron.

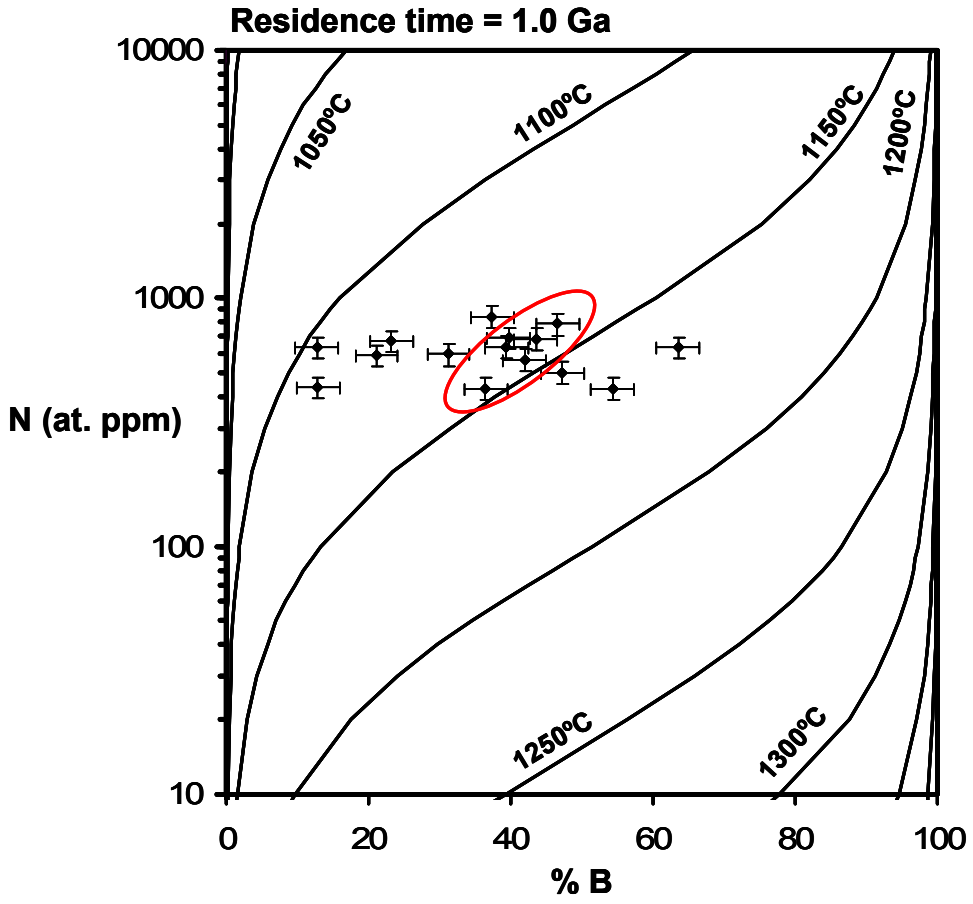

Figure 86 – Total nitrogen concentration (atomic ppm) versus nitrogen aggregation state (expressed as relative percentage of the fully aggregated nitrogen B-centre) for the 15 Ural diamonds that contained the sulphides analysed for Re-Os. Sulphides from the diamonds within the red oblate were taken as having experienced a similar temperature-time history in the mantle and hence were used for isochron regression. Error bars are ±20% for nitrogen content and ±5% for nitrogen aggregation state. Isotherms are calculated for a mantle residence time of 1.0 Ga using constants from Taylor et al. (1990).

Figure 87 shows the initial isochron regression of the 8 sulphides within this sub-group, which gave an age of 1286 ± 230 Ma (2σ error) with an elevated initial Os isotope ratio typical of eclogitic diamonds (Pearson et al., 1998b; Richardson et al., 2001). This age is interpreted to represent the genesis age of this sub-group of diamonds. The isochron regression included two sulphides with very large uncertainties in the $^{187}Os/^{188}Os$ ratio due to their small size and low Os abundance (U82d and U91a, see Table A.4.3). If these two

samples are excluded from the regression, the resulting age is not affected, but there is a slight increase in the uncertainty, implying that these two samples probably belonged to this diamond population.

From the six remaining samples, which include two sulphides released from the same diamond (U82a and U82e), a genesis age of 1280 ± 310 Ma (2σ error) was obtained (Figure 88). Of the specimens not included in the sub-set, the only other diamond containing two sulphides was sample U80 (Table A.4.3), which yielded an imprecise age of 1612 ± 320 Ma (2σ error). Whilst this age is within error of that obtained from the first sub-group of diamonds, it is deemed not to be part of the same population, as the FTIR signature of the host diamond has experienced a cooler (by ~50°C) time-integrated mantle residence.

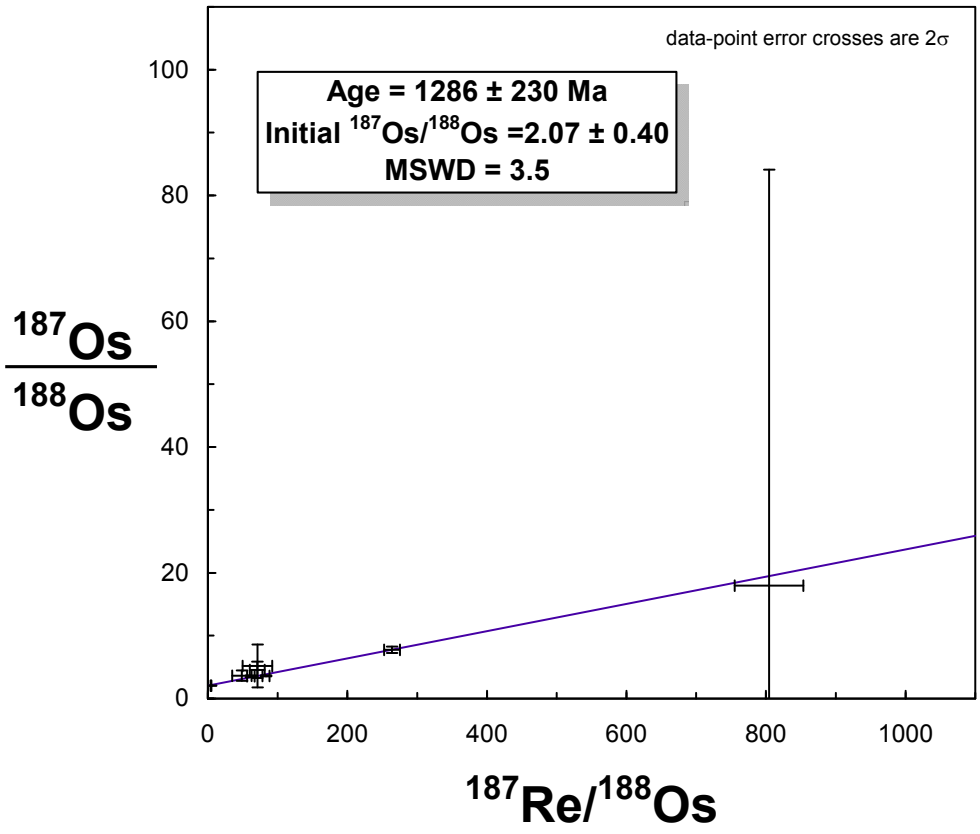

Figure 87 – Re-Os isochron diagram for samples U68c, U69b, U73b, U81a, U82a, U82d, U82e and U91a, selected on the basis of their similar nitrogen paleothermometry results (Isoplot Model 3 regression).

This Re-Os isochron age is thought reliable because: a) it includes two sulphides released from the same diamond; b) the diamonds show a narrow temperature range from N-aggregation considerations (about 20ºC), and this is comparable to the range observed in a suite of 59 diamonds recovered from a single xenolith that were interpreted by Thomassot

et al. (2007) to have all formed during a single diamond growth event; and c) the carbon and nitrogen isotopic compositions of this group of diamonds define a narrow compositional range (-6.8 to -4.2‰ for $\delta^{13}C$ and -6.9 to -4.1‰ for $\delta^{15}N$, see Chapter 4) which are consistent with an evolution from the same fluid or melt.

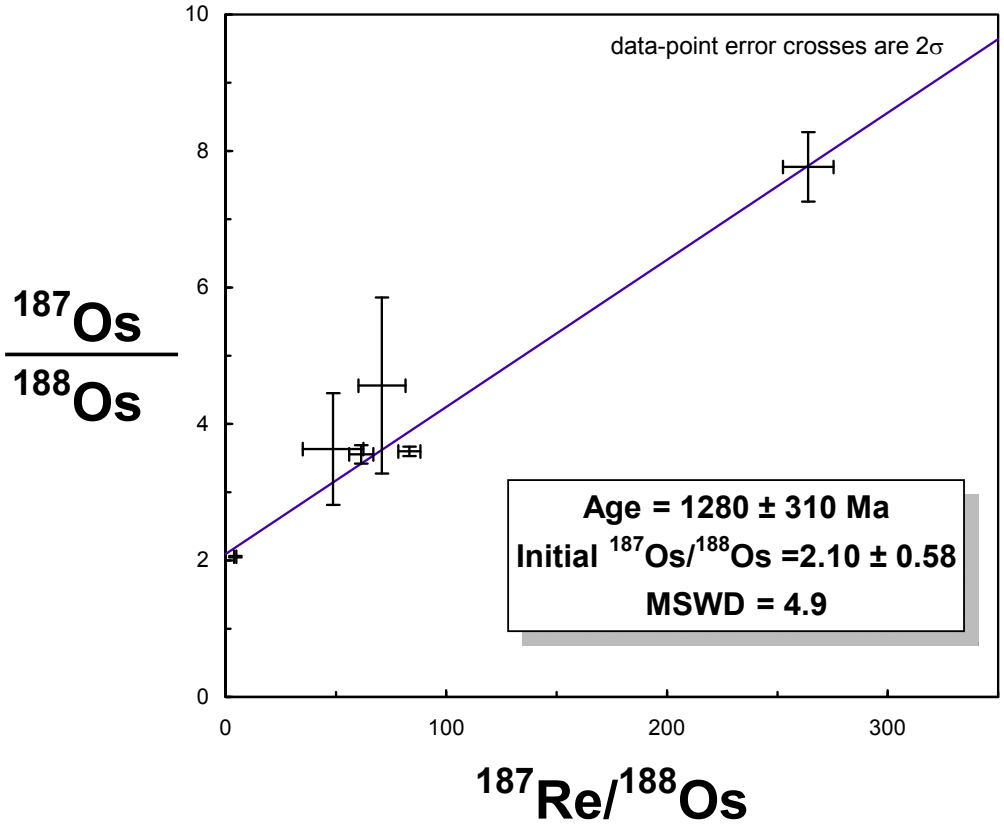

Figure 88 – Re-Os isochron diagram for the six selected eclogitic sulphide inclusions in diamonds from the Urals (Isoplot Model 3 regression). Error bars include full propagation of blank uncertainties and are at 2-sigma level.

The 1280 ± 310 Ma isochron age indicated for this sub-set of the Ural diamonds is further evidence for episodic eclogitic diamond formation. The present genesis age appears older, but within error of the 1028 ± 99 Ma to 1040 ± 120 Ma Ga for Re-Os systematics diamond formation events reported at both Orapa (Shirey et al., 2001; 2008) and Koffiefontein (Pearson et al., 1998b), but is more similar to the ~1.5 Ga genesis age determined for Jwaneng (Richardson et al. (2004); see Table A.4.1). If one considers eclogitic diamond formation as a whole lithosphere-scale event, the genesis of the Ural diamonds may also be linked to a proposed tectono-thermal mantle melting event that occurred on a worldwide basis at around 1.2 Ga (Pearson et al., 2007).

The elevated initial $^{187}Os/^{188}Os$ ratio (2.10 ± 0.58) of the 1280 ± 310 Ma isochron is in-keeping with other eclogitic sulphide inclusion isochrones (e.g. Pearson et al., 1998b;

Richardson et al., 2001). Such an elevated initial Os isochron indicates sulphide formation from a protolith, or fluids derived from a protolith, which had a suprachondritic Re/Os ratio for a considerable length of time before the inclusions were encapsulated (e.g. Pearson et al., 1998b; Richardson et al., 2001). A possible precursor with these characteristics could be a slab of oceanic crust (Roy-Barman and Allegre, 1995) subducted into a cratonic mantle keel (e.g. the East European Craton) where it was preserved by a structural mechanism such as tectonic imbrication (Helmstaedt and Schulze, 1989). Evolution from an initial $^{187}Os/^{188}Os$ of 0.12 (typical of Mesoproterozoic mantle) to the initial ratio of the Urals sulphides (using a typical MORB $^{187}Re/^{188}Os$ ratio of ~1200 (Gannoun et al., 2004)) requires a length of time of ~100 Ma. Such a period is consistent with the timescale required for oceanic crust to subduct and be subsequently emplaced in the lithospheric mantle.

6.4 Ar-Ar isotope study of clinopyroxene inclusions in the Ural diamonds

Two pre-eruption (extraneous) argon components might be present in diamond/mineral inclusion systems and need to be considered for the purposes of this study. The adopted definitions of those components follow the suggestion of Phillips et al. (2004a):

i) Excess argon: ambient ("parentless") mantle ^{40}Ar incorporated into mineral inclusions at the time of diamond crystallisation and inclusion encapsulation; i.e., derived from sources external to the diamond-inclusion system.

ii) Inherited argon: radiogenic argon ($^{40}Ar^*$) generated from in situ decay of potassium during mantle residence and retained by clinopyroxene inclusions; i.e., radiogenic argon produced between the times of diamond crystallization and kimberlite eruption.

Although excess argon is known to be present in fibrous diamonds (e.g. Ozima et al., 1989), Phillips et al. (2004a) found evidence that most gem-quality diamonds do not contain measurable quantities of excess argon. In this study, we adopt the view that any pre-eruption argon retained by the clinopyroxene inclusions is solely radiogenic argon ($^{40}Ar^*$) generated from in-situ decay of potassium during mantle residence.

6.4.1 *Obtaining an eruption age for the Ural diamonds: a collaborative effort*

The $^{40}Ar/^{39}Ar$ analysis of the Urals clinopyroxene inclusions was the product of a collaborative effort of three people: the author and two senior experts in that field of study.

The clinopyroxene inclusions were mechanically extracted from the diamonds by the author in Glasgow. They were then cleaned and sent in soda glass vials to Dr. David Phillips in the University of Melbourne, Australia, for $^{40}Ar/^{39}Ar$ analysis. Full details of the analytical procedures are given in 6.4.3.

Once the $^{40}Ar/^{39}Ar$ step-heating laser probe mass spectrometry analysis was completed, Dr. Phillips provided the author with a spreadsheet containing the raw data only (Table A.4.6). The data was then manipulated by the author with the help of Dr. Ray Burgess at the University of Manchester. In particular, the data was corrected for inclusion weights and isotopic interferences (($^{36}Ar/^{37}Ar)_{Ca}$; ($^{39}Ar/^{37}Ar)_{Ca}$; ($^{40}Ar/^{39}Ar)_{K}$); the concentrations of K, Ca and Cl in the samples were estimated according to Phillips et al. (2004a); and all errors were recalculated to 2σ. The final $^{40}Ar/^{39}Ar$ results are presented in Table A.4.5.

6.4.2 *Sample preparation*

A total of seven pale green eclogitic clinopyroxene inclusions were extracted from five Ural diamonds. All inclusions were contained within the body of the diamond, with no cracks to the surface, and exhibited imposed cubo-octahedral morphologies, a typical feature of syngenetic mineral inclusions (see Harris, 1992).

Two inclusions (U41 and U92a) were recovered as whole grains and the remainder as multiple (up to 13) fragments, all being between 70 to 380 μm in length. The weights of individual inclusions were estimated from their physical dimensions (measured under a binocular microscope, see Table A.4.4), assuming a density of 3.3 $g.cm^{-3}$ (Table A.4.5).

The clinopyroxenes were ultrasonically cleaned in de-ionised water and acetone, and then individually wrapped in aluminium foil packets and placed in a quartz glass vial, together with interspersed aliquots of the irradiation standard GA1550 (Renne et al., 1998) and packets of CaF_2 and K-glass to monitor interfering isotopes. The samples were then irradiated in position 5c of the McMaster University Research reactor, in Hamilton, Ontario, Canada.

After irradiation and cooling, the samples removed from their packaging and loaded into a copper sample tray for laser step-heating analyses. The inclusions were then baked at ~120°C for 24 hours, prior to mass spectrometry analysis.

6.4.3 *Step heating laser probe mass spectrometry*

The $^{40}Ar/^{39}Ar$ analyses were conducted at the University of Melbourne, using analytical procedures analogous to those described by Phillips et al. (2004a) and Phillips and Harris (2008). The inclusions were individually step-heated in two increments, using a defocused Spectron Nd:YAG laser. Gas purification was achieved by means of two SAES NP10 getter pumps, operated at 400°C and 20°C, respectively. Argon isotopic analyses were carried out on a MM5400 mass spectrometer, equipped with a Daly detector.

The J-values (irradiation parameters that reflect the neutron flux in the reactor and are determined from a standard with a known age which is irradiated at the same time as the samples whose ages will be determined, see McDougall and Harrison (1999)) were calculated relative to an age of 98.8 ± 0.5 Ma for the GA1550 biotite standard (Renne et al., 1998). Mass discrimination was monitored by analyses of standard air volumes from a Nupro® pipette system. Typical line blanks were $<6 \times 10^{-17}$ moles for ^{40}Ar and $<5 \times 10^{-19}$ moles for ^{39}Ar, ^{38}Ar, ^{37}Ar and ^{36}Ar. Extended line blanks (10 – 20 minutes) demonstrated atmospheric $^{40}Ar/^{36}Ar$ compositions. Correction factors for interfering reactions are as follows: $(^{39}Ar/^{37}Ar)_{Ca} = 0.000679 \pm 0.000005$; $(^{36}Ar/^{37}Ar)_{Ca} = 0.000270 \pm 0.000005$; $(^{40}Ar/^{39}Ar)_{K} = 0.0282 \pm 0.0006$; $(^{38}Ar/^{39}Ar)_{K} = 0.013 \pm 0.001$.

The reported data have been corrected for mass spectrometer backgrounds, mass discrimination, radioactive decay of ^{39}Ar and ^{37}Ar and reactor interferences. $^{40}Ar/^{39}Ar$ ages were additionally corrected for atmospheric contamination and neutron flux gradients. Unless otherwise stated, the errors are two sigma (2σ) uncertainties and exclude uncertainties in the J-value, the age of the GA1550 standard and decay constants. Decay constants are those recommended in Steiger and Jager (1977). Details of all the above information including ages are shown in Table A.4.5.

6.4.4 *Results*

The results of the $^{40}Ar/^{39}Ar$ step-heating experiments are also given in Table A.4.5. Where a clinopyroxene grain from the same diamond had fragmented into more than one piece, these were combined in a single step-heating experiment, each of which consisted of two

heating increments. A "low" temperature step, which involved heating the inclusions to the point of melting, maximised the release of pre-eruption argon. The samples were then subjected to a "high" temperature step which fused the inclusions and achieved efficient degassing of radiogenic argon (^{40}Ar*) generated during mantle residence (Phillips and Harris, 2008).

Total potassium contents of the inclusions were estimated according to Phillips et al. (2004a) and cover a wide range, from 265 ± 3 ppm to 3593 ± 37 ppm (2σ) (see Table A.4.5). Similar wide ranges in total potassium contents have also been reported for clinopyroxene inclusions in diamonds from other localities worldwide (e.g. Phillips et al., 2004a; Phillips and Harris, 2008). As monitored from reactor-produced ^{38}Ar, all inclusions contained only very low (0 to ~2.4 ppm) concentrations of chlorine. The Ca/K values increased slightly across the step-heating increments for both single and pooled inclusion fragments and it is thus unlikely that this reflects compositional zoning (not seen in the Urals clinopyroxene inclusions subjected to electron microprobe analysis) or non-uniform step-heating. Thus the dissimilarity in the argon apparent ages given by the "low" and "high" temperature steps is solely attributed to variations in the concentration of radiogenic argon (Phillips et al., 2004a) and not to any compositional, mineralogical or alteration effects.

Five clinopyroxene inclusions gave "low" temperature and "fusion" apparent ^{40}Ar/^{39}Ar ages within error of each other, the "low" temperature ages ranging from 410 ± 51 Ma to 519 ± 33 Ma, and "fusion ages" between 454 ± 38 Ma and 493 ± 11 Ma (2σ). Samples U85a and U85b (recovered from the same diamond) gave very dissimilar "low" temperature ages of 1153 ± 92 Ma and 1709 ± 43 Ma, respectively, but the "fusion" step ages are in better agreement (678 ± 22 Ma and 689 ± 17 Ma for U85a and U85b, respectively). There are no obvious correlations between apparent ^{40}Ar/^{39}Ar ages and sample weights, potassium contents or Ca/K ratios (Table A.4.5).

6.4.5 *Ar-Ar systematics and the eruption age of the Ural diamonds*

The "low" temperature heating steps are designed to reduce the amount of pre-eruption ^{40}Ar retained by extracted clinopyroxene inclusions. As pointed out by Phillips et al. (2004a), when both "low" and "high" temperature steps from individual inclusions yield analogous results, this suggests minimal retention of the inherited argon and the "fusion" step values can be interpreted as a reasonable estimate of the source age. In their study of

clinopyroxene inclusions from Orapa diamonds, Phillips and Harris (2008) found that 35% of fusion ages were within error of the time of Orapa eruption (~93 Ma; Davis (1977)), with 92% within 100 Ma of this time. Thus individual $^{40}Ar/^{39}Ar$ fusion ages should be regarded as maximum estimates of source kimberlite/lamproite eruption; however, the youngest ages from an inclusion population should approximate the time of eruption.

Of the seven samples analysed in the current study, five clinopyroxene inclusions (from four diamonds) yielded very similar "low" temperature and "fusion" ages of 462 ± 86 Ma and 472 ± 28 Ma (2σ). The results of the "fusion" steps for these five samples are presented in Figure 89.

The two other clinopyroxene inclusions (U85a and U85b, recovered from a single stone) gave "low" temperature ages older than the subsequent fusion results. This age discrepancy may reflect incomplete loss of the pre-eruption argon and thus only the "high" temperature ages can be viewed as possible maximum estimates of the source age (Phillips et al., 2004a). Alternatively, the > 200 Ma difference in the fusion ages between these two clinopyroxene inclusions and the five younger samples may indicate an older and distinct eruption age at about 684 ± 16 Ma (2σ) (Figure 89).

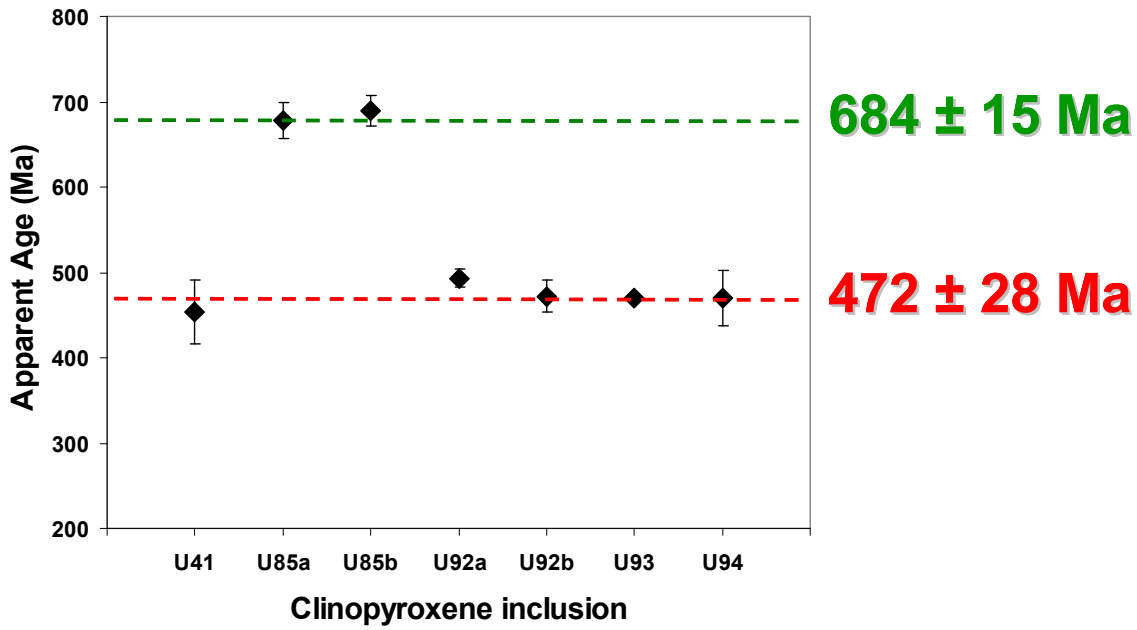

Figure 89 – $^{40}Ar/^{39}Ar$ laser fusion step-heating results for seven eclogitic clinopyroxene inclusions extracted from five Ural diamonds. Error bars are at 2-sigma level.

The 472 ± 28 Ma main eruption age presented in this work allows, for the first time, reasonable constraints to be placed on the possible primary sources of the Ural diamonds.

If the above-mentioned Orapa results of Phillips and Harris (2008) are generally applicable, then the Ural data could be linked to diamond eruption events equal to or possibly slightly younger than ~450 Ma (aspects considered in Chapter 7).

7. Discussion and Conclusions

7.1 The provenance of the diamonds in Urals alluvial deposits: assessment of the existing hypotheses

The main eruption age (472 ± 28 Ma, see Chapter 6) presented in this work allow, for the first time, constraints to be placed on the possible primary sources of the Ural diamonds. These ages are additionally constrained because the diamondiferous sedimentary rocks in the Urals are of Emsian age (Brown et al., 2006b), covering the period from 407 to 397 Ma. This Devonian age range implies that the five clinopyroxenes which gave the younger eruption ages do not contain a significant level of pre-eruption argon, indicating that the $^{40}Ar/^{39}Ar$ age has to be particularly close to the kimberlite eruption age. Therefore, the age of the source kimberlite(s)/lamproite(s) is constrained to a period of ~60 Ma, between ~410 Ma and ~470 Ma (Figure 90).

Figure 91 shows the known main localities of primary diamond deposits from Scandinavia to Siberia and from the Kola Peninsula to the Ukraine. The micro-diamonds that occur in high-grade metamorphic rocks of the Kokchetav massif in Kazakhstan have been interpreted as part of the metamorphic mineral assemblage (Sobolev and Shatsky, 1990), and thus are obviously unrelated to the Urals occurrence. Those found in the Popigai region of Siberia are confined to a impact crater of meteoritic origin (Masaitis, 1998). The origin of the micro-diamonds found in the Dniester and Pri-Azov alluvial placers in the Ukraine is unknown, but their morphology (predominantly cubes, see Yurk, 1973) and size distribution (<0.5 mm) exclude any genetic relationship to the Ural diamonds.

A contribution of diamonds from the Siberian kimberlites is also unlikely as they are located in another craton and at a distance of more than 3500 km from the Uralian placers. Even assuming that the Urals diamonds could have been transported for such a distance, the Siberian kimberlites erupted some 380 to 340 Ma ago (see Gurney et al., 2005 for a compilation of eruption ages), and thus are not only younger than the Emsian (407-397

Ma) Takaty Formation that contains the Ural diamonds (see Figure 90), but were also separated from the East European Craton (EEC) by an ocean at that time (Brown et al., 2006b).

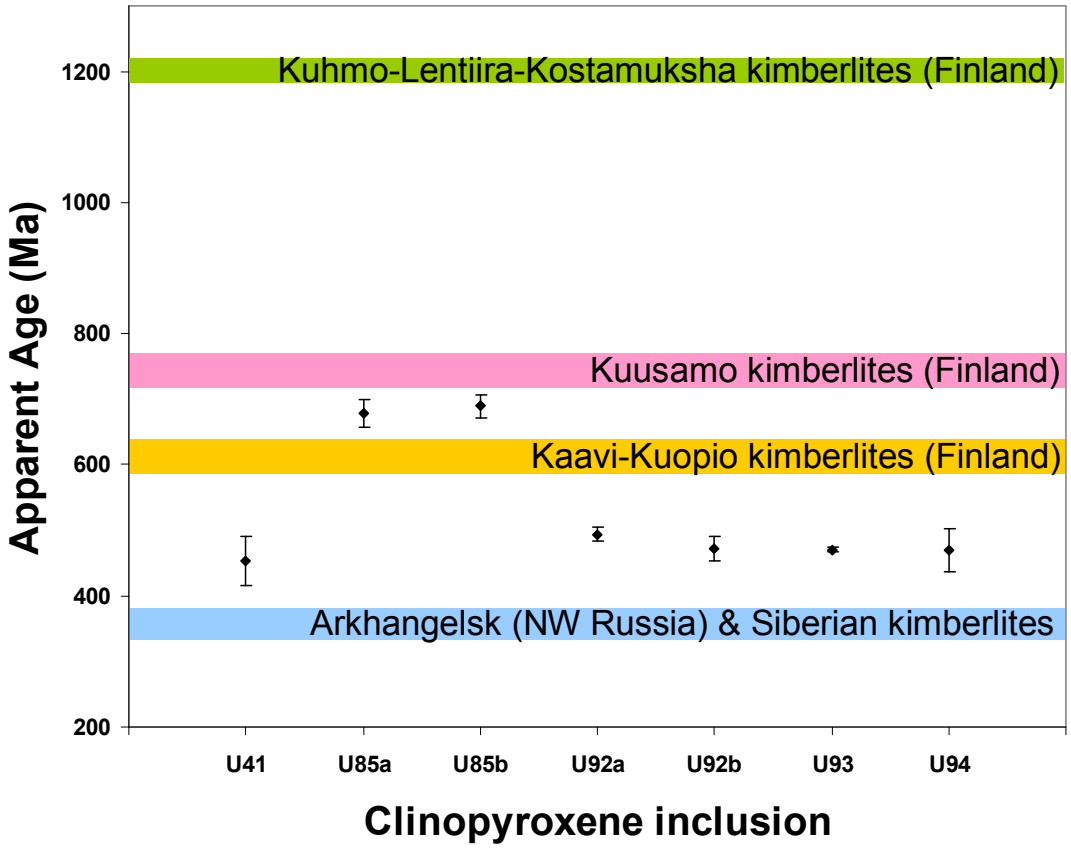

Figure 90 – $^{40}Ar/^{39}Ar$ laser fusion step-heating results for seven eclogitic clinopyroxene inclusions extracted from five Ural diamonds. Error bars are at 2-sigma level. Also plotted are the ranges in eruption ages for known kimberlites in Russia (see Beard et al., 1996; Gurney et al., 2005) and Finland (O'Brien et al., 2005; 2007; O'Brien and Bradley, 2008).

Within the EEC, the kimberlite pipes of the Kaavi-Kuopio and Kuhmo-Lentiira-Kostamuksha regions of Finland have been dated at 589-626 Ma and about 1200 Ma, respectively (O'Brien et al., 2005; 2007). Those of the Kuusamo region are still to be fully resolved (O'Brien and Bradley, 2008) but preliminary data points to an age of about 745-775 Ma. Clearly these ages are considerably older than the 472 ± 28 Ma Ural eruption age and cannot be linked to the Ural alluvial deposits (see Figure 90). It might be argued that the 684 ± 16 Ma $^{40}Ar/^{39}Ar$ eruption age obtained for one Ural diamond may be linked to the Kaavi-Kuopio kimberlites, but that kimberlite province is over 1500 km away from the Urals. In addition, the diamond morphology and size distribution of the Finnish diamonds does not appear to match that of the Urals.

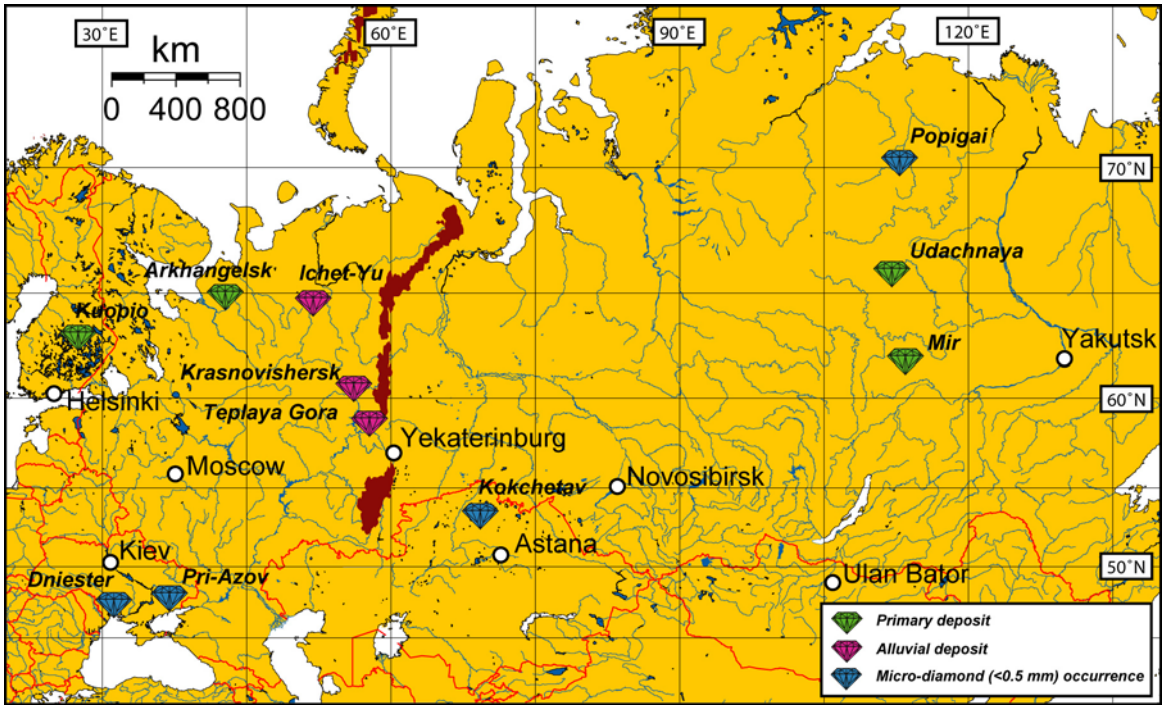

Figure 91 – The location of the main primary and alluvial macro- and micro-diamond (<0.5 mm) occurrences in Europe and Russia.

The diamonds from the pipes of the Arkhangelsk region on the EEC predominantly consist of rounded dodecahedra similar in size to those found in the Urals (Garanin et al., 2000). However, the Arkhangelsk region kimberlites are again younger (380-340 Ma, Beard et al., 1996) than both the estimated eruption age for the Ural diamonds and the age of the sedimentary rocks in which they are found (see Figure 90). Moreover, the kimberlites of Arkhangelsk still display crater facies kimberlite, indicative of minimal erosion since eruption and as Garanin et al. (2000) first suggested, it is most unlikely that this locality could be the source for the diamonds in the Urals placers.

Even if factors such as plate tectonics, kimberlite weathering and diamond transportation are not considered in this discussion, the Ural diamonds are not derived from the present known sources in the region, because their eruption ages are either too old or seriously overlap with the date of diamond deposition.

7.2 An integrated model for the genesis, eruption and accumulation of the Ural diamonds in the context of the evolution of the East European Craton

The East European Craton (EEC) is the core of the Baltica proto-plate and within it are rocks amongst the oldest known (Bogdanova, 2005; Cocks and Torsvik, 2005). The EEC is composed of three crustal segments which differ in their tectonic patterns, the ages of the crust-forming processes in the Archaean and the Proterozoic, and particularly in their Palaeoproterozoic crustal dynamics (Gorbatschev and Bogdanova, 1993; Bogdanova et al., 1996; 2001).

The northern segment (present coordinates) of the EEC is known as Fennoscandia. It features a crust which is made up of several terranes that range in thickness between 30 and 60 km and whose ages do not exceed 3.5 Ga (Korja et al., 1993; Bogdanova et al., 1996). Between 3.5 and 2.7 Ga ago, Fennoscandia was subjected to major stages of accretion and gradual growth of the Archaean continental crust. Subsequent mantle-plume events from 2.5 to 2.0 Ga ago triggered crustal rifting and fragmentation, and the opening of minor "intra-continental" oceans (Bogdanova, 2005). The 2.0 to 1.8 Ga evolution of Fennoscandia involved the closure of the small oceans and the reassembling of the previously dispersed Archaean blocks during several accretionary (subductional-collisional) orogenic episodes (Karlstrom et al., 2001). After the creation of the EEC, the south-western margin of the Fennoscandia segment was affected by a number of orogenic events at about 1.6, 1.5 and 1.2-0.95 Ga ago (Gorbatschev and Bogdanova, 1993).

Sarmatia is the southernmost (present coordinates) crustal segment of the EEC. This domain has an average crustal thickness of about 48 km and is composed of several, once independent, Archaean terranes with different ages ranging from 3.7 to 2.8 Ga, which were welded together at ca. 2.3-2.1 Ga ago (Bogdanova et al., 1996; Shchipansky and Bogdanova, 1996). Since then, Sarmatia remained a stable Archaean craton bounded by marginal folded belts, the last major crust-forming event being a 1.8-1.75 Ga widespread anorthosite-rapakivi magmatism related triggered by the collision with Fennoscandia (Bogdanova et al., 1996).

The easternmost (present coordinates) crustal segment of the EEC is named Volgo-Uralia. It is characterised by average crustal thickness of about 48 km, which is buried completely beneath a sedimentary cover locally reaching about 20 km in thickness (Bogdanova et al.,

1996; Nikishin et al., 1996). Information on the crystalline basement of Volgo-Uralia is therefore solely based on geophysical data and deep drill cores obtained from the companies that are currently exploring the high oil and gas potential of the region (Bogdanova et al., 2001). The upper crust of Volgo-Uralia is dominated by Meso- to Neo-Archaean amphibolite and granulite facies rocks affected by deformation and crustal doming at some time between 2.7 and 2.1 Ga (Bogdanova, 2005). The Volgo-Uralia crust was affected by latter stages of deformation at ca. 2.1-2.0 and 1.9-1.8 Ga, the older age recording the collision with Sarmatia, and the younger event representing the final amalgamation of the EEC (Bogdanova et al., 1996).

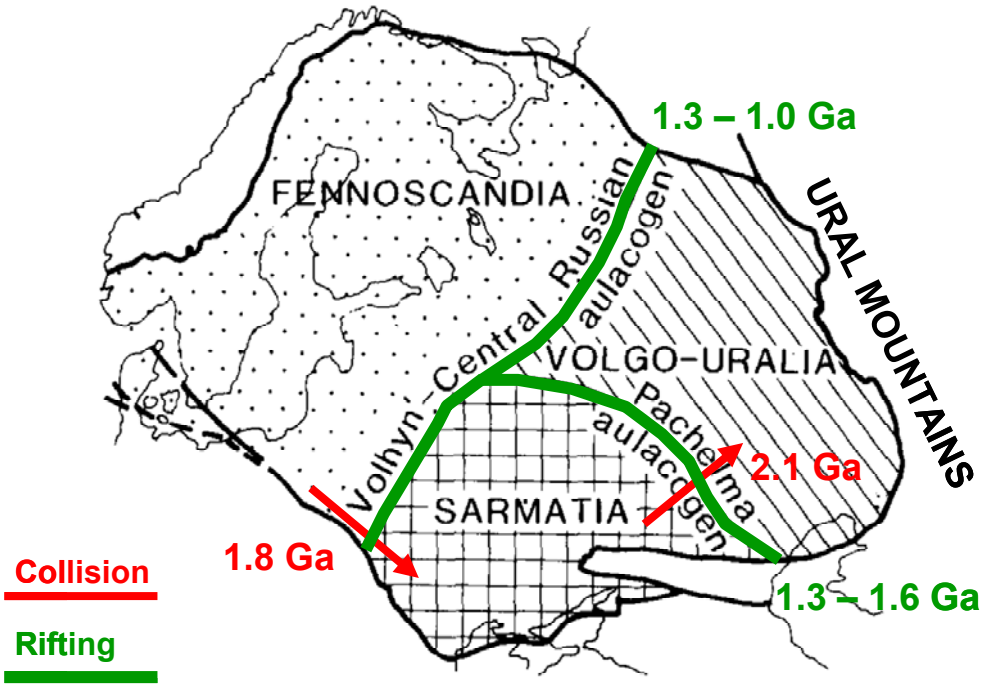

Figure 92 – Sketch map of the three crustal segments of the East European Craton (Fennoscandia, Sarmatia and Volgo-Uralia), modified from Gorbatschev and Bogdanova (1993). The red arrows indicate the timing of accretion ages for each of the crustal components. The intracratonic rift systems that developed at the intersegment suture zones after the assembly of the East European Craton are shown in green.

The evolutionary model for the EEC is described in detail by Bogdanova et al. (1996). In general terms, at about 2.1-2.0 Ga, the ocean that separated Sarmatia from Volgo-Uralia closed and these two continental segments collided, causing the overthrusting of Volgo-Uralia onto Sarmatia along the Pachelma suture (Figure 92). The two crustal segments shared a synchronous tectonic evolution after 2.0 Ga as a new, larger, Volgo-Sarmatia proto-craton. At about 1.8-1.7 Ga, south-eastwards dipping subduction started along the northern margin of Volgo-Sarmatia sub-plate (present coordinates), resulting in the amalgamation of Volgo-Sarmatia with Fennoscandia along the present-day Volhyn-Orsha

suture (Figure 92). The collision of Volgo-Uralia and the Archaean part of Fennoscandia apparently involved a substantial component of strike-slip movement that can be seen along the Central Russian suture.

Shortly after the assembly of the EEC, intracratonic rifting began, particularly in the suture zones separating the three main crustal segments (Bogdanova et al., 2001). The Pachelma rift system developed at about 1.6-1.3 Ga (Artemieva, 2003) and the transcratonic Volhyn-Orsha – Central Russian rift system was formed at about 1.3-1.0 Ga (Figure 92). The intense rift-related magmatism principally at ca. 1.3 Ga is believed to have been related to a mantle-plume event (Lobkovsky et al., 1996). In the east, rifting and formation of a passive margin occurred at ca. 1.6-1.5 Ga (Maslov, 2004). Only in the western parts of the EEC did active-margin tectonic settings continue to influence that part of the craton, until the formation of the Rodinia supercontinent at ca. 1.2 to 1.0 Ga (Bogdanova, 2005).

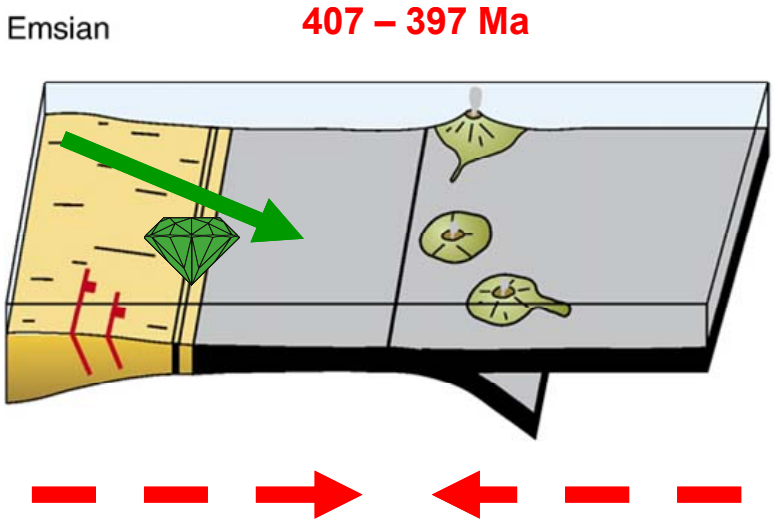

Figure 93 – Proposed model for coastal-marine diamondiferous sediment deposition along the eastern margin of the East European Craton (EEC) in Emsian times (sketch modified from Brown et al. (2006b)). The red arrows illustrate the intra-oceanic subduction taking place to the east of the craton margin, which eventually leads to the collision of the EEC with the Kazakhstan and the Siberia plates. The alluvial diamond production from the Urals shows that diamond sizes decrease southwards and towards the east, which implies a diamond source to the northwest (present coordinates), the green arrow depicting that direction.

The Re-Os genesis age of the Ural diamonds does not appear to be linked to the timing of the accretion of the EEC, even if errors are considered. The 1280 ± 310 Ma age is more likely to be associated with the upper mantle processes which gave rise to the creation, within the EEC, of the Central Russian Rift system at 1.3 Ga. A further link to trigger diamond formation at this time might be the extensive mantle melting event at about 1.2

Ga, proposed by Pearson et al. (2007) and in this region identified from osmiridium grains in the Urals placer deposits.

Subsequent to kimberlite/lamproite eruption at 472 ± 28 Ma, diamonds were eroded from the primary deposit and accumulated in sediments associated with the Takaty Formation in the Middle and North Urals. This Formation is composed of quartz sandstones with interlayers of weakly cemented conglomerates and gravelstones in the basal member (Konstantinovskii, 2003). Diamonds are mostly found in the lowermost conglomerate bed which is 0.1 to 5 metres thick (Kukharenko, 1955), and consists of alluvial sediments which have been subjected to partial rewashing within a coastal-marine zone (Konstantinovskii, 2003). Its thicker beds are confined to ancient erosional downcuttings or karstic sinkholes in the carbonate bedrock (Konstantinovskii and Prokopchuk, 1978).

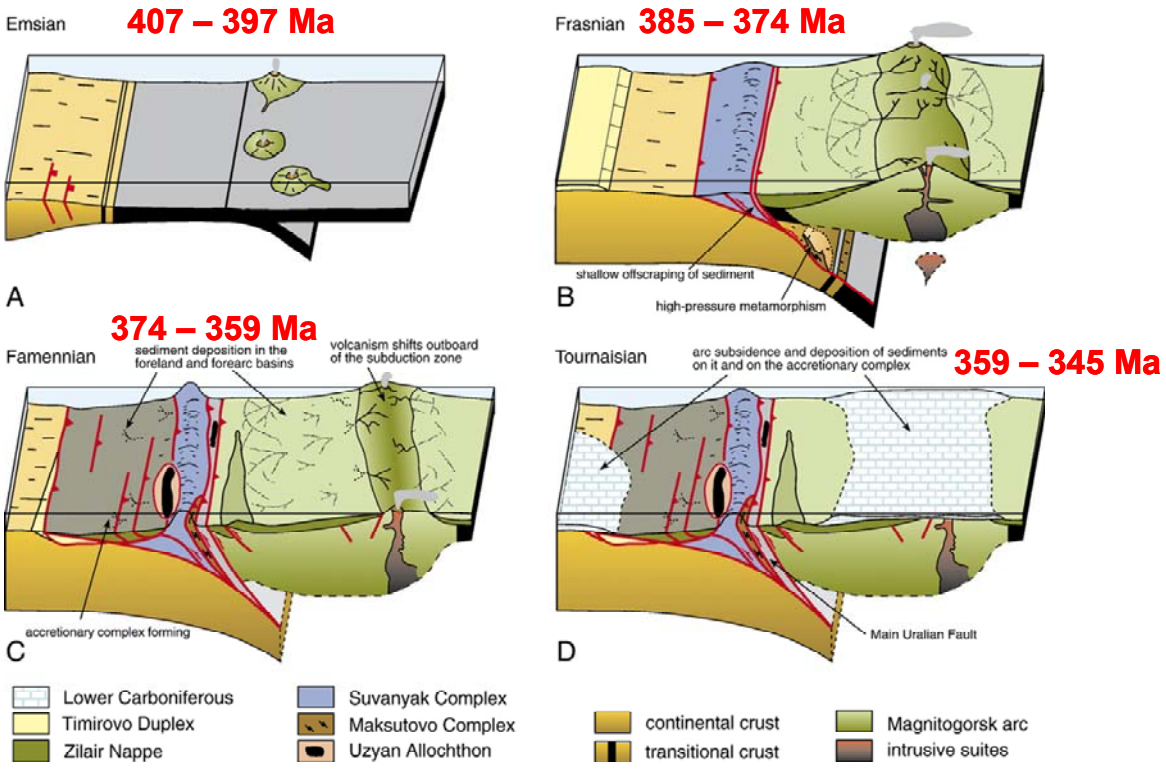

Figure 94 – Model outlining the tectonic processes that took place in the southern section of the Urals during arc-continent collision from ~407 to ~345 Ma ago (adapted from Brown et al. (2006b)). A similar set of processes is believed to have operated in the Middle section of the Urals, where most diamonds are found. During this collision, the Emsian diamondiferous formation became part of the western accretion zone and on diagram C would be in the region to the left of the main spine of the developing Ural Mountains.

During the Devonian (see Figure 93), the diamondiferous sediments are believed to have accumulated on and along the eastern margin of the EEC under coastal-marine conditions (Stepanov and Sychkin, 1996; Posukhova, 2007). Kukharenko (1955) noted that, in general

terms, the size of the Ural diamonds decreased towards the south and the east. This trend in diamond size distribution is indicative of sediment transportation from the north-west, with the larger stones being close to a palaeo-river mouth and the smaller crystals being transported further south, along the continental margin (Figure 93).

The diamondiferous sedimentary accumulation in the Urals is envisaged as being analogous to that presently found along the Namaqualand Namibian coastal belt in the western margin of southern Africa (Posukhova, 2007). Since at least Middle Eocene times, the Orange river has transported diamonds in its coarse sediment load from kimberlitic and sedimentary sources within its drainage network in southern Africa to the Namibian sector of the Atlantic Coast (Bluck et al., 2005). The mouth of the Orange river is characterised by a wave-dominated delta that is subjected to a powerful northward longshore drift under the prevailing southerly wind and South Atlantic derived south-westerly swell regimes (Jacob et al., 2006). As a consequence, onshore gravel beach deposits and offshore marine sediments along the continental shelf (Bluck et al., 2005; Spaggiari et al., 2006) have been sorted away from the mouth in an overall northward-fining trend for over 150km (Sutherland, 1982). However, the total length of the dispersal system is possibly more than 1000 km as small diamonds have been recovered at Hoanib on the Skeleton Coast (Bluck et al., 2005).

A principal difference between the above situation and the one in the Urals is that the Namaqualand-Namibia deposits are on a passive craton margin, whereas at ~400 Ma ago the eastern margin of the EEC was part of an active convergent margin (see Figure 94). During the construction of the Ural Mountains, both the alluvial and coastal-marine diamondiferous sediments became part of the western accretion zone when the EEC united with the Kazakhstan and Siberia plates during late Devonian through to late Triassic times (Brown et al., 2006b).

Subsequent to their deposition and inclusion in the formation of the Ural Mountains, reworking of the sediments of the Takaty Formation liberated and concentrated diamonds in tertiary deposits (Ishkov, 1966). As a result, the diamonds are now mined mostly from Quaternary alluvial terrace deposits and from river gravels preserved in Meso-Cenozoic karst depressions.

7.3 Conclusions

As stated at the beginning of this thesis, the principal aim of this work was to investigate the geological origin of the diamonds from the Urals. The following conclusions can be summarised from this study:

- In terms of their physical characteristics (see Chapter 2), the vast majority of the studied diamonds are rounded dodecahedra, which indicates that this diamond population have experienced major resorption after crystallisation. Throughout the diamond population there are similar and common surface features and the majority of the diamonds show signs of transportation. The diamonds that do not display evidence of transportation exhibit similar characteristics to those that do, so they are probably related in origin. More than half of the stones were affected by radiation damage, illustrated by the presence of green spots or coats on the surface of the diamonds. This similarity in physical characteristics across the Ural diamonds is consistent with the work of Kukharenko (1955) and strongly suggests that they are all part of a single population.

- The diamond nitrogen contents and nitrogen aggregation states determined by FTIR (Chapter 3) cover a large range and do not appear to match those of previous Urals studies (Khachatryan and Kaminsky, 2003). This suggests that the studied diamond population most probably consists of a "blend" of samples collected from different placer deposits in the Urals. In addition, when compared to the studied population, diamonds from primary deposits in the East European Craton show distinct FTIR signatures. Nitrogen thermometry results suggest that the diamonds likely crystallised under similar pressure-temperature conditions. This may be indicative of a single primary diamond source or of a spatial proximity between primary contributory sources of the Urals alluvial deposits.

- From a stable isotope point of view (Chapter 4), $\delta^{15}N - \delta^{13}C$ variations recorded by the peridotitic diamonds most likely reflect the existence of isotopic fractionation of mantle fluids/melts introduced into peridotites through metasomatic processes. The $\delta^{15}N - \delta^{13}C$ similarity between the peridotitic and some eclogitic diamonds suggests derivation from a similar, initially homogenous, mantle carbon source which has been subjected to metasomatic-induced isotopic fractionation. However, for some $\delta^{15}N$-enriched – $\delta^{13}C$-depleted eclogitic diamonds, the possibility of

crystallisation from subduction-related metasomatic fluids/melts cannot be excluded.

- The chemistry of syngenetic mineral inclusions (Chapter 5) indicates an almost complete overlap with previous Urals studies and the worldwide database. Inclusions of the eclogitic paragenesis are more abundant than peridotitic, with a minor websteritic phase also present. Pressure and temperature calculations of inclusion equilibration conditions show an overall agreement between the three inclusion parageneses, suggesting crystallisation at 1050-1300°C, at minimum depths of about 165 km, within a diamondiferous lithosphere extending to at least 230 km at the time of diamond formation.

- Re-Os isotopic dating of a set of eclogitic sulphide inclusions yielded a genesis age of 1280 ± 310 Ma (Chapter 6). This genesis age is likely to be associated with the upper mantle processes which gave rise to the creation, within the East European Craton, of the Central Russian Rift system at 1.3 Ga (Chapter 7). In addition, if one considers eclogitic diamond formation as a whole lithosphere-scale event, the genesis of the Ural diamonds may be linked to a proposed tectono-thermal mantle melting event that occurred on a worldwide basis at around 1.2 Ga (Pearson et al., 2007).

- $^{40}Ar/^{39}Ar$ isotopic dating carried out on a set of eclogitic clinopyroxene inclusions yielded a 472 ± 28 Ma main eruption age (Chapter 6). This age implies that the Ural diamonds are not derived from any of the present known sources in the East European Craton, because their eruption ages are either too old or seriously overlap with the 407-397 Ma diamond deposition event (Chapter 7).

- The diamondiferous sedimentary accumulation in the Urals is envisaged as being analogous to that presently found along the Namaqualand Namibian coastal belt in the western margin of southern Africa. Diamond size distribution is indicative of sediment transportation from the north-west, with the larger stones being close to a palaeo-river mouth and the smaller crystals being transported further south, along the continental margin. During the construction of the Ural Mountains, the diamondiferous sediments became part of the western accretion zone when the East European Craton united with the Kazakhstan and Siberia plates during late Devonian through to late Triassic times (Chapter 7).

Finally, the evidence presented in this thesis indicates that the Ural diamonds are likely to be derived from a kimberlite/lamproite primary source, probably on the Volgo-Uralia section of the East European Craton, which is yet to be discovered. From a prospecting point of view, the potential bad news is that the Volgo-Uralia source is likely to be under as much as 20 km of Phanerozoic sedimentary cover (Bogdanova et al., 1996; Nikishin et al., 1996).

References

Allen, B.P. and Evans, T., 1981. Aggregation of nitrogen in diamond, including platelet formation. Proceedings of the Royal Society of London, A375: 93-104.

Allsopp, H.L., Bristow, J.W., Smith, C.B., Brown, R., Gleadow, A.J.W., Kramers, J.D. and Garvie, O.G., 1989. A summary of radiometric dating methods applicable to kimberlites and related rocks. In: J.L. Ross (Editor), Kimberlites and related rocks: Their composition, occurrence, origin and emplacement. Blackwell, Carlton, pp. 343-357.

Anfilogov, V.N., Korablev, A.G. and Kabanova, L.Y., 2000. Fluid-tectonic mobilization of the buried crusts of kimberlite weathering and origin of the Urals diamond deposits. Journal of Geochemical Exploration, 69: 327-331.

Artemieva, I.M., 2003. Lithospheric structure, composition, and thermal regime of the East European Craton: implications for the subsidence of the Russian platform. Earth and Planetary Science Letters, 213: 431-446.

Aulbach, S., Shirey, S.B., Stachel, T., Creighton, S., Muehlenbachs, K. and Harris, J.W., in press. Diamond formation episodes at the southern margin of the Kaapvaal Craton: Re-Os systematics of sulfide inclusions from the Jagersfontein Mine. Contributions to Mineralogy and Petrology.

Barron, L.M., 2003. A simple model for the pressure preservation index of inclusions in diamond. American Mineralogist, 88(10): 1615-1619.

Bea, F., Fershtater, G. and Montero, P., 2002. Granitoids of the Urals: implications for the evolution of the orogen. In: D. Brown, C. Juhlin and V. Puchkov (Editors), Mountain Building in the Uralides: Pangea to the Present. American Geophysical Union, Washington, DC, pp. 211-232.

Beard, B.L., Fraracci, K.N., Taylor, L.A., Snyder, G.A., Clayton, R.A., Mayeda, T.K. and Sobolev, N.V., 1996. Petrography and geochemistry of eclogites from the Mir kimberlite, Yakutia, Russia. Contributions to Mineralogy and Petrology, 125(4): 293-310.

Bebout, G.E. and Fogel, M., 1992. Nitrogen isotope compositions of metasedimentary rocks in the Catalina Schist, California: implications for a metamorphic devolatilization history. Geochimica et Cosmochimica Acta, 56: 2839-2849.

Bekker, Y.R., Bekasova, N.B. and Ishkov, A.D., 1970. Diamond-bearing placers in the Devonian rocks of the Northern Urals. Lithology of Raw Materials, 4: 65-75.

Berzin, R., Oncken, O., Knapp, J.H., Perez-Estaun, A., Hismatulin, T., Yunusov, N. and Lipilin, A., 1996. Orogenic evolution of the Ural Mountains: results from an integrated seismic experiment. Science, 274: 220-221.

Bibby, D.M., 1982. Impurities in natural diamond. Chemistry and Physics of Carbon, 18: 3-91.

Bluck, B.J., Ward, J.D. and De Wit, M.C.J., 2005. Diamond mega-placers: southern Africa and the Kaapvaal craton in a global context. In: I. McDonald, A.J. Boyce, I.B. Butler, R.J. Herrington and D.A. Polya (Editors), Mineral Deposits and Earth Evolution. Geological Society, London, pp. 213-245.

Bogdanova, S.V., Pashkevich, I.K., Gorbatschev, R. and Orlyuk, M.I., 1996. Riphean rifting and major Paleoproterozoic crustal boundaries in the basement of the East European Craton: geology and geophysics. Tectonophysics, 268: 1-21.

Bogdanova, S.V., Gorbatschev, R. and Stephenson, R.A., 2001. EUROBRIDGE: Palaeoproterozoic accretion of Fennoscandia and Sarmatia. Tectonophysics, 339: vii-x.

Bogdanova, S.V., 2005. The East European Craton: some aspects of the Proterozoic evolution in its south-west. Mineralogical Society of Poland - Special Papers, 26: 18-24.

Borisevich, D.V., 1992. Neotectonics of the Urals. Geotectonics, 26: 41-47.

Bottinga, Y., 1969. Carbon isotope fractionation between graphite, diamond and carbon dioxide. Earth and Planetary Science Letters, 5(5): 301-307.

Boyd, F.R., 1973. A pyroxene geotherm. Geochimica et Cosmochimica Acta, 37: 2533-2546.

Boyd, S.R., Mattey, D.P., Pillinger, C.T., Milledge, H.J., Mendelssohn, M. and Seal, M., 1987. Multiple growth events during diamond genesis: an integrated study of carbon and nitrogen isotopes and nitrogen aggregation state in coated stones. Earth and Planetary Science Letters, 86(2): 341-353.

Boyd, S.R., Pillinger, C.T., Milledge, H.J. and Seal, M.J., 1992. C and N isotopic composition and the infrared absorption spectra of coated diamonds: evidence for the regional uniformity of CO_2 -H_2O rich fluids in lithospheric mantle. Earth and Planetary Science Letters, 108(1-3): 139-150.

Boyd, S.R., Wright, I.P. and Pillinger, C.T., 1993. Accurate determination of nitrogen concentrations by static vacuum mass-spectrometry. Measurement Science & Technology, 4(9): 1000-1005.

Boyd, S.R., Kiflawi, I. and Woods, G.S., 1994a. The relationship between infrared absorption and the A defect concentration in diamond. Philosophical Magazine B, 69(4): 1149-1153.

Boyd, S.R. and Pillinger, C.T., 1994. A preliminary study of $^{15}N/^{14}N$ in octahedral growth form diamonds. Chemical Geology, 116(1-2): 43-59.

Boyd, S.R., Rejou-Michel, A. and Javoy, M., 1994b. Noncryogenic Purification of Nanomole Quantities of Nitrogen Gas for Isotopic Analysis. Analytical Chemistry, 66(9): 1396-1402.

Boyd, S.R., Kiflawi, I. and Woods, G.S., 1995a. Infrared absorption by the B nitrogen aggregate in diamond. Philosophical Magazine B, 72(3): 351-361.

Boyd, S.R., Rejou-Michel, A. and Javoy, M., 1995b. Improved techniques for the extraction, purification and quantification of nanomole quantities of nitrogen gas: the nitrogen-content of diamond. Measurement Science & Technology, 6(3): 297-305.

Brey, G.P. and Kohler, T., 1990. Geothermobarometry in four-phase lherzolites II. New thermobarometers, and practical assessment of existing thermobarometers. Journal of Petrology, 31: 1353-1378.

Brey, G.P., Kohler, T. and Nickel, K.G., 1990. Geothermobarometry in four-phase lherzolites I. Experimental results from 10 to 60 kb. Journal of Petrology, 31: 1313-1352.

Brey, G.P., Doroshev, A. and Kogarko, L., 1991. The join pyrope-knorringite: experimental constraints for a new geothermobarometer for coexisting garnet and spinel, Fifth international kimberlite conference extended abstracts. CPRM Special Publication, pp. 26-28.

Brown, D., Alvarez-Marron, J., Perez-Estaun, A., Gorozhanina, Y., Baryshev, V. and Puchkov, V., 1997. Geometric and kinematic evolution of the foreland thrust and fold belt in the Southern Urals. Tectonics, 16: 551-562.

Brown, D. and Spadea, P., 1999. Processes of forearc and accretionary complex formation during arc-continent collision in the southern Ural Mountains. Geology, 27(7): 649-652.

Brown, D., Juhlin, C., Tryggvason, A., Steer, D., Ayarza, P., Beckholmen, M., Rybalka, A. and Bliznetsov, M., 2002. The crustal architecture of the Southern and Middle Urals from the URSEIS, ESRU, and Alapaev Reflection Seismic Surveys. In: D. Brown, C. Juhlin and V. Puchkov (Editors), Mountain Building in the Uralides: Pangea to the Present. American Geophysical Union, Washington, DC, pp. 33-48.

Brown, D., Puchkov, V., Alvarez-Marron, J., Bea, F. and Perez-Estaun, A., 2006a. Tectonic processes in the Southern and Middle Urals: an overview. In: D.G. Gee and R.A. Stephenson (Editors), European Lithosphere Dynamics. Geological Society of London, London, pp. 407-419.

Brown, D., Spadea, P., Puchkov, V., Alvarez-Marron, J., Herrington, R., Willner, A.P., Hetzel, R., Gorozhanina, Y. and Juhlin, C., 2006b. Arc-continent collision in the Southern Urals. Earth-Science Reviews, 79: 261-287.

Bruton, E., 1977. Diamonds. Chilton Book Company, Radnor, Pennsylvania, 532 pp.

Bulanova, G.P., 1995. The formation of diamond. Journal of Geochemical Exploration, 53(1-3): 1-23.

Bulanova, G.P., Griffin, W.L., Ryan, C.G., Shestakova, O.Y. and Barnes, S.J., 1996. Trace elements in sulfide inclusions from Yakutian diamonds. Contributions to Mineralogy and Petrology, 124(2): 111-125.

Burgess, R., Turner, G., Laurenzi, M. and Harris, J.W., 1989. ^{40}Ar-^{39}Ar laser probe dating of individual clinopyroxene inclusions in Premier eclogitic diamonds. Earth and Planetary Science Letters, 94(1-2): 22-28.

Burgess, R., Turner, G. and Harris, J.W., 1992. ^{40}Ar-^{39}Ar laser probe studies of clinopyroxene inclusions in eclogitic diamonds. Geochimica et Cosmochimica Acta, 56(1): 389-402.

Burgess, R., Phillips, D., Harris, J.W. and Robinson, D., 1998. Antarctic diamonds in south-eastern Australia? Hints from ^{40}Ar-^{39}Ar laser probe dating of clinopyroxene inclusions from Copeton diamonds, 7th International Kimberlite Conference, Cape Town, pp. 119-121 (Extended Abstracts).

Burgess, R., Kiviets, G.B. and Harris, J.W., 2004. Ar-Ar age determinations of eclogitic clinopyroxene and garnet inclusions in diamonds from the Venetia and Orapa kimberlites. Lithos, 77(1-4): 113-124.

Canil, D. and Wei, K., 1992. Constraints on the origin of mantle-derived low Ca garnets. 109: 421-430.

Canil, D., 1996. An experimental calibration of the nickel in garnet geothermometer with applications: reply. Contributions to Mineralogy and Petrology, 124: 219-223.

Cartigny, P., 1997. Concentration, composition isotopique et origine de l'azote dans le manteau terrestre (PhD Thesis), Université Denis Diderot - Paris VII, Paris, 259 pp.

Cartigny, P., Boyd, S.R., Harris, J.W. and Javoy, M., 1997. Nitrogen isotopes in peridotitic diamonds from Fuxian, China: the mantle signature. Terra Nova, 9(4): 175-179.

Cartigny, P., Harris, J.W. and Javoy, M., 1998a. Eclogitic diamond formation at Jwaneng: No room for a recycled component. Science, 280(5368): 1421-1424.

Cartigny, P., Harris, J.W., Phillips, D., Girard, M. and Javoy, M., 1998b. Subduction-related diamonds? The evidence for a mantle-derived origin from coupled δ^{13}C - δ^{15}N determinations. Chemical Geology, 147(1-2): 147-159.

Cartigny, P., Harris, J.W. and Javoy, M., 1999. Eclogitic, peridotitic and metamorphic diamonds and the problems of carbon recycling: the case of Orapa (Botswana). In: J.J. Gurney, J.L. Gurney, M.D. Pascoe and S.H. Richardson (Editors), Proceedings of the VIIth International Kimberlite Conference. Red Roof Design, Cape Town, pp. 117-124.

Cartigny, P., De Corte, K., Shatsky, V.S., Ader, M., De Paepe, P., Sobolev, N.V. and Javoy, M., 2001a. The origin and formation of metamorphic microdiamonds from the Kokchetav massif, Kazakhstan: a nitrogen and carbon isotopic study. Chemical Geology, 176(1-4): 265-281.

Cartigny, P., Harris, J.W. and Javoy, M., 2001b. Diamond genesis, mantle fractionations and mantle nitrogen content: a study of δ^{13}C-N concentrations in diamonds. Earth and Planetary Science Letters, 185(1-2): 85-98.

Cartigny, P., Harris, J.W., Taylor, A., Davies, R. and Javoy, M., 2003. On the possibility of a kinetic fractionation of nitrogen stable isotopes during natural diamond growth. Geochimica et Cosmochimica Acta, 67(8): 1571-1576.

Cartigny, P., Stachel, T., Harris, J.W. and Javoy, M., 2004. Constraining diamond metasomatic growth using C- and N-stable isotopes: examples from Namibia. Lithos, 77(1-4): 359-373.

Cartigny, P., 2005. Stable isotopes and the origin of diamond. Elements, 1(2): 79-84.

Cherniak, D.J. and Watson, E.B., 2003. Diffusion in Zircon. In: J.M. Hanchar and P.W.O. Hoskin (Editors), Zircon. Reviews in Mineralogy and Geochemistry. Mineralogical Society of America, Washington D.C., pp. 113-143.

Chrenko, R.M., 1973. Boron, the dominant acceptor in semiconducting diamond. Physical Review B, 7(10): 4560-4567.

Cocks, L.R.M. and Torsvik, T.H., 2005. Baltica from the late Precambrian to mid-Palaeozoic times: the gain and loss of a terrane's identity. Earth-Science Reviews, 72: 39-66.

Cooper, G.I., Mendelssohn, M.J. and Milledge, H.J., 1989. High pressure/ temperature experiments with natural diamond. 28th International Geological Congress: 14-17.

Craig, H., 1957. Isotopic standards for carbon and oxygen and correction factors for mass-spectroscopic analysis of carbon dioxide. Geochimica et Cosmochimica Acta, 12: 133-149.

Craig, J.R. and Kullerud, G., 1969. Phase relations in the Cu-Fe-Ni-S system and their application to magmatic ore deposits. Economic Geology Monographs, 4: 344-358.

Cumming, G.L. and Richards, J.R., 1975. Ore lead isotope ratios in a continuously changing Earth. Earth and Planetary Science Letters, 28: 155-171.

Dana, E.S., 1958. A textbook of Mineralogy (Fourth Edition, revised and enlarged by W. E. Ford). John Wiley and Sons, New York.

Davies, R.M., O'Reilly, S.Y. and Griffin, W.L., 1999. Diamonds from Wellington, NSW: insights into the origin of eastern Australian diamonds. Mineralogical Magazine, 63(4): 447-471.

Davis, G.L., 1977. The ages and uranium contents of zircons from kimberlites and associated rocks. Carnegie Institution of Washington Yearbook, 76: 631-635.

Deines, P. and Wickman, F.E., 1975. A contribution to the stable carbon isotope geochemistry of iron meteorites. Geochimica et Cosmochimica Acta, 39: 547-557.

Deines, P., 1980. The carbon isotopic composition of diamonds: relationship to diamond shape, color, occurrence and vapor composition. Geochimica et Cosmochimica Acta, 44(7): 943-961.

Deines, P., Gurney, J.J. and Harris, J.W., 1984. Associated chemical and carbon isotopic composition variations in diamonds from Finsch and Premier kimberlite, South Africa. Geochimica et Cosmochimica Acta, 48(2): 325-342.

Deines, P., Harris, J.W. and Gurney, J.J., 1987. Carbon isotopic composition, nitrogen content and inclusion composition of diamonds from the Roberts Victor Kimberlite, South Africa; evidence for $\delta^{13}C$ depletion in the mantle. Geochimica et Cosmochimica Acta, 51(5): 1227-1243.

Deines, P., Harris, J.W., Spear, P.M. and Gurney, J.J., 1989. Nitrogen and $\delta^{13}C$ content of Finsch and Premier diamonds and their implications. Geochimica et Cosmochimica Acta, 53(6): 1367-1378.

Deines, P., Harris, J.W. and Gurney, J.J., 1991a. The carbon isotopic composition and nitrogen content of lithospheric and asthenospheric diamonds from the

Jagersfontein and Koffiefontein Kimberlite, South Africa. Geochimica et Cosmochimica Acta, 55(9): 2615-2625.

Deines, P., Harris, J.W., Robinson, D.N., Gurney, J.J. and Shee, S.R., 1991b. Carbon and oxygen isotope variations in diamond and graphite eclogites from Orapa, Botswana, and the nitrogen content of their diamonds. Geochimica et Cosmochimica Acta, 55(2): 515-524.

Deines, P., Harris, J.W. and Gurney, J.J., 1993. Depth-related carbon isotope and nitrogen concentration variability in the mantle below the Orapa Kimberlite, Botswana, Africa. Geochimica et Cosmochimica Acta, 57(12): 2781-2796.

Deines, P. and Harris, J.W., 1995. Sulfide inclusion chemistry and carbon isotopes of African diamonds. Geochimica et Cosmochimica Acta, 59(15): 3173-3188.

Deines, P., Harris, J.W. and Gurney, J.J., 1997. Carbon isotope ratios, nitrogen content and aggregation state, and inclusion chemistry of diamonds from Jwaneng, Botswana. Geochimica et Cosmochimica Acta, 61(18): 3993-4005.

DeVries, R.C., 1975. Plastic deformation and "work-hardening" of diamond. Materials Research Bulletin, 10: 1193-1200.

Dickin, A.P., 1995. Radiogenic isotope geology. Cambridge University Press, New York, 452 pp.

Dickinson, J.Y., 2001. The book of diamonds: their history and romance from ancient India to modern times. Courier Dover Publications, 256 pp.

Doroshev, A.M., Brey, G.P., Girnis, A.V., Turkin, A.I. and Kogarko, L.N., 1997. Pyrope-knorringite garnets in the Earth's upper mantle: experiments in the MgO-Al_2O_3-SiO_2-Cr_2O_3 system. Russian Geology and Geophysics, 38: 559-586.

Droop, G.T.R., 1987. A general equation for estimating Fe^{3+} concentrations in ferromagnesian silicates and oxides from microprobe analyses, using stoichiometric criteria. Mineralogical Magazine, 51(361): 431-435.

Echtler, H.P., Stiller, M., Steinhoff, F., Krawczyk, C.M., Suleimanov, A., Spiridonov, V., Knapp, J.H., Menshikov, Y., Alvarez-Marron, J. and Yunusov, N., 1996. Preserved collisional crustal architecture of the Southern Urals - Vibroseis CMP-profiling. Science, 274: 224-226.

Eldridge, C.S., Compston, W., Williams, I.S., Harris, J.W. and Bristow, J.W., 1991. Isotope Evidence for the Involvement of Recycled Sediments in Diamond Formation. Nature, 353: 649-653.

Eldridge, C.S., Compston, W., Williams, I.S., Harris, J.W., Bristow, J.W. and Kinny, P.D., 1995. Applications of the SHRIMP I ion microprobe to the understanding of processes and timing of diamond formation. Economic Geology and the Bulletin of the Society of Economic Geologists, 90(2): 271-280.

Ellis, D.J. and Green, D.H., 1979. An experimental study of the effect of Ca upon garnet-clinopyroxene Fe-Mg exchange equilibria. Contributions to Mineralogy and Petrology, 71(1): 13-22.

Evans, T., Qi, Z. and Maguire, J., 1981. The stages of nitrogen aggregation in diamond. Journal of Physics, C: Solid State Physics. 14(12): L379-L384.

Evans, T. and Qi, Z., 1982. The kinetics of the aggregation of nitrogen atoms in diamond. Proceedings of the Royal Society of London, Series A: Mathematical and Physical Sciences, 381(1780): 159-178.

Evans, T. and Harris, J.W., 1989. Nitrogen aggregation, inclusion equilibration temperatures and the age of diamonds. Special Publication Geological Society of Australia, 14(2): 1001-1006.

Evans, T., 1992. Aggregation of nitrogen in diamond. In: J.E. Field (Editor), The Properties of Natural and Synthetic Diamond. Academic Press, London, pp. 259-290.

Finnerty, A.A. and Boyd, F.R., 1984. Evaluation of thermobarometers for garnet peridotites. Geochimica et Cosmochimica Acta, 48: 15-27.

Fogel, M.L. and Cifuentes, L.A., 1993. Isotope fractionation during primary production. In: S. Macko and M. Engel (Editors), Organic geochemistry: principles and applications. Plenum Press, New York, pp. 73-100.

Frank, F.C., Puttick, K.E. and Wilks, E.M., 1958. Etch pits and trigons on diamond: I. Philosophical Magazine, 3: pp. 1262-1272.

Friberg, M., Juhlin, C., Green, A.C., Horstmeyer, J., Roth, A., Rybalka, A. and Bliznetsov, M., 2000. Europrobe seismic reflection profiling across the eastern Middle Urals and West Siberian Basin. Terra Nova, 12: 252-257.

Galimov, E.M., Kaminskiy, F.V. and Ivanovskaya, I.N., 1978. Carbon-isotope compositions of diamonds from the Urals, Timan, Sayan, the Ukraine, and elsewhere. Geochemistry International, 15(2): 11-18.

Galimov, E.M., 1985. The relation between formation conditions and variations in isotope composition of diamonds. Geochemistry International, 22(1): 118-142.

Galimov, E.M., Sobolev, N.V., Yefimova, E.S., Shemanina, Y.I. and Maltsev, K.A., 1990. Carbon-isotope composition of inclusion-bearing diamonds from North Urals placers. Geochemistry International, 27(4): 131-138.

Galimov, E.M., 1991. Isotope fractionation related to kimberlite magmatism and diamond formation. Geochimica et Cosmochimica Acta, 55(6): 1697-1708.

Gannoun, A., Burton, K.W., Thomas, L.E., Parkinson, I.J., van Calsteren, P. and Schiano, P., 2004. Osmium isotope heterogeneity in the constituent phases of mid- ocean ridge basalts. Science, 303(5654): 70-72.

Garanin, V.K., Gonzaga, G.M., Campos, J.E.G. and Kudryavtseva, G.P., 2000. A new theory of the glacial origin of diamond placers in the Ural region. Moscow University Geology Bulletin, 55(5): 54-58.

Gorbatschev, R. and Bogdanova, S.V., 1993. Frontiers in the Baltic Shield. Precambrian Research, 64: 3-21.

Gradstein, F.M., Ogg, J.G., Smith, A.G., Agterberg, F.P., Bleeker, W., Cooper, R.A., Davydov, V., Gibbard, P., Hinnov, L.A., House, M.R., Lourens, L., Luterbacher, H.P., McArthur, J., Melchin, M.J., Robb, L.J., Shergold, J., Villeneuve, M., Wardlaw, B.R., Ali, J., Brinkhuis, H., Hilgen, F.J., Hooker, J., Howarth, R.J., Knoll, A.H., Laskar, J., Monechi, S., Plumb, K.A., Powell, J., Raffi, I., Röhl, U.,

Sadler, P., Sanfilippo, A., Schmitz, B., Shackleton, N.J., Shields, G.A., Strauss, H., Van Dam, J., van Kolfschoten, T., Veizer, J. and Wilson, D., 2004. A Geologic Time Scale 2004. Cambridge University Press, 589 pp.

Griffin, W.L., Jaques, A.L., Sie, S.H., Ryan, C.G., Cousens, D.R. and Suter, G.F., 1988. Conditions of diamond growth - a proton microprobe study of inclusions in West Australian diamonds. Contributions to Mineralogy and Petrology, 99(2): 143-158.

Griffin, W.L., Gurney, J.J. and Ryan, C.G., 1992. Variations in trapping temperatures and trace elements in peridotite-suite inclusions from African diamonds - evidence for two inclusion suites, and implications for lithosphere stratigraphy. Contributions to Mineralogy and Petrology, 110(1): 1-15.

Griffin, W.L., Sobolev, N.V., Ryan, C.G., Pokhilenko, N.P., Win, T.T. and Yefimova, E.S., 1993. Trace elements in garnets and chromites - diamond formation in the Siberian lithosphere. Lithos, 29(3-4): 235-256.

Griffin, W.L. and Ryan, C.G., 1995. Trace elements in indicator minerals - area selection and target evaluation in diamond exploration. Journal of Geochemical Exploration, 53(1-3): 311-337.

Griffin, W.L., Doyle, B.J., Ryan, C.G., Pearson, N.J., O' Reilly, S.Y., Davies, R., Kivi, K., Van Achtenbergh, E. and Natapov, L.M., 1999a. Layered Mantle Lithosphere in the Lac de Gras Area, Slave Craton - Composition, Structure and Origin. Journal of Petrology, 40(5): 705-727.

Griffin, W.L., Fisher, N.I., Friedman, J., Ryan, C.G. and O'Reilly, S.Y., 1999b. Cr-pyrope garnets in the lithospheric mantle I. Compositional systematics and relations to tectonic setting. Journal of Petrology, 40: 679-704.

Grutter, H.S., Apter, D.B. and Kong, J., 1999. Crust-mantle coupling - evidence from mantle-derived xenocrystic garnets. In: J.J. Gurney, J.L. Gurney, M.D. Pascoe and S.H. Richardson (Editors), Proceedings of the VIIth International Kimberlite Conference, the J.B. Dawson Volume. Red Roof Design, Cape Town, pp. 307-313.

Grutter, H.S., Gurney, J.J., Menzies, A.H. and Winter, F., 2004. An updated classification scheme for mantle-derived garnet, for use by diamond explorers. Lithos, 77(1-4): 841-857.

Grutter, H.S., Latti, D. and Menzies, A., 2006. Cr-saturation arrays in concentrate garnet compositions from kimberlite and their use in mantle barometry. Journal of Petrology, 47: 801-820.

Gurney, J.J. and Switzer, G.S., 1973. The discovery of garnets closely related to diamonds in the Finsch Pipe, South Africa. Contributions to Mineralogy and Petrology, 39(2): 103-116.

Gurney, J.J., Harris, J.W. and Rickard, R.S., 1984. Silicate and oxide inclusions in diamonds from the Orapa Mine, Botswana. In: J. Kornprobst (Editor), Kimberlites II: the mantle and crust-mantle relationships. Elsevier, Amsterdam, pp. 3-9.

Gurney, J.J., Harris, J.W., Rickard, R.S. and Moore, R.O., 1985. Inclusions in Premier Mine diamonds. Transactions of the Geological Society of South Africa, 88(2): 301-310.

Gurney, J.J., Helmstaedt, H.H., Le Roex, A.P., Nowicki, T.E., Richardson, S.H. and Westerlund, K.J., 2005. Diamonds: crustal distribution and formation processes in time and space and an integrated deposit model. Economic Geology, 100: 143-177.

Haendel, D., Muhle, K., Nitzsche, H., Stiehl, G. and Wand, U., 1986. Isotopic variations of the fixed nitrogen in metamorphic rocks. Geochimica et Cosmochimica Acta, 50: 749-758.

Haggerty, S.E., 1999. A diamond trilogy: superplumes, supercontinents and supernovae. Science, 285: 851-860.

Hall, A.E. and Smith, C.B., 1985. Lamproite diamonds: are they different? In: J.E. Glover and P.G. Harris (Editors), Kimberlite occurrence and origin: a basis for conceptual models in exploration. Geology Department and Extension Service, University of Western Australia, pp. 167-212.

Harlow, G.E. and Davies, R., 2004. Status report on stability of K-rich phases at mantle conditions. Lithos, 77(1-4): 647-653.

Harris, J.W., 1968a. The recognition of diamond inclusions. Part 2: epigenetic mineral inclusions. Industrial Diamond Review, 28: 558-561.

Harris, J.W., 1968b. The recognition of diamond inclusions. Part 1: syngenetic mineral inclusions. Industrial Diamond Review, 28: 402-410.

Harris, J.W., 1972. Black material on mineral inclusions and in internal fracture planes in diamond. Contributions to Mineralogy and Petrology, 35(1): 22-33.

Harris, J.W., Hawthorne, J.B., Oosterveld, M. and Wehmeyer, E., 1975. A classification scheme for diamond and a comparative study of South African diamond characteristics. Physics and Chemistry of the Earth, 9 (First international conference on kimberlites): 765-783.

Harris, J.W. and Gurney, J.J., 1979. Inclusions in diamond. In: J.E. Field (Editor), The properties of diamond. Academic Press, London, pp. 555-591.

Harris, J.W., 1987. Recent physical, chemical, and isotopic research of diamond. In: P.H. Nixon (Editor), Mantle Xenoliths. John Wiley & Sons Ltd, London, pp. 477-500.

Harris, J.W., 1992. Diamond Geology. In: J.E. Field (Editor), The Properties of Natural and Synthetic Diamond. Academic Press, London, pp. 345-393.

Harte, B., Gurney, J.J. and Harris, J.W., 1980. The formation of peridotitic suite inclusions in diamonds. Contributions to Mineralogy and Petrology, 72(2): 181-190.

Hauri, E.H., Pearson, D.G., Bulanova, G.P. and Milledge, H.J., 1998. Microscale variations in C and N isotopes within mantle diamonds as revealed by SIMS. VIIth International Kimberlite Conference extended abstracts volume: 317-319.

Heaney, P.J., Vicenzi, E.P. and De, S., 2005. Strange diamonds: The mysterious origins of carbonado and framesite. Elements, 1(2): 85-89.

Helmstaedt, H.H. and Schulze, D.J., 1989. Southern African kimberlites and their mantle sample: implications for Archean tectonics and lithosphere evolution. In: J. Ross et al. (Editors), Kimberlites and related rocks. Geological Society of Australia Special Publication No. 14. Blackwell, Carlton, pp. 358-368.

Herrington, R.J., Armstrong, R.N., Zaykov, V.V., Maslennikov, V.V., Tessalina, S.G., Orgeval, J.-J. and Taylor, R.N.A., 2002. Massive sulfide deposits in the South Urals: geological setting within the framework of the Uralide Orogen. In: D. Brown, C. Juhlin and V. Puchkov (Editors), Mountain Building in the Uralides: Pangea to the Present. American Geophysical Union, Washington, DC, pp. 155-182.

Hershey, J.W., 1940. The book of diamonds: their curious lore, properties, tests and synthetic manufacture. Kessinger Publishing, LLC, London, 160 pp.

Hoefs, J., 2004. Stable Isotope Geochemistry (fifth edition). Springer.

Honma, H. and Itihara, Y., 1981. Distribution of ammonium in minerals of metamorphic and granitic rocks. Geochimica et Cosmochimica Acta, 45: 983-988.

Irifune, T., Ohtani, E. and Kumazawa, M., 1982. Stability field of knorringite $Mg_3Cr_2Si_3O_{12}$ at high pressure and its implication to the occurrence of Cr-rich pyrope in the upper mantle. Physics of the Earth and Planetary Interiors, 27: 263-272.

Irifune, T. and Hariya, Y., 1983. Phase relationships in the system $Mg_3Al_2Si_3O_{12}$-$Mg_3Cr_2Si_3O_{12}$ at high pressure and some mineralogical properties of synthetic garnet solid solutions. Mineralogical Journal, 11(6): 269-281.

Irifune, T., 1987. An experimental investigation of the pyroxene garnet transformation in a pyrolite composition and its bearing on the constitution of the mantle. Physics of the Earth and Planetary Interiors, 45: 324-336.

Ishkov, A.D., 1966. Sources of diamond in Uralian placers: evidence from the Krasnaya Vishera region, All-Union conference on geology of diamond deposits. Perm University, Perm, pp. 42-48.

Jacob, D., Jagoutz, E., Lowry, D., Mattey, D. and Kudrjavtseva, G., 1994. Diamondiferous eclogites from Siberia: Remnants of Archean oceanic crust. Geochimica et Cosmochimica Acta, 58: 5191-5207.

Jacob, J., Ward, J.D., Bluck, B.J., Scholz, R.A. and Frimmel, H.E., 2006. Some observations on diamondiferous bedrock gully trapsites on Late Cainozoic, marine-cut platforms of the Sperrgebiet, Namibia. Ore Geology Reviews, 28: 493-506.

Jaques, A.L., Hall, A.E., Sheraton, J.W., Smith, C.B., Sun, S.S., Drew, R.M., Foudoulis, C. and Ellingsen, K., 1989. Composition of crystalline inclusions and C-isotopic composition of Argyle and Ellendale diamonds. In: J. Ross et al. (Editors), Kimberlites and related rocks. Geological Society of Australia Special Publication. Blackwell, Carlton, pp. 966-989.

Javoy, M., Pineau, F. and Demaiffe, D., 1984. Nitrogen and carbon isotopic composition in the diamonds of Mbuji Mayi (Zaire). Earth and Planetary Science Letters, 68(3): 399-412.

Javoy, M., Pineau, F. and Delorme, H., 1986. Carbon and nitrogen isotopes in the mantle. Chemical Geology, 57: 41-62.

Javoy, M. and Pineau, F., 1991. The volatiles record of a popping rock from the Mid-Atlantic ridge at 14ºN: chemical and isotopic compositions of gas trapped in the vesicles. Earth and Planetary Science Letters, 107: 598-611.

Kaminsky, F.V., Zakharchenko, O.D., Griffin, W.L., Channer, D.M.D. and Khachatryan-Blinova, G.K., 2000. Diamond from the Guaniamo area, Venezuela. Canadian Mineralogist, 38: 1347-1370.

Kaminsky, F.V. and Khachatryan, G.K., 2001. Characteristics of nitrogen and other impurities in diamond, as revealed by infrared absorption data. Canadian Mineralogist, 39: 1733-1745.

Karlstrom, K.E., Ahall, K.I., Harlan, S.S., Williams, M.L., McLelland, J. and Geissman, J.W., 2001. Long-lived (1.8-1.0 Ga) convergent orogen in southern Laurentia, its extensions to Australia and Baltica, and implications to refining Rodinia. Precambrian Research, 111: 5-30.

Kennedy, C.S. and Kennedy, G.C., 1976. Equilibrium boundary between graphite and diamond. Journal of Geophysical Research, 81(14): 2467-2470.

Kesson, S.E. and Ringwood, A.E., 1989. Slab-mantle interactions: 2. The formation of diamonds. Chemical Geology, 78(2): 97-118.

Khachatryan, G.K. and Kaminsky, F.V., 2003. "Equilibrium" and "non-equilibrium" diamond crystals from deposits in the East European platform, as revealed by infrared absorption data. Canadian Mineralogist, 41: 171-184.

Kinny, P.D. and Meyer, H.O.A., 1994. Zircon from the mantle - a new way to date old diamonds. Journal of Geology, 102(4): 475-481.

Kinny, P.D., Griffin, B.J., Heaman, L.M., Brakhfogel, F.F. and Spetsius, Z.V., 1997. SHRIMP U/Pb ages of perovskite and zircon from Yakutian kimberlites. Russian Geology & Geophysics, 38: 97-105.

Kirkley, M.B. and Gurney, J.J., 1989. Carbon isotope modelling of biogenic origins for carbon in eclogitic diamonds. Extended abstracts: Workshop on Diamonds, 28th International Geological Conference 40-43.

Kirkley, M.B., Gurney, J.J., Otter, M.L., Hill, S.J. and Daniels, L.R., 1991. The application of C isotope measurements to the identification of the sources of C in diamonds: a review. Applied Geochemistry, 6(5): 477-494.

Klein-BenDavid, O., Izraeli, E.S., Hauri, E. and Navon, O., 2004. Mantle fluid evolution - a tale of one diamond. Lithos, 77(1-4): 243-253.

Kohler, T.P. and Brey, G.P., 1990. Calcium exchange between olivine and clinopyroxene calibrated as a geothermobarometer for natural peridotites from 2 to 60 kb with applications. Geochimica et Cosmochimica Acta, 54: 2375-2388.

Komar, I.V. and Chikishev, A.G., 1968. Ural i Priural'e (The Urals and Ural Region). Nauka, Moscow.

Konstantinovskii, A.A. and Prokopchuk, B.I., 1978. Middle Devonian quartz-sand Formation of the eastern margin of Russian Platform. Izvestiya Akademii Nauk SSSR 9: 119-130.

Konstantinovskii, A.A., 2003. Epochs of diamond placer formation in the Precambrian and Phanerozoic. Lithology and Mineral Resources, 38(6): 530-546.

Korja, A., Korja, T., Luosto, U. and Heikkinen, P., 1993. Seismic and geoelectric evidence for collisional and extensional events in the Fennoscandian Shield - implications for Precambrian crustal evolution. Tectonophysics, 219: 129-152.

Koryakova, L.N. and Epimakhov, A.V., 2007. The Urals and Western Siberia in the Bronze and Iron Ages. Cambridge University Press, 383 pp.

Koval'skiy, V.V. and Cherskiy, N.V., 1972. Isotope composition of carbon in diamonds and possible sources of carbon for diamond formation. Geologiya i Geofizika, 9: 10-15.

Koval'skiy, V.V., Galimov, E.M. and Prokhorov, V.S., 1973. Isotopic composition of carbon from colored Yakutian diamonds. Transactions (Doklady) of the USSR Academy of Sciences, 203(1-6): 118-119.

Kramers, J.D., 1979. Lead, uranium, strontium, potassium and rubidium in inclusion-bearing diamonds and mantle-derived xenoliths from southern Africa. Earth and Planetary Science Letters, 42(1): 58-70.

Krogh, E.J., 1988. The Garnet-Clinopyroxene Fe-Mg Geothermometer - a reinterpretation of existing experimental data. Contributions to Mineralogy and Petrology, 99(1): 44-48.

Kukharenko, A.A., 1955. Diamonds of the Urals. Gosgeolizdat, Moscow, 515 pp.

Lang, A.R., 1964. Dislocations and the origin of trigons. Proceedings of the Royal Society of London, A278: pp. 234-242.

Lindsley, D.H. and Dixon, S.A., 1976. Coexisting diopside and enstatite at 20 kbar and 900º-1200ºC. American Journal of Science, 276: 1285-1301.

Lobkovsky, L.I., Cloetingh, S., Nikishin, A.M., Volozh, Y.A., Lankreijer, A.C., Belyakov, S.L., Groshev, V.G., Fokin, P.A., Milanovsky, E.E., Pevzner, L.A., Gorbachev, V.I. and Korneev, M.A., 1996. Extensional basins of the former Soviet Union - structure, basin formation mechanisms and subsidence history. Tectonophysics, 266: 251-285.

Ludwig, K.R., 2003. Isoplot 3.00: a geochronological toolkit for Microsoft Excel. Special Publication Number 4. Berkeley Geochronology Center, Berkeley, 70 pp.

MacGregor, I.D., 1974. The system MgO-Al_2O_3-SiO_2: Solubility of Al_2O_3 in enstatite for spinel and garnet peridotite compositions. American Mineralogist, 59: 110-119.

Maki, J.M., Tuomisto, F., Kelly, C., Fisher, D. and Martineau, P., 2007. Effects of thermal treatment on optically active vacancy defects in CVD diamonds. Physica B: Condensed Matter, 401-402: 613-616.

Marty, B. and Humbert, F., 1997. Nitrogen and argon isotopes in oceanic basalts. Earth and Planetary Science Letters, 152: 101-112.

Masaitis, V.L., 1998. Popigai crater: Origin and distribution of diamond-bearing impactites. Meteoritics & Planetary Science, 33(2): 349-359.

Maslov, A.V., 2004. Riphean and Vendian sedimentary sequences of the Timanides and Uralides, the eastern periphery of the East European Craton. In: D.G. Gee and V.

Pease (Editors), The Neoproterozoic Timanide Orogen of Eastern Baltica. Geological Society of London, London, pp. 19-35.

McDougall, I. and Harrison, T.M., 1999. Geochronology and thermochrology by the $^{40}Ar/^{39}Ar$ method (2nd edition). Oxford University Press, New York, 269 pp.

Mendelssohn, M.J. and Milledge, H.J., 1995a. Morphological characteristics of diamond populations and relation to temperature-dependent growth and dissolution rates. International Geology Review, 37: 285-312.

Mendelssohn, M.J. and Milledge, H.J., 1995b. Geologically significant information from routine analysis of the mid-infrared spectra of diamonds. International Geology Review, 37: 95-110.

Meyer, H.O.A., 1968. Mineral inclusions in diamonds. Year Book Carnegie Institution of Washington: 446-450.

Meyer, H.O.A. and Boyd, F.R., 1969. Mineral inclusions in diamonds. Year Book Carnegie Institution of Washington: 130-135.

Meyer, H.O.A. and Boyd, F.R., 1972. Composition and origin of crystalline inclusions in natural diamonds. Geochimica et Cosmochimica Acta, 36(11): 1255-1273.

Meyer, H.O.A. and Svisero, D.P., 1975. Mineral inclusions in Brazilian diamonds. Physics and Chemistry of the Earth, 9(First international conference on kimberlites): 785-795.

Meyer, H.O.A., 1985. Genesis of diamond - a mantle saga. American Mineralogist, 70(3-4): 344-355.

Meyer, H.O.A., 1987. Inclusions in diamond. In: P.H. Nixon (Editor), Mantle Xenoliths. John Wiley & Sons Ltd, London, pp. 501-522.

Mitchell, R.H., 1977. Ultramafic xenoliths from the Elwin bay kimberlite: the first Canadian paleogeotherm. Canadian Journal of Earth Sciences, 14: 1202-1210.

Moore, M. and Lang, A.R., 1974. On the origin of the rounded dodecahedral habit of natural diamond. Journal of Crystal Growth, 26(1): 133-139.

Moore, R.O. and Gurney, J.J., 1985. Pyroxene solid solution in garnets included in diamond. Nature (London), 318(6046): 553-555.

Moore, R.O. and Gurney, J.J., 1989. Mineral inclusions in diamond from the Monastry kimberlite, South Africa. In: J. Ross (Editor), Proceedings of the Fourth International Kimberlite Conference. Blackwell Scientific Publication, Australia, pp. 1028-1041.

Navon, O., Hutcheon, I.D., Rossman, G.R. and Wasserburg, G.J., 1988. Mantle-derived fluids in diamond micro-inclusions. Nature, 335(6193): 784-789.

Navon, O., 1999. Diamond formation in the Earth's mantle. In: J.J. Gurney, Gurney, J. L., Pascoe, M. D., Richardson, S. H. (Editor), Proceedings of the 7th International Kimberlite Conference. Red Roof Design, Cape Town, pp. 584-604.

Nickel, K.G. and Green, D.H., 1985. Empirical geothermobarometry for garnet peridotites and implications for the nature of the lithosphere, kimberlites and diamonds. Earth and Planetary Science Letters, 73(1): 158-170.

Nier, A.O. and Gulbrasen, E.A., 1939. Variations in the relative abundance of the carbon isotopes. Journal of the American Chemical Society, 61(3): 697-698.

Nikishin, A.M., Ziegler, P.A., Stephenson, R.A., Cloetingh, S.A.P.L., Furne, A.V., Fokin, P.A., Ershov, A.V., Bolotov, S.N., Korotaev, M.V., Alekseev, A.S., Gorbachev, V.I., Shipilov, E.V., Lankreijer, A., Bembinova, E.Y. and Shalimov, I.V., 1996. Late Precambrian to Triassic history of the East European Craton: dynamics of sedimentary basin evolution. Tectonophysics, 268: 23-63.

Nimis, P. and Taylor, W.R., 2000. Single clinopyroxene thermobarometry for garnet peridotites. Part I. Calibration and testing of a Cr-in-Cpx barometer and an enstatite-in-Cpx thermometer. Contributions to Mineralogy and Petrology, 139: 541-554.

Nisbet, E.G., Mattey, D.P. and Lowry, D., 1994. Can diamonds be dead bacteria? Nature, 367(6465): 694.

O'Brien, H., Peltonen, P. and Vartiainen, H., 2005. Kimberlites, carbonatites and alkaline rocks. In: M. Lehtinen (Editor), Precambrian Geology of Finland - Key to the Evolution of the Fennoscandian Shield. Elsevier Science B.V., Amsterdam, pp. 605-644.

O'Brien, H., Phillips, D. and Spencer, R., 2007. Isotopic ages of Lentiira – Kuhmo – Kostomuksha olivine lamproite - Group II kimberlites. Bulletin of the Geological Society of Finland, 79: 203-215.

O'Brien, H. and Bradley, J., 2008. New kimberlite discoveries in Kuusamo, northern Finland. 9th International Kimberlite Conference Extended Abstract: 9IKC-A-00346.

O'Neill, H.S. and Wood, B.J., 1979. An experimental study of Fe-Mg partitioning between garnet and olivine and its calibration as a geothermometer. Contributions to Mineralogy and Petrology, 70: 59-70.

O'Neill, H.S., 1980. An experimental study of Fe-Mg partitioning between garnet and olivine and its calibration as a geothermometer: corrections. Contributions to Mineralogy and Petrology, 72: 337.

Orlov, Y.L., 1977. The mineralogy of the diamond. John Wiley and Sons, New York, 235 pp.

Ozima, M., Zashu, S., Takigami, Y. and Turner, G., 1989. Origin of the anomalous ^{40}Ar-^{39}Ar age of Zaire cubic diamonds; excess ^{40}Ar in pristine mantle fluids. Nature (London), 337(6204): 226-229.

Pearson, D.G., Davies, R.M., Shirey, S.B., Carlson, R.W. and Griffin, W.L., 1998a. The age and origin of eastern Australian diamonds: Re-Os isotope evidence from sulfide inclusions in two diamonds from Wellington, New South Wales, 7th International Kimberlite Conference, Cape Town, pp. 644-666 (Extended Abstracts).

Pearson, D.G., Shirey, S.B., Harris, J.W. and Carlson, R.W., 1998b. Sulphide inclusions in diamonds from the Koffiefontein kimberlite, S Africa: constraints on diamond ages and mantle Re-Os systematics. Earth and Planetary Science Letters, 160(3-4): 311-326.

Pearson, D.G. and Shirey, S.B., 1999. Isotopic dating of diamonds. In: J. Ruiz and D.D. Lambert (Editors), Application of radiogenic isotopes to ore deposit research and exploration. Reviews in Economic Geology. Society of Economic Geologists, Denver, pp. 143-171.

Pearson, D.G., Shirey, S.B., Bulanova, G.P., Carlson, R.W. and Milledge, H.J., 1999. Re-Os isotope measurements of single sulfide inclusions in a Siberian diamond and its nitrogen aggregation systematics. Geochimica et Cosmochimica Acta, 63(5): 703-711.

Pearson, D.G. and Harris, J.W., 2004. Age constraints for diamonds from Koffiefontein mine, S. Africa: a Re-Os isotope and N-aggregation study. Geochimica et Cosmochimica Acta, 68(11): A714-A714.

Pearson, D.G., Parman, S.W. and Nowell, G.M., 2007. A link between large mantle melting events and continent growth seen in osmium isotopes. Nature, 449(7159): 202-205.

Peters, K.E., Sweeney, R.E. and Kaplan, I.R., 1978. Correlation of carbon and nitrogen stable isotope ratios in sedimentary organic matter. Limnology and Oceanography, 23: 598-604.

Phaal, C., 1965. Surface studies of diamond. Industrial Diamond Review, 25: 486-489.

Phillips, D., Onstott, T.C. and Harris, J.W., 1989. $^{40}Ar/^{39}Ar$ laser-probe dating of diamond inclusions from the Premier kimberlite. Nature, 340: 460-462.

Phillips, D., Harris, J.W., Kivets, G.B. and Burgess, R., 1998. $^{40}Ar/^{39}Ar$ laser probe analyses of clinopyroxene diamond inclusions from the Orapa and Mbuyi-Miya mines, 7th International Kimberlite Conference, Cape Town, pp. 687-689 (Extended Abstracts).

Phillips, D., Kiviets, G.B., Barton, E.S., Smith, C.B., Viljoen, K.S. and Fourie, L.F., 1999. $^{40}Ar/^{39}Ar$ dating of kimberlites and related rocks: problems and solutions. In: J.L.G. J.J. Gurney, M.D. Pascoe & S.H. Richardson (Editor), Proceedings of the 7th International Kimberlite Conference. National Book Printer, Cape Town, pp. 677-688.

Phillips, D., Harris, J.W. and Kiviets, G.B., 2004a. $^{40}Ar/^{39}Ar$ analyses of clinopyroxene inclusions in African diamonds: Implications for source ages of detrital diamonds. Geochimica et Cosmochimica Acta, 68(1): 151-165.

Phillips, D., Harris, J.W. and Viljoen, K.S., 2004b. Mineral chemistry and thermobarometry of inclusions from De Beers Pool diamonds, Kimberley, South Africa. Lithos, 77(1-4): 155-179.

Phillips, D. and Harris, J.W., 2008. Provenance studies from $^{40}Ar/^{39}Ar$ dating of mineral inclusions in diamonds: Methodological tests on the Orapa kimberlite, Botswana. Earth and Planetary Science Letters(274): 169-178.

Pollack, H.N. and Chapman, D.S., 1977. On the regional variation of heat flow, geotherms and lithospheric thickness. Tectonophysics, 38: 279-296.

Posukhova, T.V., 2007. Morphogenesis of diamond and associated minerals from diamondiferous deposits in the Urals and Timan. Moscow University Geology Bulletin, 62(3): 198-205.

Powell, R., 1985. Regression diagnostics and robust regression in geothermometer/geobarometer calibration: the garnet-clinopyroxene geothermometer revisited. Journal of Metamorphic Geology, 3(231-243).

Prinz, M., Manson, D.V., Hlava, P.F. and Keil, K., 1975. Inclusions in diamonds; garnet lherzolite and eclogite assemblages. Physics and Chemistry of the Earth, 9 (First international conference on kimberlites): 797-815.

Puchkov, V., 1997. Structure and geodynamics of the Uralian orogen. In: J.-P. Burg and M. Ford (Editors), Orogeny Through Time. Geological Society Special Publication, pp. 201-236.

Puchkov, V., 2002. Paleozoic evolution of the East European continental margin involved in the Uralide orogeny. In: D. Brown, C. Juhlin and V. Puchkov (Editors), Mountain Building in the Uralides: Pangea to the Present. American Geophysical Union, Washington, DC, pp. 9-31.

Renne, P.R., Swisher, C.C., Deino, A.L., Karner, D.B., Owens, T. and Depaolo, D.J., 1998. Intercalibration of standards, absolute ages and uncertainties in $^{40}Ar/^{39}Ar$ dating. Chemical Geology, 145: 117-152.

Richardson, S.H., Gurney, J.J., Erlank, A.J. and Harris, J.W., 1984. Origin of diamonds in old enriched mantle. Nature, 310(5974): 198-202.

Richardson, S.H., 1986. Latter-day origin of diamonds of eclogitic paragenesis. Nature, 322(6080): 623-626.

Richardson, S.H., Erlank, A.J., Harris, J.W. and Hart, S.R., 1990. Eclogitic diamonds of Proterozoic age from Cretaceous kimberlites. Nature, 346(6279): 54-56.

Richardson, S.H., Harris, J.W. and Gurney, J.J., 1993. Three generations of diamonds from old continental mantle. Nature (London), 366(6452): 256-258.

Richardson, S.H. and Harris, J.W., 1997. Antiquity of peridotitic diamonds from the Siberian craton. Earth and Planetary Science Letters, 151(3-4): 271-277.

Richardson, S.H., Chinn, I. and Harris, J.W., 1999. Age and origin of eclogitic diamonds from the Jwaneng kimberlite. In: J.J. Gurney, Gurney, J. L., Pascoe, M. D., Richardson, S. H. (Editor), Proceedings of the 7th International Kimberlite Conference. Red Roof Design, Cape Town, pp. 709-713.

Richardson, S.H., Shirey, S.B., Harris, J.W. and Carlson, R.W., 2001. Archean subduction recorded by Re-Os isotopes in eclogitic sulfide inclusions in Kimberley diamonds. Earth and Planetary Science Letters, 191(3-4): 257-266.

Richardson, S.H., Shirey, S.B. and Harris, J.W., 2004. Episodic diamond genesis at Jwaneng, Botswana, and implications for Kaapvaal craton evolution. Lithos, 77(1-4): 143-154.

Richardson, S.H., Harris, J.W. and Poml, P.F., 2006. Antiquity of harzburgitic diamonds from the Venetia kimberlite, Limpopo belt, Kaapvaal craton. Geochimica et Cosmochimica Acta, 70(18): A531-A531.

Rickard, R.S., Harris, J.W., Gurney, J.J. and Cardoso, P., 1989. Mineral inclusions in diamonds from Koffiefontein Mine. Special Publication Geological Society of Australia, 14(2): 1054-1062.

Robertson, R., Fox, J.J. and Martin, A.E., 1934. Two types of diamond. Philosophical Transactions of the Royal Society of London Series A - Mathematical Physical and Engineering Sciences, A232: 463-535.

Robinson, D.N., 1978. The characteristics of natural diamond and their interpretation. Minerals Science and Engineering, 10(2): 55-72.

Robinson, D.N., 1979. Surface textures and other features of diamonds. Ph.D. Thesis, University of Cape Town, South Africa.

Robinson, D.N., 1981. Diamonds and their surface features. Quarterly News Bulletin Geological Society of South Africa = Kwartaallikse Nuusbulletin Geologiese Vereniging van Suid Africa, 24(4): 39.

Robinson, D.N., Scott, J.A., Van Niekerk, A. and Anderson, V.G., 1989. The sequence of events reflected in the diamonds of some Southern African kimberlites. Special Publication Geological Society of Australia, 14(2): 990-1000.

Roy-Barman, M. and Allegre, C.J., 1995. $^{187}Os/^{186}Os$ in Oceanic Island Basalts - Tracing Oceanic-Crust Recycling in the Mantle. Earth and Planetary Science Letters, 129(1-4): 145-161.

Rudnick, R.L., Eldridge, C.S. and Bulanova, G.P., 1993. Diamond growth history from in situ measurement of Pb and S isotopic compositions of sulphide inclusions. Geology, 21: 13-16.

Ryan, C.G., Griffin, W.L. and Pearson, N.J., 1996. Garnet geotherms: a technique for derivation of P-T data from Cr-pyrope garnets. Journal of Geophysical Research, 101: 5611-5625.

Rybal'chenko, A.Y., Kolobyanin, V.Y., Luk'yanova, L.I., Lobkova, L.P., Protasov, B.B., Sokolov, O.V., Kirillov, V.A., Morozov, G.G., Evdokimov, A.M., Sidtikov, I.S., Rybal'chenko, T.M., Kurbatskaya, F.A., Ostroumov, V.R. and Tupyrev, Y.B., 1997. A new type of the native sources of diamonds in the Urals. Transactions (Doklady) of the Russian Academy of Sciences, 353(2): 223-226.

Satish-Kumar, M., Wada, H. and Santosh, M., 2002. Constraints on the application of carbon isotope thermometry in high- to ultrahigh-temperature metamorphic terranes. Journal of Metamorphic Geology, 20: 335-350.

Scarrow, J.H., Ayala, C. and Kimbell, G.S., 2002a. Insights into orogenesis: getting to the root of a continent-ocean-continent collision, Southern Urals, Russia. Journal of the Geological Society, 159: 659-671.

Scarrow, J.H., Hetzel, R., Gorozhanin, V.M., Dinn, M., Glodny, J., Gerdes, A., Ayala, C. and Montero, P., 2002b. Four decades of geochronological work in the Southern and Middle Urals: a review. In: D. Brown, C. Juhlin and V. Puchkov (Editors),

Mountain Building in the Uralides: Pangea to the Present. American Geophysical Union, Washington, DC, pp. 233-255.

Scharer, U., Corfu, F. and Demaiffe, D., 1997. U-Pb and Lu-Hf isotopes in baddeleyite and zircon megacrysts from the Mbuji-Mayi kimberlite: constraints on the subcontinental mantle. Chemical Geology, 143: 1-16.

Schrauder, M. and Navon, O., 1993. Solid carbon-dioxide in a natural diamond. Nature, 365(6441): 42-44.

Schulze, D.J., Wiese, D. and Steude, J., 1996. Abundance and distribution of diamonds in eclogite revealed by volume visualization of CT X-ray scans. Journal of Geology, 104(1): 109-114.

Seward, D., Brown, D., Hetzel, R., Friberg, M., Gerdes, A., Petrov, G.A. and Perez-Estaun, A., 2002. The syn- and post-orogenic low temperature events in the Southern and Middle Urals: evidence from fission-track analysis. In: D. Brown, C. Juhlin and V. Puchkov (Editors), Mountain Building in the Uralides: Pangea to the Present. American Geophysical Union, Washington, DC, pp. 257-272.

Shchipansky, A.A. and Bogdanova, S.V., 1996. The Sarmatian crustal segment: Precambrian correlation between the Voronezh Massif and the Ukrainian Shield across the Dniepr-Donets Aulacogen. Tectonophysics, 268: 109-125.

Shirey, S.B., Carlson, R.W., Richardson, S.H., Menzies, A., Gurney, J.J., Pearson, D.G., Harris, J.W. and Wiechert, U., 2001. Archean emplacement of eclogitic components into the lithospheric mantle during formation of the Kaapvaal Craton. Geophysical Research Letters, 28(13): 2509-2512.

Shirey, S.B., Harris, J.W., Richardson, S.H., Fouch, M., James, D.E., Cartigny, P., Deines, P. and Viljoen, F., 2003. Regional patterns in the paragenesis and age of inclusions in diamond, diamond composition, and the lithospheric seismic structure of Southern Africa. Lithos, 71(2-4): 243-258.

Shirey, S.B., Richardson, S.H. and Harris, J.W., 2004a. Integrated models of diamond formation and craton evolution. Lithos, 77(1-4): 923-944.

Shirey, S.B., Richardson, S.H. and Harris, J.W., 2004b. Age, paragenesis and composition of diamonds and evolution of the Precambrian mantle lithosphere of southern Africa. South African Journal of Geology, 107(1-2): 91-106.

Shirey, S.B., Richardson, S.H. and Harris, J.W., 2008. Mesoarchean to Mesoproterozoic Re-Os ages for sulfide inclusions in Orapa diamonds and implications for Kaapvaal-Zimbabwe craton development. 9th International Kimberlite Conference Extended Abstract: 9IKC-A-00365.

Smith, C.B., Gurney, J.J., Harris, J.W., Otter, M.L., Kirkley, M.B. and Jagoutz, E., 1991. Neodymium and Strontium isotope systematics of eclogite and websterite paragenesis inclusions from single diamonds, Finsch and Kimberley Pool, RSA. Geochimica et Cosmochimica Acta, 55(9): 2579-2590.

Smith, G.F.H., 1912. Gemstones and their distinctive characters. Kessinger Publishing Co., London, 372 pp.

Sobolev, N.V., Gnevushev, M.A., Mikhailovskaya, L.N., Futergendler, S.I., Shemanina, E.I., Lavrentyev, Y.G. and Pospelova, L.N., 1971. Composition of garnet and

pyroxene inclusions in Ural diamonds. Doklady Akademii Nauk SSSR, 198(1): 190-193.

Sobolev, N.V., 1977. Deep-seated inclusions in kimberlites and the problem of the composition of the upper mantle. (Translated from the Russian edition, 1974). American Geophysical Union, Washington D. C., 279 pp.

Sobolev, N.V., Galimov, E.M., Ivanovskaya, I.N. and Yefimova, E.S., 1979. Isotopic composition of carbon of diamonds containing crystalline inclusions. Docklady Akademy Nauk SSSR, 249: 1217-1220.

Sobolev, N.V., 1984. Crystalline inclusions in diamonds from New South Wales, Australia. In: J.E. Glover and P.G. Harris (Editors), Kimberlite occurrence and origin: a basis for conceptual models in exploration. University of western Australia, Perth, pp. 213-226.

Sobolev, N.V. and Shatsky, V.S., 1990. Diamond inclusions in garnets from metamorphic rocks - a new environment for diamond formation. Nature, 343(6260): 742-746.

Sobolev, N.V., Kaminsky, F.V., Griffin, W.L., Yefimova, E.S., Win, T.T., Ryan, C.G. and Botkunov, A.I., 1997. Mineral inclusions in diamonds from the Sputnik kimberlite pipe, Yakutia. Lithos, 39(3-4): 135-157.

Spaggiari, R.I., Bluck, B.J. and Ward, J.D., 2006. Characteristics of diamondiferous Plio-Pleistocene littoral deposits within the palaeo-Orange River mouth, Namibia. Ore Geology Reviews, 28: 475-492.

Stacey, J.S. and Kramers, J.D., 1975. Approximation of terrestrial lead isotope evolution by a two-stage model. Earth and Planetary Science Letters, 26: 207-221.

Stachel, T. and Harris, J.W., 1997. Syngenetic inclusions in diamond from the Birim field (Ghana) - A deep peridotitic profile with a history of depletion and re-enrichment. Contributions to Mineralogy and Petrology, 127(4): 336-352.

Stachel, T., Harris, J.W. and Brey, G.P., 1998. Rare and unusual mineral inclusions in diamonds from Mwadui, Tanzania. Contributions to Mineralogy and Petrology, 132(1): 34-47.

Stachel, T., Brey, G.P. and Harris, J.W., 2000a. Kankan diamonds (Guinea) I: from the lithosphere down to the transition zone. Contributions to Mineralogy and Petrology, 140(1): 1-15.

Stachel, T., Harris, J.W., Brey, G.P. and Joswig, W., 2000b. Kankan diamonds (Guinea) II: lower mantle inclusion parageneses. Contributions to Mineralogy and Petrology, 140(1): 16-27.

Stachel, T., Aulbach, S., Brey, G.P., Harris, J.W., Leost, I., Tappert, R. and Viljoen, K.S., 2004. The trace element composition of silicate inclusions in diamonds: a review. Lithos, 77(1-4): 1-19.

Stachel, T., Brey, G.P. and Harris, J.W., 2005. Inclusions in sublithospheric diamonds: Glimpses of deep Earth. Elements, 1(2): 73-78.

Stachel, T. and Harris, J.W., 2008. The origin of cratonic diamonds - constraints from mineral inclusions. Ore Geology Reviews, 34: 5-32.

Stachel, T., Harris, J.W. and Muehlenbachs, K., submitted. Sources of carbon in inclusion bearing diamonds. Submitted to Proceedings Volume of the 9th Internantional Kimberlite Conference, Frankfurt, 2008.

Steiger, R.H. and Jager, E., 1977. Subcommission on geochronology: convention of the use of decay constants in geo- and cosmochronology. Earth and Planetary Science Letters, 36: 359-362.

Stepanov, I.S., 1971. On the sources of diamonds in the Ural placers. Sovetskaya Geologiya, 5: 85-95.

Stepanov, I.S. and Sychkin, G.N., 1996. Geomorphological and paleogeographical conditions of formation and evolution of the diamond placers that have lost links to their primary sources: example from the Urals. Bulletin of the Russian Geological Society, 128(4): 89-94.

Strauss, H., 1986. Carbon and sulphur isotopes in Precambrian sediments from the Canadian shield. Geochimica et Cosmochimica Acta, 50: 2653-2662.

Sunagawa, I., 1984. Morphology of natural and synthetic diamond crystals. In: I. Sunagawa (Editor), Materials Science of the Earth's Interior. Terra Scientific publishing Co., Tokyo, pp. 303-330.

Sutherland, D.G., 1982. The transport and sorting of diamonds by fluvial and marine processes. Economic Geology, 77(7): 1613-1620.

Sutton, J.R., 1928. Diamond, a descriptive treatise. Thomas Murby and Co., London.

Svisero, D.P., 1981. Composicao quimica e origem de minerais inclusos em diamantes brasileiros - granadas. Anais da Academia Brasileira de Ciencias, 53(1): 153-163.

Svisero, D.P., 1983. Composicao quimica e origem de minerais inclusos em diamantes brasileiros - olivinas e piroxenios. Anais da Academia Brasileira de Ciencias, 55(4): 395-407.

Tappert, R., Stachel, T., Harris, J.W., Muehlenbachs, K., Ludwig, T. and Brey, G.P., 2005. Diamonds from Jagersfontein (South Africa): messengers from the sublithospheric mantle. Contributions to Mineralogy and Petrology, 150(5): 505-522.

Taylor, L.A., Milledge, H.J., Bulanova, G.P., Snyder, G.A. and Keller, R.A., 1998. Metasomatic eclogitic diamond growth: Evidence from multiple diamond inclusions. International Geology Review, 40(8): 663-676.

Taylor, L.A., Anand, M., Promprated, P., Floss, C. and Sobolev, N.V., 2003. The significance of mineral inclusions in large diamonds from Yakutia, Russia. American Mineralogist, 88(5-6): 912-920.

Taylor, L.A. and Anand, M., 2004. Diamonds: time capsules from the Siberian Mantle. Chemie Der Erde-Geochemistry, 64(1): 1-74.

Taylor, W.R., Jaques, A.L. and Ridd, M., 1990. Nitrogen-defect aggregation characteristics of some Australasian diamonds: time-temperature constraints on the source regions of pipe and alluvial diamonds. American Mineralogist, 75: 1290-1310.

Taylor, W.R., Canil, D. and Milledge, H.J., 1996. Kinetics of Ib to IaA nitrogen aggregation in diamond. Geochimica Et Cosmochimica Acta, 60(23): 4725-4733.

Thomassot, E., Cartigny, P., Harris, J.W. and Viljoen, K.S., 2007. Methane-related diamond crystallization in the Earth's mantle: Stable isotope evidences from a single diamond-bearing xenolith. Earth and Planetary Science Letters, 257: 362-371.

Urusovskaya, A.A. and Orlov, Y.L., 1964. Nature of plastic deformation in natural diamond. Doklady Akademii Nauk SSSR, 154: 112-115.

Van Heerden, L.A., Boyd, S.R., Milledge, H.J. and Pillinger, C.T., 1995. The carbon- and nitrogen-isotope characteristics of the Argyle and Ellendale diamonds, Western Australia. International Geology Review, 37(1): 39-50.

Vance, E.R. and Milledge, H.J., 1972. Natural and laboratory alpha-particle irradiation of diamond. Mineralogical Magazine, 38(299): 878-881.

Vance, E.R., Harris, J.W. and Milledge, H.J., 1973. Possible origins of alpha-particle damage in diamonds from kimberlite and alluvial sources. Mineralogical Magazine, 39(303): 349-360.

Veizer, J. and Hoefs, J., 1976. The nature of $^{18}O/^{16}O$ and $^{13}C/^{12}C$ secular trends in sedimentary carbonate rocks. Geochimica et Cosmochimica Acta, 40: 1387-1395.

Vinogradov, A.P., Kropotova, O.I., Orlov, Y.L. and Grinenko, V.A., 1966. Isotopic composition of diamond and carbonado crystals. Geochemistry International, 3(6): 1123-1125.

Wagner, P.A., 1914. The diamond fields of southern Africa. Transvaal leader, Johannesburg, 347 pp.

Welke, H.J., Allsopp, H.L. and Harris, J.W., 1974. Measurements of K, Rb, U, Sr and Pb in diamonds containing inclusions. Nature (London), 252(5478): 35-37.

Wells, P.R., 1977. Pyroxene thermometry in simple and complex systems. Contributions to Mineralogy and Petrology, 62: 129-139.

Westerlund, K.J., Shirey, S.B., Richardson, S.H., Carlson, R.W., Gurney, J.J. and Harris, J.W., 2006. A subduction wedge origin for Paleoarchean peridotitic diamonds and harzburgites from the Panda kimberlite, Slave craton: evidence from Re-Os isotope systematics. Contributions to Mineralogy and Petrology, 152(3): 275-294.

Wilks, E. and Wilks, J., 1994. Properties and applications of diamond. Butterworth-Heinemann, Oxford, 525 pp.

Williams, A.F., 1932. The genesis of the diamond. Ernest Benn Ltd., London.

Wood, B.J., 1974. The solubility of alumina in orthopyroxene coexisting with garnet. Contributions to Mineralogy and Petrology, 46: 1-15.

Woods, G.S., 1976. Electron microscopy of "giant" platelets on cube planes in diamond. Philosophical Magazine, 34(6): 993-1012.

Woods, G.S. and Collins, A.T., 1983. Infrared absorption spectra of hydrogen complexes in Type I diamonds. Journal of Physics and Chemistry of Solids, 44(5): 471-475.

Yamaoka, S., Kanda, H. and Setaka, N., 1980. Etching of diamond octahedrons at high temperatures and pressures with controlled oxygen partial pressure. Journal of Materials Science, 15: 332-336.

Yastrebov, Y.V., 2008. Ural Mountains, Encyclopædia Britannica Online.

Yefimova, E.S., Sobolev, N.V. and Pospelova, L.N., 1983. Sulfide inclusions in diamond and specific features of their paragenesis (in Russian). Zapiski Vsesoyuznogo Mineralogicheskogo Obshchestva, 112: 300-310.

Yurk, Y.Y., 1973. Diamonds from sandy depositions of Ukraine. Naukova Dumka, Kiev.

Zingg, T., 1935. Beiträge zur Schotteranalyse. Schweizerische Mineralogische und Petrologische Mitteilungen, 15: 39-140.

Appendices

A.1. Nitrogen contents and aggregation states

Table A.1 - FTIR characteristics of the Ural diamonds.

Sample	Type	N (at. ppm)	%B	H_2 peak	Paragenesis
U1	IaA/B	156	51	No	P
U2	IaA/B	546	55	No	E
U3	IaA/B	233	75	Yes	P
U4	IaA/B	163	82	Yes	P
U5	IaA/B	76	6	No	P
U6	IaA/B	250	38	No	P
U7	IaA/B	130	34	No	P
U8	IaA/B	88	30	No	P
U9	IaA/B	614	31	Yes	U
U11	IaA/B	644	23	Yes	E
U12	IaA/B	73	25	No	P
U13	IaA/B	717	59	Yes	E
U14	IaA/B	305	36	Yes	P
U15	IaA/B	763	2	No	E
U16	IaA/B	247	23	No	P
U17	IaA/B	135	77	Yes	P
U18	IaA/B	56	62	Yes	P
U19	IaA/B	42	66	Yes	P
U20	IaA/B	345	32	Yes	P
U21	IaA/B	402	26	No	P
U22	IaA/B	115	74	Yes	P
U23	IaA/B	209	78	Yes	W
U24	IaA/B	382	88	Yes	P
U25	IaA/B	586	53	No	E
U26	IaA/B	831	21	No	P
U27	IaA/B	257	22	No	P
U28	IaA/B	497	24	No	P
U29	IaA/B	802	44	No	P
U30	IaA/B	624	73	No	P
U31	IaA/B	696	58	No	P
U32	IaA/B	593	79	Yes	E
U33	IaA/B	546	55	Yes	E
U34	IaA/B	866	52	Yes	E
U35	IaA/B	472	59	Yes	E
U36	IaA/B	374	62	No	E
U37	IaA/B	97	42	Yes	E
U38	IaA/B	675	46	Yes	E
U39	IaA/B	662	58	Yes	E
U40	II	0	0	No	P
U41	IaA/B	473	53	Yes	E
U42	IaA/B	546	24	Yes	E
U43	IaA/B	515	7	Yes	E
U44	IaA/B	619	45	Yes	E
U45	IaA/B	355	21	No	W
U46	IaA/B	909	64	Yes	E
U47	IaA/B	205	54	Yes	E
U48	IaA/B	629	60	Yes	E
U49	IaA/B	652	50	No	E
U50	IaA/B	461	42	Yes	E
U51	IaA/B	654	87	Yes	E
U52	IaA/B	635	40	Yes	E
U53	IaA/B	1540	73	Yes	E
U54	IaA/B	422	62	Yes	E
U55	IaA/B	542	43	Yes	E
U56	IaA/B	549	33	Yes	E
U57	IaA/B	170	65	Yes	E
U58	IaA/B	698	85	Yes	E
U59	IaA/B	568	62	Yes	E
U60	IaA/B	508	10	No	E
U61	IaA/B	509	32	Yes	E
U62	IaA/B	539	49	Yes	E
U63	IaA/B	597	46	Yes	U
U64	IaA/B	580	26	Yes	U
U65	IaA/B	280	19	No	U
U66	IaA/B	249	56	Yes	U
U67	IaA/B	587	21	Yes	U
U68	IaA/B	688	44	Yes	E
U69	IaA/B	788	47	Yes	U
U70	IaA/B	711	52	Yes	U
U71	IaA	578	0	No	E
U72	IaA/B	462	52	Yes	E
U73	IaA/B	433	37	Yes	E
U74	IaA/B	633	13	Yes	E
U75	IaA/B	866	63	Yes	E
U76	IaA/B	807	34	Yes	E
U77	IaA/B	644	20	Yes	E
U78	IaA/B	846	37	Yes	U
U79	IaA/B	594	31	Yes	E
U80	IaA/B	438	13	Yes	E
U81	IaA/B	639	39	Yes	E
U82	IaA/B	567	42	Yes	E
U83	IaA/B	846	48	Yes	E
U84	IaA/B	431	55	No	E
U85	IaA/B	493	66	Yes	E
U86	IaA/B	361	69	No	E
U87	IaA/B	433	54	Yes	U
U88	IaA/B	670	23	Yes	U
U89	IaA/B	635	64	Yes	U
U90	IaA/B	502	47	Yes	U
U91	IaA/B	691	40	Yes	U
U92	IaA/B	869	27	Yes	E
U93	IaA/B	714	50	Yes	E
U94	IaA/B	359	38	Yes	E

N - Diamond nitrogen contents in atomic ppm

(%B) - percentage of the nitrogen B-defect

A.2. Carbon and nitrogen isotopes

Table A.2.1 - $\delta^{13}C$ and nitrogen contents (determined by FTIR) in diamonds from the Urals.

Sample	Paragenesis	Weight (mg)	$\delta^{13}C$ (‰)	N FTIR (ppm)	Sample	Paragenesis	Weight (mg)	$\delta^{13}C$ (‰)	N FTIR (ppm)
U1	P	1.5292	-7.47	130	U51	E	0.4527	-4.13	749
U2	E	0.9299	-5.13	585	U52	E	1.8262	-5.51	594
U3	P	0.5464	-8.86	393	U53	E	1.1858	-8.28	1528
U4	P	1.3487	-4.45	295	U54	E	1.1709	-5.61	474
U5	P	1.6399	2.31	113	U55	E	1.2182	-5.45	627
U6	P	0.5989	-2.11	230	U56	E	1.8603	-5.53	548
U7	P	2.1899	-4.36	164	U57	E	0.2675	-5.37	188
U8	P	0.2257	-2.54	133	U58	E	2.8971	-4.64	742
U9	U	1.123	-5.62	646	U59	E	0.407	-6.72	805
U11	E	1.346	-6.29	748	U60	E	0.742	-5.19	652
U12	P	1.8574	-1.48	48	U61	E	0.6913	-5.84	601
U13	E	0.6169	-6.00	886	U62	E	0.6683	-6.30	1011
U14	P	0.8074	-1.72	329	U63	U	0.7564	-5.61	651
U15	E	0.674	-11.91	696	U64	U	0.9458	-5.94	547
U16	P	1.4856	-3.66	229	U65	U	0.4751	-3.97	332
U17	P	1.0234	-4.96	211	U66	U	0.4289	-5.24	272
U18	P	0.5068	-4.94	62	U67	U	1.459	-5.28	658
U19	P	0.296	-4.99	46	U68	E	0.8102	-5.82	715
U20	P	0.8371	-1.89	418	U69	U	1.331	-5.82	832
U21	P	0.8914	-3.90	434	U70	U	0.6971	-5.87	929
U22	P	0.4014	-5.98	125	U71	E	1.4019	-4.90	621
U23	W	0.3855	-3.73	262	U72	E	1.7635	-6.77	370
U24	P	1.8904	-3.10	486	U73	E	2.2426	-6.79	480
U25	E	0.4969	-17.48	590	U74	E	0.8868	-6.41	868
U26	P	1.0846	-4.64	899	U75	E	1.3518	-5.36	1175
U27	P	0.5731	-4.43	96	U76	E	0.2763	-5.17	927
U28	P	0.853	-2.94	673	U77	E	0.2729	-4.99	573
U29	P	0.7354	-5.98	797	U78	U	2.307	-5.27	733
U30	P	2.1904	-4.95	623	U79	E	1.859	-5.58	436
U31	P	1.2131	-5.12	741	U80	E	1.6888	-5.39	560
U32	E	1.0796	-5.12	632	U81	E	1.3409	-4.24	631
U33	E	0.4178	-6.39	308	U82	E	1.8278	-5.63	624
U34	E	1.1629	-6.07	883	U83	E	0.5062	-7.52	936
U35	E	1.3415	-6.28	490	U84	E	0.768	-5.22	686
U36	E	1.1365	-6.20	434	U85	E	1.3443	-4.98	427
U37	E	1.2303	-5.39	155	U86	E	1.0128	-7.24	377
U38	E	0.6919	-6.42	698	U87	U	1.5055	-5.79	582
U39	E	2.1785	-6.28	649	U88	U	2.4903	-6.09	671
U40	P	0.3354	-2.19	0	U89	U	1.6944	-5.20	600
U41	E	0.7166	-5.08	649	U90	U	1.8121	-4.95	669
U42	E	1.889	-6.12	542	U91	U	2.8173	-5.81	698
U43	E	0.9228	-5.11	520	U92	E	1.1042	-6.19	858
U44	E	0.5137	-5.21	596	U93	E	1.6965	-5.41	800
U45	W	1.819	-5.75	360	U94	E	1.9385	-4.74	390
U46	E	1.3965	-6.34	1040					
U47	E	1.0205	-18.93	352					
U48	E	0.7888	-6.14	806					
U49	E	1.6984	-5.65	699					
U50	E	1.8007	-5.93	764					

Inclusion parageneses: Eclogitic (E), Peridotitic (P), Websteritic (W), Unknown (U)

Table A.2.2 - $\delta^{15}N$, $\delta^{13}C$ and nitrogen contents (determined by bulk combustion) in diamonds from the Urals.

Sample	Paragenesis	Weight (mg)	$\delta^{15}N$	$\delta^{13}C$	N Comb. (ppm)
U1	P	1.5292	5.82	-7.30	176
U3	P	0.5464	8.32	-8.42	217
U5	P	1.6399	-24.06	2.39	94
U15	E	0.6740	-3.23	-11.85	444
U20	P	0.8371	-9.36	-1.67	284
U24	P	1.8904	-1.89	-2.95	407
U25	E	0.4969	1.04	-16.91	674
U30	P	2.1904	-6.74	-5.17	951
U42	E	1.8890	0.72	-6.00	643
U45	W	1.8190	-4.68	-5.48	327
U47	E	1.0205	2.23	-20.96	360
U53	E	1.1858	2.32	-7.79	1991
U69	U	1.3310	-4.41	-5.82	582
U72	E	1.7635	4.42	-5.87	479
U75	E	1.3518	1.83	-5.72	1073
U81	E	1.3409	-6.90	-3.96	716

Inclusion parageneses: Eclogitic (E), Peridotitic (P), Websteritic (W), Unknown (U)

A.3. Inclusion geochemistry

Table A.3.1 – Electron microprobe chemical analyses of peridotitic garnet inclusions in diamonds from the Urals.

Mineral	Garnet	Garnet	Garnet	Garnet	Garnet	Garnet	Garnet	Garnet
Sample	U1A	U1B	U3A	U4A	U5A	U5B	U6A	U29A
Diamond	D67	D67	D87	D148	D94	D94	D37	D112
Assemblage	2 gt, 2 ol	2 gt, 2 ol	gt, ol	gt, ol	2gt, ol	2gt, ol	gt	gt, chr
Paragenesis	*p (H)*	*p (H)*	*p (H)*	*p (H)*	*p (H)*	*p (H)*	*p (H)*	*p (H)*
P_2O_5	0.01	0.02	0.08	0.02	0.01	0.02	0.00	0.02
SiO_2	41.93	42.69	40.76	40.61	42.28	42.44	42.53	40.95
TiO_2	0.05	0.04	1.00	0.08	0.00	0.02	0.02	0.32
Al_2O_3	14.39	14.60	12.02	11.24	16.59	16.71	20.38	12.88
Cr_2O_3	11.05	10.93	13.49	14.91	10.23	10.17	4.54	13.71
FeO	6.00	5.94	5.18	6.26	4.10	4.04	6.77	5.92
MnO	0.28	0.27	0.27	0.34	0.23	0.23	0.30	0.34
NiO	0.01	0.01	0.00	0.02	0.01	0.00	0.00	0.01
MgO	22.33	22.51	22.39	22.02	25.38	25.48	23.47	20.55
CaO	4.19	4.12	3.04	2.03	1.31	1.30	2.34	5.28
Na_2O	0.01	0.01	0.04	0.02	0.03	0.03	0.01	0.06
K_2O	0.00	0.00	0.00	0.00	0.00	0.01	0.01	0.00
ZnO	0.02	0.01	0.00	0.00	0.04	0.00	0.04	0.02
Totals	100.26	101.15	98.26	97.55	100.21	100.44	100.40	100.07

Total iron expressed as FeO
p (H) = peridotitic (harzburgitic) paragenesis

Number of cations on the basis of 24 oxygens

P	0.001	0.002	0.010	0.003	0.002	0.003	0.000	0.002
Si	6.078	6.119	6.051	6.110	6.005	6.008	6.006	6.027
Ti	0.005	0.004	0.111	0.009	0.000	0.002	0.002	0.036
Al	2.459	2.466	2.103	1.993	2.777	2.788	3.392	2.234
Cr	1.267	1.239	1.583	1.774	1.149	1.138	0.507	1.595
Fe	0.727	0.712	0.643	0.788	0.487	0.478	0.800	0.729
Mn	0.034	0.033	0.033	0.043	0.027	0.027	0.036	0.043
Ni	0.001	0.002	0.000	0.002	0.001	0.000	0.000	0.002
Mg	4.826	4.810	4.955	4.939	5.374	5.377	4.941	4.509
Ca	0.651	0.633	0.484	0.327	0.199	0.197	0.354	0.833
Na	0.003	0.003	0.010	0.007	0.009	0.007	0.002	0.016
K	0.000	0.000	0.000	0.000	0.000	0.001	0.002	0.000
Zn	0.002	0.001	0.000	0.000	0.005	0.000	0.004	0.002
Totals	16.054	16.023	15.984	15.996	16.034	16.027	16.045	16.027

Mg #	86.9	87.1	88.5	86.2	91.7	91.8	86.1	86.1
Ca #	11.9	11.6	8.9	6.2	3.6	3.5	6.7	15.6
Cr #	34.0	33.4	43.0	47.1	29.3	29.0	13.0	41.7

Mg # = 100Mg/(Mg + Fe^{2+}), Ca # = 100Ca/(Ca + Mg) and Cr # = 100Cr/(Cr + Al) by atom

Endmembers (mol. %)

Pyrope (Mg)	77.8	78.2	81.5	81.6	88.7	88.8	81.1	74.3
Almandine (Fe)	11.7	11.6	10.6	13.0	8.0	7.9	13.1	12.0
Grossular (Ca)	10.5	10.3	8.0	5.4	3.3	3.3	5.8	13.7

Al/Cr ratio	1.94	1.99	1.33	1.12	2.42	2.45	6.69	1.40
$Mg\#_{Ca\text{-}corr}$	88.2	88.4	89.5	86.9	92.1	92.2	86.8	87.8

$Mg\#_{Ca\text{-}corr}$ = Mg# + 2Ca

Table A.3.2 – Electron microprobe chemical analyses of eclogitic garnet inclusions in diamonds from the Urals.

Mineral	Garnet	Garnet	Garnet	Garnet	Garnet	Garnet	Garnet	Garnet
Sample	U34A	U35C	U35D	U36A	U36B	U36C	U38A	U38B
Diamond	D99-C	D99-E	D99-E	D117	D117	D117	D29-A	D29-A
Assemblage	gt, cpx	2 gt, 2 cpx	2 gt, 2 cpx	3 gt	3 gt	3 gt	2 gt	2 gt
Paragenesis	*e*	*e*	*e*	*e*	*e*	*e*	*e*	*e*
P_2O_5	0.04	0.03	0.03	0.05	0.03	0.05	0.07	0.09
SiO_2	40.35	40.83	40.38	40.52	40.68	40.55	41.34	40.28
TiO_2	0.48	0.44	0.44	0.27	0.28	0.29	0.42	0.41
Al_2O_3	22.43	22.78	22.33	22.30	22.55	22.34	22.95	22.25
Cr_2O_3	0.05	0.05	0.05	0.07	0.05	0.06	0.03	0.03
FeO	17.17	16.70	16.39	16.45	16.52	16.38	16.47	16.57
MnO	0.27	0.33	0.31	0.33	0.32	0.33	0.38	0.40
NiO	0.00	0.01	0.00	0.01	0.00	0.00	0.01	0.00
MgO	10.63	11.86	11.84	13.03	13.13	13.05	13.89	13.56
CaO	9.04	8.15	8.07	6.90	6.81	6.87	5.66	5.73
Na_2O	0.21	0.16	0.21	0.15	0.15	0.14	0.20	0.18
K_2O	0.00	0.01	0.00	0.00	0.00	0.00	0.00	0.00
ZnO	0.03	0.02	0.03	0.03	0.03	0.04	0.02	0.03
Totals	100.69	101.36	100.08	100.12	100.55	100.09	101.43	99.53

Total iron expressed as FeO
e = *eclogitic* paragenesis

Number of cations on the basis of 24 oxygens

P	0.005	0.003	0.004	0.006	0.004	0.006	0.008	0.011
Si	5.994	5.992	6.000	6.000	5.994	6.002	6.008	5.987
Ti	0.054	0.048	0.049	0.030	0.030	0.032	0.045	0.046
Al	3.927	3.940	3.910	3.892	3.916	3.897	3.931	3.897
Cr	0.006	0.005	0.006	0.008	0.006	0.007	0.004	0.004
Fe	2.133	2.050	2.037	2.037	2.036	2.027	2.002	2.060
Mn	0.033	0.040	0.039	0.041	0.040	0.041	0.046	0.050
Ni	0.000	0.001	0.000	0.001	0.000	0.000	0.001	0.000
Mg	2.354	2.595	2.623	2.876	2.884	2.879	3.009	3.004
Ca	1.439	1.281	1.285	1.095	1.075	1.089	0.881	0.912
Na	0.061	0.046	0.059	0.044	0.042	0.040	0.056	0.052
K	0.000	0.001	0.000	0.000	0.000	0.000	0.000	0.000
Zn	0.003	0.003	0.003	0.004	0.004	0.004	0.002	0.003
Totals	16.009	16.005	16.016	16.033	16.030	16.025	15.995	16.027

Mg #	52.5	55.9	56.3	58.5	58.6	58.7	60.1	59.3
Ca #	37.9	33.1	32.9	27.6	27.2	27.4	22.7	23.3
Cr #	0.1	0.1	0.2	0.2	0.2	0.2	0.1	0.1

Mg # = $100Mg/(Mg + Fe^{2+})$, Ca # = 100Ca/(Ca + Mg) and Cr # = 100Cr/(Cr + Al) by atom

Endmembers (mol. %)

Pyrope (Mg)	39.7	43.8	44.1	47.9	48.1	48.0	51.1	50.3
Almandine (Fe)	36.0	34.6	34.3	33.9	34.0	33.8	34.0	34.5
Grossular (Ca)	24.3	21.6	21.6	18.2	17.9	18.2	15.0	15.3

Al/Cr ratio	711.40	738.20	652.68	468.20	659.11	555.02	1069.09	1005.07
$Mg\#_{Ca\text{-}corr}$	55.3	58.4	58.9	60.7	60.8	60.9	61.8	61.2

$Mg\#_{Ca\text{-}corr}$ = Mg# + 2Ca

Table A.3.2 (cont.) – Electron microprobe chemical analyses of eclogitic garnet inclusions in diamonds from the Urals.

Mineral	Garnet	Garnet	Garnet	Garnet	Garnet	Garnet	Garnet	Garnet
Sample	U42A	U43A	U43B	U44A	U44B	U46A	U46B	U47A
Diamond	D10-B	D101	D101	D11-B	D11-B	D18	D18	D32
Assemblage	gt, coe, 3 sul	2 gt, 3 sul	2 gt, 3 sul	2 gt	2 gt	2 gt	2 gt	2 gt
Paragenesis	*e*	*e*	*e*	*e*	*e*	*e*	*e*	*e*
P_2O_5	0.04	0.04	0.05	0.05	0.04	0.04	0.04	0.05
SiO_2	40.17	40.51	39.97	39.71	40.10	40.75	40.27	41.27
TiO_2	0.43	0.58	0.56	0.56	0.56	0.31	0.32	0.10
Al_2O_3	22.11	22.46	22.16	22.20	22.21	22.32	22.33	23.06
Cr_2O_3	0.06	0.05	0.04	0.04	0.05	0.05	0.06	0.04
FeO	17.71	17.72	17.75	18.09	18.08	17.29	17.03	10.49
MnO	0.27	0.30	0.31	0.30	0.29	0.31	0.31	0.31
NiO	0.00	0.00	0.00	0.00	0.00	0.01	0.00	0.00
MgO	10.13	9.84	9.69	8.87	8.84	11.45	11.41	14.94
CaO	9.15	9.26	9.24	10.21	10.15	7.95	8.01	9.47
Na_2O	0.19	0.25	0.26	0.23	0.23	0.18	0.16	0.13
K_2O	0.00	0.00	0.00	0.00	0.00	0.00	0.00	0.00
ZnO	0.01	0.04	0.04	0.00	0.03	0.02	0.04	0.02
Totals	100.27	101.05	100.07	100.26	100.58	100.68	99.98	99.89

Total iron expressed as FeO
e = *eclogitic* paragenesis

Number of cations on the basis of 24 oxygens

P	0.005	0.005	0.006	0.006	0.005	0.005	0.005	0.006
Si	6.012	6.013	6.002	5.978	6.011	6.034	6.005	5.995
Ti	0.048	0.065	0.063	0.064	0.063	0.034	0.036	0.011
Al	3.900	3.929	3.922	3.939	3.924	3.895	3.925	3.948
Cr	0.007	0.006	0.005	0.004	0.006	0.006	0.007	0.005
Fe	2.217	2.200	2.229	2.277	2.266	2.141	2.124	1.274
Mn	0.034	0.038	0.040	0.038	0.037	0.039	0.040	0.039
Ni	0.000	0.000	0.000	0.000	0.000	0.001	0.000	0.000
Mg	2.260	2.178	2.169	1.991	1.975	2.528	2.537	3.235
Ca	1.467	1.473	1.487	1.647	1.630	1.261	1.280	1.474
Na	0.055	0.071	0.075	0.068	0.067	0.052	0.047	0.038
K	0.000	0.000	0.000	0.000	0.000	0.000	0.000	0.000
Zn	0.001	0.005	0.004	0.000	0.003	0.002	0.005	0.002
Totals	16.006	15.983	16.001	16.012	15.988	15.999	16.009	16.027

Mg #	50.5	49.7	49.3	46.6	46.6	54.1	54.4	71.7
Ca #	39.4	40.3	40.7	45.3	45.2	33.3	33.5	31.3
Cr #	0.2	0.2	0.1	0.1	0.2	0.2	0.2	0.1

Mg # = 100Mg/(Mg + Fe^{2+}), Ca # = 100Ca/(Ca + Mg) and Cr # = 100Cr/(Cr + Al) by atom

Endmembers (mol. %)

Pyrope (Mg)	38.0	37.2	36.9	33.7	33.6	42.6	42.7	54.1
Almandine (Fe)	37.3	37.6	37.9	38.5	38.6	36.1	35.8	21.3
Grossular (Ca)	24.7	25.2	25.3	27.8	27.8	21.3	21.5	24.6

Al/Cr ratio	540.31	631.70	847.00	894.40	662.15	665.43	583.97	838.41
$Mg\#_{Ca\text{-}corr}$	53.4	52.7	52.3	49.9	49.8	56.7	57.0	74.7

$Mg\#_{Ca\text{-}corr}$ = Mg# + 2Ca

Table A.3.2 (cont.) – Electron microprobe chemical analyses of eclogitic garnet inclusions in diamonds from the Urals.

Mineral	Garnet	Garnet	Garnet	Garnet	Garnet	Garnet	Garnet	Garnet
Sample	U47B	U48A	U48B	U48C	U49A	U50A	U51A	U51B
Diamond	D32	D36-D	D36-D	D36-D	D61-A	D110	D135	D135
Assemblage	2 gt	3 gt	3 gt	3 gt	gt	gt	3 gt	3 gt
Paragenesis	*e*	*e*	*e*	*e*	*e*	*e*	*e*	*e*
P_2O_5	0.06	0.04	0.03	0.12	0.02	0.02	0.04	0.02
SiO_2	41.71	40.98	40.59	40.01	41.13	41.78	41.53	41.07
TiO_2	0.11	0.30	0.38	0.48	0.45	0.20	0.30	0.29
Al_2O_3	23.14	22.43	22.19	22.06	22.28	22.87	22.64	22.57
Cr_2O_3	0.05	0.03	0.03	0.03	0.05	0.04	0.03	0.02
FeO	10.52	16.22	16.36	16.83	11.29	13.76	15.27	15.77
MnO	0.31	0.34	0.34	0.35	0.26	0.30	0.39	0.38
NiO	0.00	0.00	0.00	0.00	0.02	0.00	0.00	0.01
MgO	16.08	11.98	11.01	9.65	9.82	16.33	13.42	12.71
CaO	8.16	7.74	8.92	10.15	14.66	4.92	6.95	7.42
Na_2O	0.13	0.17	0.19	0.22	0.13	0.14	0.18	0.16
K_2O	0.00	0.01	0.00	0.00	0.00	0.01	0.00	0.01
ZnO	0.00	0.03	0.03	0.01	0.02	0.00	0.02	0.00
Totals	100.29	100.26	100.07	99.89	100.12	100.36	100.77	100.43

Total iron expressed as FeO
e = *eclogitic* paragenesis

Number of cations on the basis of 24 oxygens

P	0.008	0.005	0.004	0.015	0.003	0.002	0.004	0.002
Si	6.009	6.057	6.042	6.007	6.072	6.045	6.063	6.043
Ti	0.012	0.033	0.043	0.054	0.049	0.021	0.033	0.032
Al	3.929	3.907	3.893	3.903	3.876	3.900	3.896	3.914
Cr	0.006	0.003	0.003	0.003	0.005	0.005	0.004	0.002
Fe	1.267	2.005	2.037	2.113	1.394	1.665	1.864	1.940
Mn	0.038	0.042	0.043	0.044	0.033	0.037	0.048	0.047
Ni	0.000	0.000	0.000	0.000	0.002	0.000	0.000	0.002
Mg	3.453	2.640	2.443	2.160	2.161	3.522	2.921	2.788
Ca	1.259	1.226	1.423	1.633	2.319	0.763	1.087	1.170
Na	0.037	0.048	0.055	0.063	0.037	0.038	0.052	0.045
K	0.000	0.001	0.000	0.000	0.000	0.001	0.000	0.001
Zn	0.000	0.003	0.003	0.001	0.002	0.000	0.002	0.000
Totals	16.018	15.971	15.988	15.995	15.952	15.998	15.973	15.987

Mg #	73.2	56.8	54.5	50.5	60.8	67.9	61.0	59.0
Ca #	26.7	31.7	36.8	43.1	51.8	17.8	27.1	29.6
Cr #	0.2	0.1	0.1	0.1	0.1	0.1	0.1	0.1

Mg # = $100Mg/(Mg + Fe^{2+})$, Ca # = 100Ca/(Ca + Mg) and Cr # = 100Cr/(Cr + Al) by atom

Endmembers (mol. %)

Pyrope (Mg)	57.7	45.0	41.4	36.6	36.8	59.2	49.7	47.3
Almandine (Fe)	21.2	34.2	34.5	35.8	23.7	28.0	31.7	32.9
Grossular (Ca)	21.1	20.9	24.1	27.6	39.5	12.8	18.5	19.8

Al/Cr ratio	638.78	1152.95	1323.12	1133.93	722.00	811.70	992.61	1602.11
$Mg\#_{Ca\text{-}corr}$	75.7	59.3	57.4	53.8	65.4	69.4	63.2	61.3

$Mg\#_{Ca\text{-}corr}$ = Mg# + 2Ca

Table A.3.2 (cont.) – Electron microprobe chemical analyses of eclogitic garnet inclusions in diamonds from the Urals.

Mineral	Garnet	Garnet	Garnet	Garnet	Garnet	Garnet	Garnet	Garnet
Sample	U51C	U52A	U52B	U52C	U52D	U52E	U53A	U53B
Diamond	D135	D139	D139	D139	D139	D139	D144	D144
Assemblage	3 gt	5 gt	5 gt	5 gt	5 gt	5 gt	3 gt	3 gt
Paragenesis	*e*	*e*	*e*	*e*	*e*	*e*	*e*	*e*
P_2O_5	0.03	0.09	0.07	0.05	0.07	0.10	0.07	0.04
SiO_2	40.94	39.95	39.74	40.09	40.10	40.47	40.58	40.73
TiO_2	0.30	0.68	0.65	0.63	0.63	0.63	0.50	0.48
Al_2O_3	22.44	22.19	21.85	22.03	22.23	22.26	22.16	22.42
Cr_2O_3	0.04	0.05	0.04	0.07	0.05	0.05	0.05	0.06
FeO	15.59	18.76	18.58	18.21	18.43	18.83	17.56	17.26
MnO	0.37	0.27	0.27	0.26	0.29	0.27	0.29	0.28
NiO	0.00	0.01	0.00	0.00	0.00	0.00	0.00	0.00
MgO	12.79	9.67	9.30	9.54	9.62	9.81	10.54	10.69
CaO	7.37	8.27	8.73	8.46	8.71	8.13	8.92	8.58
Na_2O	0.17	0.26	0.25	0.24	0.27	0.28	0.22	0.19
K_2O	0.00	0.00	0.00	0.01	0.00	0.00	0.00	0.00
ZnO	0.02	0.04	0.03	0.04	0.01	0.01	0.01	0.01
Totals	100.06	100.24	99.52	99.63	100.42	100.85	100.89	100.73

Total iron expressed as FeO
e = *eclogitic* paragenesis

Number of cations on the basis of 24 oxygens

P	0.003	0.011	0.009	0.007	0.009	0.013	0.008	0.004
Si	6.043	5.997	6.016	6.041	6.005	6.029	6.023	6.036
Ti	0.033	0.077	0.074	0.072	0.071	0.070	0.056	0.054
Al	3.904	3.926	3.898	3.913	3.924	3.908	3.876	3.916
Cr	0.005	0.006	0.005	0.008	0.006	0.006	0.005	0.007
Fe	1.924	2.355	2.352	2.295	2.308	2.346	2.180	2.139
Mn	0.047	0.034	0.035	0.033	0.036	0.034	0.037	0.035
Ni	0.000	0.001	0.000	0.000	0.000	0.000	0.000	0.000
Mg	2.814	2.164	2.099	2.143	2.148	2.179	2.332	2.362
Ca	1.166	1.330	1.416	1.366	1.398	1.298	1.418	1.362
Na	0.048	0.076	0.075	0.070	0.078	0.081	0.062	0.055
K	0.000	0.000	0.000	0.001	0.000	0.000	0.000	0.000
Zn	0.002	0.005	0.003	0.004	0.002	0.001	0.001	0.001
Totals	15.989	15.982	15.982	15.953	15.985	15.965	15.999	15.970

Mg #	59.4	47.9	47.2	48.3	48.2	48.2	51.7	52.5
Ca #	29.3	38.1	40.3	38.9	39.4	37.3	37.8	36.6
Cr #	0.1	0.1	0.1	0.2	0.2	0.2	0.1	0.2

Mg # = $100Mg/(Mg + Fe^{2+})$, Ca # = 100Ca/(Ca + Mg) and Cr # = 100Cr/(Cr + Al) by atom

Endmembers (mol. %)

Pyrope (Mg)	47.7	37.0	35.8	36.9	36.7	37.4	39.3	40.3
Almandine (Fe)	32.6	40.3	40.1	39.5	39.4	40.3	36.8	36.5
Grossular (Ca)	19.7	22.7	24.1	23.5	23.9	22.3	23.9	23.2

Al/Cr ratio	760.24	689.12	740.25	497.57	637.26	650.63	734.07	586.33
$Mg\#_{Ca\text{-}corr}$	61.7	50.5	50.0	51.0	51.0	50.7	54.5	55.2

$Mg\#_{Ca\text{-}corr}$ = Mg# + 2Ca

Table A.3.2 (cont.) – Electron microprobe chemical analyses of eclogitic garnet inclusions in diamonds from the Urals.

Mineral	Garnet	Garnet	Garnet	Garnet	Garnet	Garnet	Garnet	Garnet
Sample	U53C	U54F	U54G	U54H	U55A	U56E	U56F	U57A
Diamond	D144	D4-B	D4-B	D4-B	D12-C	D47-A	D47-A	D58
Assemblage	3 gt	3 gt, 5 sul	3 gt, 5 sul	3 gt, 5 sul	gt, 3 sul	2 gt, rut, 2 sul	2 gt, rut, 2 sul	2 gt
Paragenesis	*e*	*e*	*e*	*e*	*e*	*e*	*e*	*e*
P_2O_5	0.07	0.05	0.08	0.08	0.10	0.10	0.06	0.07
SiO_2	39.95	39.61	40.27	40.39	40.81	40.38	39.71	40.14
TiO_2	0.46	0.70	0.67	0.65	0.56	0.63	0.64	0.57
Al_2O_3	21.77	22.06	22.11	22.11	22.34	22.44	22.17	22.19
Cr_2O_3	0.06	0.03	0.05	0.04	0.08	0.05	0.05	0.04
FeO	17.41	18.48	18.56	18.46	17.47	19.02	19.04	15.71
MnO	0.30	0.30	0.30	0.30	0.27	0.27	0.30	0.28
NiO	0.00	0.00	0.00	0.00	0.01	0.00	0.00	0.02
MgO	10.44	9.52	9.48	9.51	9.45	10.15	10.02	9.80
CaO	8.78	8.90	8.87	8.87	10.02	7.80	7.82	11.00
Na_2O	0.21	0.29	0.26	0.27	0.29	0.26	0.29	0.24
K_2O	0.00	0.00	0.00	0.00	0.00	0.00	0.01	0.00
ZnO	0.02	0.05	0.03	0.03	0.03	0.03	0.06	0.03
Totals	99.47	99.99	100.66	100.72	101.42	101.13	100.16	100.08

Total iron expressed as FeO
e = *eclogitic* paragenesis

Number of cations on the basis of 24 oxygens

P	0.009	0.007	0.010	0.010	0.012	0.013	0.008	0.009
Si	6.018	5.972	6.020	6.031	6.038	5.999	5.972	5.999
Ti	0.053	0.080	0.075	0.073	0.062	0.070	0.073	0.064
Al	3.865	3.920	3.896	3.891	3.895	3.929	3.930	3.908
Cr	0.007	0.004	0.005	0.004	0.009	0.006	0.006	0.005
Fe	2.193	2.330	2.321	2.305	2.162	2.363	2.395	1.963
Mn	0.038	0.038	0.038	0.038	0.034	0.034	0.038	0.035
Ni	0.000	0.000	0.000	0.000	0.001	0.000	0.000	0.002
Mg	2.345	2.140	2.113	2.117	2.084	2.248	2.246	2.183
Ca	1.417	1.438	1.421	1.419	1.588	1.242	1.260	1.761
Na	0.061	0.085	0.074	0.079	0.082	0.075	0.086	0.068
K	0.000	0.000	0.000	0.000	0.000	0.000	0.002	0.000
Zn	0.003	0.005	0.003	0.004	0.004	0.003	0.006	0.003
Totals	16.010	16.019	15.976	15.972	15.971	15.982	16.020	16.001

Mg #	51.7	47.9	47.7	47.9	49.1	48.8	48.4	52.7
Ca #	37.7	40.2	40.2	40.1	43.2	35.6	35.9	44.7
Cr #	0.2	0.1	0.1	0.1	0.2	0.1	0.1	0.1

Mg # = 100Mg/(Mg + Fe^{2+}), Ca # = 100Ca/(Ca + Mg) and Cr # = 100Cr/(Cr + Al) by atom

Endmembers (mol. %)

Pyrope (Mg)	39.4	36.2	36.1	36.2	35.7	38.4	38.1	37.0
Almandine (Fe)	36.8	39.4	39.6	39.5	37.0	40.4	40.6	33.2
Grossular (Ca)	23.8	24.3	24.3	24.3	27.2	21.2	21.4	29.8

Al/Cr ratio	579.50	996.49	732.41	890.77	421.54	711.71	703.15	787.57
$Mg\#_{Ca\text{-}corr}$	54.5	50.7	50.5	50.7	52.3	51.2	50.9	56.2

$Mg\#_{Ca\text{-}corr}$ = Mg# + 2Ca

Table A.3.2 (cont.) – Electron microprobe chemical analyses of eclogitic garnet inclusions in diamonds from the Urals.

Mineral	Garnet	Garnet	Garnet	Garnet	Garnet	Garnet	Garnet	Garnet
Sample	U57B	U58A	U58B	U58C	U58D	U58E	U58F	U59B
Diamond	D58	D129	D129	D129	D129	D129	D129	D122-B
Assemblage	2 gt	6 gt	6 gt	6 gt	6 gt	6 gt	6 gt	3 gt, cpx
Paragenesis	*e*	*e*	*e*	*e*	*e*	*e*	*e*	*e*
P_2O_5	0.08	0.04	0.05	0.04	0.01	0.02	0.03	0.04
SiO_2	40.34	40.46	40.48	40.35	40.04	40.30	40.62	40.54
TiO_2	0.64	0.47	0.47	0.42	0.44	0.43	0.46	0.23
Al_2O_3	22.11	22.33	22.39	22.11	22.26	22.22	22.38	22.53
Cr_2O_3	0.06	0.05	0.04	0.04	0.04	0.05	0.04	0.04
FeO	18.54	17.46	17.44	17.42	17.84	17.82	17.40	15.91
MnO	0.27	0.30	0.29	0.29	0.30	0.31	0.29	0.32
NiO	0.01	0.00	0.02	0.01	0.00	0.01	0.00	0.01
MgO	9.89	12.31	12.29	12.03	11.89	12.06	12.30	13.90
CaO	7.71	6.67	6.67	6.39	6.91	6.69	6.57	6.30
Na_2O	0.28	0.19	0.23	0.20	0.23	0.19	0.21	0.17
K_2O	0.00	0.00	0.01	0.00	0.00	0.00	0.00	0.00
ZnO	0.03	0.02	0.02	0.05	0.01	0.02	0.03	0.00
Totals	99.96	100.29	100.39	99.34	99.97	100.12	100.33	99.98

Total iron expressed as FeO
e = *eclogitic* paragenesis

Number of cations on the basis of 24 oxygens

P	0.010	0.005	0.007	0.005	0.002	0.003	0.004	0.005
Si	6.051	6.002	5.999	6.038	5.980	6.002	6.018	5.984
Ti	0.072	0.052	0.052	0.047	0.049	0.048	0.051	0.026
Al	3.909	3.904	3.911	3.900	3.918	3.900	3.908	3.919
Cr	0.007	0.006	0.005	0.004	0.005	0.006	0.005	0.004
Fe	2.326	2.166	2.161	2.180	2.228	2.219	2.156	1.964
Mn	0.034	0.038	0.036	0.037	0.038	0.039	0.036	0.040
Ni	0.001	0.000	0.002	0.001	0.000	0.002	0.000	0.001
Mg	2.211	2.722	2.715	2.684	2.647	2.678	2.716	3.059
Ca	1.239	1.060	1.059	1.025	1.106	1.068	1.043	0.996
Na	0.080	0.053	0.065	0.057	0.065	0.056	0.061	0.047
K	0.000	0.000	0.001	0.000	0.000	0.000	0.000	0.000
Zn	0.003	0.002	0.002	0.005	0.001	0.002	0.004	0.000
Totals	15.944	16.010	16.015	15.983	16.040	16.021	16.001	16.045

Mg #	48.7	55.7	55.7	55.2	54.3	54.7	55.8	60.9
Ca #	35.9	28.0	28.1	27.6	29.5	28.5	27.7	24.6
Cr #	0.2	0.1	0.1	0.1	0.1	0.2	0.1	0.1

Mg # = 100Mg/(Mg + Fe^{2+}), Ca # = 100Ca/(Ca + Mg) and Cr # = 100Cr/(Cr + Al) by atom

Endmembers (mol. %)

Pyrope (Mg)	38.3	45.8	45.7	45.6	44.3	44.9	45.9	50.8
Almandine (Fe)	40.3	36.4	36.4	37.0	37.3	37.2	36.4	32.6
Grossular (Ca)	21.5	17.8	17.8	17.4	18.5	17.9	17.6	16.6

Al/Cr ratio	558.62	708.22	794.67	915.52	809.32	636.97	775.84	883.81
$Mg\#_{Ca\text{-}corr}$	51.2	57.8	57.8	57.2	56.5	56.8	57.8	62.9

$Mg\#_{Ca\text{-}corr}$ = Mg# + 2Ca

Table A.3.2 (cont.) – Electron microprobe chemical analyses of eclogitic garnet inclusions in diamonds from the Urals.

Mineral	Garnet	Garnet	Garnet	Garnet	Garnet	Garnet	Garnet	Garnet
Sample	U59C	U59D	U60A	U61A	U62A	U62B	U68A	U71A
Diamond	D122-B	D122-B	D11-D	D28	D30	D30	D107-A	D12-B
Assemblage	3 gt, cpx	3 gt, cpx	gt, sul	gt	2 gt	2 gt	gt, 2 sul	gt
Paragenesis	*e*	*e*	*e*	*e*	*e*	*e*	*e*	*e*
P_2O_5	0.04	0.03	0.02	0.06	0.03	0.04	0.04	0.12
SiO_2	40.42	40.91	40.57	39.96	41.17	40.22	39.68	39.47
TiO_2	0.18	0.18	0.28	0.63	0.38	0.40	0.76	0.73
Al_2O_3	22.36	22.69	22.28	22.03	22.47	22.34	22.12	22.08
Cr_2O_3	0.04	0.06	0.08	0.05	0.04	0.04	0.01	0.05
FeO	15.85	15.72	18.78	17.40	17.12	17.41	16.79	19.50
MnO	0.33	0.33	0.34	0.36	0.34	0.34	0.39	0.28
NiO	0.01	0.01	0.02	0.00	0.01	0.00	0.00	0.00
MgO	13.92	14.16	14.01	9.39	12.04	11.73	12.09	9.98
CaO	6.19	6.16	4.04	10.19	7.24	7.44	8.04	7.41
Na_2O	0.13	0.11	0.16	0.23	0.18	0.21	0.05	0.32
K_2O	0.00	0.01	0.00	0.00	0.00	0.00	0.00	0.00
ZnO	0.02	0.02	0.01	0.03	0.02	0.03	0.04	0.03
Totals	99.47	100.39	100.59	100.33	101.04	100.20	100.01	99.97

Total iron expressed as FeO
e = *eclogitic* paragenesis

Number of cations on the basis of 24 oxygens

P	0.004	0.004	0.003	0.007	0.004	0.005	0.005	0.015
Si	5.995	6.001	5.993	5.993	6.052	5.988	5.923	5.955
Ti	0.020	0.020	0.031	0.071	0.042	0.045	0.085	0.083
Al	3.909	3.923	3.879	3.894	3.893	3.920	3.891	3.926
Cr	0.004	0.006	0.009	0.006	0.005	0.005	0.001	0.006
Fe	1.966	1.929	2.320	2.183	2.105	2.168	2.096	2.460
Mn	0.041	0.040	0.042	0.046	0.042	0.043	0.050	0.035
Ni	0.001	0.001	0.002	0.000	0.001	0.000	0.000	0.000
Mg	3.078	3.097	3.085	2.100	2.639	2.604	2.690	2.245
Ca	0.984	0.968	0.639	1.638	1.140	1.187	1.286	1.198
Na	0.036	0.032	0.047	0.067	0.050	0.060	0.014	0.093
K	0.000	0.002	0.000	0.000	0.000	0.000	0.000	0.000
Zn	0.002	0.003	0.001	0.004	0.002	0.003	0.005	0.003
Totals	16.040	16.026	16.051	16.008	15.976	16.027	16.045	16.020
Mg #	61.0	61.6	57.1	49.0	55.6	54.6	56.2	47.7
Ca #	24.2	23.8	17.2	43.8	30.2	31.3	32.3	34.8
Cr #	0.1	0.2	0.2	0.2	0.1	0.1	0.0	0.2

Mg # = 100Mg/(Mg + Fe^{2+}), Ca # = 100Ca/(Ca + Mg) and Cr # = 100Cr/(Cr + Al) by atom

Endmembers (mol. %)

Pyrope (Mg)	51.1	51.7	51.0	35.5	44.8	43.7	44.3	38.0
Almandine (Fe)	32.6	32.2	38.4	36.9	35.8	36.4	34.5	41.7
Grossular (Ca)	16.3	16.2	10.6	27.7	19.4	19.9	21.2	20.3
Al/Cr ratio	900.85	614.97	431.33	619.61	858.85	756.85	4710.50	632.96
$Mg\#_{Ca\text{-}corr}$	63.0	63.6	58.4	52.3	57.9	56.9	58.8	50.1

$Mg\#_{Ca\text{-}corr}$ = Mg# + 2Ca

Table A.3.2 (cont.) – Electron microprobe chemical analyses of eclogitic garnet inclusions in diamonds from the Urals.

Mineral	Garnet	Garnet	Garnet	Garnet	Garnet	Garnet	Garnet	Garnet
Sample	U73A	U74B	U75D	U76B	U77B	U79A	U80A	U81B
Diamond	D14-C	D16-B	D22-A	D40-C	D45-B	D105	D107-B	D118-A
Assemblage	2 gt, sul	3 gt, cpx	4 gt, sul	2 gt	gt, sul	gt	gt	gt
Paragenesis	*e*	*e*	*e*	*e*	*e*	*e*	*e*	*e*
P_2O_5	0.06	0.06	0.05	0.08	0.09	0.08	0.03	0.07
SiO_2	40.47	39.98	40.39	39.51	39.90	40.08	40.45	39.98
TiO_2	0.40	0.54	0.31	0.48	0.64	0.52	0.54	0.80
Al_2O_3	22.39	21.97	21.97	21.79	22.04	22.76	22.36	21.73
Cr_2O_3	0.02	0.05	0.08	0.04	0.05	0.05	0.05	0.04
FeO	16.97	17.79	19.27	19.58	18.21	17.31	18.49	18.56
MnO	0.37	0.29	0.29	0.34	0.25	0.33	0.27	0.33
NiO	0.00	0.00	0.00	0.00	0.00	0.01	0.00	0.00
MgO	13.25	9.82	13.06	8.41	10.15	11.32	11.27	8.99
CaO	5.92	9.22	4.36	9.61	8.37	8.06	6.94	9.71
Na_2O	0.18	0.22	0.15	0.21	0.27	0.26	0.25	0.26
K_2O	0.00	0.00	0.00	0.00	0.00	0.00	0.00	0.00
ZnO	0.03	0.02	0.00	0.03	0.02	0.03	0.02	0.04
Totals	100.05	99.96	99.91	100.08	99.99	100.81	100.67	100.52

Total iron expressed as FeO
e = *eclogitic* paragenesis

Number of cations on the basis of 24 oxygens

P	0.007	0.007	0.006	0.010	0.012	0.010	0.004	0.009
Si	5.993	6.010	6.024	5.994	5.993	5.939	6.009	6.009
Ti	0.045	0.061	0.035	0.055	0.072	0.058	0.061	0.091
Al	3.908	3.892	3.862	3.896	3.902	3.975	3.915	3.850
Cr	0.002	0.006	0.009	0.005	0.006	0.006	0.006	0.004
Fe	2.102	2.236	2.404	2.484	2.287	2.145	2.297	2.333
Mn	0.046	0.037	0.036	0.044	0.031	0.041	0.034	0.042
Ni	0.000	0.000	0.000	0.000	0.000	0.001	0.000	0.000
Mg	2.925	2.201	2.904	1.902	2.273	2.501	2.496	2.014
Ca	0.939	1.485	0.697	1.562	1.347	1.280	1.105	1.564
Na	0.051	0.064	0.042	0.060	0.078	0.074	0.071	0.075
K	0.000	0.000	0.000	0.000	0.000	0.000	0.000	0.000
Zn	0.003	0.002	0.000	0.004	0.003	0.003	0.002	0.005
Totals	16.022	16.001	16.018	16.016	16.003	16.034	15.999	15.997

Mg #	58.2	49.6	54.7	43.4	49.8	53.8	52.1	46.3
Ca #	24.3	40.3	19.4	45.1	37.2	33.9	30.7	43.7
Cr #	0.0	0.2	0.2	0.1	0.2	0.1	0.2	0.1

Mg # = 100Mg/(Mg + Fe^{2+}), Ca # = 100Ca/(Ca + Mg) and Cr # = 100Cr/(Cr + Al) by atom

Endmembers (mol. %)

Pyrope (Mg)	49.0	37.2	48.4	32.0	38.5	42.2	42.3	34.1
Almandine (Fe)	35.2	37.8	40.0	41.8	38.7	36.2	39.0	39.5
Grossular (Ca)	15.7	25.1	11.6	26.3	22.8	21.6	18.7	26.5

Al/Cr ratio	2086.00	629.81	414.56	832.86	657.09	706.82	628.89	875.46
$Mg\#_{Ca\text{-}corr}$	60.1	52.6	56.1	46.5	52.5	56.4	54.3	49.5

$Mg\#_{Ca\text{-}corr}$ = Mg# + 2Ca

Table A.3.2 (cont.) – Electron microprobe chemical analyses of eclogitic garnet inclusions in diamonds from the Urals.

Mineral	Garnet	Garnet	Garnet	Garnet	Garnet
Sample	U82C	U83A	U84A	U85A	U86C
Diamond	D119	D122-A	D131	D132	D133-E
Assemblage	2 gt	gt	gt, sul	gt, 6 cpx, coe, sul	3 gt
Paragenesis	*e*	*e*	*e*	*e*	*e*
P_2O_5	0.06	0.06	0.07	0.09	0.05
SiO_2	39.53	40.47	39.87	39.68	40.16
TiO_2	0.80	0.37	0.64	0.72	0.54
Al_2O_3	21.48	22.37	22.40	21.50	22.14
Cr_2O_3	0.05	0.05	0.05	0.04	0.05
FeO	18.67	17.75	18.35	19.23	17.92
MnO	0.34	0.31	0.28	0.44	0.25
NiO	0.01	0.01	0.00	0.01	0.00
MgO	8.85	11.32	10.09	8.62	9.48
CaO	9.84	7.78	8.42	9.58	9.52
Na_2O	0.27	0.22	0.27	0.19	0.23
K_2O	0.00	0.00	0.00	0.00	0.01
ZnO	0.04	0.01	0.02	0.01	0.02
Totals	99.94	100.71	100.45	100.12	100.37

Total iron expressed as FeO
e = *eclogitic* paragenesis

Number of cations on the basis of 24 oxygens

P	0.008	0.007	0.009	0.012	0.007
Si	5.991	6.004	5.965	6.010	6.016
Ti	0.092	0.041	0.072	0.082	0.061
Al	3.837	3.912	3.950	3.838	3.909
Cr	0.006	0.006	0.005	0.005	0.006
Fe	2.366	2.202	2.296	2.436	2.245
Mn	0.043	0.039	0.035	0.056	0.032
Ni	0.001	0.002	0.000	0.001	0.000
Mg	1.999	2.504	2.250	1.946	2.117
Ca	1.598	1.237	1.350	1.555	1.528
Na	0.078	0.064	0.078	0.057	0.068
K	0.000	0.000	0.000	0.000	0.002
Zn	0.004	0.001	0.002	0.001	0.002
Totals	16.023	16.018	16.011	15.998	15.991

Mg #	45.8	53.2	49.5	44.4	48.5
Ca #	44.4	33.1	37.5	44.4	41.9
Cr #	0.2	0.1	0.1	0.1	0.1

Mg # = 100Mg/(Mg + Fe^{2+}), Ca # = 100Ca/(Ca + Mg) and Cr # = 100Cr/(Cr + Al) by atom

Endmembers (mol. %)

Pyrope (Mg)	33.5	42.1	38.2	32.8	35.9
Almandine (Fe)	39.7	37.1	38.9	41.0	38.1
Grossular (Ca)	26.8	20.8	22.9	26.2	25.9

Al/Cr ratio	627.83	680.53	725.89	728.39	673.54
$Mg\#_{Ca\text{-}corr}$	49.0	55.7	52.2	47.5	51.6

$Mg\#_{Ca\text{-}corr}$ = Mg# + 2Ca

Table A.3.3 – Electron microprobe chemical analyses of clinopyroxene inclusions in diamonds from the Urals.

Mineral	Cpx	Cpx	Cpx	Cpx	Cpx	Cpx	Cpx	Cpx
Sample	U2B	U2D	U13A med	U13A dark	U13A light	U23A	U34B	U35A
Diamond	D12-A	D12-A	D33	D33	D33	D84	D99-C	D99-E
Assemblage	2 cpx, sul	2 cpx, sul	cpx	oligoclase?	cpx?	ol, cpx	gt, cpx	2 gt, 2 cpx
Paragenesis	*e*	*e*	*e*	*e*	*e*	*w*	*e*	*e*
P_2O_5	0.01	0.00	0.00	0.02	0.00	0.04	0.01	0.00
SiO_2	55.84	55.55	56.29	64.12	52.70	54.58	55.92	56.33
TiO_2	0.26	0.26	0.51	0.29	0.65	0.61	0.45	0.46
Al_2O_3	7.59	7.50	15.34	21.83	13.58	6.29	14.64	14.44
Cr_2O_3	0.12	0.10	0.05	0.00	0.09	0.12	0.07	0.06
FeO	7.07	7.07	3.33	1.82	4.22	6.40	3.96	3.69
MnO	0.11	0.11	0.05	0.03	0.06	0.08	0.04	0.06
NiO	0.06	0.06	0.01	0.01	0.02	0.06	0.02	0.02
MgO	14.59	14.60	6.42	1.58	9.18	11.50	6.66	7.01
CaO	9.75	9.67	10.09	3.18	14.28	15.40	9.90	9.86
Na_2O	4.37	4.37	7.60	4.14	5.35	3.59	7.42	7.24
K_2O	0.16	0.19	0.21	0.67	0.01	0.07	0.14	0.13
ZnO	0.03	0.00	0.03	0.04	0.01	0.04	0.01	0.02
Totals	99.95	99.48	99.92	97.73	100.14	98.77	99.24	99.31

Total iron expressed as FeO
e = *eclogitic* paragenesis
w = *websteritic* paragenesis

Number of cations on the basis of 6 oxygens

P	0.000	0.000	0.000	0.000	0.000	0.001	0.000	0.000
Si	1.991	1.991	1.972	2.148	1.879	1.996	1.977	1.985
Ti	0.007	0.007	0.013	0.007	0.017	0.017	0.012	0.012
Al	0.319	0.317	0.633	0.862	0.571	0.271	0.610	0.600
Cr	0.003	0.003	0.001	0.000	0.003	0.003	0.002	0.002
Fe	0.211	0.212	0.098	0.051	0.126	0.196	0.117	0.109
Mn	0.003	0.003	0.001	0.001	0.002	0.003	0.001	0.002
Ni	0.002	0.002	0.000	0.000	0.000	0.002	0.001	0.000
Mg	0.776	0.780	0.335	0.079	0.488	0.627	0.351	0.368
Ca	0.373	0.371	0.379	0.114	0.546	0.603	0.375	0.372
Na	0.302	0.304	0.516	0.269	0.370	0.255	0.509	0.495
K	0.007	0.009	0.009	0.029	0.001	0.003	0.006	0.006
Zn	0.001	0.000	0.001	0.001	0.000	0.001	0.000	0.001
Totals	3.995	3.998	3.960	3.562	4.002	3.977	3.962	3.952

Mg #	78.6	78.6	77.5	60.8	79.5	76.2	75.0	77.2
Ca #	32.4	32.3	53.0	59.1	52.8	49.0	51.7	50.3
Cr #	1.0	0.9	0.2	0.0	0.4	1.2	0.3	0.3

Mg # = $100Mg/(Mg + Fe^{2+})$, Ca # = $100Ca/(Ca + Mg)$ and Cr # = $100Cr/(Cr + Al)$ by atom

Endmembers (mol. %)

Wollastonite (Ca)	27.4	27.2	46.7	46.8	47.1	42.3	44.5	43.8
Enstatite (Mg)	57.1	57.2	41.3	32.4	42.1	44.0	41.6	43.4
Ferrossilite (Fe)	15.5	15.5	12.0	20.9	10.9	13.7	13.9	12.8

Table A.3.3 (cont.) – Electron microprobe chemical analyses of clinopyroxene inclusions in diamonds from the Urals.

Mineral	Cpx	Cpx	Cpx	Cpx	Cpx	Cpx	Cpx	Cpx
Sample	U35B	U37A	U37B	U39A	U41A	U59A	U74D	U85B
Diamond	D99-E	D23-B	D23-B	D21	D91	D122-B	D16-B	D132
Assemblage	2 gt, 2 cpx	2 cpx	2 cpx	cpx	cpx	3 gt, cpx	3 gt, cpx	gt, 6 cpx, coe, sul
Paragenesis	*e*	*e*	*e*	*e*	*e*	*e*	*e*	*e*
P_2O_5	0.01	0.01	0.01	0.01	0.02	0.00	0.00	0.01
SiO_2	55.73	54.69	54.94	55.39	55.16	56.15	54.96	54.37
TiO_2	0.52	0.43	0.43	0.54	0.31	0.25	0.49	0.62
Al_2O_3	14.57	11.71	11.55	11.21	8.50	11.57	13.72	8.23
Cr_2O_3	0.06	0.03	0.04	0.03	0.05	0.05	0.06	0.03
FeO	3.67	7.46	7.26	5.47	7.08	4.19	4.79	6.89
MnO	0.04	0.07	0.08	0.09	0.13	0.09	0.04	0.07
NiO	0.02	0.03	0.03	0.02	0.02	0.02	0.03	0.01
MgO	7.23	7.30	7.25	8.88	12.62	9.66	7.20	9.63
CaO	10.50	11.41	11.29	10.39	9.82	11.21	11.04	14.86
Na_2O	7.02	6.23	6.46	6.74	5.00	6.13	6.70	4.59
K_2O	0.15	0.09	0.09	0.38	0.12	0.18	0.15	0.27
ZnO	0.03	0.03	0.03	0.03	0.03	0.01	0.04	0.02
Totals	99.55	99.48	99.46	99.18	98.85	99.51	99.22	99.60

Total iron expressed as FeO
e = *eclogitic* paragenesis

Number of cations on the basis of 6 oxygens

P	0.000	0.000	0.000	0.000	0.001	0.000	0.000	0.000
Si	1.965	1.973	1.981	1.986	1.991	1.990	1.960	1.977
Ti	0.014	0.012	0.012	0.015	0.008	0.007	0.013	0.017
Al	0.605	0.498	0.491	0.474	0.362	0.483	0.577	0.353
Cr	0.002	0.001	0.001	0.001	0.002	0.001	0.002	0.001
Fe	0.108	0.225	0.219	0.164	0.214	0.124	0.143	0.210
Mn	0.001	0.002	0.003	0.003	0.004	0.003	0.001	0.002
Ni	0.001	0.001	0.001	0.000	0.001	0.001	0.001	0.000
Mg	0.380	0.393	0.390	0.475	0.679	0.510	0.383	0.522
Ca	0.397	0.441	0.436	0.399	0.380	0.426	0.422	0.579
Na	0.480	0.436	0.452	0.469	0.350	0.421	0.463	0.324
K	0.007	0.004	0.004	0.018	0.005	0.008	0.007	0.013
Zn	0.001	0.001	0.001	0.001	0.001	0.000	0.001	0.000
Totals	3.960	3.986	3.989	4.004	3.996	3.975	3.973	3.997

Mg #	77.8	63.6	64.0	74.3	76.1	80.4	72.8	71.4
Ca #	51.1	52.9	52.8	45.7	35.9	45.5	52.4	52.6
Cr #	0.3	0.2	0.2	0.2	0.4	0.3	0.3	0.2

Mg # = 100Mg/(Mg + Fe^{2+}), Ca # = 100Ca/(Ca + Mg) and Cr # = 100Cr/(Cr + Al) by atom

Endmembers (mol. %)

Wollastonite (Ca)	44.8	41.7	41.7	38.5	29.8	40.1	44.5	44.2
Enstatite (Mg)	42.9	37.1	37.3	45.7	53.4	48.1	40.4	39.8
Ferrossilite (Fe)	12.2	21.3	21.0	15.8	16.8	11.7	15.1	16.0

Table A.3.3 (cont.) – Electron microprobe chemical analyses of clinopyroxene inclusions in diamonds from the Urals.

Mineral	Cpx	Cpx	Cpx
Sample	U92B	U93A	U94B
Diamond	D100	D115-A	D121
Assemblage	2 cpx	cpx	2 cpx
Paragenesis	*e*	*e*	*e*
P_2O_5	0.03	0.01	0.01
SiO_2	56.29	55.73	56.02
TiO_2	0.46	0.44	0.47
Al_2O_3	12.39	9.04	12.40
Cr_2O_3	0.03	0.08	0.04
FeO	4.05	3.41	4.09
MnO	0.08	0.08	0.07
NiO	0.03	0.06	0.03
MgO	8.95	12.18	8.85
CaO	9.59	12.24	9.62
Na_2O	7.37	5.22	7.39
K_2O	0.09	0.45	0.09
ZnO	0.01	0.00	0.01
Totals	99.36	98.94	99.09

Total iron expressed as FeO
e = *eclogitic* paragenesis

Number of cations on the basis of 6 oxygens

P	0.001	0.000	0.000
Si	1.992	1.993	1.989
Ti	0.012	0.012	0.012
Al	0.517	0.381	0.519
Cr	0.001	0.002	0.001
Fe	0.120	0.102	0.121
Mn	0.002	0.002	0.002
Ni	0.001	0.002	0.001
Mg	0.472	0.649	0.468
Ca	0.364	0.469	0.366
Na	0.506	0.362	0.509
K	0.004	0.020	0.004
Zn	0.000	0.000	0.000
Totals	3.991	3.995	3.994

Mg #	79.8	86.4	79.4
Ca #	43.5	41.9	43.9
Cr #	0.2	0.6	0.2

Mg # = 100Mg/(Mg + Fe^{2+}), Ca # = 100Ca/(Ca + Mg) and Cr # = 100Cr/(Cr + Al) by atom

Endmembers (mol. %)

Wollastonite (Ca)	38.0	38.4	38.3
Enstatite (Mg)	49.4	53.2	49.0
Ferrossilite (Fe)	12.5	8.4	12.7

Table A.3.4 – Electron microprobe chemical analyses of orthopyroxene inclusions in diamonds from the Urals.

Mineral	Opx	Opx	Opx	Opx	Opx	Opx
Sample	U45A	U45B	U45C	U45D	U45E	U45F
Diamond	D16-A	D16-A	D16-A	D16-A	D16-A	D16-A
Assemblage	6 opx	6 opx	6 opx	6 opx	6 opx	6 opx
Paragenesis	*w*	*w*	*w*	*w*	*w*	*w*
P_2O_5	0.00	0.00	0.00	0.00	0.01	0.00
SiO_2	57.48	57.27	57.04	57.56	57.96	56.84
TiO_2	0.09	0.08	0.09	0.08	0.09	0.09
Al_2O_3	1.20	1.17	1.18	1.17	1.20	1.20
Cr_2O_3	0.09	0.10	0.09	0.09	0.10	0.09
FeO	6.61	6.71	6.62	6.48	6.57	6.49
MnO	0.09	0.10	0.11	0.11	0.11	0.11
NiO	0.19	0.21	0.19	0.19	0.19	0.18
MgO	33.13	33.16	33.20	33.27	33.36	32.98
CaO	0.62	0.62	0.59	0.59	0.62	0.63
Na_2O	0.37	0.36	0.38	0.35	0.39	0.39
K_2O	0.01	0.00	0.01	0.00	0.00	0.00
ZnO	0.04	0.03	0.06	0.03	0.03	0.04
Totals	99.92	99.81	99.54	99.91	100.61	99.04

Total iron expressed as FeO
w = websteritic paragenesis

Number of cations on the basis of 6 oxygens

P	0.000	0.000	0.000	0.000	0.000	0.000
Si	1.987	1.984	1.981	1.989	1.989	1.983
Ti	0.002	0.002	0.002	0.002	0.002	0.002
Al	0.049	0.048	0.048	0.048	0.048	0.049
Cr	0.003	0.003	0.002	0.003	0.003	0.003
Fe	0.191	0.194	0.192	0.187	0.189	0.189
Mn	0.003	0.003	0.003	0.003	0.003	0.003
Ni	0.005	0.006	0.005	0.005	0.005	0.005
Mg	1.708	1.713	1.719	1.714	1.707	1.716
Ca	0.023	0.023	0.022	0.022	0.023	0.023
Na	0.025	0.024	0.026	0.023	0.026	0.026
K	0.000	0.000	0.000	0.000	0.000	0.000
Zn	0.001	0.001	0.001	0.001	0.001	0.001
Totals	3.997	4.000	4.004	3.996	3.996	4.002

Mg #	89.9	89.8	89.9	90.2	90.1	90.1
Ca #	1.3	1.3	1.3	1.3	1.3	1.4
Cr #	4.9	5.6	4.6	5.0	5.1	4.9

Mg # = 100Mg/(Mg + Fe^{2+}), Ca # = 100Ca/(Ca + Mg) and Cr # = 100Cr/(Cr + Al) by atom

Endmembers (mol. %)

Wollastonite (Ca)	1.2	1.2	1.1	1.1	1.2	1.2
Enstatite (Mg)	88.9	88.7	88.9	89.1	89.0	89.0
Ferrossilite (Fe)	9.9	10.1	9.9	9.7	9.8	9.8

Table A.3.5 – Electron microprobe chemical analyses of olivine inclusions in diamonds from the Urals.

Mineral	Olivine	Olivine	Olivine	Olivine	Olivine	Olivine	Olivine	Olivine
Sample	U1C	U1D	U3B	U4B	U5C	U7A	U14A	U16A
Diamond	D67	D67	D87	D148	D94	D25	D36-A	D55
Assemblage	2 gt, 2 ol	2 gt, 2 ol	gt, ol	gt, ol	2gt, ol	ol	ol	ol
Paragenesis	*p (H)*	*p (H)*	*p (H)*	*p (H)*	*p (H)*	*p*	*p*	*p*
P_2O_5	0.00	0.00	0.00	0.01	0.01	0.00	0.00	0.00
SiO_2	41.74	41.09	40.89	40.88	41.40	40.74	40.47	41.43
TiO_2	0.00	0.00	0.00	0.01	0.00	0.00	0.00	0.01
Al_2O_3	0.04	0.04	0.02	0.01	0.02	0.04	0.03	0.02
Cr_2O_3	0.12	0.11	0.10	0.06	0.06	0.08	0.07	0.05
FeO	7.80	7.65	6.37	6.82	4.41	8.24	8.66	7.20
MnO	0.13	0.12	0.09	0.10	0.06	0.13	0.13	0.10
NiO	0.35	0.35	0.35	0.38	0.35	0.37	0.38	0.38
MgO	51.45	50.59	51.48	51.48	53.72	50.74	50.01	51.99
CaO	0.07	0.06	0.03	0.01	0.01	0.07	0.07	0.03
Na_2O	0.01	0.00	0.02	0.01	0.02	0.02	0.02	0.03
K_2O	0.00	0.00	0.00	0.00	0.00	0.00	0.00	0.00
ZnO	0.02	0.02	0.04	0.05	0.02	0.01	0.05	0.08
Totals	101.72	100.02	99.38	99.82	100.08	100.44	99.88	101.31

Total iron expressed as FeO
p (H) = peridotitic (harzburgitic) paragenesis
p = peridotitic (unspecified) paragenesis

Number of cations on the basis of 4 oxygens

P	0.000	0.000	0.000	0.000	0.000	0.000	0.000	0.000
Si	0.997	0.998	0.995	0.992	0.991	0.990	0.991	0.992
Ti	0.000	0.000	0.000	0.000	0.000	0.000	0.000	0.000
Al	0.001	0.001	0.000	0.000	0.001	0.001	0.001	0.001
Cr	0.002	0.002	0.002	0.001	0.001	0.002	0.001	0.001
Fe	0.156	0.155	0.130	0.138	0.088	0.167	0.177	0.144
Mn	0.003	0.002	0.002	0.002	0.001	0.003	0.003	0.002
Ni	0.007	0.007	0.007	0.007	0.007	0.007	0.007	0.007
Mg	1.833	1.832	1.867	1.863	1.917	1.837	1.825	1.856
Ca	0.002	0.002	0.001	0.000	0.000	0.002	0.002	0.001
Na	0.000	0.000	0.001	0.000	0.001	0.001	0.001	0.001
K	0.000	0.000	0.000	0.000	0.000	0.000	0.000	0.000
Zn	0.000	0.000	0.001	0.001	0.000	0.000	0.001	0.001
Totals	3.001	3.000	3.005	3.007	3.008	3.010	3.009	3.007

Mg #	92.2	92.2	93.5	93.1	95.6	91.7	91.1	92.8
Ca #	0.1	0.1	0.0	0.0	0.0	0.1	0.1	0.0
Cr #	69.1	67.6	80.9	80.4	67.9	57.9	58.4	60.1

Mg # = 100Mg/(Mg + Fe^{2+}), Ca # = 100Ca/(Ca + Mg) and Cr # = 100Cr/(Cr + Al) by atom

Endmembers (mol. %)

Forsterite (Mg)	92.0	92.1	93.4	93.0	95.5	91.5	91.0	92.7
Fayalite (Fe)	7.8	7.8	6.5	6.9	4.4	8.3	8.8	7.2
Tp (Mn)	0.1	0.1	0.1	0.1	0.1	0.1	0.1	0.1

Table A.3.5 (cont.) – Electron microprobe chemical analyses of olivine inclusions in diamonds from the Urals.

Mineral	Olivine	Olivine	Olivine	Olivine	Olivine	Olivine	Olivine	Olivine
Sample	U17A	U18A	U18B	U19A	U20A	U21A	U22A	U22B
Diamond	D57-A	D75	D75	D77-A	D93-A	D104	D82	D82
Assemblage	ol	2 ol	2 ol	ol	ol	ol	2 ol	2 ol
Paragenesis	*p*	*p*	*p*	*p*	*p*	*p*	*p*	*p*
P_2O_5	0.00	0.01	0.01	0.02	0.00	0.00	0.01	0.01
SiO_2	41.19	41.58	40.82	40.85	40.31	41.09	41.06	40.75
TiO_2	0.00	0.00	0.00	0.01	0.00	0.01	0.00	0.00
Al_2O_3	0.03	0.01	0.02	0.02	0.01	0.04	0.02	0.02
Cr_2O_3	0.06	0.06	0.06	0.09	0.03	0.03	0.06	0.07
FeO	7.09	6.19	6.19	6.78	6.37	7.01	6.80	6.74
MnO	0.11	0.10	0.08	0.11	0.09	0.09	0.09	0.11
NiO	0.38	0.35	0.34	0.35	0.38	0.39	0.36	0.37
MgO	51.63	52.99	51.81	51.25	51.24	51.57	51.44	51.22
CaO	0.01	0.01	0.02	0.01	0.01	0.01	0.02	0.01
Na_2O	0.02	0.01	0.01	0.01	0.00	0.01	0.02	0.01
K_2O	0.01	0.00	0.01	0.00	0.00	0.00	0.00	0.00
ZnO	0.02	0.04	0.02	0.05	0.04	0.01	0.02	0.03
Totals	100.53	101.34	99.39	99.55	98.49	100.26	99.90	99.34

Total iron expressed as FeO
p = peridotitic (unspecified) paragenesis

Number of cations on the basis of 4 oxygens

P	0.000	0.000	0.000	0.000	0.000	0.000	0.000	0.000
Si	0.994	0.991	0.992	0.994	0.990	0.993	0.995	0.994
Ti	0.000	0.000	0.000	0.000	0.000	0.000	0.000	0.000
Al	0.001	0.000	0.001	0.001	0.000	0.001	0.001	0.001
Cr	0.001	0.001	0.001	0.002	0.001	0.001	0.001	0.001
Fe	0.143	0.123	0.126	0.138	0.131	0.142	0.138	0.137
Mn	0.002	0.002	0.002	0.002	0.002	0.002	0.002	0.002
Ni	0.007	0.007	0.007	0.007	0.008	0.008	0.007	0.007
Mg	1.857	1.882	1.877	1.859	1.877	1.859	1.859	1.862
Ca	0.000	0.000	0.000	0.000	0.000	0.000	0.000	0.000
Na	0.001	0.000	0.001	0.000	0.000	0.000	0.001	0.000
K	0.000	0.000	0.000	0.000	0.000	0.000	0.000	0.000
Zn	0.000	0.001	0.000	0.001	0.001	0.000	0.000	0.001
Totals	3.006	3.008	3.007	3.004	3.009	3.006	3.004	3.005

Mg #	92.8	93.8	93.7	93.1	93.5	92.9	93.1	93.1
Ca #	0.0	0.0	0.0	0.0	0.0	0.0	0.0	0.0
Cr #	59.9	72.9	64.1	74.6	61.8	36.1	67.2	66.8

Mg # = 100Mg/(Mg + Fe^{2+}), Ca # = 100Ca/(Ca + Mg) and Cr # = 100Cr/(Cr + Al) by atom

Endmembers (mol. %)

Forsterite (Mg)	92.7	93.8	93.6	93.0	93.4	92.8	93.0	93.0
Fayalite (Fe)	7.1	6.1	6.3	6.9	6.5	7.1	6.9	6.9
Tp (Mn)	0.1	0.1	0.1	0.1	0.1	0.1	0.1	0.1

Table A.3.5 (cont.) – Electron microprobe chemical analyses of olivine inclusions in diamonds from the Urals.

Mineral	Olivine	Olivine	Olivine
Sample	U23B	U24A	U40A
Diamond	D84	D54	D78
Assemblage	ol, cpx	ol	ol
Paragenesis	*w*	*p*	*p*
P_2O_5	0.02	0.00	0.00
SiO_2	39.29	41.25	40.69
TiO_2	0.01	0.00	0.01
Al_2O_3	0.04	0.02	0.02
Cr_2O_3	0.03	0.05	0.01
FeO	15.75	6.75	6.22
MnO	0.23	0.11	0.09
NiO	0.19	0.39	0.35
MgO	43.82	51.52	51.76
CaO	0.34	0.02	0.01
Na_2O	0.02	0.00	0.01
K_2O	0.01	0.00	0.00
ZnO	0.05	0.01	0.02
Totals	99.80	100.11	99.19

Total iron expressed as FeO
p = peridotitic (unspecified) paragenesis
w = websteritic paragenesis

Number of cations on the basis of 4 oxygens

P	0.000	0.000	0.000
Si	0.995	0.997	0.991
Ti	0.000	0.000	0.000
Al	0.001	0.000	0.000
Cr	0.001	0.001	0.000
Fe	0.333	0.136	0.127
Mn	0.005	0.002	0.002
Ni	0.004	0.008	0.007
Mg	1.654	1.857	1.880
Ca	0.009	0.001	0.000
Na	0.001	0.000	0.000
K	0.000	0.000	0.000
Zn	0.001	0.000	0.000
Totals	3.004	3.002	3.008

Mg #	83.2	93.2	93.7
Ca #	0.6	0.0	0.0
Cr #	29.6	68.1	37.0

Mg # = 100Mg/(Mg + Fe^{2+}), Ca # = 100Ca/(Ca + Mg) and Cr # = 100Cr/(Cr + Al) by atom

Endmembers (mol. %)

Forsterite (Mg)	83.0	93.1	93.6
Fayalite (Fe)	16.7	6.8	6.3
Tp (Mn)	0.2	0.1	0.1

Table A.3.6 – Electron microprobe chemical analyses of chromite inclusions in diamonds from the Urals.

Mineral	Chromite	Chromite	Chromite	Chromite	Chromite	Chromite	Chromite	Chromite
Sample	U8B	U8C	U12A	U12B	U27A	U28A	U28B	U28C
Diamond	D60-C	D60-C	D57-B	D57-B	D38	D149	D149	D149
Assemblage	3 chr	3 chr	2 chr	2 chr	chr	3 chr	3 chr	3 chr
Paragenesis	*p*	*p*	*p*	*p*	*p*	*p*	*p*	*p*
P_2O_5	0.00	0.00	0.00	0.01	0.00	0.00	0.00	0.01
SiO_2	0.20	0.18	0.25	0.23	0.25	0.14	0.14	0.14
TiO_2	0.21	0.20	0.10	0.08	0.03	0.35	0.34	0.35
Al_2O_3	7.01	6.91	7.61	7.59	10.16	6.89	6.68	6.63
Cr_2O_3	64.09	63.89	64.32	64.04	59.85	63.41	63.35	63.47
$Fe_2O_{3\ calc}$	3.23	3.37	0.46	1.69	2.90	3.57	3.15	3.18
FeO	10.87	10.84	13.44	12.54	11.41	11.79	12.23	12.26
MnO	0.25	0.25	0.26	0.29	0.28	0.28	0.26	0.26
NiO	0.10	0.10	0.11	0.12	0.11	0.09	0.10	0.09
MgO	14.72	14.65	12.81	13.48	14.34	14.15	13.69	13.67
CaO	0.00	0.00	0.00	0.00	0.00	0.00	0.00	0.00
Na_2O	0.01	0.01	0.00	0.02	0.00	0.00	0.00	0.02
K_2O	0.00	0.00	0.00	0.00	0.00	0.00	0.00	0.00
ZnO	0.07	0.06	0.10	0.03	0.09	0.07	0.07	0.09
Totals	100.75	100.47	99.45	100.11	99.41	100.74	100.01	100.16

Ferric iron calculated from stoichiometry after Droop (1987)
p = peridotitic (unspecified) paragenesis

Number of cations on the basis of 32 oxygens

P	0.000	0.000	0.000	0.002	0.000	0.000	0.000	0.002
Si	0.050	0.048	0.065	0.060	0.065	0.037	0.037	0.036
Ti	0.041	0.038	0.019	0.015	0.005	0.068	0.067	0.068
Al	2.130	2.107	2.360	2.330	3.089	2.103	2.060	2.043
Cr	13.062	13.066	13.382	13.191	12.206	12.987	13.108	13.119
Fe^{3+}	0.626	0.656	0.090	0.331	0.562	0.695	0.620	0.626
Fe^{2+}	2.344	2.344	2.958	2.733	2.462	2.554	2.676	2.680
Mn	0.054	0.055	0.058	0.063	0.060	0.061	0.058	0.058
Ni	0.021	0.022	0.023	0.024	0.022	0.020	0.021	0.019
Mg	5.657	5.649	5.025	5.235	5.514	5.464	5.341	5.327
Ca	0.000	0.000	0.000	0.000	0.000	0.000	0.000	0.000
Na	0.004	0.006	0.000	0.010	0.000	0.000	0.000	0.008
K	0.000	0.000	0.000	0.000	0.000	0.000	0.000	0.000
Zn	0.013	0.011	0.020	0.006	0.018	0.014	0.014	0.016
Totals	24.002	24.003	24.000	24.001	24.002	24.003	24.002	24.002

Mg #	70.7	70.7	63.0	65.7	69.1	68.1	66.6	66.5
Ca #	0.0	0.0	0.0	0.0	0.0	0.0	0.0	0.0
Cr #	86.0	86.1	85.0	85.0	79.8	86.1	86.4	86.5

Mg # = $100Mg/(Mg + Fe^{2+})$, Ca # = 100Ca/(Ca + Mg) and Cr # = 100Cr/(Cr + Al) by atom

Table A.3.6 (cont) – Electron microprobe chemical analyses of chromite inclusions in diamonds from the Urals.

Mineral	Chromite	Chromite	Chromite
Sample	U29B	U30A	U31A
Diamond	D112	D115-B	D123
Assemblage	gt, chr	chr	chr
Paragenesis	*p (H)*	*p*	*p*
P_2O_5	0.00	0.01	0.00
SiO_2	0.16	0.20	0.08
TiO_2	0.66	0.40	0.04
Al_2O_3	5.99	5.51	6.71
Cr_2O_3	63.81	63.80	64.60
$Fe_2O_{3\ calc}$	3.03	4.01	3.59
FeO	12.11	12.58	11.02
MnO	0.28	0.27	0.27
NiO	0.11	0.11	0.10
MgO	13.90	13.50	14.46
CaO	0.00	0.00	0.00
Na_2O	0.00	0.01	0.00
K_2O	0.00	0.00	0.00
ZnO	0.08	0.06	0.04
Totals	100.12	100.47	100.91

Ferric iron calculated from stoichiometry after Droop (1987)
p (H) = peridotitic (harzburgitic) paragenesis
p = peridotitic (unspecified) paragenesis

Number of cations on the basis of 32 oxygens

P	0.000	0.002	0.000
Si	0.042	0.053	0.020
Ti	0.129	0.079	0.008
Al	1.848	1.704	2.043
Cr	13.209	13.233	13.196
Fe^{3+}	0.597	0.792	0.699
Fe^{2+}	2.652	2.760	2.380
Mn	0.062	0.060	0.058
Ni	0.023	0.024	0.021
Mg	5.425	5.279	5.569
Ca	0.000	0.000	0.000
Na	0.000	0.006	0.000
K	0.000	0.000	0.000
Zn	0.015	0.012	0.008
Totals	24.002	24.004	24.003

Mg #	67.2	65.7	70.1
Ca #	0.0	0.0	0.0
Cr #	87.7	88.6	86.6

Mg # = 100Mg/(Mg + Fe^{2+}), Ca # = 100Ca/(Ca + Mg) and Cr # = 100Cr/(Cr + Al) by atom

Table A.3.7 – Electron microprobe chemical analyses of a rutile inclusion in a diamond from the Urals.

Mineral	Rutile
Sample	U56A
Diamond	D47-A
Assemblage	2 gt, rut, 2 sul
Paragenesis	*e*
P_2O_5	0.01
SiO_2	0.02
TiO_2	98.74
Al_2O_3	0.70
Cr_2O_3	0.11
FeO	0.16
MnO	0.00
NiO	0.00
MgO	0.01
CaO	0.00
Na_2O	0.00
K_2O	0.00
ZnO	0.00
Totals	99.74

Total iron expressed as FeO
e = *eclogitic* paragenesis

Number of cations on the basis of 12 oxygens

P	0.000
Si	0.000
Ti	0.990
Al	0.011
Cr	0.001
Fe	0.002
Mn	0.000
Ni	0.000
Mg	0.000
Ca	0.000
Na	0.000
K	0.000
Zn	0.000
Totals	1.004

Table A.3.8 – Electron microprobe chemical analyses of kyanite inclusions in diamonds from the Urals.

Mineral	Kyanite	Kyanite
Sample	U25A	U32A
Diamond	D60-B	D128
Assemblage	ky	ky
Paragenesis	*e*	*e*
P_2O_5	0.02	0.01
SiO_2	36.90	36.90
TiO_2	0.14	0.30
Al_2O_3	62.05	61.64
Cr_2O_3	0.04	0.10
FeO	0.24	0.39
MnO	0.01	0.00
NiO	0.00	0.00
MgO	0.10	0.18
CaO	0.00	0.00
Na_2O	0.00	0.02
K_2O	0.00	0.01
ZnO	0.01	0.04
Totals	99.51	99.59

Total iron expressed as FeO
e = *eclogitic* paragenesis

Number of cations on the basis of 10 oxygens

P	0.001	0.001
Si	2.004	2.005
Ti	0.006	0.012
Al	3.971	3.948
Cr	0.002	0.004
Fe	0.011	0.018
Mn	0.000	0.000
Ni	0.000	0.000
Mg	0.008	0.015
Ca	0.000	0.000
Na	0.000	0.002
K	0.000	0.000
Zn	0.000	0.002
Totals	6.003	6.007

Table A.3.9 – Electron microprobe chemical analyses of coesite inclusions in diamonds from the Urals.

Mineral	Coesite	Coesite	Coesite	Coesite	Coesite	Coesite
Sample	U11A	U11B	U15A	U42E	U72F	U85C
Diamond	D11-A	D11-A	D39	D10-B	D14-B	D132
Assemblage	2 coe	2 coe	coe	gt, coe, 3 sul	coe, sul	gt, 6 cpx, coe, sul
Paragenesis	*e*	*e*	*e*	*e*	*e*	*e*
P_2O_5	0.00	0.00	0.00	0.00	0.00	0.00
SiO_2	99.84	99.16	100.03	99.90	100.52	99.89
TiO_2	0.00	0.00	0.00	0.00	0.00	0.00
Al_2O_3	0.04	0.03	0.03	0.02	0.05	0.04
Cr_2O_3	0.00	0.00	0.00	0.01	0.01	0.02
FeO	0.00	0.00	0.00	0.00	0.00	0.00
MnO	0.00	0.00	0.01	0.01	0.00	0.00
NiO	0.00	0.00	0.00	0.00	0.02	0.00
MgO	0.00	0.00	0.01	0.00	0.01	0.01
CaO	0.00	0.00	0.00	0.00	0.00	0.00
Na_2O	0.01	0.00	0.01	0.00	0.01	0.00
K_2O	0.00	0.01	0.00	0.00	0.00	0.01
ZnO	0.02	0.02	0.02	0.01	0.00	0.00
Totals	99.91	99.22	100.10	99.95	100.61	99.97

Total iron expressed as FeO
e = *eclogitic* paragenesis

Number of cations on the basis of 12 oxygens

P	0.000	0.000	0.000	0.000	0.000	0.000
Si	5.997	5.998	5.997	5.998	5.996	5.997
Ti	0.000	0.000	0.000	0.000	0.000	0.000
Al	0.003	0.002	0.002	0.001	0.003	0.003
Cr	0.000	0.000	0.000	0.000	0.000	0.001
Fe	0.000	0.000	0.000	0.000	0.000	0.000
Mn	0.000	0.000	0.001	0.001	0.000	0.000
Ni	0.000	0.000	0.000	0.000	0.001	0.000
Mg	0.000	0.000	0.001	0.000	0.001	0.001
Ca	0.000	0.000	0.000	0.000	0.000	0.000
Na	0.001	0.000	0.001	0.000	0.001	0.000
K	0.000	0.001	0.000	0.000	0.000	0.001
Zn	0.001	0.001	0.001	0.001	0.000	0.000
Totals	6.002	6.001	6.002	6.001	6.002	6.002

Table A.3.10 – Electron microprobe chemical analyses of sulphide inclusions in diamonds from the Urals.

Mineral	mss			po	po	popn	
Phase	mss	pn	mss	po	po	pn	po
Sample	U2A med	U2A light	U2A dark	U9A	U33A	U42B light	U42B dark
Diamond	D12-A	D12-A	D12-A	D81-B	D20	D10-B	D10-B
Assemblage	2 cpx, sul	2 cpx, sul	2 cpx, sul	sul	sul	gt, coe, 3 sul	gt, coe, 3 sul
Paragenesis	*e*	*e*	*e*	*?*	*?*	*e*	*e*
Cu	1.19	0.06	0.22	1.83	1.11	0.05	0.44
Fe	53.76	30.22	55.56	58.20	58.45	28.67	58.94
Ni	6.49	34.31	4.80	0.29	0.19	32.46	0.26
Co	0.20	0.88	0.18	0.08	0.09	4.64	0.08
Zn	0.01	0.03	0.01	0.01	0.00	0.02	0.02
Cr	0.01	0.01	0.02	0.02	0.00	0.01	0.01
Se	0.00	0.01	0.01	0.00	0.01	0.00	0.00
S	37.54	33.25	38.42	38.88	38.99	32.97	38.98
Totals	99.21	98.78	99.22	99.29	98.83	98.82	98.72

e = *eclogitic* paragenesis
? = *undetermined* paragenesis
mss = monosulphide solid solution
popn = pyrrhotite + pentlandite
po = pyrrhotite
pn = pentlandite

Sulfur normalised to 4 cations

Cu	0.064	0.004	0.012	0.095	0.057	0.003	0.023
Fe	3.289	2.087	3.322	3.439	3.443	1.997	3.473
Ni	0.378	2.255	0.273	0.016	0.010	2.151	0.014
Co	0.011	0.058	0.010	0.004	0.005	0.306	0.005
Zn	0.000	0.002	0.000	0.000	0.000	0.001	0.001
Cr	0.001	0.001	0.001	0.001	0.000	0.001	0.000
Se	0.000	0.001	0.000	0.000	0.000	0.000	0.000
S	4.000	4.000	4.000	4.000	4.000	4.000	4.000
Σcations	7.743	8.407	7.618	7.555	7.517	8.460	7.516
Σcations/S	1.94	2.10	1.90	1.89	1.88	2.11	1.88
(Fe,Ni)/S	1.60	1.94	1.57	1.50	1.50	1.85	1.52
Atomic proportions							
Cu	0.019	0.001	0.003	0.029	0.017	0.001	0.007
Fe	0.963	0.541	0.995	1.042	1.047	0.513	1.055
Ni	0.111	0.585	0.082	0.005	0.003	0.553	0.004
Co	0.003	0.015	0.003	0.001	0.002	0.079	0.001
Zn	0.000	0.000	0.000	0.000	0.000	0.000	0.000
Cr	0.000	0.000	0.000	0.000	0.000	0.000	0.000
Se	0.000	0.000	0.000	0.000	0.000	0.000	0.000
S	1.171	1.037	1.198	1.212	1.216	1.028	1.216
Totals	2.267	2.179	2.282	2.290	2.285	2.175	2.284

Table A.3.10 (cont.) – Electron microprobe chemical analyses of sulphide inclusions in diamonds from the Urals.

Mineral	popn		po	po	mss	po	popn	
Phase	pn	po	po	po	mss	po	pn	po
Sample	U42C light	U42C dark	U42D	U43C	U43D	U43E	U54A light	U54A dark
Diamond	D10-B	D10-B	D10-B	D101	D101	D101	D4-B	D4-B
Assemblage	gt, coe, 3 sul	gt, coe, 3 sul	gt, coe, 3 sul	2 gt, 3 sul	2 gt, 3 sul	2 gt, 3 sul	3 gt, 5 sul	3 gt, 5 sul
Paragenesis	*e*	*e*	*e*	*e*	*e*	*e*	*e*	*e*
Cu	0.16	0.30	0.24	0.68	4.66	1.04	0.05	0.29
Fe	34.06	59.09	59.27	57.74	54.48	57.71	29.28	58.98
Ni	29.69	0.19	0.23	1.53	1.83	0.66	33.85	0.52
Co	0.35	0.09	0.08	0.16	0.23	0.10	3.08	0.10
Zn	0.05	0.02	0.01	0.00	0.01	0.01	0.00	0.00
Cr	0.01	0.01	0.01	0.01	0.01	0.01	0.01	0.00
Se	0.01	0.00	0.01	0.00	0.01	0.01	0.00	0.01
S	33.88	38.54	38.41	38.33	38.55	38.85	33.14	39.03
Totals	98.20	98.23	98.25	98.46	99.78	98.38	99.40	98.93

e = *eclogitic* paragenesis
mss = monosulphide solid solution
popn = pyrrhotite + pentlandite
po = pyrrhotite
pn = pentlandite

Sulfur normalised to 4 cations

Cu	0.009	0.016	0.013	0.036	0.244	0.054	0.003	0.015
Fe	2.309	3.521	3.544	3.460	3.246	3.412	2.029	3.470
Ni	1.915	0.010	0.013	0.087	0.103	0.037	2.232	0.029
Co	0.022	0.005	0.004	0.009	0.013	0.006	0.202	0.005
Zn	0.003	0.001	0.000	0.000	0.001	0.000	0.000	0.000
Cr	0.001	0.001	0.000	0.001	0.001	0.000	0.000	0.000
Se	0.001	0.000	0.000	0.000	0.000	0.000	0.000	0.000
S	4.000	4.000	4.000	4.000	4.000	4.000	4.000	4.000
Σcations	8.260	7.554	7.575	7.593	7.608	7.510	8.466	7.520
Σcations/S	2.07	1.89	1.89	1.90	1.90	1.88	2.12	1.88
(Fe,Ni)/S	1.88	1.54	1.55	1.55	1.46	1.50	1.90	1.52
Atomic proportions								
Cu	0.002	0.005	0.004	0.011	0.073	0.016	0.001	0.005
Fe	0.610	1.058	1.061	1.034	0.976	1.033	0.524	1.056
Ni	0.506	0.003	0.004	0.026	0.031	0.011	0.577	0.009
Co	0.006	0.002	0.001	0.003	0.004	0.002	0.052	0.002
Zn	0.001	0.000	0.000	0.000	0.000	0.000	0.000	0.000
Cr	0.000	0.000	0.000	0.000	0.000	0.000	0.000	0.000
Se	0.000	0.000	0.000	0.000	0.000	0.000	0.000	0.000
S	1.056	1.202	1.198	1.195	1.202	1.211	1.034	1.217
Totals	2.182	2.270	2.268	2.269	2.287	2.275	2.188	2.289

Table A.3.10 (cont.) – Electron microprobe chemical analyses of sulphide inclusions in diamonds from the Urals.

Mineral	popn?	popn		popn		popn?	popn	
Phase	po	pn	po	pn	po	po	pn	po
Sample	U54B dark	U54C light	U54C dark	U54D light	U54D dark	U54E dark	U55B light	U55B dark
Diamond	D4-B	D4-B	D4-B	D4-B	D4-B	D4-B	D12-C	D12-C
Assemblage	3 gt, 5 sul	3 gt, 5 sul	3 gt, 5 sul	3 gt, 5 sul	3 gt, 5 sul	3 gt, 5 sul	gt, 3 sul	gt, 3 sul
Paragenesis	*e*	*e*	*e*	*e*	*e*	*e*	*e*	*e*
Cu	0.35	0.22	0.37	0.03	0.39	0.26	0.03	0.60
Fe	59.34	32.21	58.82	27.32	58.81	58.86	28.74	58.68
Ni	0.27	30.39	0.94	34.55	0.65	0.58	33.89	0.45
Co	0.07	3.46	0.10	3.91	0.09	0.09	2.91	0.09
Zn	0.01	0.00	0.02	0.01	0.03	0.00	0.00	0.02
Cr	0.01	0.00	0.00	0.00	0.01	0.01	0.01	0.00
Se	0.00	0.01	0.00	0.00	0.01	0.00	0.00	0.00
S	38.45	34.45	38.60	32.62	38.16	38.39	32.51	38.08
Totals	98.50	100.74	98.85	98.44	98.14	98.19	98.08	97.92

e = *eclogitic* paragenesis
popn = pyrrhotite + pentlandite
po = pyrrhotite
pn = pentlandite

Sulfur normalised to 4 cations

Cu	0.019	0.013	0.019	0.002	0.021	0.014	0.002	0.032
Fe	3.545	2.147	3.500	1.924	3.540	3.522	2.031	3.539
Ni	0.015	1.928	0.053	2.315	0.037	0.033	2.278	0.026
Co	0.004	0.219	0.006	0.261	0.005	0.005	0.195	0.005
Zn	0.001	0.000	0.001	0.001	0.001	0.000	0.000	0.001
Cr	0.000	0.000	0.000	0.000	0.000	0.001	0.000	0.000
Se	0.000	0.001	0.000	0.000	0.000	0.000	0.000	0.000
S	4.000	4.000	4.000	4.000	4.000	4.000	4.000	4.000
Σcations	7.584	8.308	7.579	8.502	7.605	7.574	8.506	7.603
Σcations/S	1.90	2.08	1.89	2.13	1.90	1.89	2.13	1.90
(Fe,Ni)/S	1.55	1.82	1.55	1.90	1.56	1.55	1.93	1.55
Atomic proportions								
Cu	0.006	0.003	0.006	0.000	0.006	0.004	0.000	0.009
Fe	1.063	0.577	1.053	0.489	1.053	1.054	0.515	1.051
Ni	0.005	0.518	0.016	0.589	0.011	0.010	0.577	0.008
Co	0.001	0.059	0.002	0.066	0.001	0.001	0.049	0.002
Zn	0.000	0.000	0.000	0.000	0.000	0.000	0.000	0.000
Cr	0.000	0.000	0.000	0.000	0.000	0.000	0.000	0.000
Se	0.000	0.000	0.000	0.000	0.000	0.000	0.000	0.000
S	1.199	1.074	1.204	1.017	1.190	1.197	1.014	1.188
Totals	2.273	2.231	2.281	2.162	2.262	2.267	2.156	2.257

Table A.3.10 (cont.) – Electron microprobe chemical analyses of sulphide inclusions in diamonds from the Urals.

Mineral	popn?		po	po	po	popn	
Phase	pn?	po	po	po	po	pn	po
Sample	U55C light	U55C dark	U55D	U56C	U56D	U60B light	U60B dark
Diamond	D12-C	D12-C	D12-C	D47-A	D47-A	D11-D	D11-D
Assemblage	gt, 3 sul	gt, 3 sul	gt, 3 sul	2 gt, rut, 2 sul	2 gt, rut, 2 sul	gt, sul	gt, sul
Paragenesis	*e*	*e*	*e*	*e*	*e*	*e*	*e*
Cu	0.09	0.44	0.34	0.33	0.49	0.12	0.11
Fe	36.48	58.29	58.19	58.30	58.28	34.06	58.07
Ni	24.92	1.10	0.72	0.29	0.38	29.31	0.95
Co	2.59	0.11	0.10	0.09	0.08	1.61	0.12
Zn	0.03	0.00	0.01	0.01	0.00	0.02	0.01
Cr	0.00	0.01	0.01	0.01	0.01	0.01	0.01
Se	0.01	0.00	0.00	0.00	0.01	0.00	0.01
S	35.00	38.13	38.41	38.39	38.32	33.13	37.98
Totals	99.12	98.07	97.78	97.40	97.56	98.26	97.25

e = *eclogitic* paragenesis
popn = pyrrhotite + pentlandite
po = pyrrhotite
pn = pentlandite

Sulfur normalised to 4 cations

Cu	0.005	0.023	0.018	0.017	0.026	0.007	0.006
Fe	2.394	3.511	3.479	3.488	3.493	2.361	3.511
Ni	1.556	0.063	0.041	0.016	0.022	1.933	0.055
Co	0.161	0.006	0.006	0.005	0.004	0.106	0.007
Zn	0.001	0.000	0.001	0.000	0.000	0.001	0.000
Cr	0.000	0.000	0.001	0.000	0.001	0.001	0.000
Se	0.000	0.000	0.000	0.000	0.000	0.000	0.000
S	4.000	4.000	4.000	4.000	4.000	4.000	4.000
Σcations	8.118	7.604	7.545	7.527	7.546	8.409	7.580
Σcations/S	2.03	1.90	1.89	1.88	1.89	2.10	1.89
(Fe,Ni)/S	1.75	1.56	1.53	1.53	1.53	1.91	1.55
Atomic proportions							
Cu	0.001	0.007	0.005	0.005	0.008	0.002	0.002
Fe	0.653	1.044	1.042	1.044	1.044	0.610	1.040
Ni	0.425	0.019	0.012	0.005	0.006	0.499	0.016
Co	0.044	0.002	0.002	0.001	0.001	0.027	0.002
Zn	0.000	0.000	0.000	0.000	0.000	0.000	0.000
Cr	0.000	0.000	0.000	0.000	0.000	0.000	0.000
Se	0.000	0.000	0.000	0.000	0.000	0.000	0.000
S	1.092	1.189	1.198	1.197	1.195	1.033	1.185
Totals	2.215	2.260	2.260	2.253	2.254	2.172	2.245

Table A.3.10 (cont.) – Electron microprobe chemical analyses of sulphide inclusions in diamonds from the Urals.

Mineral	popn		popn		mss?	po	po
Phase	pn	po	pn	po	mss?	po	po
Sample	U63A light	U63A dark	U64A light	U64A dark	U65A light	U66A	U67A
Diamond	D17	D17	D35-B	D35-B	D46	D48	D99-A
Assemblage	sul	sul	sul	sul	sul	sul	4 sul
Paragenesis	*?*	*?*	*?*	*?*	*?*	*?*	*?*
Cu	0.33	0.65	0.04	0.70	0.25	0.68	0.09
Fe	30.71	58.41	28.19	57.83	41.24	58.58	59.06
Ni	31.11	0.28	34.01	0.72	21.04	0.49	0.57
Co	3.61	0.09	3.59	0.11	0.33	0.09	0.13
Zn	0.02	0.03	0.00	0.01	0.01	0.00	0.00
Cr	0.01	0.01	0.00	0.01	0.02	0.01	0.01
Se	0.00	0.01	0.00	0.01	0.01	0.01	0.00
S	32.83	38.30	32.76	38.39	35.50	38.96	39.13
Totals	98.61	97.77	98.60	97.77	98.39	98.82	98.99

? = *undetermined* paragenesis
mss = monosulphide solid solution
popn = pyrrhotite + pentlandite
po = pyrrhotite
pn = pentlandite

Sulfur normalised to 4 cations

Cu	0.020	0.034	0.003	0.037	0.014	0.035	0.005
Fe	2.149	3.502	1.976	3.459	2.668	3.453	3.467
Ni	2.071	0.016	2.269	0.041	1.295	0.027	0.032
Co	0.240	0.005	0.239	0.006	0.020	0.005	0.007
Zn	0.001	0.001	0.000	0.000	0.001	0.000	0.000
Cr	0.000	0.000	0.000	0.000	0.001	0.001	0.001
Se	0.000	0.000	0.000	0.000	0.000	0.000	0.000
S	4.000	4.000	4.000	4.000	4.000	4.000	4.000
Σcations	8.480	7.560	8.487	7.544	8.000	7.522	7.512
Σcations/S	2.12	1.89	2.12	1.89	2.00	1.88	1.88
(Fe,Ni)/S	1.88	1.53	1.90	1.52	1.75	1.52	1.52
Atomic proportions							
Cu	0.005	0.010	0.001	0.011	0.004	0.011	0.001
Fe	0.550	1.046	0.505	1.035	0.738	1.049	1.058
Ni	0.530	0.005	0.579	0.012	0.358	0.008	0.010
Co	0.061	0.002	0.061	0.002	0.006	0.002	0.002
Zn	0.000	0.000	0.000	0.000	0.000	0.000	0.000
Cr	0.000	0.000	0.000	0.000	0.000	0.000	0.000
Se	0.000	0.000	0.000	0.000	0.000	0.000	0.000
S	1.024	1.194	1.022	1.197	1.107	1.215	1.220
Totals	2.171	2.258	2.168	2.258	2.214	2.285	2.291

Table A.3.10 (cont.) – Electron microprobe chemical analyses of sulphide inclusions in diamonds from the Urals.

Mineral	po?		popn		popn		popn	
Phase	po	mss?	po	pn	pn	po	pn	po
Sample	U67B dark	U67B light	U67C dark	U67C light	U67D light	U67D dark	U68B light	U68B dark
Diamond	D99-A	D99-A	D99-A	D99-A	D99-A	D99-A	D107-A	D107-A
Assemblage	4 sul	4 sul	4 sul	4 sul	4 sul	4 sul	gt, 2 sul	gt, 2 sul
Paragenesis	*?*	*?*	*?*	*?*	*?*	*?*	*e*	*e*
Cu	0.17	0.35	0.20	0.06	0.11	0.22	0.02	0.10
Fe	58.57	39.98	59.26	28.85	30.25	58.97	28.66	58.31
Ni	1.00	20.50	0.26	32.60	32.85	0.30	31.93	0.90
Co	0.14	2.93	0.09	3.87	2.87	0.09	4.73	0.11
Zn	0.02	0.01	0.03	0.02	0.03	0.02	0.01	0.01
Cr	0.01	0.01	0.00	0.00	0.01	0.00	0.01	0.00
Se	0.01	0.01	0.00	0.01	0.00	0.01	0.01	0.00
S	39.16	34.13	39.35	32.90	33.01	38.67	32.92	39.22
Totals	99.08	97.90	99.18	98.31	99.11	98.28	98.29	98.65

e = *eclogitic* paragenesis
? = *undetermined* paragenesis
mss = monosulphide solid solution
popn = pyrrhotite + pentlandite
po = pyrrhotite
pn = pentlandite

Sulfur normalised to 4 cations

Cu	0.009	0.020	0.010	0.004	0.007	0.011	0.001	0.005
Fe	3.436	2.690	3.458	2.014	2.105	3.502	2.000	3.415
Ni	0.056	1.312	0.014	2.165	2.175	0.017	2.120	0.050
Co	0.008	0.187	0.005	0.256	0.189	0.005	0.313	0.006
Zn	0.001	0.000	0.001	0.001	0.002	0.001	0.000	0.001
Cr	0.001	0.001	0.000	0.000	0.000	0.000	0.001	0.000
Se	0.000	0.000	0.000	0.000	0.000	0.000	0.000	0.000
S	4.000	4.000	4.000	4.000	4.000	4.000	4.000	4.000
Σcations	7.510	8.211	7.489	8.441	8.477	7.537	8.436	7.477
Σcations/S	1.88	2.05	1.87	2.11	2.12	1.88	2.11	1.87
(Fe,Ni)/S	1.52	1.77	1.51	1.87	1.91	1.53	1.84	1.51
Atomic proportions								
Cu	0.003	0.005	0.003	0.001	0.002	0.003	0.000	0.002
Fe	1.049	0.716	1.061	0.517	0.542	1.056	0.513	1.044
Ni	0.017	0.349	0.004	0.555	0.560	0.005	0.544	0.015
Co	0.002	0.050	0.001	0.066	0.049	0.001	0.080	0.002
Zn	0.000	0.000	0.000	0.000	0.000	0.000	0.000	0.000
Cr	0.000	0.000	0.000	0.000	0.000	0.000	0.000	0.000
Se	0.000	0.000	0.000	0.000	0.000	0.000	0.000	0.000
S	1.221	1.064	1.227	1.026	1.029	1.206	1.027	1.223
Totals	2.293	2.185	2.298	2.165	2.181	2.272	2.165	2.286

Table A.3.10 (cont.) – Electron microprobe chemical analyses of sulphide inclusions in diamonds from the Urals.

Mineral	mss?			mss		mss	mss?	
Phase	pn	po?	mss	mss	mss	mss	pn	mss?
	U68C	U68C		U69A	U69A		U70A	U70A
Sample	light	dark	U68C med	light	dark	U69B	light	dark
Diamond	D107-A	D107-A	D107-A	D15-B	D15-B	D15-B	D109	D109
Assemblage	gt, 2 sul	gt, 2 sul	gt, 2 sul	2 sul	2 sul	2 sul	sul	sul
Paragenesis	*e*	*e*	*e*	*?*	*?*	*?*	*?*	*?*
Cu	0.02	0.46	0.40	0.60	15.26	3.99	0.16	2.22
Fe	29.75	57.01	54.31	56.25	45.72	52.22	30.00	55.04
Ni	34.01	1.84	5.14	2.45	1.22	4.28	33.04	2.20
Co	1.42	0.13	0.24	0.23	0.12	0.46	1.27	0.19
Zn	0.00	0.00	0.00	0.01	0.00	0.00	0.01	0.01
Cr	0.00	0.01	0.00	0.00	0.01	0.01	0.00	0.01
Se	0.00	0.01	0.01	0.02	0.00	0.00	0.01	0.00
S	33.10	38.65	38.60	38.60	36.72	38.53	33.61	38.74
Totals	98.31	98.10	98.68	98.16	99.06	99.48	98.10	98.40

e = *eclogitic* paragenesis
? = *undetermined* paragenesis
mss = monosulphide solid solution
po = pyrrhotite
pn = pentlandite

Sulfur normalised to 4 cations

Cu	0.001	0.024	0.021	0.031	0.839	0.209	0.010	0.115
Fe	2.065	3.388	3.232	3.347	2.860	3.113	2.050	3.263
Ni	2.245	0.104	0.291	0.139	0.073	0.243	2.148	0.124
Co	0.093	0.007	0.013	0.013	0.007	0.026	0.082	0.011
Zn	0.000	0.000	0.000	0.000	0.000	0.000	0.001	0.001
Cr	0.000	0.000	0.000	0.000	0.000	0.000	0.000	0.001
Se	0.000	0.000	0.000	0.001	0.000	0.000	0.000	0.000
S	4.000	4.000	4.000	4.000	4.000	4.000	4.000	4.000
Σcations	8.405	7.524	7.557	7.532	7.779	7.591	8.291	7.514
Σcations/S	2.10	1.88	1.89	1.88	1.94	1.90	2.07	1.88
(Fe,Ni)/S	1.93	1.52	1.54	1.52	1.28	1.47	1.88	1.48
Atomic proportions								
Cu	0.000	0.007	0.006	0.009	0.240	0.063	0.003	0.035
Fe	0.533	1.021	0.972	1.007	0.819	0.935	0.537	0.985
Ni	0.579	0.031	0.088	0.042	0.021	0.073	0.563	0.037
Co	0.024	0.002	0.004	0.004	0.002	0.008	0.021	0.003
Zn	0.000	0.000	0.000	0.000	0.000	0.000	0.000	0.000
Cr	0.000	0.000	0.000	0.000	0.000	0.000	0.000	0.000
Se	0.000	0.000	0.000	0.000	0.000	0.000	0.000	0.000
S	1.032	1.205	1.204	1.204	1.145	1.202	1.048	1.208
Totals	2.169	2.267	2.274	2.267	2.227	2.280	2.173	2.270

Table A.3.10 (cont.) – Electron microprobe chemical analyses of sulphide inclusions in diamonds from the Urals.

Mineral	popn		mss	mss	mss	po-mss	
Phase	pn	po	mss	mss	mss	mss	po
	U72G	U72G				U84B	U84B
Sample	light	dark	U73B	U75E	U77A	light	dark
Diamond	D14-B	D14-B	D14-C	D22-A	D45-B	D131	D131
Assemblage	coe, sul	coe, sul	2 gt, sul	4 gt, sul	gt, sul	gt, sul	gt, sul
Paragenesis	*e*	*e*	*e*	*e*	*e*	*e*	*e*
Cu	0.01	1.54	1.79	2.19	2.09	0.22	0.38
Fe	27.61	58.20	55.38	57.08	55.68	40.29	58.85
Ni	31.07	0.65	2.07	0.98	2.76	22.24	0.24
Co	6.32	0.15	0.30	0.12	0.22	1.76	0.10
Zn	0.00	0.00	0.01	0.02	0.02	0.01	0.02
Cr	0.00	0.00	0.00	0.01	0.00	0.00	0.00
Se	0.02	0.01	0.00	0.01	0.01	0.00	0.00
S	33.54	38.79	39.01	38.87	38.98	35.39	39.54
Totals	98.56	99.33	98.57	99.27	99.75	99.90	99.13

e = *eclogitic* paragenesis
mss = monosulphide solid solution
po-mss = pyrrhotite + monosulphide solid solution
popn = pyrrhotite + pentlandite
po = pyrrhotite
pn = pentlandite

Sulfur normalised to 4 cations

Cu	0.000	0.080	0.093	0.114	0.108	0.012	0.019
Fe	1.891	3.446	3.260	3.373	3.280	2.615	3.418
Ni	2.024	0.037	0.116	0.055	0.155	1.373	0.013
Co	0.410	0.008	0.017	0.007	0.012	0.108	0.006
Zn	0.000	0.000	0.000	0.001	0.001	0.000	0.001
Cr	0.000	0.000	0.000	0.000	0.000	0.000	0.000
Se	0.001	0.000	0.000	0.000	0.000	0.000	0.000
S	4.000	4.000	4.000	4.000	4.000	4.000	4.000
Σcations	8.327	7.571	7.486	7.550	7.556	8.109	7.457
Σcations/S	2.08	1.89	1.87	1.89	1.89	2.03	1.86
(Fe,Ni)/S	1.75	1.52	1.47	1.49	1.50	1.77	1.49
Atomic proportions							
Cu	0.000	0.024	0.028	0.034	0.033	0.003	0.006
Fe	0.494	1.042	0.992	1.022	0.997	0.721	1.054
Ni	0.529	0.011	0.035	0.017	0.047	0.379	0.004
Co	0.107	0.003	0.005	0.002	0.004	0.030	0.002
Zn	0.000	0.000	0.000	0.000	0.000	0.000	0.000
Cr	0.000	0.000	0.000	0.000	0.000	0.000	0.000
Se	0.000	0.000	0.000	0.000	0.000	0.000	0.000
S	1.046	1.210	1.217	1.212	1.216	1.104	1.233
Totals	2.177	2.290	2.277	2.288	2.297	2.237	2.299

Table A.3.10 (cont.) – Electron microprobe chemical analyses of sulphide inclusions in diamonds from the Urals.

Mineral	pocp		po-mss		po
Phase	cp	po	mss	po	po
Sample	U85D light	U85D dark	U90B light	U90B dark	U90C
Diamond	D132	D132	D69	D69	D69
Assemblage	gt, 6 cpx, coe, sul	gt, 6 cpx, coe, sul	3 sul	3 sul	3 sul
Paragenesis	*e*	*e*	*?*	*?*	*?*
Cu	32.94	0.18	1.68	1.01	0.49
Fe	31.01	60.02	49.15	55.71	57.45
Ni	0.02	0.37	9.93	2.53	1.03
Co	0.05	0.11	0.56	0.20	0.15
Zn	0.00	0.02	0.02	0.00	0.00
Cr	0.00	0.00	0.01	0.00	0.01
Se	0.00	0.01	0.01	0.01	0.02
S	34.94	38.78	38.22	38.91	39.22
Totals	98.96	99.48	99.57	98.38	98.36

e = *eclogitic* paragenesis
? = *undetermined* paragenesis
mss = monosulphide solid solution
po-mss = pyrrhotite + monosulphide solid solution
pocp = pyrrhotite + chalcopyrite
po = pyrrhotite
cp = chalcopyrite

Sulfur normalised to 4 cations

Cu	1.903	0.009	0.089	0.053	0.025
Fe	2.038	3.555	2.953	3.289	3.365
Ni	0.001	0.021	0.567	0.142	0.058
Co	0.003	0.006	0.032	0.011	0.008
Zn	0.000	0.001	0.001	0.000	0.000
Cr	0.000	0.000	0.000	0.000	0.001
Se	0.000	0.000	0.000	0.000	0.001
S	4.000	4.000	4.000	4.000	4.000
Σcations	7.945	7.592	7.643	7.495	7.457
Σcations/S	1.99	1.90	1.91	1.87	1.86
(Fe,Ni)/S	0.89	1.56	1.55	1.50	1.49

Atomic proportions

Cu	0.518	0.003	0.027	0.016	0.008
Fe	0.555	1.075	0.880	0.998	1.029
Ni	0.000	0.006	0.169	0.043	0.018
Co	0.001	0.002	0.010	0.003	0.003
Zn	0.000	0.000	0.000	0.000	0.000
Cr	0.000	0.000	0.000	0.000	0.000
Se	0.000	0.000	0.000	0.000	0.000
S	1.090	1.209	1.192	1.213	1.223
Totals	2.165	2.295	2.278	2.274	2.280

A.4. Radiogenic isotope dating of mineral inclusions

Table A.4.1 – A Compilation of Diamond Dating Studies - adapted from Stachel and Harris (2008).

Isotope system	Locality	Method	Inclusion mineral and Paragenesis	Age (Ma)	Eruption Age (Ma)	Reference
Pb-Pb/U-Pb	Premier SA	model age	Sulphides (?)	~ 1500	1180 ± 30	1
	Premier SA	model age	Sulphides (?)	~ 1200	1180 ± 30	2
	Finsch SA	model age	Sulphides (?)	> 2000	118 ± 3	2
	Kimberley SA	model age	Sulphides (?)	> 2000	95	2
	Udachnaya	model age	Sulphide (?)	~ 2000	361 ± 6	3
	Dem. Rep. of Congo	model age	Zircon (?)	628 ±12	73.1 ± 1.1	4
Sm-Nd	Kimberley SA	model age	P-type gnt	3200 ± 100	95	5
	Finsch SA	model age	P-type gnt	3200 ± 100	118 ± 3	5
	Argyle AUS	isochron	E-type gnt + cpx	1580 ± 60	1129 ± 9	6
	Kimberley SA	model age	W-type cpx (single)	2111± 120	118 ± 3	7
	Finsch SA	model age	E-type gnt (single)	1443 ± 166	118 ± 3	7
	Finsch SA	model age	E-type gnt (single)	1657 ± 77	118 ± 3	7
	Finsch SA	isochron	E-type gnt + cpx	1580 ± 50	118 ± 3	8
	Orapa BOTS	isochron	E-type gnt + cpx	990 ± 50	93± 3	8
	Premier SA	isochron	E-type gnt + cpx	1150 ± 60	1180 ± 30	6
	Premier SA	isochron	P-type gnt + cpx Lhz	1930 ± 60	1180 ± 30	9
	Udachnaya RU	isochron	P-type gnt	2010 ± 60	361 ± 6	10
	Jwaneng BOTS	isochron	E-type gnt + cpx	1540 ± 20	235 ± 4	11
	Venetia SA	isochron	P-type gnt	2300 ± 40	519	12
Re-Os	Koffiefontein SA	isochron	P-type sulphides	68 ± 30	90	13
	Koffiefontein SA	isochron	E-type sulphides	1048 ± 120	90	13
	Wellington AUS	model age	P-type sulphides	3609 ± 300	341 ± 25	14
	Wellington AUS	model age	P-type sulphides	2374 ± 300	341 ± 25	14
	Udachnaya RU	model age	P-type sulphides	3100 to 3500 ± 300	361 ± 6	15
	Udachnaya RU	model age	P-type sulphides	3502 ± 100	361 ± 6	15
	Kimberley RA	isochron	E-type sulphides	2890 ± 60	95	16
	Orapa BOTS	isochron	E-type sulphides	2500 to 3000	93	17
	Orapa BOTS	isochron	E-type sulphides	1000	93	17
	Jwaneng BOTS	isochron	E-type sulphides	1500	235 ± 4	18
	Jwaneng BOTS	isochron	E-type sulphides	2900	235 ± 4	18
	Koffiefontein SA	isochron	E-type sulphides	1000 ± 40	90	19
	Koffiefontein SA	isochron	E-type sulphides	2600 ± 300	90	19
	Panda CAN	isochron	P-type sulphides	3520 ± 170	53	20

Ar-Ar	Premier SA	cleaved single crystals	E-type cpx	1185 ± 94	1180 ± 30	21
	Premier SA	cleaved single crystals	E-type cpx	1198 ± 28	1180 ± 30	22
	Jwaneng BOTS	cleaved single crystals	E-type cpx	244 (233 to 417, n=7)	235 ± 4	23
	Jwaneng BOTS	cleaved single crystals	E-type cpx	241 ± 8	235 ± 4	24
	Jwaneng BOTS	cleaved single crystals	E-type cpx	233 ± 12	236 ± 4	24
	Orapa BOTS	cleaved single crystals	E-type cpx	102 (96 to 655, n=10)	93	23
	Orapa BOTS	cleaved single crystals	P-type cpx	105 to 176 ± 5	93	24
	Argyle AUS	cleaved single crystals	E-type cpx	1159 to 1540	1129 ± 9	23
	Udachnaya RU	cleaved single crystals	E-type cpx	425 (349 to 461, n=7)	361 ± 6	23
	Udachnaya RU	buried single crystal	E-type cpx	1149 ± 37	361 ± 6	23
	Dem. Rep. of Congo	cleaved single crystals	E-type cpx	(106 to 801, n=5)	73.1 ± 1.1	24
	Copeton AUS	cleaved single crystals	E-type cpx	355 ± 14	Alluvial	25
	Copeton AUS	cleaved single crystals	E-type cpx	327 ± 34	Alluvial	25
	Copeton AUS	cleaved single crystals	E-type cpx	340 ± 28	Alluvial	25
	Orapa BOTS	buried single crystal	E-type cpx	906 to 1032	93	26
	Orapa BOTS	buried single crystal	E-type cpx	> 2500	93	26
	Venetia SA	buried single crystal	E-type cpx	~ 520	519	26

Eruption ages from Allsopp et al., (1989), Kinny et al., (1997) and Gurney et al., (2005).

1 = Welke et al., (1974): 2 = Kramers, (1979): 3 = Rudnick et al., (1993): 4 = Kinny and Meyer, (1994): 5 = Richardson, et al., (1984)
6 = Richardson (1986): 7 = Smith et al., (1991): 8 = Richardson et al., (1990): 9 = Richardson et al., (1993)
10 = Richardson and Harris, (1997): 11 = Richardson etal., (1999): 12 = Richardson et al (2006): 13 = Pearson et al., (1998b)
14 = Pearson et al., (1998a): 15 = Pearson et al., (1999): 16 = Richardson et al., (2001): 17 = Shirey et al., (2001): 18 = Richardson et al., (2004)
19 = Pearson and Harris (2004): 20 = Westerlund et al., (2006): 21 = Burgess et al., (1989): 22 = Phillips et al., (1989)
23 = Burgess et al., (1992): 24 = Phillips et al., (1998): 25 = Burgess et al., (1998): 26 = Burgess et al., (2004).

Table A.4.2 – Dimensions of the Urals sulphide inclusions analysed for Re-Os.

Sample	Size of inclusions (μm)	Explanation
U67A	220x120x110; 150x90x60; 120x70x30; 100x80x60	1 inclusion - 4 fragments
U68C	130x110x50; 100x80x60; 90x90x50; 80x60x50	1 inclusion - 4 fragments
U69B	110x70x50; 100x90x60; 90x60x50; 70x50x20; 60x40x30	1 inclusion - 5 fragments
U73B	220x160x120; 120x90x60; 100x40x30; 80x50x40; 80x40x40; 80x40x40; 70x50x40; 70x50x40; 70x50x30; 50x40x30; 50x30x30; 50x30x30	1 inclusion - 12 fragments
U74E	170x120x60; 110x50x30; 80x60x40; 70x60x40; 50x30x20	1 inclusion - 5 fragments
U78B	110x70x50; 110x60x20; 80x60x20; 60x30x20; 70x20x20; 60x30x20; 50x20x20	1 inclusion - 7 fragments
U79B	200x20x20; 120x90x60; 120x70x50; 120x60x30; 110x90x50; 90x70x20; 90x40x30; 70x60x50; 70x40x20; 60x40x30; 50x30x20; 50x30x20	1 inclusion - 12 fragments
U80B	290x90x80	1 inclusion
U80C	120x80x60; 130x90x50; 100x90x80; 100x60x30; 90x90x30; 90x70x40; 90x80x30; 90x60x30; 80x50x30; 60x40x20; 50x30x20; 50x20x20; 50x30x20; 50x30x20	1 inclusion - 14 fragments
U81A	150x100x50; 150x90x40; 120x100x50; 120x120x60; 120x60x40; 100x90x50; 100x80x50; 100x70x50; 100x60x40; 100x50x30; 90x60x40; 90x50x40; 90x80x50; 90x60x40; 90x60x40; 80x50x40; 90x30x30; 60x50x40;	1 inclusion - 18 fragments
U82A	110x60x40; 90x50x30; 80x60x30; 60x50x20; 50x30x30	1 inclusion - 5 fragments
U82D	120x100x70	1 inclusion
U82E	130x80x60	1 inclusion
U87A	330x180x150; 300x180x170; 250x200x120; 210x150x120; 210x40x40; 200x40x40; 180x140x100; 180x100x80; 180x120x100; 150x90x60; 150x130x80; 150x150x60; 120x90x50; 120x80x50; 120x100x80; 110x60x40; 90x70x50; 90x70x50; 90x90x50; 80x60x50	1 inclusion - 20 fragments
U87B	170x120x60	1 inclusion
U87C	170x70x70	1 inclusion
U88A	210x90x60; 160x90x60; 190x100x50; 180x120x50; 180x70x50; 150x110x100; 150x50x40; 140x50x40; 120x70x50; 120x60x50; 120x50x50; 120x70x50; 120x60x50; 100x70x50; 100x60x50; 90x60x40; 90x40x30; 80x70x50; 60x30x20; 60x60x50	1 inclusion - 20 fragments
U89A	160x120x80; 140x40x30; 120x70x50; 110x110x90; 110x60x40; 70x50x30; 70x60x30; 60x40x30; 50x40x30; 50x30x20	1 inclusion - 10 fragments
U90A	160x80x60; 120x100x90; 120x60x40; 90x50x30; 80x50x30; 70x50x30; 60x50x30; 60x40x30; 50x30x20; 50x30x20; 50x30x20; 50x30x20; 50x20x20	1 inclusion - 13 fragments
U91A	220x160x120; 180x130x100; 180x100x60; 170x100x60; 150x100x70; 120x110x80; 120x90x50; 120x60x40; 120x50x40; 110x70x50; 100x50x40; 90x60x50; 70x50x40; 70x50x40; 70x50x30; 60x50x40; 60x40x40; 50x50x30; 50x40x30; 50x30x20	1 inclusion - 20 fragments

Table A.4.3 – Re-Os isotope measurements of the Ural diamonds sulphide inclusions.

Sample	Sample weight (µg)	Os conc (fg)	Os conc (ppb)	Common Os (ppb)	Re conc (ppb)	$^{187}Os/^{188}Os$	2σ uncertainty $^{187}Os/^{188}Os$	$^{187}Re/^{188}Os$	2σ uncertainty $^{187}Re/^{188}Os$	$[N_T]$ (at. ppm)	%IaB	Fe (at.%)	Ni (at.%)	Cu (at.%)	Co (ppm)
U67A	7.0	115	15.3	10.9	400	3.127	0.196	175.493	13.047	587	21	88.5	9.6	2.0	4165
U68C	4.7	208	42.7	29.4	377	3.554	0.136	61.487	5.441	688	44	87.5	9.0	3.4	3895
U69B	3.5	1257	356.9	284.3	258	2.055	0.011	4.359	0.493	788	47	91.8	5.5	2.7	2887
U73B	16.9	220	12.6	6.3	345	7.767	0.510	263.977	11.435	433	37	92.2	5.5	2.4	2730
U74E	6.4	139	20.5	17.7	87	1.289	0.031	23.423	2.070	633	13	96.7	2.4	1.4	1389
U78B	3.3	2564	774.5	608.3	289	2.194	0.009	2.283	0.261	846	37	84.4	12.8	2.5	2527
U79B	9.6	828	85.5	74.1	663	1.284	0.008	42.987	2.689	594	31	98.1	1.2	1.2	711
U80B	11.0	115	9.7	5.2	215	6.849	0.941	199.529	13.430	438	13	94.8	3.3	2.2	2094
U80C	9.2	538	58.8	47.7	169	1.882	0.020	17.050	1.816	438	13	95.6	3.0	1.8	1541
U81A	21.3	355	16.3	11.2	194	3.601	0.069	83.307	5.030	639	39	93.2	3.3	3.6	2197
U82A	2.8	60	18.7	11.8	174	4.563	1.289	70.862	10.631	567	42	95.3	2.9	2.1	1770
U82D	1.9	60	27.7	16.6	246	5.194	3.411	71.041	21.132	567	42	94.7	3.4	2.1	3220
U82E	2.4	87	33.1	22.6	230	3.634	0.819	48.729	13.792	567	42	93.3	4.5	2.4	1854
U87A	80.3	314	3.8	1.8	249	8.895	0.421	672.432	22.396	433	54	93.7	3.9	2.6	1711
U87B	4.0	78	17.6	8.2	967	8.876	6.295	566.210	96.641	433	54	93.2	4.1	2.9	n.d.
U87C	3.7	33	6.9	5.2	198	2.669	1.423	183.148	38.288	433	54	93.6	3.9	2.7	2241
U88A	28.2	360	12.5	3.1	230	24.340	8.241	369.112	18.114	670	23	94.1	2.6	3.4	2239
U89A	9.9	188	18.3	9.6	325	7.044	0.604	162.942	13.539	635	64	95.3	2.8	2.2	1652
U90A	8.4	225	25.9	21.6	130	1.616	0.036	28.866	2.986	502	47	91.3	5.9	2.9	1515
U91A	27.1	91	3.1	0.9	154	17.961	66.168	804.317	49.236	691	40	94.7	1.9	3.5	1898

Errors in $^{187}Os/^{188}Os$ are the sum of Os run precision (2σ), weighing errors and uncertainty in Os blank correction (variation in blank abundance, blank isotopic composition and spike calibration).

Errors in $^{187}Re/^{188}Os$ are the sum of $^{187}Re/^{185}Re$ and $^{190}Os/^{188}Os$ run precision (2σ), weighing errors, Re and Os spike calibration and uncertainty in Re and Os blank correction.

Diamond nitrogen contents $[N_T]$ and percentage of the nitrogen B-defect (%IaB) determined by Fourier Transform Infrared Spectroscopy.

The Re/Os isotopic ratios of that sample U67 are only indicative, as several fragments were accidentally lost during micro-manipulation.

n.d. - not determined.

Table A.4.4 – Dimensions of the Urals clinopyroxene inclusions analysed for $^{40}Ar/^{39}Ar$.

Sample	Size of inclusions (μm)	Explanation
U41	370x240x140	1 inclusion
U85a	160x130x90; 160x60x50; 150x90x60; 120x70x60; 90x80x50	1 inclusion - 5 fragments
U85b	210x90x60; 200x160x60; 170x130x70; 150x120x60; 150x120x60; 150x120x50; 150x120x40; 140x60x40; 100x70x40; 90x60x40; 90x70x20; 90x50x30; 90x90x30	1 inclusion - 13 fragments
U92a	180x120x100	1 inclusion
U92b	360x280x80; 320x210x120; 320x220x120; 300x150x80; 260x150x80; 240x120x100; 240x150x60; 160x160x60; 180x150x60; 180x160x60	1 inclusion - 10 fragments
U93	380x360x200; 360x210x50; 240x100x50; 140x70x50; 80x50x30; 80x50x30; 70x50x30; 70x50x30	1 inclusion - 8 fragments
U94	300x210x140; 240x150x100	1 inclusion - 2 fragments

Table A.4.5 – $^{40}Ar/^{39}Ar$ analytical results for eclogitic clinopyroxene inclusions in diamonds from the Ural Mountains.

Sample (Mass, µg)	Step No	Cum.% ^{39}Ar	^{40}Ar (±) ($x10^{-13}$ moles)	^{39}Ar (±) ($x10^{-14}$ moles)	^{38}Ar (±) ($x10^{-16}$ moles)	^{37}Ar (±) ($x10^{-16}$ moles)	^{36}Ar (±) ($x10^{-16}$ moles)	Ca/K (±)	$^{40}Ar^*$ %	$^{40}Ar^*/^{39}Ar$ (±)	K (±) ppm	Cl (±) ppm	Ca (±) wt%	Age (±) Ma
J-Value = 0.013111 ± 0.000034														
U41	1	19.8	0.0041 (0.0000)	0.0014 (0.0001)	0.0014 (0.0016)	4.6422 (0.1883)	0.0049 (0.0012)	58.5 (3.8)	65.4	19.5 (2.7)	83 (4)	0.1 (0.2)	0.55 (0.02)	410 (51)
(41.0 µg)	2	100.0	0.0137 (0.0001)	0.0056 (0.0001)	0.0009 (0.0025)	20.4698 (0.4341)	0.0048 (0.0038)	63.5 (1.9)	89.6	21.8 (2.0)	335 (7)	0.0 (0.4)	2.43 (0.05)	454 (38)
	Total		0.0179 (0.0001)	0.0070 (0.0001)	0.0023 (0.0023)	25.1121 (0.3855)	0.0097 (0.0033)	62.5 (2.3)	84.8	21.4 (2.2)	285 (6)	0.0 (0.3)	2.06 (0.05)	445 (40)
J-Value = 0.013097 ± 0.000033														
U85a	1	23.2	0.0190 (0.0001)	0.0027 (0.0001)	0.0006 (0.0024)	6.0638 (0.2172)	0.0024 (0.0064)	39.6 (1.8)	96.3	68.3 (7.4)	492 (14)	0.1 (1.4)	2.23 (0.08)	1153 (92)
(13.3 µg)	2	100.0	0.0320 (0.0002)	0.0089 (0.0002)	0.0010 (0.0022)	22.1443 (0.2225)	0.0034 (0.0033)	43.6 (1.0)	96.8	34.8 (1.3)	1633 (34)	0.1 (1.0)	8.14 (0.08)	678 (22)
	Total		0.0510 (0.0002)	0.0116 (0.0002)	0.0016 (0.0022)	28.2081 (0.2212)	0.0058 (0.0040)	42.7 (1.2)	96.7	42.6 (2.7)	1368 (30)	0.1 (1.0)	6.76 (0.08)	788 (38)
J-Value = 0.013097 ± 0.000033														
U85b	1	33.7	0.0364 (0.0002)	0.0030 (0.0001)	0.0011 (0.0030)	5.6114 (0.1895)	0.0025 (0.0040)	33.2 (1.3)	98.0	120.6 (4.7)	225 (4)	0.1 (0.5)	0.85 (0.03)	1709 (43)
(32.1 µg)	2	100.0	0.0214 (0.0002)	0.0058 (0.0001)	0.0008 (0.0019)	14.4609 (0.1414)	0.0026 (0.0018)	43.6 (0.8)	96.5	35.5 (1.1)	442 (7)	0.1 (0.3)	2.20 (0.02)	689 (17)
	Total		0.0578 (0.0002)	0.0088 (0.0001)	0.0019 (0.0023)	20.0723 (0.1576)	0.0050 (0.0025)	40.1 (1.0)	97.0	64.2 (2.3)	369 (6)	0.1 (0.4)	1.75 (0.02)	1033 (26)
J-Value = 0.013097 ± 0.000033														
U92a	1	28.6	0.0146 (0.0001)	0.0051 (0.0001)	0.0038 (0.0024)	24.4773 (0.4517)	0.0058 (0.0030)	84.3 (2.2)	88.2	25.4 (1.8)	1739 (33)	1.8 (1.8)	16.76 (0.31)	519 (33)
(7.1 µg)	2	100.0	0.0307 (0.0002)	0.0127 (0.0001)	0.0041 (0.0017)	66.4911 (0.7249)	0.0011 (0.0023)	91.9 (1.3)	99.0	24.0 (0.6)	4335 (38)	2.6 (1.4)	45.53 (0.50)	493 (11)
	Total		0.0454 (0.0002)	0.0177 (0.0001)	0.0078 (0.0019)	90.9684 (0.6467)	0.0069 (0.0025)	89.7 (1.6)	95.9	24.4 (0.9)	3593 (37)	2.4 (1.5)	37.30 (0.44)	501 (17)
J-Value = 0.013097 ± 0.000033														
U92b	1	21.3	0.0448 (0.0003)	0.0047 (0.0001)	0.0255 (0.0026)	19.2215 (0.3543)	0.1166 (0.0044)	71.2 (2.4)	23.1	21.9 (2.9)	85 (2)	0.1 (0.1)	0.69 (0.01)	455 (53)
(136.0 µg)	2	100.0	0.0587 (0.0004)	0.0175 (0.0002)	0.0141 (0.0037)	87.5528 (1.1214)	0.0636 (0.0060)	87.7 (1.4)	68.0	22.8 (1.1)	314 (3)	0.1 (0.2)	3.14 (0.04)	472 (19)
	Total		0.1035 (0.0004)	0.0222 (0.0002)	0.0396 (0.0035)	106.7743 (0.9580)	0.1803 (0.0057)	84.2 (1.6)	58.4	22.6 (1.5)	265 (3)	0.1 (0.2)	2.62 (0.03)	469 (26)
J-Value = 0.013097 ± 0.000033														
U93	1	25.7	0.0845 (0.0005)	0.0335 (0.0002)	0.0070 (0.0039)	31.5122 (0.4647)	0.0158 (0.0057)	16.5 (0.3)	94.5	23.8 (0.5)	745 (5)	0.2 (0.2)	1.40 (0.02)	490 (10)
(109.8 µg)	2	100.0	0.2220 (0.0014)	0.0968 (0.0004)	0.0032 (0.0067)	120.6316 (1.5123)	0.0061 (0.0029)	21.8 (0.3)	99.2	22.8 (0.2)	2151 (9)	0.1 (0.3)	5.36 (0.07)	471 (4)
	Total		0.3065 (0.0012)	0.1303 (0.0004)	0.0102 (0.0060)	152.1438 (1.2431)	0.0219 (0.0036)	20.4 (0.3)	98.0	23.0 (0.3)	1789 (8)	0.1 (0.3)	4.34 (0.06)	475 (5)
J-Value = 0.013097 ± 0.000033														
U94	1	23.1	0.0066 (0.0000)	0.0026 (0.0001)	0.0007 (0.0025)	9.6576 (0.1156)	0.0036 (0.0022)	63.9 (1.9)	83.7	20.8 (2.6)	157 (4)	0.0 (0.3)	1.15 (0.01)	435 (48)
(41 µg)	2	100.0	0.0208 (0.0001)	0.0088 (0.0001)	0.0001 (0.0021)	41.8755 (0.8080)	0.0029 (0.0053)	83.4 (2.0)	95.9	22.7 (1.8)	523 (8)	0.0 (0.4)	4.99 (0.10)	469 (33)
	Total		0.0274 (0.0001)	0.0114 (0.0001)	0.0008 (0.0022)	51.5331 (0.6481)	0.0065 (0.0046)	78.9 (2.0)	93.1	22.3 (2.0)	439 (7)	0.0 (0.4)	4.10 (0.08)	462 (36)

i) Errors are two sigma uncertainties and exclude uncertainties in the J-value.
ii) Molar data are corrected for mass spectrometer backgrounds, discrimination, radioactive decay and isotopic interferences.
iii) Interference corrections: $(^{36}Ar/^{37}Ar)_{Ca} = 2.70x10^{-4}$; $(^{39}Ar/^{37}Ar)_{Ca} = 6.80x10^{-4}$; $(^{40}Ar/^{39}Ar)_{K} = 5.0x10^{-4}$.
iv) J-value is based on an age of 98.8 ± 0.5 Ma for GA1550 biotite (Renne et al., 1998).
v) $^{40}Ar^* = (^{40}Ar_{total} - {}^{40}Ar_{atmosphere})/{}^{40}Ar_{total}$.
vi) Total values for each inclusion are weighted averages using size of step weighing.

Table A.4.6 – $^{40}Ar/^{39}Ar$ analytical raw data for clinopyroxene inclusions in diamonds from the Ural Mountains.

Sample ID	Step No	Cum.% ^{39}Ar	^{40}Ar (x10^{-13} moles)	±	^{39}Ar (x10^{-14} moles)	±	^{38}Ar (x10^{-16} moles)	±	^{37}Ar (x10^{-16} moles)	±	^{36}Ar (x10^{-16} moles)	±	Ca/K	±	%^{40}Ar*	^{40}Ar*/^{39}Ar	±	Age (Ma)	±
Sample U41																			
J-Value =	0.013111	0.000034																	
U41	1	19.8	0.0041	0.0000	0.0014	0.0000	0.0014	0.0008	4.6422	0.0942	0.0049	0.0006	58.4561	1.9124	65.4	19.47	1.34	410.2	25.3
U41	2	100.0	0.0137	0.0000	0.0056	0.0001	0.0009	0.0012	20.4698	0.2171	0.0048	0.0019	63.5035	0.9455	89.6	21.82	1.02	453.9	18.8
Sample U85																			
J-Value =	0.013097	0.000033																	
U85	1	23.2	0.0190	0.0000	0.0027	0.0000	0.0006	0.0012	6.0638	0.1086	0.0024	0.0032	39.6131	0.8982	96.3	68.32	3.69	1153.0	46.0
U85a	2	100.0	0.0320	0.0001	0.0089	0.0001	0.0010	0.0011	22.1443	0.1112	0.0034	0.0016	43.5842	0.5071	96.8	34.82	0.67	677.9	10.8
Sample U85b																			
J-Value =	0.013097	0.000033																	
U85b	1	33.7	0.0364	0.0001	0.0030	0.0000	0.0011	0.0015	5.6114	0.0947	0.0025	0.0020	33.1957	0.6429	98.0	120.58	2.34	1709.3	21.5
U85b	2	100.0	0.0214	0.0001	0.0058	0.0000	0.0008	0.0010	14.4609	0.0707	0.0026	0.0009	43.5543	0.3923	96.5	35.54	0.54	689.4	8.7
Sample U92a																			
J-Value =	0.013097	0.000033																	
U92a	1	28.6	0.0146	0.0000	0.0051	0.0000	0.0038	0.0012	24.4773	0.2258	0.0058	0.0015	84.3356	1.1207	88.2	25.42	0.92	518.5	16.3
U92a	2	100.0	0.0307	0.0001	0.0127	0.0001	0.0041	0.0009	66.4911	0.3624	0.0011	0.0011	91.8972	0.6456	99.0	24.02	0.30	493.4	5.3
Sample U92b																			
J-Value =	0.013097	0.000033																	
U92b	1	21.3	0.0448	0.0001	0.0047	0.0001	0.0255	0.0013	19.2215	0.1772	0.1166	0.0022	71.2350	1.2135	23.1	21.90	1.43	455.0	26.3
U92b	2	100.0	0.0587	0.0002	0.0175	0.0001	0.0141	0.0019	87.5528	0.5607	0.0636	0.0030	87.6536	0.7041	68.0	22.85	0.53	472.3	9.7
Sample U93																			
J-Value =	0.013097	0.000033																	
U93	1	25.7	0.0845	0.0003	0.0335	0.0001	0.0070	0.0019	31.5122	0.2323	0.0158	0.0028	16.4513	0.1314	94.5	23.81	0.27	489.8	4.9
U93	2	100.0	0.2220	0.0007	0.0968	0.0002	0.0032	0.0033	120.6316	0.7562	0.0061	0.0014	21.8125	0.1446	99.2	22.75	0.10	470.5	1.8
Sample U94																			
J-Value =	0.013097	0.000033																	
U94	1	23.1	0.0066	0.0000	0.0026	0.0000	0.0007	0.0012	9.6576	0.0578	0.0036	0.0011	63.9003	0.9272	83.7	20.82	1.29	435.1	23.9
U94	2	100.0	0.0208	0.0000	0.0088	0.0001	0.0001	0.0011	41.8755	0.4040	0.0029	0.0026	83.3690	1.0044	95.9	22.69	0.90	469.5	16.4